The University Of Sheffield.

Understanding the role of glucose metabolism during macrophage challenge with *Streptococcus pneumoniae*

By:

Miss Emily Fisk

A thesis submitted in partial fulfilment of the requirements for the degree of Doctor of Philosophy

The University of Sheffield
Faculty of Medicine, Dentistry and Health
Department of Infection, Immunity and Cardiovascular Disease

December 2018

Contents page

List of Figures

List of Tables

Acknowledgements

Throughout my PhD, I have received a wealth of support both from within and outside of academia, and it is these people I truly thank for helping me through this (often hellish) rollercoaster of an experience!

Firstly, I would like to thank my supervisors, Prof David Dockrell and Dr. Helen Marriott for providing me this opportunity and for pushing me through to this final point! I am particularly grateful for the time you have taken to give feedback on my writing.

Second, I would like to express my thanks to my research group and the technical staff who have helped me along the way. Martin Bewley - you taught the students all we know and supplied some terrible yet brilliant jokes along the way, so thank you for both your academic and comedic support. Paul Collini, Paul Morris and Joby Cole – the fact that each of you have done your PhDs with young families and hectic medic timetables has felt like total madness, but it's been truly inspirational and I have admired your abilities in managing it all! You have always discussed and counselled my experimental problems during this PhD, and I will be forever grateful for all your help (also for the coffee and cookies Joby!) Jon Kilby, Katie Cooke and Lynne Williams - my work would not have been possible without each of you, and I am extremely grateful for your technical assistance and company in the lab. MD Mohasin - thanks for putting up with me being so bossy and I look forward to seeing where you head next. Andrea Hounslow – your support and guidance in the NMR Facility has been truly invaluable and I genuinely wouldn't have gotten anywhere without you there. I would like to thank you for your patience, guidance and for introducing me to people in the field, particularly those at Liverpool.

One of the biggest reasons I have reached this point of my PhD is because I have had unfathomable support from my colleagues and fellow PGR students. Primarily, I would like to thank Dr. Lucy Morris. You have been a patient teacher, an idol lab colleague, a great gym buddy, an incredible friend and someone whom I hope never to lose contact with. I can brazenly say I wouldn't have lasted past my confirmation review without you, so thank you for everything! Dr Furaha Asani and Miss Chloë Marshall – you were my Florey pals throughout. Furaha, you have been truly inspirational and I have admired the passion and drive you channel into all that you do. Chloë, I'm glad I pestered you

into being my friend and I've admired your strength and stubbornness in getting the best out of this PhD and landing such a great job. Dr. Billy Bryan – although our PhDs were in completely different subjects, we spent a lot of time working together and I am very grateful for the experiences we shared in boosting PGR representation and running some kick-ass charity bake sales. Dr Devon Smith – I am so extremely lucky to have met you and to have worked on both Pint of Science and PubhD with you – you are my SciComm guru, thank you for all you've taught me. I would also like to thank my other colleagues, Dr. Andreea Ciuntu, Dr. Apoorva Mulay, Dr Clair Fellows, Dr Grace Manley, Dr Isobel Williams, Dr Jake Mills, Dr Jess Tarrant and Dr. Sayali Haldipurkar. It's been lovely to work with you all, and we have shared some brilliant times, from the chaos of Health Challenge to the all night panic of BiotechYES.

Another network of support I couldn't have done this without is the Broomgrove Badminton Club. You guys have been so lovely and playing badminton has served as a wonderful distraction during stress of the lab and PhD life. I have also loved our little dinner parties and socials across the years – they were all fab! I would have gone stir-crazy without you guys to smash some cocks with twice a week, so thank you to you all: Ada, Adam, Alice, Andrew, Becca, Ben, Cat, Dave G, Dave J, Evan, Franck, Gerry, Hannah, Jarek, James A, James S, Joe, Jonathon, Kat, Kate, Laura, Louise, Mark, Mike, Mahmoud, Patrick, Rich C, Rich G, Sally, Sam, Sarah, Sonja and Verity.

Finally, I would like to thank my family. Mum, Dad, Lucy and Ad – whilst you may have no idea what I've really been doing these past 4 years, I couldn't have done it without your love and support. Maybe now I'll get to come home and see you all more often! And last but by no means least, Thomas Brooker – you have been my best friend and confidant throughout this PhD, dealing with all my tearful tantrums and ceaseless complaining. I cannot begin to describe how lucky I am to have you, and how thankful I am that you have supported me all this way - from practicing presentations and reading each other's work, to distracting me with games, baking and incredible holiday escapes. Thank you with all my heart.

Declaration

All work presented in this thesis is my own. Dr. Helen Marriott and Ms. Lynne Williams were responsible for culling mice and extracting bones for bone marrow culture. Lucy Morris and MD Mohasin also helped with maintaining these murine cell cultures. Animal work was carried out in accordance with the Animals Act 1986, with approval of the Sheffield Ethical Review Committee, UK. MD Mohasin also assisted during preliminary Seahorse XF assay optimisations.

Abstract

In 2015, the WHO recorded lower respiratory infections as the leading cause of mortality by infection worldwide (World Health Organization 2017). *Streptococcus pneumoniae* is just one bacterial species responsible for this burden. This pathogen is managed through using antibiotics, however it's recognised that pathogens can rapidly adapt to the selective pressure of antibiotics and acquire resistant mechanisms. Therefore, as the affliction of AMR grows wider, alternative treatments for bacterial infections are urgently required. One suggested method involves the development of host-based therapies. This requires a thorough understanding of host-pathogen interactions, to appropriately control host immune responses without causing excessive inflammation or host damage. This is particularly important for bacteria such as *S. pneumoniae,* which frequently colonise hosts without causing serious disease.

Metabolism has emerged as a key regulator of innate immune responses, particularly macrophages activated with the bacterial component LPS (O'Neill et al. 2016); however, few studies have sought to uncover the importance of metabolism during macrophage challenge with live bacteria. Therefore, the work reported herein aimed to understand how *S. pneumoniae* modulates murine macrophage metabolism, with a view to honing host responses to improve infection outcome, as a potential alternative to antibiotics.

This thesis outlines the optimisation and use of Seahorse XF Analysis and NMR Spectroscopy, to understand changes in macrophage metabolism, following stimulation with *S. pneumoniae* compared to the pro-inflammatory macrophage stimulus LPS. I have also addressed the use of glycolytic inhibitors, to probe the importance of glucose metabolism in regulating macrophage effector functions, such as phagocytosis and cytokine release. My principal finding is that *S. pneumoniae* does not induce the same metabolic changes as recorded for LPS in the literature. I propose that bacterial stimulation induces distinct macrophage activation phenotypes that depend on tailored host-pathogen interactions, which are likely to be unique for different pathogens of interest.

Abbreviations

2DG	2-deoxyglucose
AAAS	Arginosuccinate shunt
AAM	Alternatively-activated macrophage
AM	Alveolar macrophages
AMR	Antimicrobial resistance
ATP	Adenosine triphosphate
BCAA	Branched chain amino acid
BHI	Brain-heart infusion
BMDM	Bone marrow-derived macrophage
CAM	Classically-activated macrophage
CCR	Carbon catabolite repression
CFU	Colony forming units
COPD	Chronic obstructive pulmonary disease
COX2	Cyclooxygenase-2
D_2O	Deuterium oxide
DAF-FM	4-amino-5-methylamino-2',7'-difluorofluorescein diacetate
DAMP	Danger-associated molecular pathogen
DCF-DA	2',7'–dichlorofluorescin diacetate
DHEA	Dehydroepiandrosterone
DMEM	Dulbecco's Modified Eagle Medium
ECAR	Extracellular acidification rate
ELISA	Enzyme-linked immunosorbent assay
FCCP	Carbonyl cyanide-4-(trifluoromethoxy)phenylhydrazone
GABA	Gamma-aminobutyric acid
GAPDH	Glyceraldehyde-3-phosphate dehydrogenase
HIFCS	Heat-inactivated foetal calf serum
HMDB	Human metabolome database
INFy	Interferon gamma
iNOS	Inducible nitric oxide synthase
Iodo	Iodoacetate
LAMP	Lysosome-associated membrane protein
LPS	Lipopolysaccharide

MDM	Monocyte-derived macrophage
MIC	Minimum Inhibitory concentration
MM-VC	Miles Misra viable count
MOI	Multiplicity of infection
MRSA	Methicillin-resistant *Staphylococcus aureus*
MS	Mass Spectrometry
NADH	Nicotinamide adenine dinucleotide
NMR	Nuclear magnetic resonance
NO	Nitric oxide
OCR	Oxygen consumption rate
OD	Optical density
Oligo	Oligomycin A
OXPHOS	Oxidative phosphorylation
PAMP	Pathogen-associated molecular pattern
PBS	Phosphate-buffered solution
PCV	Pneumococcal conjugate vaccine
PI3K	Phosphatidlinositol 3-kinase
PPP	Pentose phosphate pathways
PPV	Pneumococcal polysaccharide vaccine
PRR	Pathogen recognition receptor
ROS	Reactive oxygen species
RNS	Reactive nitrogen species
Spn	*Streptococcus pneumoniae*
STING	Stimulator of interferon genes
TCA	Tricarboxylic acid
TLR	Toll-like receptor
TSP	Trimethylsilyl propionate
UNS	Unstimulated
XF	Extracellular flux
XFAM	Extracellular flux assay media

Chapter 1 - Introduction

1.1. Antimicrobial Resistance

1.1.1. Early antibiotic discovery

In 1928, Sir Alexander Fleming serendipitously discovered penicillin (Fleming 1929). Howard Florey and Ernst Chain then purified this compound, enabling it to be used to treat clinical bacterial infections, and saving millions of lives during World War II. This discovery is now considered as one of the biggest medical breakthroughs of the 20th century (Kardos & Demain 2011; Neushul 1993). Despite this, during his Nobel Lecture, Fleming foretold the principal of antibiotic resistance with the following statement:

"It is not difficult to make microbes resistant to penicillin in the laboratory by exposing them to concentrations not sufficient to kill them, and the same thing has occasionally happened in the body. The time may come when penicillin can be bought by anyone in the shops. Then there is the danger that the ignorant man may easily underdose himself and by exposing his microbes to non-lethal quantities of the drug, make them resistant." (Fleming 1964).

A century on and hundreds of antibiotics are now available, but with many classes facing bacterial resistance (Clatworthy et al. 2007). Antimicrobial Resistance (AMR) is the overarching term for when a microorganism becomes resistant to an antimicrobial compound, with which it was originally treated; for example, *Staphylococcus aureus* was previously treated with methicillin, however, this drug is now administered more selectively, since the emergence of methicillin-resistant *S. aureus* (MRSA) in the 1960s (Jevons 1961; Cetin 1962). AMR has been forecast to cost the globe $100 trillion by 2050, if no further action is taken, which could increase the death doll by 10 million lives each year – equating to an estimated increase of one person every three seconds (Taylor et al. 2014). During the 1940s-1960s, a time referred to as the 'Golden Era of Antibiotic Discovery', many antibiotics were isolated through screening of soil samples, as demonstrated by Selma Waksman and his work with Streptomyces (Walsh & Wencewicz 2014; Lewis 2013). However, after 20 years no new antibiotics had been identified and resistance was already emerging, which instead prompted the chemical manipulation of current antibiotics and target compounds. The last major antibiotic class identified in 1986 were the lipopeptides, specifically the drug Daptomycin (Lewis 2013; Steenbergen

et al. 2005). However, regardless of advances in scientific technologies – including the ability to sequence and profile bacterial genomes – new approaches to AMR are still urgently required.

1.1.2. Modern antibiotic discovery and new antimicrobial approaches

Despite the increasing burden of AMR, pharmaceutical industries were not investing in the development of new antimicrobials. It can cost up to $800million for a drug to reach market, making it clear why drugs for chronic diseases or long term usage were a more attractive pipeline (Norrby et al. 2005; O'Neill 2015). Pharmaceuticals therefore focused their efforts on drugs that provided better return, to recover the costs of research and development, from basic bench science through to clinical trials, whilst also making profits on sales (Cole 2014). This idea of money versus morals caused increasing debate, and governing bodies have since implemented plans and incentives to increase research into antimicrobial strategies. For example, in 2015 alone, the World Health Organization (WHO), United States and G7 Health Ministers all launched action plans to develop AMR research (World Health Organization 2015; The White House Administration 2015; G7 Gesundheitsministertreffen 2015). In 2014, economist Jim O'Neill chaired the UK independent review on AMR, with the final report published in 2016, detailing the ensuing devastation AMR will cause if left unchallenged, with recommended actions suggested to be carried out on a global scale (O'Neill 2016). This review also prompted the Industry Declaration by Pharmaceutical, Biotechnological and Diagnostic companies, calling for governments to reform the market of antimicrobials and diagnostics (Review on Antimicrobial Resistance 2016). With this financial and collaborative support, the search for new antimicrobials is now back on the rise. One example of new technologies in recent antimicrobial studies can be demonstrated by (Ling et al. 2015). There had been no new antibiotic classes founded for over 30 years, but the advanced technology used by Ling et al. to grow unculturable soil organisms, resulted in the identification of the novel antimicrobial Teixobactin (Ling et al. 2015).

Whilst an increase in antimicrobial and therapeutic enhancements are recommended in the O'Neill review, they also suggest that the development of vaccines and alternatives to antimicrobials are conducted (O'Neill 2016). One alternative method could be to target the host immune system, as opposed to targeting bacteria; for example, by

boosting natural host immune responses to better fight infection. This requires a thorough understanding of immune responses and the interplay with bacteria (Czaplewski et al. 2016). With this approach to AMR, valuable insight could be achieved into how 'healthy' people remain healthy and why the immune system can result in illness, even during colonisation with commensal bacteria. The understanding of host-pathogen interactions could provide information on how to promote more efficient immune responses, or how to hinder the initial interaction of bacteria with their hosts, and prevent bacteria from colonising, thriving, and causing disease when in association with our bodies. This is very much the view of the University of Sheffield's Florey Institute: researching the host-pathogen interactions of *S. aureus* and *S. pneumoniae*, with a view to identifying novel antimicrobial strategies, using the notion of bench-to-bedside research (The University of Sheffield 2015). The work reported herein focuses specifically on the pathogen *S. pneumoniae* and its interaction with cell cultures, as a model of pneumococcal respiratory infection.

1.2. *S. pneumoniae*

S. pneumoniae is a Gram-positive human-commensal bacterium that is commonly found in the upper respiratory tract (Gray 1980). However, given the opportunity it can cause disease - for example, when opposed by a weakened host immune response, as is typically observed in children, the elderly and immunocompromised. In these individuals, the bacterium colonises the lower respiratory environment, induces disease and disseminates through the blood (van der Poll & Opal 2009; Weiser 2010). *S. pneumoniae* causes a wide range of diseases, including meningitis, bacteraemia, otitis media (Musher 1992), and it is a leading cause of community-acquired pneumonia. It is also a cause of infectious exacerbations in Chronic Obstructive Pulmonary Disease (COPD), which was previously recorded to affect between 30-80% of patients (Garau & Calbo 2008; Garcia-Vidal et al. 2009), although more recent estimates have since been below 20% (Williams et al. 2017; Lin et al. 2016). In 2000, it was estimated that 14.5 million cases of serious pneumococcal disease were recorded, with more than 800,000 of these resulting in deaths of children under the age of five (World Health Organization 2011). With such high mortality and the increasing spread of AMR, *S. pneumoniae* is still one of the leading causes of death by infection, worldwide.

1.2.1. *S. pneumoniae* virulence factors

S. pneumoniae uses a combination of different virulence techniques, to successfully colonise, invade and infect different tissue niches (van der Poll & Opal 2009), with a large proportion of genes having been acquired through horizontal transfer, from both genetic recombination and mobile genetic elements (Chaguza et al. 2015). The genome of *S. pneumoniae* is roughly two million base pairs and contains between 1,500-1,800 core genes, which are commonly shared across serotypes (Tettelin et al. 2001; Makarewicz et al. 2017; Chaguza et al. 2015). These genes are likely to transcribe proteins that contribute to essential functions, including viability, core metabolic pathways, colonisation, and expression of virulence factors, such as the pneumolysin toxin, autolysin, hyaluronidase, and metal ion transporter channels (Obert et al. 2006). A large component of the genome regulates metabolic function and its consequences, for example the ability to withstand oxidative stress (Tettelin et al. 2001; Aberdein et al. 2013). The genome also consists of variable regions, which are also referred to as

accessory regions (ARs) or regions of diversity. Whilst virulence factors have been noted to cluster at ARs, they are not exclusively transcribed within these regions (Obert et al. 2006), and differential expression of virulence determinants is suggested to be dependent on the serotype and infection site, with no definitive or distinguishable trend for ARs noted during invasive infections (Ogunniyi et al. 2002; Blomberg et al. 2009). In this section, two key virulence factors are described in detail, with further factors also discussed briefly.

1.2.1.1. Polysaccharide capsule

The pneumococcal capsule is arguably the most important virulence factor for the pathogenicity of the pneumococcus. It plays a fundamental role in the pathogens ability to colonise, invade and disseminate from the respiratory tract to other tissues. It supports bacterial evasion of phagocytosis, as the capsule coats the external surface of the bacterium, hiding pneumococcal surface structures that would otherwise be bound or identified by complement and antibodies of the host immune response (Kalin 1998). The capsule also restricts mucosal clearance of the pathogen, as it is highly negatively charged and exerts a strong electrostatic repulsion against mucosal surfaces (Nelson et al. 2007). Further to this, capsular size and viscosity have been shown to influence colonisation of the bacterium; pneumococci with thinner, transparent capsules are shown to be more successful during binding of the host, in early colonisation and biofilm formation, whilst thicker, opaque capsules promote a more planktonic phenotype and are better suited for tissue invasion and pathogen dissemination. It is reported that many pneumococcal variants have the ability to switch between these two capsule types, through displaying phase variation (Weiser et al. 1994). Currently, there are over 90 different capsular polysaccharide variants recorded (Bentley et al. 2006; Geno et al. 2015), and it has been shown that non-encapsulated strains are more susceptible to immune clearance and present a loss of virulence compared to their encapsulated counterparts (Hyams et al. 2010). That said, increasing numbers of non-encapsulated strains have been isolated from patients with conjunctivitis and otitis media, and in rare cases of invasive pneumococcal disease (Keller et al. 2016). This capsule is also the principal target for current pneumococcal vaccines, as discussed later in this section.

1.2.1.2. Pneumolysin

Pneumolysin is the 53kDa cholesterol-dependent pore-forming toxin produced by *S. pneumoniae*, which shows strong similarity to the *Clostridium perfringens* toxin, perfringolysin. Pneumolysin is released by the bacterium as a soluble monomer, consisting of four domains and with primarily β-sheet structures. These monomer units bind to cholesterol in host cell lipid membranes, where they oligomerise to a 30-50 subunit pore, with a diameter of up to 450Å (Gilbert et al. 1999). When present in high enough concentrations, the pores leach the contents of host cells, and induce cell death through lysis (Van Pee et al. 2016; Hirst et al. 2004). The toxin is usually found in the cytoplasm of the bacteria, and is considered to be released through autolysis of the bacterium via the autolysin LytA; however the mechanism of its release is still widely debated as it has also been shown to occur independently of LytA (Balachandran et al. 2001). Aside from it's pore-forming capabilities, pneumolysin has been reported to cause other pathological effects at lower concentrations, including the inhibition of epithelial ciliary action, the stimulation of cytokine production by immune cells, and activation of T-cell subsets (Hirst et al. 2004). The toxin has also been shown to play an important role in the ability of pneumococci to replicate and disseminate in the alveolar environment and in the activation of complement *in vivo* (Rubins et al. 1995). Further to this, it is proposed that pneumolysin can promote biofilm formation of pneumococci, independent of its pore-forming ability (Shak et al. 2013). Interestingly non-haemolytic pneumolysin mutants of *S. pneumoniae* have been isolated from patients with invasive pneumococcal disease, demonstrating that a functional pore-forming toxin is not necessarily required for virulence, and may also confer a selective advantage for dissemination and survival in the host bloodstream (Kirkham et al. 2006; Harvey et al. 2011)

1.2.1.3. Other virulence factors and mechanisms

Sheltered beneath the polysaccharide capsule, *S. pneumoniae* has an array of surface proteins that contribute to bacterial virulence. These include LPXTG-anchored proteins, such as neuraminidase and hyaluronidase, and choline binding proteins, including LytA and the pneumococcal surface proteins PspA and PspC (PspC also known as CbpA). The sialidase enzyme, neuraminidase, has been shown to be important in removal of glycan

sugars from host receptors, in order to aid bacterial adhesion to host cell surfaces, particularly to cells of the epithelium (Brittan et al. 2012). Likewise, hyaluronidase has been suggested to break down extracellular matrix components, to aid spread of infection between tissues (Kadioglu et al. 2008). Meanwhile, PspA and PspC are important for interference of the host complement response, and for binding lactoferrin and the complement regulator Factor H, respectively (Mitchell & Mitchell 2010; Kadioglu et al. 2008). This allows extended evasion of opsonophagocytosis and hinders host clearance of the bacterium. The expression of pneumococcal surface lipoproteins is vital in pro-inflammatory activation of immune cells, including macrophages (Tomlinson et al. 2014). Additionally, natural IgM antibodies to pneumococcal surface proteins are known to be effective in opsonising *S. pneumoniae* TIGR4 in the absence of capsular antibodies (Wilson et al. 2017), although further work is required to confirm this for other serotypes. Lastly, external to the capsular environment, some pneumococcal variants present a pilus, which is suggested to play a role in binding, adherence and pro-inflammatory stimulation of the host (Barocchi et al. 2006).

Whilst the pneumococcus has a plethora of ways to prevent phagocytosis and immune evasion, the bacterium can still be phagocytosed by immune cells. In this intracellular environment, the bacterium has further strategies to prevent killing by the host. In the nasopharynx, *S. pneumoniae* kills competing bacteria through the release of hydrogen peroxide and uses the manganese-containing superoxide dismutase, MnSOD, to oppose damage to itself; this therefore allows *S. pneumoniae* to also resist oxidative killing mechanisms induced in the phagolysosome of host cells (Yesilkaya et al. 2000). The bacterium is also equipped to impede oxidative killing by other factors, including the pyruvate oxidase, SpxB, which generates further reactive oxygen species (ROS) but prevents ATP depletion (Pericone et al. 2003); the nicotinamide adenine dinucleotide (NADH) oxidase, Nox, which converts free oxygen into water to avoid it being used for ROS generation (Yu et al. 2001); and the pneumococcal surface antigen protein complex, PsaABC, which transports manganese required for MnSOD function, in association with the thiol peroxidase PsaD (McAllister et al. 2004; Tseng et al. 2002).

In addition to roles in virulence, some metabolic enzymes have been shown to locate at the cell walls of *S. pneumoniae, S. agalactiae* and *S. pyogenes*, including glyceraldehyde-3-phosphate dehydrogenase (GAPDH), glucose-6-phosphate isomerase and enolase

(D'Costa et al. 2000; Ling et al. 2004). These enzymes have been proposed to support functions in adhesion and binding of host factors, such as plasminogen and epithelial cell surfaces (Henderson & Martin 2011; Daniely et al. 2006). This is puzzling, as most of these proteins do not have sequences or motifs targeting them to this region, and therefore requires further research to understand their full purpose here. However, it has been shown that these cytoplasmic proteins could provide immunogenicity and a potential avenue for vaccine targeting (Zysk et al. 2000).

1.2.1.4. Pneumococcal metabolism

S. pneumoniae is a fermentative anaerobe, that heavily depends on sugar metabolism for biosynthesis, growth and virulence. It completely lacks the genes required for respiration and only a few genes of the Krebs cycle are found in specific pneumococcal serotypes; that said, a functional ATPase is present and genomic analysis of strain TIGR4 has shown the potential for synthesis and utilisation of up to 14 amino acids (Tettelin et al. 2001). Like many lactic acid bacteria, *S. pneumoniae* obtains its energy requirements most efficiently from carbohydrates, including compounds such as glucose, galactose and mannose, which feed the Embden-Meyerhof glycolytic pathway; however this typically depends on what is available to the bacterium in its environmental niche (Hoskins et al. 2001). The bacterium can sense and utilise sugars in the local environment via carbon catabolite repression (CCR), a process that silences genes of metabolic enzymes when they are not required – i.e. when they cannot process the sugars currently available. A key regulator of this process is catabolite control protein A, CcpA, which is important in steering the appropriate metabolic changes for colonisation in the nasopharynx (Iyer et al. 2005). In the nasopharynx, free glucose is limited, so the bacterium utilises glycosidases to cleave glycans from the epithelium and mucosal surfaces; whilst in the blood stream and inflammatory environments, glucose is present in much higher concentrations and is readily used by the bacterium (Shelburne et al. 2008; Philips et al. 2003).

1.2.2. Therapy for *S. pneumoniae* infections

To treat pneumococcal infections, antibiotics are the method of choice. However, AMR-pneumococcal strains have already emerged against major antibiotics, including penicillin, the macrolides, tetracyclines and fluoroquinolones (Adam 2002; Gill et al. 1999; Riedel et al. 2007). The patient and site of infection can influence the course of antibiotic treatment – for example, there are different approaches for an elderly patient with meningitis, versus an infant with community-acquired pneumonia. Treatment methods can also be influenced by patient allergy history, as some people are allergic to penicillin. The choice of antibiotic can additionally be influenced by geographical trends of resistance; for example, penicillin resistance has previously been shown to vary considerably between different countries, with the percentage of resistant clinical isolates in 1989 shown to be below 3% for England, but up to 5% in France, 44% in Spain and 57% in Hungary (Appelbaum 1992). However, where susceptible, the main method of treatment is with β-lactam antimicrobials such as penicillin and amoxicillin. It is also suggested that the chosen drugs should be ones that lower the propensity for driving resistance, particularly in regions where resistance is already high (Riedel et al. 2007). In the case of bacterial pneumonia, oral amoxicillin is the first line antibiotic used to treat previously healthy infants, children and adolescents, whilst penicillin or intravenous ampicillin are chosen to treat more severe cases, and ceftriaxone or cefotaxime used for meningitis. Some infections by strains with raised minimum inhibitory concentrations (MIC) to penicillin may still be treated with a cephalosporin, but meningitis may require use of other agents, such as vancomycin, which doesn't get into the cerebrospinal fluid very well, or in combination with linezolid. With penicillin allergy, macrolides or doxycycycline may be used for milder infections (Bradley et al. 2011; Mandell et al. 2007).

Strategies to prevent pneumococcal disease at the community level have largely focused on vaccination strategies. Currently, there are two main vaccines used against the pneumococcus: the pneumococcal conjugate vaccine (PCV) and the pneumococcal polysaccharide vaccine (PPV). PCV13 contains the capsular polysaccharide of thirteen of the most prominent, clinically observed strains in severe paediatric infections and most adult cases. The polysaccharides are conjugated to the non-toxic but highly immunogenic diphtheria toxin protein, CRM_{197}, which acts to provoke a strong T-cell-

dependent immune response to the polysaccharides. This in turn induces a mature B-cell response with class switching, immunological memory and the production of life-long immunity via antibody production. The vaccine is suitable for children under the age of five, and healthy adults between the ages of 18-65 (U.S. Department of Health and Human Services 2013). However, the vaccine only covers a small proportion of existing serotypes, and the composition of the vaccine does not match prevailing serotypes as closely in other regions of the world, such as Africa and Asia (Johnson et al. 2010). The PCV13, however, not only reduces invasive pneumococcal disease (eg. bacteraemia), but also cases of pneumonia. Alternatively, the PPV23 vaccine contains the purified polysaccharides of 23 pneumococcal serotypes, but provides a lower immunogenicity: the vaccine provokes T-cell independent responses but fails to generate immunological memory, whilst memory B-cell production is weak and a vaccine booster is required every 5 years, especially if the patient is at high risk of *S. pneumoniae* infection (Schwarz & Pauksens 2013; NHS Choices 2016; Centers for Disease Control and Prevention 2016). PPV23 is the recommended vaccine for older adults and some patients with co-morbidities. With continued cases of pneumococcal disease due to replacement of vaccine colonising strains with other non-vaccine serotypes (Dagan 2009), and with the number of identifiable *S. pneumoniae* serotypes considered to be greater than 90, vaccination strategies alone are not able to produce complete protection or full, cost-effective control of pneumococcal disease. Additionally, some groups are shown to have reduced responses to vaccines, such as the elderly or those with significant immune-compromised conditions, (Ljungman 2012; Park & Nahm 2011). In view of the limited number of capsular types that can be covered with capsule-based vaccines and the potential replacement of vaccine serotypes with non-vaccine serotypes, significant research efforts have focused on trying to develop PPVs to target specific proteins, for examples pneumolysin or PsPA, which would not be restricted to specific serotypes (Ginsburg et al. 2012).

1.3. The immune system

The human body has evolved to protect the host against bacterial infections and their associated complications, not just through physical barriers such as the skin and mucosal surfaces, but also through the development of a functional immune system. Immunity can be divided into two main systems: innate or adaptive. The innate immune system acts rapidly using non-specific mediators, such as the complement system and phagocytic cells, including macrophages and neutrophils, which phagocytose and kill invading pathogens. Key features of the innate immune system are the development of rapid and broad responses to a range of microbial structures. On the other hand, the adaptive immune system acts over a much longer timescale, using specific mediators such as antibodies, B-cells and T-cells, which provide immune memory for subsequent infections (Murphy et al. 2012). The adaptive immune response is much more specific, and acts against very precise antigenic determinants. Although the immune system has been classically divided in this way, the identification of lymphoid subsets that contribute to innate immune responses, and the identification of innate immune memory through epigenetic modifications have started to blur this classical division (Netea et al. 2015; Quintin et al. 2014).

Immune cells are produced through a procedure known as haematopoiesis, a term that describes the growth and proliferation of different blood cell lineages from haematopoietic precursor cells (Murphy et al. 2012). This process begins in the yolk sac soon after development and shifts transiently to the liver during the emergence of blood circulation. Prior to birth, the niche of blood cell progenitors moves again to the bone marrow and thymus, where they remain throughout adulthood (Jagannathan-Bogdan & Zon 2013). The common progenitor that gives rise to all immune cells is the pluripotent haematopoietic stem cell, which are located within bone marrow. From this point, the stem cells divide into more specialised groups, which mirror the division of immunity. B-cells and T-cells, found in adaptive immunity, are produced through the emergence of the common lymphoid progenitor, whilst the common myeloid progenitors give rise to further progenitors for megakaryocytes, erythrocytes and granulocytes, which become platelets, red blood cells and neutrophils, macrophages and monocytes respectively (Murphy et al. 2012).

Interactions by commensal bacteria, formation of the microbiome, and development of the immune system are of key interest, as a fine balance must be achieved to limit bacterial replication and prevent bacterial spread or tissue invasion that could then lead to clinical disease, whilst also preventing inappropriate inflammation and the tissue injury associated with inappropriate immune activation (Ivanov & Littman 2011). Receptors and regulatory pathways of immune cells are essential for this purpose, as defects in key, rapid cellular mediators have been shown to decrease bacterial clearance, resulting in bacterial outgrowth and increased susceptibility to invasive disease. An example of this can be demonstrated by modulation of receptor family signalling, such as those involving the Toll-like receptors (TLR), which are stimulated by microbial and danger-associated stimuli (Albiger et al. 2005; Ku et al. 2007). Innate immune functions are therefore carefully controlled by expression of recognition receptors and their downstream signalling pathways, to produce an appropriate cytokine and inflammatory response, both to commensal flora and following dynamic changes in the microbiome, including acquisition of potentially pathogenic strains. The focus of work in this thesis considers the importance of one innate immune cell, the macrophage, and the role of changes in metabolism on its innate function.

1.3.1. Macrophages

The role and function of macrophages can be traced back to the discovery of phagocytes, by Élie Metchnikoff, who was jointly awarded the Nobel Prize in Medicine in 1908. Metchnikoff described the active internalisation, vacuole acidification and destruction of foreign bodies in leukocytes (Gordon 2008; Metchnikoff & Binnie 1906). During this time, it was thought that the sole function of the macrophage was to clear infection and debris, hence the direct Greek translation of 'big eater'; however, it is now more recognised that macrophages have additional roles in wound healing and tissue homeostasis (Wynn et al. 2013). Macrophages are a highly conserved component of the innate immune system, dating back 500 million years and found in organisms such as starfish that lack a vascular system (Gordon 2008; Metchnikoff & Binnie 1906).

Macrophages arise from two sources – the maturation of monocytes that have migrated from the bloodstream to specific tissue environments via chemotactic gradients, and also embryonically derived mature macrophages that persist independently from the

vasculature and self-sustain within tissues (Epelman et al. 2014; Hashimoto et al. 2013). Different tissue macrophage populations have different origins; the tissue macrophages that make up the brain (microglia) are derived from a yolk-sac progenitor, while those forming alveolar macrophage are derived from haematopoietic liver cell progenitors, and those forming gut macrophages are predominantly derived from blood-derived monocytes (Epelman et al. 2014). The variation in origin and environmental niche underpins the heterogeneity in tissue macrophage populations, with adaptations to patrol different tissue niches, including the liver (Kupffer cells), intestine, blood (monocytes) and bone (osteoclasts). These mononuclear phagocytic cells ingest foreign particles, engulfing them in an increasingly acidified vacuole, where they are degraded and the antigens redirected to the outer cell membrane for antigen presentation at the surface. Degradation products can also be used to activate pattern recognition receptors (PRRs), macrophage signalling and cytokine release, which causes downstream recruitment of neutrophils, dendritic cells and T-cells, and induce inflammation (Gordon & Taylor 2005; Murphy et al. 2012). Alveolar macrophages (AMs) are particularly important for bacterial clearance and immune responses in the lungs and airways, preventing migration, excessive growth and translocation of microorganisms from the upper to lower respiratory tract. Upon aspiration of bacteria, resident AMs are among the first immune cells to respond at the site. It is critical that macrophages not only act rapidly, but also appropriately, as pneumonia can result from inappropriately activated host immune responses, either resulting in a reduced or excessive response (Murphy et al. 2012). Macrophages phagocytose, kill and degrade pathogens, but also facilitate secondary antigen presentation and regulate inflammatory responses via the release of cytokines and immune mediators, and through the induction of apoptosis and efferocytosis of apoptotic cells (Savill et al. 1993; Lee et al. 2009).

1.3.2. Pathogen recognition

During initial interactions with pathogens, macrophages use a range of receptors to rapidly sense and respond to the presence of infection (Opitz et al. 2010). They are suitably adapted to this through a variety of cell surface, intracellular and secretory receptors (Taylor et al. 2005). Many receptors involved in this process of pathogen

detection are known as pattern recognition receptors (PRRs). These are germ-line encoded, fixed within the genome, and are central to rapid recognition of both non-self and endogenous 'danger signals' released by injured cells. These receptors detect conserved and/or essential pathogen structures, otherwise known as pathogen-associated molecular patterns (PAMPs). Some example PAMPS include lipopolysaccharide (LPS), and CpG motifs in DNA and dsRNA (Koppe et al. 2012). PRRs are also capable of detecting danger-associated molecular patterns (DAMPs), which are host-derived products released upon cell injury or death – for example extracellular ATP or proteins usually only found in the cell cytoplasm (Newton & Dixit 2012).

One of the largest families of membrane PRRs are the TLRs. It has been cited that TLR2, TLR4 and TLR9 are important for immune detection of *S. pneumoniae*, via detection of lipoproteins, pneumolysin and pneumococcal DNA respectively (Albiger et al. 2007; Malley et al. 2003; Tomlinson et al. 2014). These receptors signal via MyD88-dependent pathways to induce mature cytokine secretion (Takeda & Akira 2001; Marr et al. 2003). PRRs are also present in the intracellular environment, and include NOD-like Receptors (NLRs) and RIG-1-like Receptors (RLRs). NOD2 is a sensor of peptidoglycan muramyl peptide fragments from both Gram-positive and Gram-negative bacteria. It has been shown to be activated during *S. pneumoniae* infection and is also important for TLR2-mediated clearance of bacteria (Davis et al. 2011). The pneumococcal toxin, pneumolysin, can activate the NLRP3 inflammasome, a multimolecular complex that promotes cleavage and activation of Caspase-1, to allow proteolytic cleavage and mature release of IL-1β; however the mechanism by which the toxin reaches the cytoplasmic environment is still unconfirmed (McNeela et al. 2010). That said, the pneumolysin toxin aids NOD1 activation in synergistic infections of epithelial cells, in association with bacteria such as *Haemophilus influenzae,* suggesting that pore generation could assist the transport of peptidoglycan fragments into the intracellular environment (Ratner et al. 2007). Finally, it is also suggested that *S. pneumoniae* DNA could be detected by intracellular DNA sensors, via stimulator of interferon genes (STING)-mediated pathways and receptors such as melanoma differentiation-associated protein 5 (MDA5), but this is yet to be validated (Koppe et al. 2012; Ishikawa & Barber 2008).

Following interaction with bacterial stimuli, macrophages initiate signal transduction pathways to stimulate the production of cytokines, cause an acute-phase inflammatory response and recruit other cells, such as neutrophils, T-cells, innate lymphoid cells and dendritic cells, to the site. By doing this, it increases the number of immune cells to the area, to help clear the infection more efficiently. The cytokines released are typically pro-inflammatory and include IL-1β, IL-6, IL-8, IL-12 IFNα/β, TNF-α and IL-18, most of which are transcribed via NF-κB and/or IRF3 pathways (Opitz et al. 2010).

1.3.3. Phagocytosis

Following detection and binding of bacteria (or of another foreign particle) to the surface of the macrophage, receptors that recognise and bind the bacterium start to cluster at the site, binding to their cognate ligands on the bacterial surface. This prompts actin polymerisation and pseudopodial membrane extension, whereby the membrane gradually envelops the bacterium, fusing at the distal region – thus resulting in the formation of a bacterium-containing phagosome (Murphy et al. 2012). Crosstalk between GTPases, such as Dynamin-2, and actin are important for macrophage early phagosome formation, including the initial pseudopodial formation and later scission of the budding cavity from the cell membrane (Marie-Anaïs et al. 2016). Furthermore, Phosphatidlinositol 3-Kinase (PI3K) is required for the formation of pseudopodia, suggesting a role for PI3K in outer membrane insertion, to prepare for phagocytosis (Cox 1999). Following phagosome formation, progressive acidification then occurs via fission and fusion with lysosomal compartments, like that seen for the endocytic pathway. Phagosomal maturation can be traced via compartment acidification and the loss or accumulation of markers typically found in early endosomes, late endosomes and lysosomes. For example, early endosome fusion accumulates the GTPase Rab5, early endosome antigen-1 (EEA1) and vacuolar ATPases; late endosome and lysosome fusion then see acquisition of Rab7, Rab9, lysosome-associated membrane proteins (LAMPs) and cathepsin D (Trimble & Coppolino 2005). The result is an acidified compartment of roughly pH 4.5-5.0 that contains antimicrobial factors, as discussed later. A brief overview of this phagocytic process is demonstrated in Figure 1.1.

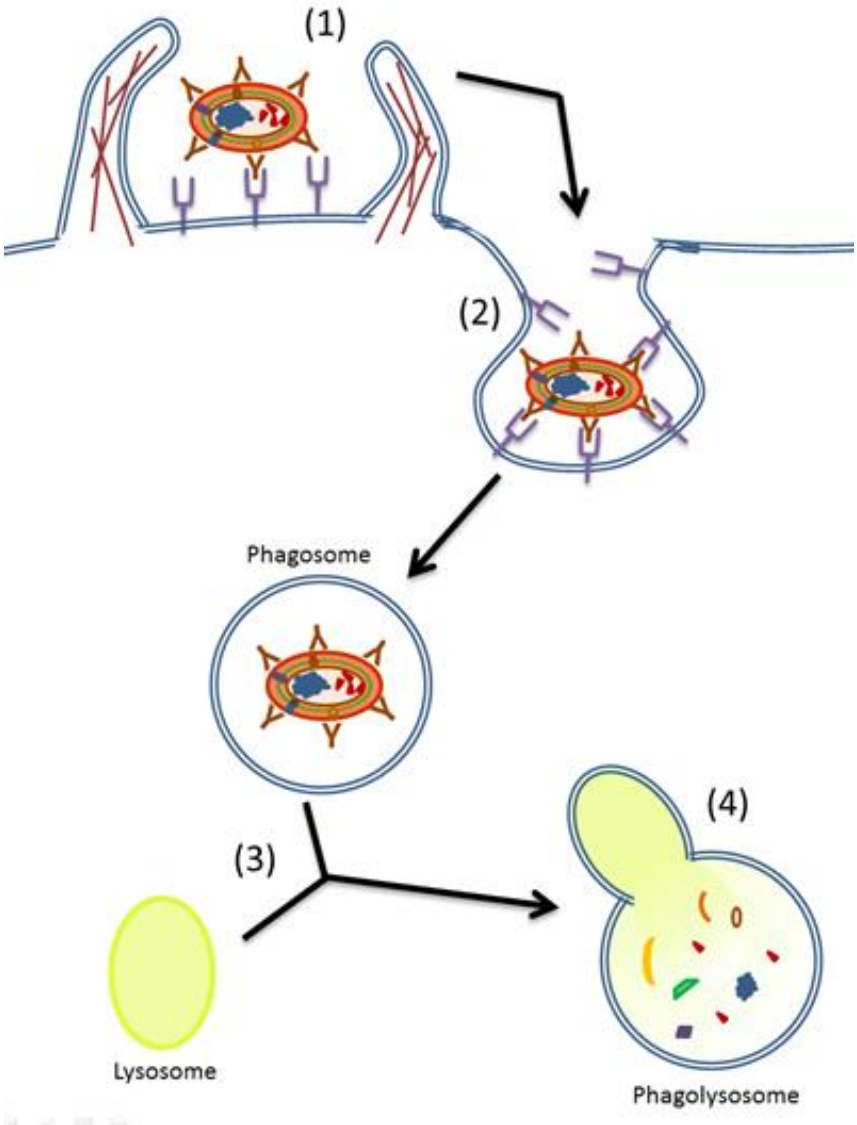

Figure 1.1: An overview of phagocytosis

In this diagram, phagocytosis is demonstrated in four simplified stages: (1) An opsonised bacterium is recognised via binding of antibodies to macrophage FcRs, with other ligands also binding their corresponding receptors, to induce receptor clustering, membrane extension and actin polymerisation; (2) the macrophage membrane engulfs the pathogen, before it encapsulates it in an intracellular phagosome; (3) the phagosome matures and eventually fuses with lysosomes, forming the phagolysosome; (4) the bacterium is degraded in the phagolysosome, by antimicrobial factors. After this, the microbial fragments are either processed and presented via Major Histocompatibility Complexes, or egested to the extracellular environment (not shown here)

In the case of *S. pneumoniae*, the polysaccharide capsule and other virulence factors impair bacterial binding and phagocytosis. Therefore other components of the immune system come into play here – specifically antibodies and the complement system. During pneumococcal challenge, antibodies bind to conserved and specific antigen epitopes on the bacterium, via the variable Fab immunoglobulin (Ig) region. This helps to promote opsonophagocytosis through binding of the antibody Fc region to Fc-receptors on phagocyte surfaces (Gordon et al. 2000). Antibodies are elicited to a range of pneumococcal structures during infection (Wilson et al. 2017), however, only capsular antibodies are currently implemented in licensed vaccines strategies (Bruyn 1992; Aliberti et al. 2014). Components of complement also opsonise and agglutinate bacteria, to promote efficient phagocytosis and bacterial clearance. The complement cascade can be activated via three main pathways: classical, alternative and lectin. The classical pathway, activated in part via IgM, is the most important pathway for innate recognition of *S. pneumoniae* (Brown et al. 2002). In its absence, mice are particularly susceptible to septicaemia following bacterial challenge. This pathway determines the proportion of bacteria binding C3 and is facilitated by binding of component C1q to conserved Fc regions of antigen-bound IgM or IgG (Brown et al. 2002). The classical pathway is also activated by C-reactive protein (CRP), in the absence of antibodies, as CRP can bind pneumococcal surfaces and activate complement independently (Kaplan & Volanakis 1974; Mold et al. 2002). C1q activation can also be achieved through directly binding bacterial surfaces (Albertí et al. 1993; Brown et al. 2002), and by SIGN-R1, a C-type lectin, after interacting with pneumococcal polysaccharides (Kang et al. 2006). The lectin pathway shows similarity to the classical pathway, but with the use of mannose-binding lectins in the place of C1q activation (Murphy et al. 2012). During pneumococcal challenge, activation of the lectin pathway is driven by Ficolin A and Collectin-11 (Ali et al. 2012). Lastly, the alternative pathway has dual function, with roles in both bacterial recognition and in amplification of the classical and lectin pathways. The alternative pathway is a key determinant of the amount of C3 binding on pneumococci (Brown et al. 2002). It is constitutively active at low levels, via spontaneous hydrolysis of C3 (Noris & Remuzzi 2013), which allows C3b deposition on bacterial surfaces. Activation of the alternative pathway is important in opsonising pneumococcal surfaces with C3b, for effective uptake and bacterial clearance (Xu et al. 2001). *S. pneumoniae* activates all three complement activation pathways, which converge at C3b formation, to induce

opsonophagocytosis and inflammatory response activation through release of the chemotactic factor C5a (Andre et al. 2017). The polysaccharide capsule inhibits binding of IgG and CRP, limiting C3b/iC3b (a proteolytically inactive cleavage product of C3b) binding via the classical pathway, while also inhibiting alternative pathway amplification of C3b binding (Hyams et al. 2010). Pneumolysin, primarily through inhibition of the classical pathway but also through inhibition of the alternative pathway, and the surface protein PsPA, through both classical and alternative pathways, also inhibit complement deposition on the bacterial surface (Yuste et al. 2005).

1.3.4. Antimicrobial killing mechanisms

1.3.4.1. Phagolysosome acidification

During maturation of the phagolysome, vacuolar ATPases are accumulated, which aid the acidification of this compartment to roughly pH 4.5-5.0, through pumping of H^+ into the phagosome. H^+ are also acquired through fusion of phagosomes with lysosomes, which contain a high concentration of these ions. Not only does this create an antagonistic environment for bacteria, reducing microbial growth and causing a loss of viability, but it also prompts activation of enzymes that aid bacterial degradation and work optimally at low pH, such as lysozyme (Ip et al. 2010). A number of pathogens, including species of *Mycobacterium, Salmonella* and *Leishmania*, have evolved mechanisms to hinder this phagosomal maturation and intracellular killing (Kinchen & Ravichandran 2008).

1.3.4.2.Oxidative antimicrobial strategies

Macrophage signalling receptors can activate a 'respiratory burst', which induces increased oxygen intake, along with the assembly and activation of nicotinamide adenine dinucleotide phosphate (NADPH)-dependent oxidase (NOX2) at the phagosomal membrane, to produce superoxide (O_2^-) (Slauch 2011). NOX2 is a heme-binding protein consisting of multiple subunits, one of which forms a transmembrane channel, through which electrons are passed from NADPH to oxygen (Yang et al. 2011). O_2^- can also be converted to hydrogen peroxide, either spontaneously or via superoxide

dismutase. These reactive oxygen species (ROS) can act as bactericidal factors in the lysosome environment (Slauch 2011). Macrophage ROS production is much lower than that seen in neutrophils; therefore an alternative role for this burst could be to produce hydrogen peroxide as a secondary signalling messenger, for pathways such as MAPK, JNK and ERK (Iles & Forman 2002).

Phagocytes are also capable of reactive nitrogen species (RNS) production, via the inducible nitric oxide synthase (iNOS, also referred to as NOS2), which is expressed during inflammatory activation of macrophages (Rath et al. 2014). iNOS is a homodimer, with each subunit comprised of a reductase domain, which transfers electrons from NADPH to flavin carriers. These electrons are then passed onto the haem of the oxygenase domain, which binds cofactor BH_4 and the substrate L-arginine. The enzyme uses oxygen, L-arginine and electrons from NAPDH, to produce L-citrulline and Nitric Oxide (NO) (Förstermann & Sessa 2012). NO can also be generated via endothelial NOS (eNOS) in lung macrophages during pneumococcal infection (Yang et al. 2014). NO can combine with other ROS species to form highly oxidising compounds; for example peroxynitrite ($ONOO^-$), which has been identified within the phagosome after NO reaction with O_2^- (Prolo et al. 2014). Both ROS and RNS are powerful oxidising agents, which attack bacterial structures and components such as DNA, lipids and proteins (Paiva & Bozza 2014). As pneumococci have been shown to resist peroxide killing, the efficacy of ROS-mediated killing has been questioned (Pericone & Park 2003), emphasising the potential importance of alternative strategies, such as those involving RNS.

1.3.4.3. Non-oxidative antimicrobial strategies

Aside from ROS and RNS production, the macrophage utilises peptides and proteins as antimicrobial factors. One of the most widely characterised enzymatic groups are the Cathepsins. These papain family proteases are produced as inactive zymogens, which are either auto-activated within the lysosome, as a result of the low pH, or through cleavage by other proteases (Weiss & Schaible 2015). There are more than 10 members in humans, all with varied functions in both innate and adaptive immunity, including pathogen killing, TLR signalling, antigen presentation and apoptosis (Conus & Simon 2010). Cathepsins B, D, G and S have specifically been demonstrated to interact with

and aid microbial killing in a range of innate immune cells, including neutrophils, macrophages and dendritic cells (Bewley et al. 2011; Steinwede et al. 2012; Hole et al. 2012). Further enzymes found in the lysosome include glycosylases, phospholipases and nucleases, and also the peptidoglycan degrading enzyme lysozyme (Weiss & Schaible 2015). These mechanisms collectively kill and degrade the bacterium, allowing remnants to be secreted and/or presented on the cell surface via interaction with major histocompatibility proteins (MHCs). These proteins bind the bacterial antigens in the lysosome and are re-directed to the macrophage surface, where they activate naïve T-cell and B-cell responses (Harding & Geuze 1992). Finally, the macrophage matrix metalloprotease protein MMP12 has also been shown to localise to murine phagolysosomes, and aids bacterial degradation through disruption of cell wall structures (Houghton et al. 2009).

In addition to destructive enzymes, macrophages also contain a number of antimicrobial peptides, many of which can disrupt bacterial membrane formation and integrity, and/or inhibit other processes such as DNA and protein synthesis (Paustian 2013). The main antimicrobial peptides in macrophages are the cathlecidins and defensins. Only one cathlecidin gene is present in humans and mice, both of which are produced as pro-forms that require cleavage, to give the active peptides LL-37 and CRAMP respectively (Gallo et al. 1997). Human cathlecidin LL-37 can induce elevated phagocytic clearance (Wan et al. 2014), aid intracellular killing of several *Mycobacterium* species (Sonawane et al. 2011) and is also thought to control LPS-induced responses to prevent endotoxic shock (Hancock & Diamond 2000). Similarly, defensins are also produced in a pro-peptide form, requiring cleavage. α- and β-defensins were initially isolated from tissue secretions and are documented as a component of neutrophil granules; however expression of β-defensins does also occur in macrophages, and is shown to increase during stimulation with LPS (Duits et al. 2002). β-defensins have antimicrobial properties including to *S. mutans, E. coli, P. gingivalis* and *C. albicans* (De Smet & Contreras 2005), and they are suggested to act as a chemoattractant for macrophages (Soruri et al. 2007). Human β-defensins 2 and 3 are induced in epithelial cells by pneumococci (Scharf et al. 2012), but less is known concerning their roles in macrophages. In addition to peptides, macrophages have also been noted to produce bioactive lipids, such as Leukotriene B_4. This is a derivative of arachidonic acid lipid metabolism, which can trigger a number of

host responses, including phagocytosis, NOX2 activation and the release of lysosomal enzymes and peptides (Flamand et al. 2007).

A further antimicrobial mechanism regards sequestering of key nutrients by the host, also referred to as nutritional immunity. An example of this is the import and export of metal ions. One of the most widely characterised channels belongs to the natural resistance associated membrane protein 1 (NRAMP1), which is thought to co-localise with LAMP1 in the late endosome (Cellier et al. 2007). NRAMP1 uses the proton gradient of the lysosome to pump out divalent iron and manganese cations, which are required for bacterial metabolism, hence limiting their intracellular viability (Flannagan et al. 2015). In addition to this, the toxicity caused by transition metals is utilised by macrophages, as they are shown to increase their uptake and lysosomal accumulation of both copper and zinc ions during inflammatory activation (Stafford et al. 2013; White et al. 2009). It is thought that these metal ions compete with ions in bacterial structures and proteins, starving the bacteria of key resources; for example, elevated zinc has been shown to outcompete and starve *S. pneumoniae* of manganese, which is required for PsaA function (McDevitt et al. 2011).

1.3.4.4. Apoptosis-associated killing

After phagocytosis has occurred and the macrophage has attempted to eradicate the ingested *S. pneumoniae*, either all bacteria will have been cleared, or viable intracellular bacteria may remain in phagolysosomes. For this reason, Dockrell et al. have suggested that a high intracellular pneumococcal burden can induce macrophage apoptosis as a final resort to prevent further bacterial replication, dissemination and disease progression (Ali et al. 2003; Dockrell et al. 2003a). They propose this switch to be regulated by the anti-apoptotic mitochondrial protein Mcl-1, which is down-regulated at late infection time points (after 16 hours sustained phagocytosis), causing loss of inner mitochondrial transmembrane potential, ($\Delta\psi_m$), mitochondrial outer membrane permeabilisation, cytochrome c release and subsequent apoptosis (H. M. Marriott et al. 2005). Bewley et al. further propose a role for the lysosomal protease, cathepsin D, in regulating this apoptotic response during pneumococcal infection, therefore forming a link between phagosome maturation and apoptotic killing (Bewley et al. 2011). Marriott et al have shown how this could be a mechanism preventing excessive inflammation

during pneumococcal infection *in vivo* (Dockrell et al. 2001; Marriott et al. 2006). Apoptosis-associated killing has also been shown during *Mycobacterium tuberculosis* infection, whereby apoptosis is activated either through TNFα-mediated pathways during low bacterial load, or through caspase-independent mechanisms following high intracellular burden (Lee et al. 2006). In this infection model, it is suggested that Mcl-1 and cathepsins again have roles in regulating apoptosis to limit bacterial burden (Sly et al. 2003). A similar mechanism of programmed cell death for host defence is also thought to occur during *Yersinia* infection of macrophages, whereby the bacterial virulence factor, YopJ, induces apoptosis through activation of receptor-interacting protein kinase 1 (RIPK1) (Peterson et al. 2017).

1.3.5. Macrophage polarisation

Macrophages can adopt different phenotypic features, depending on the cytokine or external stimulus they are faced with. When exposed to IFNy or bacterial products such as LPS, macrophages develop a pro-inflammatory, activated phenotype - also referred to as an M1 phenotype or classically-activated macrophages (CAMs) - whereas in the presence of IL-4 or IL-13 they develop an anti-inflammatory phenotype - also referred to as an M2 phenotype or alternatively-activated macrophages (AAMs) (Mosser & Edwards 2008). These names were originally adopted as the M1 and M2 subsets are similar to the activation of Th1 and Th2 cells, with similar patterns of pro-inflammatory or anti-inflammatory cytokines, and similar functional roles (Mills 2012). CAMs and AAMs were formerly thought to have predominant roles in inflammation and wound healing respectively, however their roles are now understood to be more diverse and include functions in immune regulation, cancer and chronic diseases (Murray et al. 2014; Mosser & Edwards 2008). The two polar activation states are often distinguished through differences in transcription factors, such as increased STAT6 in CAMs and increased STAT1 in AAMs, cytokine release including TNFα in CAMs and IL-10 for AAMs, and also via differences in metabolic pathways, such as that seen specifically for arginine, as discussed later in this chapter (Murray et al. 2014). Despite these findings, macrophages are extremely plastic and the CAM/AAM phenotypes mostly resemble two extremes of a variable phenotypic spectrum, with subtypes of these two groups also blurring the categorisation of activated cells (Mosser & Edwards 2008). In August 2013,

researchers in this field called for urgent clarity and new nomenclature, regarding specific stimulations and more appropriate terminology surrounding CAM/AAM-like cells (Murray et al. 2014); that said, further verification and shared best practice is still on-going. In the respiratory environment, AMs are thought to be relatively quiescent when associated with the respiratory epithelium (Lambrecht 2006), however their distinct activation status can depend on the health and lifestyle of the individual, or the model system in question. For example, increased inflammation and modulation of AM activation has been shown in smoking individuals (Woodruff et al. 2005) and patients with lung diseases such as COPD (Barnes et al. 2003), whilst reduction in specific macrophage activation responses are seen following viral infection (Didierlaurent et al. 2008). This therefore makes it difficult to predict the exact activation or polarisation status of AMs *in vivo* in any given patient population, since there are diverse stimuli that can modulate macrophage activation in health and disease, and many variations in activation state with transcriptional profiling (Mosser & Edwards 2008).

In this thesis, the interest lies predominantly with macrophages stimulated with LPS, as this type of activation is important for priming microbicidal responses and inducing a common host response, which closely resembles CAM activation (Benoit et al. 2008). It has been used as a reference for CAM and provides a suitable comparison for these studies, in view of the extensive literature on its effects on macrophages. It is likely, however, that specific changes could be pathogen-specific and therefore may not strictly replicate an LPS-induced CAM phenotype. This was shown to be the case by Nau et al. who used a DNA microarray to assess the activation status of cells, after stimulation with LPS, versus challenge with a range of individual bacterial determinants or whole bacteria (Nau et al. 2002). Here, a common host response was observed, including changes in expression for receptors and signalling pathways, but with unique differences seen between different bacterial stimulations, particularly regarding released cytokine profiles (Nau et al. 2002). Additionally, some features of AAM polarisation, as opposed to CAM polarisation, have been shown to occur during macrophage infection with certain bacteria, including *C. burnetii* (Marie Benoit et al. 2008) and *S. pyogenes* (Goldmann et al. 2007). This therefore challenges the idea of a common macrophage response to bacteria and suggests that a greater understanding of specific host-pathogen interactions is required, with comparisons made to LPS and other well-characterised CAM stimuli.

1.4. Metabolism

All life requires energy, and metabolism can be considered to encompass all chemical reactions that occur within a living system - be that a single prokaryotic cell or a complex eukaryotic organism. It encompasses a wide range of topics, from simple carbon pathways, such as those in bacteria, through to multicellular metabolic demands, for example as required in tumour growth and proliferation. Metabolic reactions can typically be classed into two groups: anabolic, describing the formation of cellular components that requires energy, such as DNA and proteins, and catabolic, describing the degradation of constituents, such as organic matter or carbohydrates which is often accompanied by the release of energy (Fromm & Hargrove 2012). This energy production comes in the form of the biologically universal energy carrier, adenosine triphosphate (ATP). Two of the major pathways that contribute to animal ATP production are glycolysis, located in the cellular cytoplasm, and the Krebs cycle (also known as the tricarboxylic acid cycle, or TCA), located in the mitochondria. See Figure 1.2 for an overview of these two pathways, or Figure 1.3 for detailed pathways of glycolysis and the pentose phosphate pathway (PPP).

The field of metabolism has become of increasing interest since Nobel Laureate Otto Warburg formed his hypothesis on the metabolism of cancer cells. In the 1920s, Warburg et al. noted an increased fermentation and conversion of glucose to lactate in tumour cells, as compared to healthy controls (Warburg et al. 1927). He postulated that tumour cells shift their energy production primarily towards fermentation - the splitting of glucose to lactic acid, also referred to as anaerobic glycolysis. It was unclear why anaerobic glycolysis would occur during plentiful oxygen supply, as complete oxidation of glucose through respiration yields far greater amounts of ATP, and would better provide for the large energy demand of proliferating or active cells. However, it is now thought that upregulation of glycolysis is much quicker than boosting mitochondrial respiration, as this simply requires induction of enzymatic pathways, as opposed to mitochondrial biogenesis – a much longer and more energy-intensive process. So, whilst boosting glycolysis may seem inefficient, ATP production can occur much faster. Furthermore, glycolysis also presents a benefit as it produces many biosynthetic precursors, supporting pathways such as amino acid and fatty acid synthesis, which are required for proliferating cells – although the latter aspect is more important for

proliferating cells, like cancer cells or replicating T-cells than macrophages, which usually do not proliferate (Heiden et al. 2009; O'Neill et al. 2016).

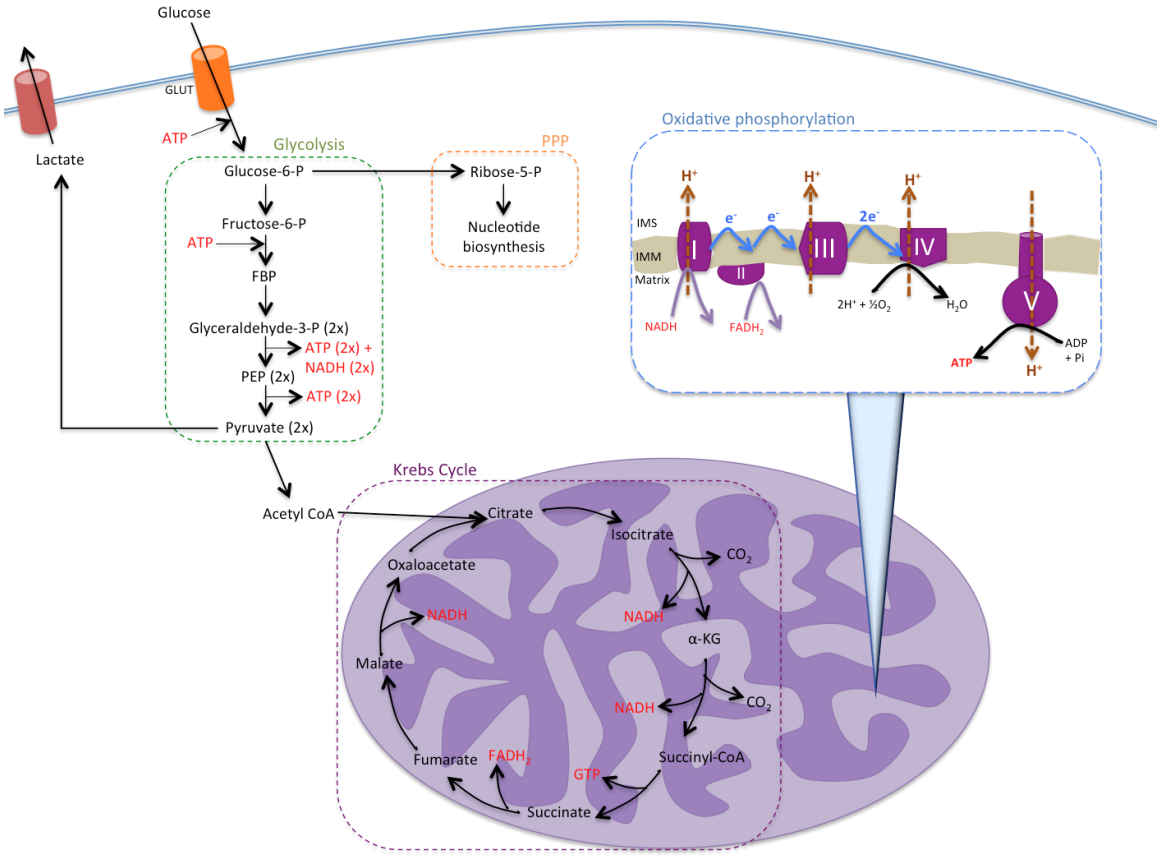

Figure 1.2: Glycolysis and Krebs Cycle metabolism

An overview of glucose metabolism, from initial entry to oxidative phosphorylation. Glucose first enters the cell via a GLUT transporter protein (typically GLUT1). To commit the molecule to glycolysis and prevent efflux of the compound, glucose is first phosphorylated. It then undergoes several enzymatic reactions, which both cost and produce ATP, as shown. The product, pyruvate, can either be transported out of the cell in the form of lactate, or enter the Krebs cycle. An alternative route for Glucose-6-Phopsphate is to enter the Pentose Phosphate Pathway (PPP), which produces intermediates for nucleotide biosynthesis. The Krebs cycle is critical in forming reducing equivalents, such as NADH, which can be used for oxidative phosphorylation. It does this through processing carbohydrates, to release carbon dioxide and water. These intermediates can also feed into or from other metabolic and biosynthetic pathways (not shown). Oxidative phosphorylation is comprised of the electron transport chain, linked to an ATP Synthase (ATPase). Reducing equivalents donate their electrons, which are shuttled across the membrane, via Complexes I-IV, and used to pump hydrogen ions across the membrane. The ATPase, also referred to as Complex V, then uses this proton gradient to produce ATP, as the hydrogen ions travel back across the membrane through the pore. (FBP = Fructose-1,6-bisphosphate; PEP = Phosphoenolpyruvate; α-KG = α-ketoglutarate; IMS = Inter membrane space; IMM = Inner mitochondrial membrane)

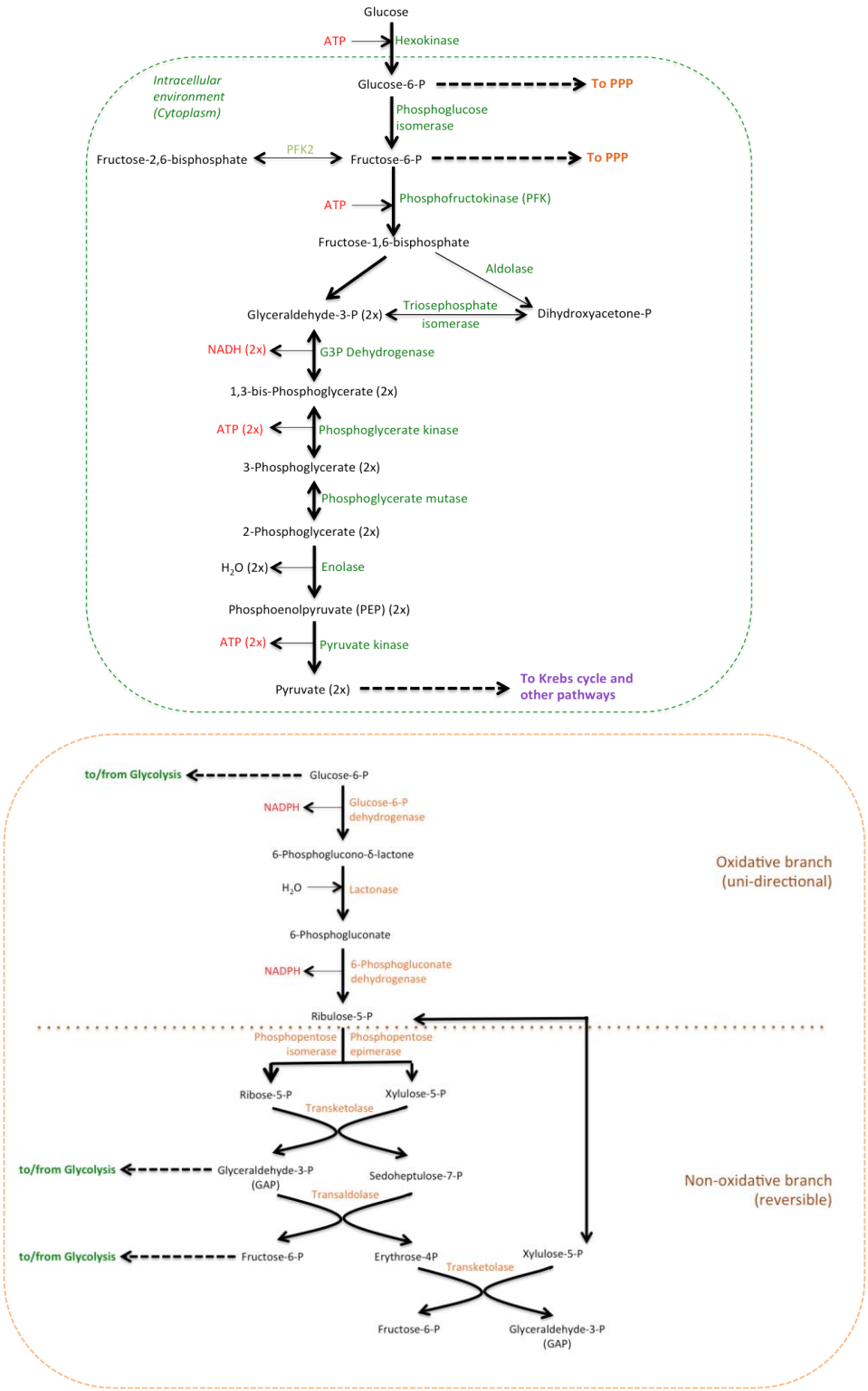

Figure 1.3: Glycolysis and Pentose Phosphate Pathway (PPP) metabolism

Details of the pathways for glycolysis (green) and the PPP (orange), highlighting enzymes, intermediates, and key interlinking regions in both. This demonstrates the interconnectivity of the pathways, and stages at which reducing equivalents are either used or produced, in the form of ATP, NADH or NAPDH.
(ATP = adenosine triphosphate, PFK = phosphofructokinase, PFK2 = phosphofructokinase-2, G3P = glyceraldeyde-3-phosphate, NADH = nicotinamide adenine dinucleotide, NADPH = nicotinamide adenine dinucleotide phosphate, PEP = phosphoenolpyruvate)

1.4.1. The field of immunometabolism

Since Warburg's hypothesis, the role of metabolism in cancer has become evident and his work has prompted research into the importance of metabolic changes in other fields. For example, in 1981 Chandra noted that obesity damages immune responses, and this has since been associated with an increased migration of macrophages to adipose tissue, where a constitutively pro-inflammatory environment is produced (Chandra 1981; Mosser & Edwards 2008). This diverts immunological and metabolic resources from other parts of the body. Roles for metabolism have also been seen in chronic diseases such as arthritis and asthma, and in increased susceptibilities to other diseases including neurodegeneration and cancer (Mathis & Shoelson 2011). With this amplified interest in metabolism, a new research field has developed over the last decade: the field of immunometabolism. Immune cells must respond appropriately to foreign signals or stimuli, but it is now clear that they must also adapt their responses depending on the nutrients or metabolites available in their local and intracellular environments, and also use these changes in metabolism to prime functional responses (Schertzer & Steinberg 2014).

1.4.1.1. Immunometabolic studies in innate immune cells

In the same way cancer cells demonstrate a metabolic switch from oxidative phosphorylation (OXPHOS) to glycolysis, macrophages, dendritic cells, T-cells and other immune subsets also follow this pattern during immune activation. Proinflammatory activation can alter their cellular metabolism in favour of glycolysis (Krawczyk et al. 2010; Newsholme et al. 1986; Tannahill & O'Neill 2011; Wahl et al. 2012). This could help prime cells for infection and classical activation by amplifying glycolytic ATP production and synthesis of biosynthetic precursors for amino acids and lipids, whilst promoting the production of cytokines (Donnelly & Finlay 2015; Vazquez et al. 2010). This switch may also be vital for cells in hypoxic conditions that need to respond to stimuli in limited oxygen availability, for example in abscesses or the lung environment during infection. Hypoxia has also been shown to extend monocyte and macrophage survival whilst enhancing glycolytic metabolism (Roiniotis et al. 2009).

1.4.1.2. LPS-induced metabolic changes of macrophages

CAMs and AAMs display different metabolic phenotypes, and metabolism could be a leading factor in controlling the phenotypic switch. For example, Freemerman et al. and Haschemi et al. have shown that increasing glycolysis in macrophages can induce a pro-inflammatory CAM state, whereas shutting off key glycolytic pathways will cause an anti-inflammatory AAM state and increases to OXPHOS (Freemerman et al. 2014; Haschemi et al. 2012). Additionally, one of the most discernible differences between these phenotypes is the metabolism of arginine: following classical activation, cells utilise arginine to produce NO via iNOS, whereas AAMs use arginase to metabolise arginine to ornithine, which can then be used in pathways required for cell proliferation (Rath et al. 2014). Much of the literature concerning M1-like metabolic changes has used LPS as a primary, bacteria-derived stimulus, therefore this switch has become relatively well characterised (O'Neill et al. 2016). In contrast, relatively little has been studied with live bacteria or other defined microbial components.

After LPS stimulation of murine macrophages, glucose uptake and transcription of the GLUT1 transporter are rapidly upregulated to increase glycolytic and PPP flux (Fukuzumi et al. 1996). It has also been suggested that Hexokinase-II associates with mitochondrial ATPases, to directly obtain ATP for the phosphorylation of glucose; however, literature supporting this idea is currently only shown in dendritic cells, and it's existence in macrophages is still to be proven (Everts et al. 2014; Shulga & Pastorino 2016). Other enzymes shown to be involved in this switch, following LPS stimulation of murine macrophages, includes: the sedoheptulose kinase CARKL, which is downregulated following LPS stimulation (Haschemi et al. 2012); the pyruvate kinase M2 isoform, which forms a dimer and associates with HIF1α to induce IL-1β and glycolytic enzyme transcription (Palsson-Mcdermott et al. 2015); the ubiquitous isoform of 6-phosphofructokinase, PFKFB3, which maintains high levels of Fructose-2,6-bisphosphate, an allosteric activator of glycolytic flux (Ruiz-García et al. 2011); and monocarboxylate transporter 4, which is considered as vital for exporting lactate from cells during increased glycolysis (Tan, Xie, Banerjee, et al. 2015). The enzyme glyceraldehyde-3-phosphate dehydrogenase (G3PDH) has also been implicated in post-transcriptional repression of TNFα mRNA, after LPS stimulation of THP-1 cells; this

interaction is not accessible during increases to glycolytic metabolism and G3PDH activity, allowing translation of TNFα to occur (Millet et al. 2016).

Despite an increase in glycolysis there is no concomitant increase in the Krebs cycle to utilise the pyruvate generated; instead, the cycle breaks at two points, resulting in the accumulation of citrate and succinate (O'Neill et al. 2016). Citrate can then be used to supplement fatty acid synthesis, or be converted to aconitate, which feeds into itaconic acid production. Itaconic acid has been shown to have bactericidal activity by inhibiting the glyoxylate shunt – a pathway required for bacterial growth in bacteria expressing isocitrate lyase, such as *M. tuberculosis* and *P. aeruginosa* (Michelucci et al. 2013). Itaconic acid has also shown to inhibit succinate dehydrogenase, further amplifying the accumulation of succinate and inhibition of mitochondrial respiration (Lampropoulou et al. 2016). Citrate levels are also maintained through the aspartate-arginosuccinate shunt (AAAS), which combines the urea cycle and Krebs cycle, to increase nitric oxide production, required for antimicrobial activity (Mills & O'Neill 2016). The accumulation of succinate after LPS stimulation is important in stabilising the transcription factor HIF1α for glycolytic enzyme up-regulation and in increasing IL-1β release (Tannahill et al. 2013). It is also suggested to play an important role as an intracellular signal and in succinylation of metabolic enzymes, including lactate dehydrogenase and glyceraldehyde-3-phosphate dehydrogenase (Du et al. 2012; Tannahill et al. 2013). As Krebs cycle flux is arrested, concentrations of succinate are augmented through alternative pathways, such as the gamma-aminobutyric acid (GABA) shunt and glutamine-dependent anaplerosis (Tannahill et al. 2013; Jha et al. 2015). The oxidation of succinate has further been shown as important for driving the CAM phenotype and specifically in repurposing of mitochondria for ROS production (Mills et al. 2016).

In parallel with increased glycolysis, LPS stimulation of macrophages induces an increase in the PPP – a source of NADPH and nucleotide precursors. In CAMs, NAPDH is required by NADPH oxidase to produce ROS, and to maintain cellular redox, which is considered to be important in regulating inflammatory cytokine release (Haschemi et al. 2012). Finally, mitochondrial respiration is also downregulated following LPS stimulation. It has been shown that mitochondria instead shift their function towards ROS production, and can localise to phagolysosomes, to help killing of internalised bacteria (West et al. 2011). Figure 1.4 summarises these metabolic changes, after LPS stimulation of macrophages.

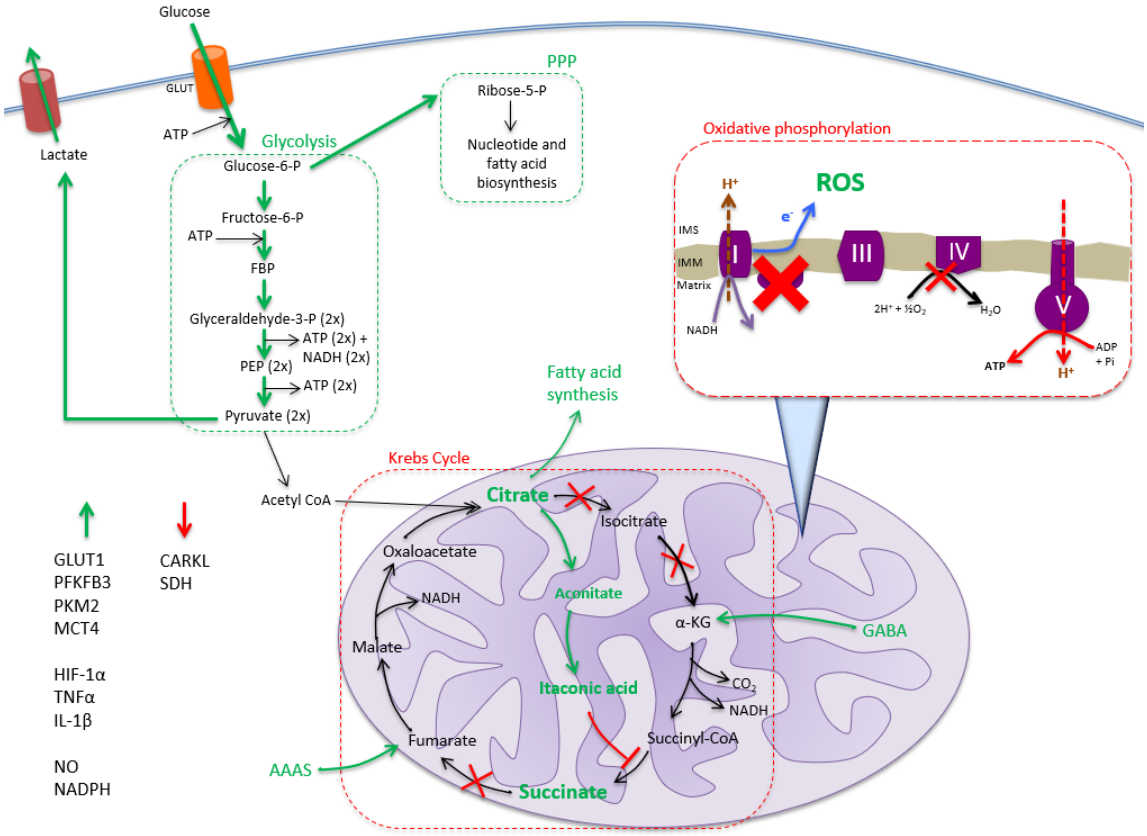

Figure 1.4: Metabolic changes after LPS stimulation of macrophages

Highlights of the metabolic changes to glycolysis, the PPP, Krebs cycle and oxidative phosphorylation during LPS stimulation of macrophages. Green indicates upregulation or an increase in metabolism/metabolites, whilst Red indicates a downregulation or decrease in metabolism/metabolites. The list in the bottom left corner indicates other changes caused by LPS stimulation (see results text for further details).
(GLUT = Glucose Transporter; PFKFB3 = 6-Phosphofructo-2-kinase/fructose-2,6-bisphosphatase isoform; PKM2 = Pyruvate Kinase M2 isoform; MCT4 = Monocarboxylate transporter 4; CARKL = Carbohydrate kinase-like (sedoheptulose kinase); SDH = Succinate Dehydrogenase; FBP = Fructose-1,6-bisphosphate; PEP = Phosphoenolpyruvate; AAAS = Aspartate-Arginosuccinate Shunt; α-KG = α-ketoglutarate; GABA = Gamma-aminobutyric

1.4.1.3. Relevance of LPS-induced metabolism in infection studies

At present, most of the literature on macrophage immunometabolism has focused on the use of LPS, a Gram-negative bacterial component, to induce a pro-inflammatory CAM status. Comparatively few studies have considered how this relates to the actual interplay between the host and whole, live pathogens of interest – particularly with regards to Gram-positive bacteria. Some studies considering the metabolic changes of host cells have instead focused on intracellular pathogens, such as *S. enterica* (Bowden et al. 2009) and *M. tuberculosis* (Shi et al. 2015). Eisenreich *et al.* have previously reviewed this field, in the context of limiting nutrient sources during intracellular infection of host cells: they highlight that pathogenic factors can interfere with host metabolism and antibacterial killing of phagolysosomes – this has been shown for factors SidK in *L. pneumophila* and PtpA in *M. tubercuolosis* both of which inhibit the host vacuolar ATPase to prevent phagosome acidification (Eisenreich et al. 2013). They also emphasise that cancer cell line models should be avoided, as these cells present an augmented metabolism compared to primary cell lines, with increased basal glycolysis and decreased basal OXPHOS (Eisenreich et al. 2013; Portnoy et al. 2016). That said, Lachmandas et al. recently compared human monocyte responses to LPS, versus stimulation with a TLR2 agonist or bacterial lysates from *E. coli, S. aureus* or *M. tuberculosis* (Lachmandas et al. 2016). Metabolic rates, enzyme gene expression and cytokine release were all compared following these stimulations, with the Gram positive bacterium *S. aureus* typically showing reduced responses compared to LPS. This provides an insight into the differences between singular TLR responses and more complex bacterial stimulation; that said, minimal details were provided by this publication regarding the preparation of bacterial components, therefore further evidence must be sought, and demonstrated in other immune cells types and for other bacterial species.

1.4.2. Methods of studying metabolism

Metabolism can be evaluated at a basic level using simple biochemical techniques: for example, the removal of metabolic substrates can be used to establish dependence, such as the removal of glucose or glutamine in a cell culture system, whilst gene knockouts for specific metabolic enzymes, transporters or transcription factors can be

used to establish more specific roles in distinct metabolic pathways. That said, many genetic knock-out models suffer from redundancy, so can provide smaller, different effects than expected (Kafri et al. 2009). Other direct methods of tracing metabolism include measuring uptake, utilisation or production of specific substrates, with many commercial suppliers now providing kits for such assay set-ups (Sigma-Aldrich Co. LLC. 2017; Promega UK 2017). A further method could be to assess changes in metabolic gene transcription or protein expression of metabolic enzymes, also referred to as the metabolic transcriptome and proteome respectively. For example, expression of the glucose transporter GLUT1 could be used to indicate changes in glycolytic status (Zhao et al. 2008).

More complex methods of studying metabolism are now starting to emerge: much like other –omics strategies, metabolomics aims to consider global changes in biological systems, with a view to characterising all small molecule metabolites, also known as the metabolome. This is an important measure of the metabolic phenotype and is considered to be indicative of the total metabolic status - with integration of gene and protein expression, metabolite concentrations and enzyme activities, all contributing to these metabolomic measures (Nielsen 2003). The metabolome is the closest representation of the cellular phenotype and is a practical candidate for understanding the phenotypic differences observed between diseases. Two of the most widely used metabolomic techniques are Mass Spectrometry (MS) and Nuclear Magnetic Resonance (NMR) Spectroscopy. Both methods can be used for untargeted metabolomic assessment. However MS currently dominates the field, due to its higher sensitivity and tandem separation processes, using techniques such as gas or liquid chromatography (Dunn & Ellis 2005). NMR Spectroscopy has alternative benefits, as it is very reproducible and can aid identification of unknown compounds through structure elucidation (Markley et al. 2017). It is also beneficial in tracing isotope-labelled substrates through pathways, such as a glycolysis – which is a traditional method of tracing metabolic pathway flux (Di Gialleonardo et al. 2016).

1.4.2.1. Seahorse Extracellular Flux Analysis

To understand the role of metabolism in cellular function, research has increasingly shifted towards omics strategies: from genomics and transcriptomics, through to

proteomics and now metabolomics. However, each of these strategies are typically representative of a snapshot in time, and limited quantitative information can be given, with comparisons usually made between independent experimental conditions or subsets (Winter & Krömer 2013; Cascante & Marin 2008). Consequently, techniques have been developed to enable estimations of metabolism in real time, to study real time production and consumption of metabolites, otherwise known as metabolic flux or fluxomics.

One of the simplest fluxomic technologies, introduced to bioscience research in 2006, is the Seahorse Extracellular Flux (XF) Analyser - now owned by Agilent Technologies. This technology measures changes in oxygen pressure and media acidity as readouts of metabolism. Oxygen pressure changes are referred to as the Oxygen Consumption Rate (OCR) and provide an indicator of mitochondrial respiration, whilst pH changes are referred to as Extracellular Acidification Rate (ECAR) and provide an indirect measure of glycolysis. The technique allows real-time and dynamic assessment of live cell cultures without the use of labelled substrates, by creating a small, transient micro-chamber between a patented-design cell culture microplate and a sensor cartridge. An example of this set-up is shown in Figure 1.4A. Cellular respiration and glycolysis cause measurable changes to the concentrations of oxygen and free protons in this micro-chamber respectively, which can be measured by built-in fluorescent probes located in the sensor cartridge, also referred to as the 'flux plate'. These probes are lowered to within 200μm of the bottom of the well and are supported by small grooves in the cell microplate, to prevent crushing or damaging the cells. The micro-chamber holds a volume of approximately 7μl.

To analyse ECAR or OCR of a living system, the user programs the Seahorse Analyser to cycle through mixing, waiting and measuring processes. As previously described, the measuring is performed by lowering of the probes to create a micro-chamber. Whilst cells metabolise, an acidified and anaerobic media is produced within this restricted portion of the microplate. This media must then be mixed and re-equilibrated to restore the original baseline detection levels of oxygen and hydrogen, prior to subsequent cycles and measurements being taken. To do this, the machine pushes the flux plate continuously up and down for several minutes, encouraging mixing of the media. A wait period then follows, allowing passive equilibration and settling of the media, ready for

the next cycle to start. Mixing and waiting stages should prevent a hypoxic or acidic local environment from being artificially induced during the assay. In addition to the sensor probes, the flux plate contains four infection ports, which provide an integrated drug delivery system. These can be used to pneumatically inject compounds of interest, to observe their effects on cellular metabolism in real-time. Agilent also supply a range of kits, to test specific metabolic pathways, including the Mitochondrial (Mito) Stress Test and Glycolysis (Glyco) Stress Test kits, which allow defined and related ways of metabolically profiling cell cultures that measure respiration and glycolysis respectively (Romero et al. 2017; Agilent Technologies 2017b). The assay profile for the Glycolysis Stress Test is shown in Figure 1.4B, highlighting the metabolic quantification that can be calculated from this type of XF Analysis.

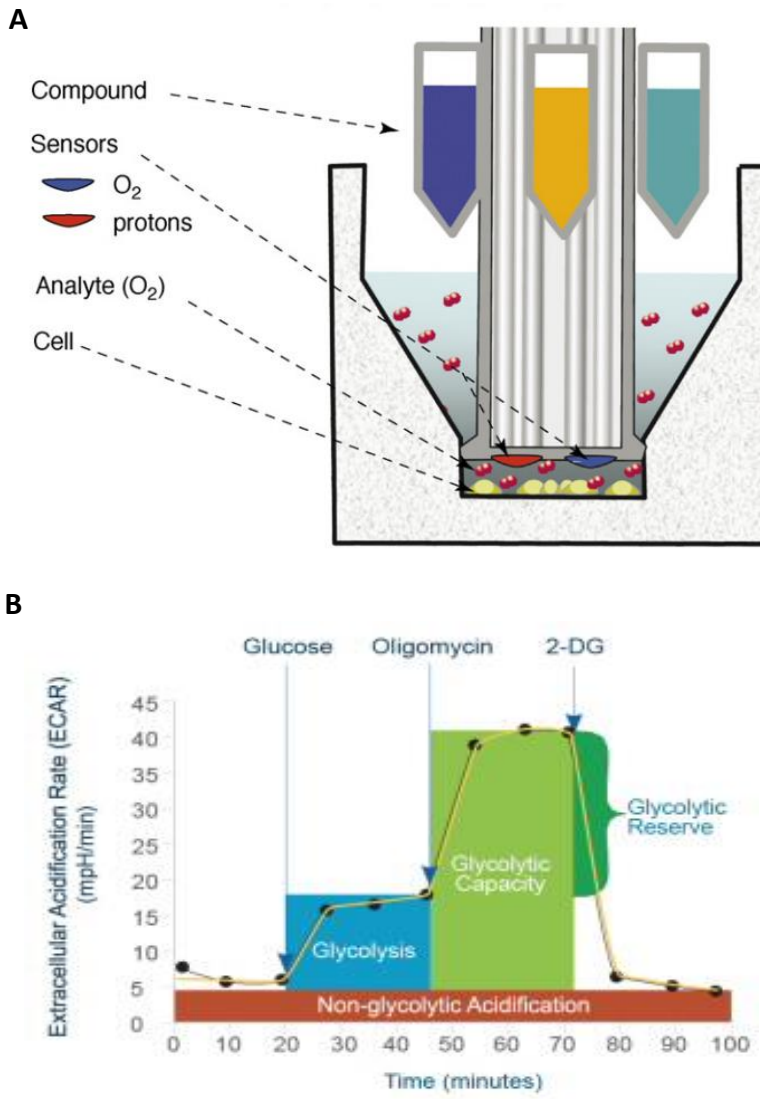

Figure 1.5: Mechanics of Seahorse XF analysis and metabolic profiling using the Glycolysis Stress Test

A) The mechanics of Seahorse XF analysis, with a focus on the cell microplate and sensor cartridge. Cells are seeded into the bottom of the wells (yellow) and covered with unbuffered media. The two sensor probes are indicated (blue and red), for oxygen and hydrogen sensing respectively. Four injection ports are also attached to the sensor cartridge (only three shown here), allowing simple injection of compounds, to stimulate cells during the assay.
(Image reprinted from Ferrick et al. (2008), Advances in measuring cellular bioenergetics using extracellular flux, Vol 13, Issue 5-6, Pages 268-274)
Copyright (2018) with permission from Elsevier (Licence no. 4265340479632).
B) The Glycolysis Stress Test assay profile, highlighting the three recommended injections for profiling glucose metabolism. Coloured areas also demonstrate quantifiable measures that can be calculated from this data (2-DG = 2-deoxyglucose)
(Image reprinted from Glycolysis Stress Test User Manual, with permission of Agilent Technologies UK & Ireland)

The Seahorse XF Analyser has been applied to a variety of research fields, including cancer, neurology, obesity, cardiovascular disease, immunology, and infection studies. The breadth of publications utilising this technique has since prompted Agilent to produce their own publication database, aiding ease of protocol and information sharing even further (Agilent Technologies 2017c). In the field of innate immune studies, the XF analyser has been used to consider the metabolism of dendritic cells (Everts et al. 2014), monocytes and macrophages (Haschemi et al. 2012; Tannahill et al. 2013). It has been shown that macrophages, including bone marrow-derived macrophages (BMDMs), increase glycolytic metabolism following stimulation with LPS and the conversion to a CAM phenotype, and this has been measured via Seahorse XF assessment (Haschemi et al. 2012; Tannahill et al. 2013; Tan, Xie, Banerjee, et al. 2015; Palsson-Mcdermott et al. 2015). Within this literature, metabolic changes to LPS stimulation have been traced in real time (Everts et al. 2014; Haschemi et al. 2012), and after both short-term and prolonged exposure (Van den Bossche et al. 2015; Haschemi et al. 2012; Tannahill et al. 2013). Significant increases in glycolysis are measured in all cases, providing reproducible methodologies and consistent results that can be taken forward when studying LPS-stimulated macrophage responses, as a control and a point of reference when examining the metabolic responses following pneumococcal stimulation of BMDMs. Furthermore, this point of reference is important since few studies have shown if these metabolic changes are the case during live bacterial infection or, more specifically, with infection by Gram-positive, extracellular bacteria such as *S. pneumoniae.* Instead, research has mainly focused on the burden of intracellular bacteria, such as *S. typhimurium* (Rosenberger et al. 2000) and *L. monocytogenes* (Cohen et al. 2000), and the use of other approaches such as transcriptomics and proteomics. Bacteria present a multitude of PAMPs and stimuli, to which macrophages must respond and the cellular responses could be very different to those seen for singular stimuli – for example the interaction of TLR4 with free LPS versus whole bacteria containing multiple PAMPS could result in very different downstream patterns of activation (Moore et al. 2000). Therefore the Seahorse XF Analysis should provide valuable insight into both immediate and long-term changes in macrophage metabolism, specifically glycolysis and oxidative respiration, following stimulation with LPS versus *S. pneumoniae*.

1.4.2.2. NMR Spectroscopy

NMR Spectroscopy is a technique typically used by chemical, biological and physical researchers to study the properties and arrangements of atoms, in different chemical states. The technique utilises the idea that all atomic nuclei have their own magnetic properties and nuclear spin, and that they are capable of absorbing and reemitting electromagnetic radiation. This atomic phenomenon is known as NMR.

Biological NMR Spectroscopy typically uses atoms that have a nuclear spin integer of ½, as these atoms are not only electrically charged, but can only be found in either one of two states: a high energy or low energy state. The most commonly used atoms in biological experiments are ^{1}H and ^{13}C - although other atoms with quadrupolar nuclei and spin integers of >½ can also be used, including ^{2}H and ^{18}O (Marion 2013). When held within an external magnet, the magnetised nuclei will either precess in the same direction as the magnetic field, the low energy +½ state, or in the opposite direction to the field, in the high energy –½ state (Thompson 1990). In a compound or mixture, not all nuclei will be in the same spin state, but by using a carefully administered dose of electromagnetic radiation, all nuclei can be excited from one energy state to another, and the radiation they emit as they return to a thermally equilibrated state can be recorded. These electromagnetic doses can also be clustered into a pulse sequence, and with more radiation being applied, a greater number of excited nuclei are observed - until the point of saturation (Bothwell & Griffin 2011). The emitted electromagnetic signals are recorded as free induction decays (FIDs) which can be mathematically converted into a frequency domain, using a Fourier Transformation. This then directly relates to the number of excited atoms in the sample (Bothwell & Griffin 2011). This alone would not be much use, as it would just appear as one large peak. However, electrons surrounding each nucleus reduce the magnetic field experienced by each atom. The electron shields are unique to not only the atom in question, but also its chemical environment and configuration in space. Therefore, a great amount of detail can be obtained about the locations and/or orientations of atoms in complex mixtures (Thomas 1998; Thompson 1990). Each atom will absorb a characteristic frequency, and the resonance emitted will shift depending on the chemical environment it is situated – this is referred to as δ (chemical shift) and it is represented on the x-axis of 1D spectra. The typical unit of measure on the x-axis is parts per million (ppm). This is the frequency

observed but normalised to the size of the applied magnet field and in relation to a reference standard, such as Trimethylsilyl propionate (TSP) or 4,4-dimethyl-4-silapentane-1-sulfonic acid (DSS). This allows comparisons to be made between spectra from different strength magnets and from different occasions (Bothwell & Griffin 2011). Information from the Fourier transform is displayed as a 1D spectral plot, with intensity on the y-axis and frequency (ppm) on the x-axis. Figure 1.6 shows a flow diagram of the processes for producing a 1D-NMR spectrum.

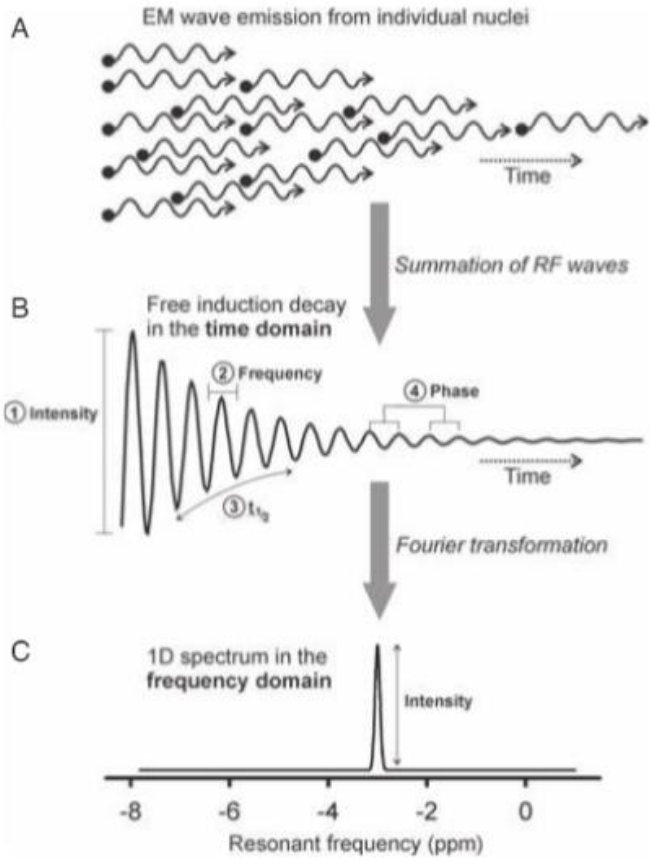

Figure 1.6: NMR spectroscopy data acquisition – from electromagnetic radiation to a transformed 1D spectra

A) Nuclei (represented by black dots) are excited to a high energy state and the electromagnetic (EM) emissions (represented by wavy lines) are recorded over time, as the nuclear energies relax back to an equilibrium state.
B) The radiofrequency (RF) waves are summed, to give a free induction decay (FID) over time. FIDs provide information from four parameters: (1) intensity of signals; (2) frequencies observed; (3) half-life of signals; (4) signal phase. Each of these parameters can be optimised to provide stronger and better resolution spectra.
C) A Fourier transform is used to mathematically convert the FID into a 1D spectra, demonstrating intensity on the y-axis and frequency (in ppm) on the x-axis. This removes the time domain from the presented spectra.
(Image reprinted from Bothwell et al. (2011), An introduction to biological nuclear magnetic resonance spectroscopy, Vol 86, Pages 493-510)

NMR spectroscopy has applications in a wide range of fields, but the focus of this thesis is its use in metabolomics. Metabolomics is the study of all metabolites in a sample, with a view to assessing changes between different stimuli, genetic modifications, or experimental stresses. This provides an observation of the dynamic metabolic system, at a snapshot in time (Cascante & Marin 2008). Tracing the metabolome is thought to provide information on the phenotype of a living system, as metabolic changes depend on differences in the genome, proteome, exposome and all other factors and influences affecting the local environment (Fiehn 2002). Approaches in metabolomics have already been shown in testing of crops and food products, through to medical diagnostics and in the potential for personalised healthcare (Collino et al. 2013; Wishart 2008). MS and NMR Spectroscopy techniques have currently dominated interest, with both techniques providing individual benefits. Whilst NMR has a lower sensitivity than MS, NMR has high reproducibility, it allows for compound structure elucidation when finding unknown compounds, and typically requires much simpler sample preparation than MS (Dunn & Ellis 2005).

To date, biologically relevant studies have focused on blood, tissue, and urine samples from patients to assess for metabolic markers of disease (Mamas et al. 2011). The use of metabolic biomarkers have been shown for a range of diseases, including cancer, diabetes, cardiovascular and neurodegenerative diseases (Emwas et al. 2013), however, it seems that comparatively few have focused on infectious diseases. For example, Weiner et al. have looked at the influence of *M. tuberculosis* infection on patient blood serum metabolites and have identified twenty metabolites which could help serve specific diagnosis of tuberculosis (Weiner et al. 2012), whilst Shin et al. have considered the changes to organ metabolomics in mouse models of tuberculosis (Shin et al. 2011). Interestingly, Slupsky et al. have used NMR Spectroscopy for considering changes in urinary metabolite profiles of patients with pneumococcal pneumonia, with comparisons made to profiles from patients infected with other pathogens, such as *H. influenzae*, or with other lung diseases, such as asthma (Slupsky et al. 2009; Slupsky 2010). A study by Chiu et al. has shown that biomarkers of *S. pneumoniae* metabolism, such as 3-hydroxybutyrate, could be used to study the progression of infant pneumonia in pleural fluid samples (Chiu et al. 2016). Also, a broader study by Gupta et al. has distinguished Gram-positive from Gram-negative bacteria in urines of both healthy and individuals with urinary tract infections (UTI), which aims to help bacterial identification,

diagnosis and trajectory of recovery. These examples demonstrate the progression and ambition of this field, using a variety of sample types to understand the metabolic signatures of host-pathogen interactions. It shows the potential to identify specific pathogens responsible for UTIs, and consequently to avoid over prescription of antibiotics and tailor more precise patient treatments.

Although clinical studies dominate in the field of NMR metabolomics, it has also been used to consider metabolic changes *in vitro,* using cell cultures. It is shown that different cell types exhibit characteristic and individual metabolic patterns (Urenjak et al. 1993). This could aid the identification and quantification of different cells types in heterogenous populations, such as those involved in 3D cell cultures or tissue models. In terms of macrophage metabolism, studies have utilised both whole cells (Ramm Sander et al. 2013) and cell extracts (Stuckey et al. 2005), to consider the role of lipid and non-lipid metabolites respectively. The sample type and preparation method can considerably influence the resulting spectra, regarding both the content detected and the signal-noise ratio, therefore identifying a suitable procedure can depend on the research question involved. For example, Lamour et al. considered the metabolic changes of the intracellular and extracellular environments of macrophages, both in the presence of CAM/AAM stimulation and during *L. major* infection (Lamour et al. 2012). Three different sample preparation methods were required - for the internal, external and isolated bacterial samples - and a longer acquisition time was required for the cell extracts, as they contained smaller concentrations compared to the extracellular culture environment. This was the first study of this kind, to consider metabolic changes of activated macrophages using NMR metabolomics. 1H-NMR spectroscopy should therefore provide a global overview of changes to metabolism, with the ability to identify highly reproducible metabolic signatures between different cell types and stimulatory conditions.

Aims and Hypotheses

The aim of this project was to characterise the changes to metabolism, in macrophages exposed to *S. pneumoniae,* and to relate these to responses seen following macrophage stimulation with LPS. It was also to determine the functional consequences of these metabolic changes to key innate immune functions. This would help establish the importance of specific metabolic changes, to the host responses seen during the host-pathogen interaction, and would reveal whether metabolism mediates changes associated with classical activation during the macrophage response to *S. pneumoniae*

The project objectives were to:

1) **Optimise and use the Seahorse XF Analyser** to assess changes in glycolytic metabolism, during *S. pneumoniae* infection, compared to LPS

2) **Optimise and use NMR Spectroscopy** to evaluate global changes in metabolites, during *S. pneumoniae* infection, compared to LPS

3) **Measure changes in macrophage effector functions** following inhibition of glycolytic metabolism during *S. pneumoniae* infection

The hypotheses of this project were:

1) *S. pneumoniae* challenge induces changes in metabolism that are comparable to those seen for LPS stimulation, such as a shift towards glycolytic metabolism.

2) Macrophage effector functions during *S. pneumoniae* challenge are dependent on a glycolytic switch, as seen during LPS stimulation.

Chapter 2 - Materials and Methods

2.1. Materials and reagents

Material	Supplier	Catalogue no.
2',7'-dichlorodihydrofluorescein diacetate (DCF-DA)	ThermoFisher	D399
2-Deoxy-D-Glucose (2DG)	Sigma	D4601
4-Amino-5-Methylamino-2',7'-Difluorofluorescein Diacetate (DAF-FM)	ThermoFisher	D23842
Accutase cell detachment solution	Merck Millipore	SCR005
BioWhittaker® Dulbecco's Modified Eagle Medium (DMEM)	Lonza	BE12-604F
BioWhittaker® Penicillin-Streptomycin stock	Lonza	17-602E
Blood Agar Plates	(made in-house by technical team)	
Carbonyl cyanide 4-(trifluoromethoxy) phenylhydrazone (FCCP)	Sigma	C2920
Clarity™ Western ECL substrate	Bio-Rad	1705061
Color Prestained Protein Ladder (Broad range)	New England Biolabs	P7711S
DC Protein Assay Kit	Bio-Rad	5000116
Dehydroepiandrosterone (DHEA)	Sigma (Cerilliant)	D-063
Fetal Bovine Serum, South America Origin (Heat-inactivation carried out in-house)	Biosera	FB-1001
Gentamicin (Cidomycin)	Sanofi (from NHS Pharmacy)	
HPLC-Grade Methanol	Fisher Scientific	A452-1
IL-6 Mouse ELISA Kit	ThermoFisher	88-7064-88
L929-cell conditioned media	(made in-house by technical team)	
Latex beads, fluorescent red	Sigma	L3030
LPS (E. coli R515)	Enzo Life Sciences	ALX-581-007-L001
Oligomycin A (Oligo)	Sigma	75351
Oxoid Brain-Heart Infusion Broth	ThermoScientific	CM1135
Paraformaldehyde	Sigma	P6148
Penicillin	Sigma	P3032
Phenol-free RPMI	Sigma	R7509

Phosphate Buffered Solution (PBS)	Lonza	BE17-517Q/12
Pneumovax®23	Merck (from NHS Pharmacy)	
Polycloncal Goat Anti-mouse HRP antibody	Dako	P0447
Purified Anti-α-Tubulin antibody, mouse monoclonal	Sigma	T6199
Purified Mouse Anti-mouse COX-2 antibody	BD Biosciences	610204
Purified Mouse Anti-mouse iNOS antibody	BD Biosciences	610432
Recombinant Murine IL-4	PeproTech	216-16
Saponin	Sigma	S7900
Seahorse XF24 FluxPak	Agilent	100850-001
Sodium Iodoacetate (Iodo)	Sigma	I2512
TNFα Mouse ELISA Kit	ThermoFisher	88-7324-88
Vectashield Mounting Medium	VWR	101098-044

2.2. Cell culture

2.2.1. Murine bone marrow-derived macrophages (BMDMs)

Wild type mice were killed by cervical dislocation and sprayed with disinfectant. The skin around the abdomen was cut and pulled down over the hind legs to expose the femurs and tibias. Bones were removed by cutting at the hip and ankle joints. Murine bone marrow cells were isolated by removing all tissue from the bones, cutting them at each end and flushing the bone marrow cells out using ~5ml Dulbecco's Modified Eagle Medium (DMEM) with L-glutamine and 4.5g/L glucose, supplemented with 100U/ml Penicillin, 100µg/ml Streptomycin, 10% Heat-Inactivated Fetal Calf Serum (HIFCS) and 10% L929 cell-conditioned media. Cells were plated at $2x10^5$ cells/ml in T75 flasks or 24-well plates, and incubated at 37°C with 5% CO_2 for five days. After this time, non-adherent cells were discarded and media changed every other day, with antibiotics removed from the media during the seven days preceding experimental use. For some experiments, coverslips were placed in 24-well plates prior to seeding, to allow adherent cells to be used for staining and microscopy. All cells were cultured for at least 12-14 days, to allow cells to differentiate and non-adherent, non-differentiated cells to be removed before use.

2.2.2. Human monocyte-derived macrophages (MDMs)

Blood isolation was carried out at the Royal Hallamshire Hospital. 300ml blood was collected in blood bags from consenting donors by a trained member of staff. Blood bags contained the anticoagulant Citrate Phosphate Dextrose Adenine. All donors were given an information sheet and signed both a consent and a screening form. These are filed in the Infectious Diseases Department. Monocyte isolation from human blood was conducted by a member of the departmental technical team with ethical approval from South Sheffield Regional Ethics Committee (07-Q2305/7). Blood was decanted into T75ml tissue culture flasks and 25ml from each donor layered onto 12.5ml Ficoll-Paque in 50ml Falcon tubes. Blood was centrifuged at 1500 rpm for 23 minutes with no braking. Cell layers were isolated and added to clean 50ml tubes and centrifuged at 1000 rpm for 13 minutes. Supernatants were discarded, and pellets resuspended in 10ml Roswell Park Memorial Institute (RPMI) media, with 10% heat-inactivated foetal bovine serum. Peripheral blood mononuclear cells were then counted using a haemocytometer and further diluted in media to $2x10^6$cells/ml prior to plating out.

2.2.3. Reseeding cells

BMDMs were grown in T75 flasks for at least twelve days prior to re-seeding. Media was removed from flasks and washed with 5ml PBS. After completely removing the PBS, 5ml accutase cell detachment solution was added and incubated in 5% CO_2 at 37°C for 15 minutes. Following this time, cells normally detach from the flask and can be seen floating in suspension, but they can be encouraged to loosen with gentle pipetting if required. The cell suspension was centrifuged at 200g for 10 minutes, the supernatant was discarded and cells were resuspended in 5ml DMEM with 10% HIFCS and 10% L929 cell-conditioned media. The cell concentration was measured using a haemocytometer, and cells were diluted to the desired density before plating into 24-well, 6-well or XF Cell Culture Microplates.

2.3. Bacterial culture

2.3.1. *S. pneumoniae*

S. pneumoniae serotype 2 strain D39 was obtained from Prof. Tim Mitchell (University of Birmingham). Long-term storage of bacteria was on Protect multi-purpose cryobeads (Technical Service Consultants, UK) stored at -80°C. The bacterial stock was prepared by streaking of a bead onto a blood agar plate and incubating at 37°C with 5% CO_2 overnight. The following day 50ml Brain-Heart Infusion Broth (BHI) with 20% HIFCS was prepared and separated into two 25ml universals. Ten bacterial colonies were selected from the blood agar plate and mixed into one of the universals, whilst the second tube acted as the blank. Universals were incubated at 37°C with 5% CO_2 for 4-7 hours with shaking. After the first four hours, 1ml from each universal was pipetted into cuvettes for reading by photospectrometer. The Optical Density (OD) of the D39-containing broth was measured at 610nm, with the broth without bacteria used as a blank. Readings were taken every half an hour until an OD of 0.6 was reached, which is in *S. pneumoniae* log-stage growth. Once the bacteria had grown to this density, the universals were removed from the incubator and 1ml aliquots of the bacteria were taken and stored at -80°C. When required, these aliquots were rapidly defrosted, spun and washed with PBS prior to use.

2.3.2. Opsonisation with mouse immune serum

For sufficient bacterial internalization of *S. pneumoniae* by murine BMDMs, bacteria were opsonized with mouse immune serum (mIS) containing antibodies against this bacterium. Balb/c mice were immunized with a combination of Pneumovax®23 (23µg/mouse) and anti-CD40 monoclonal antibody (50µg/mouse). Mice were left for at least 4 weeks to mount an immune response. They were then bled, and serum pooled from multiple mice. The mIS was kept at -80°C in 25µl aliquots and defrosted immediately before use.

2.3.3. *S. pneumoniae* infection

For live bacterial infections a 1ml D39 aliquot was rapidly thawed from -80°C, spun at 9000rpm for 3 minutes and re-suspended in 1ml PBS. This was repeated twice, and the final pellet resuspended in 225µl DMEM with 25µl mIS. Bacteria were opsonized using this serum, by incubating at 37°C with shaking for 30 minutes. Once opsonized, bacteria were pelleted by centrifugation at 3400rpm for 3 minutes and washed in 1ml PBS. Bacteria were washed a further two times in PBS, and finally re-suspended in 990µl DMEM with 10% HIFCS. Cells in 24-well plates were washed twice with 1ml PBS prior to replacing with 0.5ml DMEM with 10% HIFCS in each well. Bacteria were added to give an estimated Multiplicity of Infection (MOI) of 10, while control cells were mock-infected with equal volumes of media. Cells were then placed on ice for one hour, in order to increase adhesion of bacteria to macrophage surface membranes. After this initial hour, cells were then transferred to 37°C for three hours. At 4 hours, all wells were washed twice with PBS and, where indicated, extracellular bacteria were eradicated by treating with 1ml DMEM with 20ug/ml Gentamycin and 40U/ml Penicillin, and incubating at 37°C for 30 minutes. Cells were washed with PBS to remove residual antibiotics, and fresh media added before returning cells to 37°C until the desired time point.

A Miles-Misra viable count (MM-VC) was used to assess the true concentration of bacteria, and to calculate the actual MOI after each infection procedure. For this, eight 10-fold serial dilutions of the re-suspended bacteria were performed, by taking 100 µl of the solution and serially diluting in 900µl PBS. A blood agar plate was divided and labeled into eight segments, before three 10µl droplets of each dilution were plated onto separate areas of the plate. This was incubated overnight and counted the following day, to allow calculation of the bacterial aliquot concentration in cfu/ml. To heat-kill the bacteria, the 1ml D39 aliquot was heated to 70°C in a heat block for 40 minutes, prior to washing and opsonizing as above, with the MM-VC used to confirm loss of bacterial viability.

An R6 unencapsulated *S. pneumoniae* strain was also used, where stated in the results text. This strain was obtained from Dr. Andrew Fenton at the University of Sheffield. It did not require opsonisation but otherwise followed the same infection procedure as above.

2.3.4. Bacterial internalisation assay

Cells were infected and assessed after several hours. At defined time points, eight 1:10 serial dilutions of the cell culture media were made, to identify the number of viable bacteria in the extracellular environment. Three 10µl droplets of each dilution were plated onto separate areas of a blood agar plate and incubated at 37°C overnight. The media was then removed and cells washed three times with 1ml PBS, before adding 1ml DMEM with 20µg/ml Gentamycin and 40U/ml Penicillin, and incubating at 37°C for 30 minutes to kill any remaining extracellular bacteria. After this time, media was removed, and cells washed three times with 2ml PBS, to remove all residual antibiotic. Two 1:5 serial dilutions were made from the final PBS wash, after antibiotic treatment, to check that all extracellular bacteria had been killed. These were again plated onto agar plates as described previously. The final PBS wash was removed, and 250µl 2% saponin in PBS added to each well and incubated for a further 15 minutes (0.02% saponin in distilled water was also trialled). Following this, 750µl PBS was added to each well, and then scraped with a pipette tip and vigorously pipetted onto, in order to lyse the cells. Two final 1:5 serial dilutions were made, to assess numbers of bacteria seen within the intracellular environment. Once more, these were plated onto agar plates and left to incubate overnight. The following day, blood agar plates were counted for colonies and cfu calculations made for each of the cell environments and conditions.

2.4. Metabolic assays

2.4.1. Seahorse XF24 Extracellular Flux Analysis

The day prior to each Seahorse assay, the XF24 Flux Assay Plate was prepared, by filling each well of the Utility plate with 1ml XF Calibrant and submerging the Sensor Cartridge into the solution. The Utility plate and submerged Sensor Cartridge were then left in a non-CO_2 incubator at 37°C overnight. The XF24 Analyser was also turned on and left to equilibrate overnight.

Cells were reseeded on the day prior to assay, using the details listed in section 2.2.2. and the cell seeding protocol advised by Seahorse Bioscience (Seahorse Bioscience Inc. 2015a). Unless otherwise stated, the cell density used was 200,000 cells/well.

On the day of the assay, all assay media and compound injections were prepared, with a pH of 7.40±0.05 at 37°C. For the Glycolysis Stress Test, the medium was always supplemented with 2mM L-Glutamine. The microplate media was changed one hour prior to assay, with warm XF Assay Media (XFAM). Once again, the recommended protocol from Seahorse Bioscience was used (Seahorse Bioscience Inc. 2015b). For experiments stated in this report, final microplate media volume, prior to assay, was 630µl. Injection ports were prepared with compounds at concentrations that were 10-fold higher than the working concentration, allowing dilution to occur upon injection. E.g. 70µl of 100mM compound injected into 630µl, provides a diluted working concentration of 10mM. Guidelines for loading compounds into the Sensor Cartridge were given by Seahorse Bioscience (Seahorse Bioscience Inc. 2015c). Injection port volumes were made up to satisfy the following quantities, allowing appropriate 10-fold dilution: Port A 70µl, Port B 77µl, Port C 84µl, Port D 92µl. The Seahorse XF24 command protocol timings also varied during optimization stages. However, the final mix, wait, measure times used for $2x10^5$ BMDMs/well were 3, 12, 3 minutes respectively. Assay results were also normalized, following protein extraction and quantification from all microplate wells.

2.4.2. NMR Spectroscopy sample preparation

BMDMs were reseeded into 6-well plates at $1x10^6$cells/well (unless otherwise stated) on the day prior to use, and infected or treated as required. Whole cells, cell supernatants and cell extracts were prepared and analyzed using NMR Spectroscopy.

Whole cell samples were prepared by washing the wells twice with 1ml PBS and scraping into a final volume of 460µl PBS containing 10% D_2O. Tubes were kept on ice prior to NMR Spectrometry, and 5µl of 100mM TSP added to each sample before they were loaded into 5mm Shigemi NMR tubes. These tubes have a large susceptibility-matched solid glass bottom, which allow sample sedimentation within the sensitive volume of the NMR probe coil. This protocol was adapted from Ramm Sander et al (Ramm Sander et al. 2013).

Supernatants were collected directly from the cell culture plate, spun at 2500rpm for 2 minutes to remove cellular debris, and transferred to fresh tubes to be stored at -80°C

until analysis. On the day of NMR Spectroscopy, 300µl supernatant sample was mixed with 300µl D_2O Phosphate Buffer and 1µl 100mM Trimethylsilyl propionate (TSP). D_2O Phosphate Buffer consisted of PBS made with 70% D_2O, 30% H_2O. 550µl of the sample was transferred to a 5mm NMR tube, and a hand-crank centrifuge used to push all samples into the lower portion of tube and to remove any air bubbles. In later experiments, TSP was added to the main D_2O PBS stock to provide a concentration of 100µM throughout all samples and reduce TSP concentration variability between sample preparations.

To prepare cell extracts, cell culture media was removed and cells were washed with 1ml/well room temperature PBS. PBS was removed and 1ml ice-cold High Performance Liquid Chromatography (HPLC)-grade methanol was added to quench cell metabolism and cells were lysed on ice for 5 minutes. Cells were scraped using a cell scraper, to further encourage lysing and to harvest intracellular contents. Suspension were transferred to clean eppendorf tubes and kept on ice. A further 460µl was used to rinse each well and added to the corresponding eppendorf kept on ice. Lysates were dried overnight at 45°C using an Eppendorf Concentrator 5301. Once dried, 80% methanol extractions were performed twice on the remaining pellets using the following steps: (i) resuspend dried lysate in 500µl HPLC-grade methanol and vortex for 30 seconds, (ii) add 130µl distilled water and vortex again for 30 seconds, (iii) leave tubes on ice for 15 minutes, (iv) centrifuge samples at 13000rpm for 10 minutes and transfer lysate supernatants to fresh eppendorfs kept on ice, (v) repeat methanol extraction stages i-iv on remaining pellet. After the two methanol extractions were pooled, they were dried again overnight at 45°C using the Eppendorf Concentrator 5301. The following morning, samples were transferred to -80°C until analysis. On the day of NMR Spectroscopy, dried extracts were resuspended in 600µl D_2O Phosphate Buffer, as described for cell supernatants, with 1µl TSP. 550µl of the sample was transferred to a 5mm NMR tube and a hand-crank centrifuge used to push all samples to the lower portion of tube and to remove air bubbles. This protocol was adapted from Lamour et al (Lamour et al. 2012).

2.4.3. NMR Spectroscopy sample acquisition

Whole cells → Spectra were acquired with a Bruker 600MHz Avance DRX NMR spectrometer equipped with a TXI-cryoprobe, at 5°C. The pulse program 'zgesgp' was used, with 64 scans and processed with a line broadening of 1Hz.

Cell Supernatants → Spectra were acquired on a Bruker 800MHz Avance I NMR spectrometer equipped with a TXI probe, at 25°C. The pulse program 'ah_robust5.ptg' was used, with 128 scans and processed with a line broadening of 1Hz. The pulse program script was written in house by University of Sheffield NMR Facility technician, Miss Andrea Hounslow.

Cell Extracts→ Spectra were acquired with the same method as for supernatants, however the number of scans was increased to 512 to increase the signal:noise output.

Following Fourier transformation, all spectra were phased and baseline-corrected manually in TopSpin (Bruker processing software).

2.4.4. Metabolic inhibition

Metabolic inhibitors were diluted into cell culture media, DMEM with 10% HIFCS. Cells were washed twice with 1ml PBS, and 500µl DMEM with 10% HIFCS plus inhibitor added to each well. To infect after inhibition, bacteria were added directly into this media at an MOI of 10. Adding an equal volume of DMEM with 10%HIFCS to corresponding wells stimulated mock-infection. Alternatively, inhibitors were added 4hr post-stimulation, after two 1ml PBS washes and in the same media and volumes as above. Concentrations of inhibitors used were in accordance with the literature (Haschemi et al. 2012; Tannahill et al. 2013), and were as follows: 100mM 2DG, 100µM Iodoacetate and 200µM DHEA.

2.4.5. Measurement of ATP levels

To measure ATP, the Perkin Elmer ATPlite luminescence assay system was used. Cells were reseeded into a 96-well plate at 20,000 cells/well (100µl of 200,000 cells/ml) and left to adhere overnight. Wells were washed twice with 100µl PBS and stimulated as desired. After 4 hours, wells were again washed twice with 100µl PBS and 100µl media returned to each well. After 10 hours, the ATPlite kit was removed from the fridge and

allowed to return to room temperature. At 12 hours, media was removed and wells washed twice with 100µl PBS. 50µl lysis buffer was added to all wells and the plate was shaken for 5 minutes. 50µl substrate solution was added and the plate shaken for a further 5 minutes. Finally, 100µl PBS was added and the plate was dark-adapted for 10 minutes, before reading luminescence on a ThermoScientific VarioSkan plate reader. Control wells (containing no cells) provided the assay background. These values were subtracted from all conditions.

2.4.6. Measurement of glucose uptake

To measure glucose uptake, the Promega Glucose Uptake-Glo™ assay kit was used. Cells were reseeded into a 96-well plate at 20,000 cells/well (100µl of 200,000 cells/ml) and left to adhere overnight. Wells were washed twice with 100µl PBS and stimulated as desired. After 4 hours, wells were again washed twice with 100µl PBS and 100µl media returned to each well. After 10 hours, the Uptake-Glo™ assay kit was removed from the freezer and returned to room temperature. After 11 hours, the 2DG Detection Reagent and 2DG solutions were prepared and kept at room temperature. After 12 hours, media was removed and wells washed twice with 100µl PBS. 50µl 1mM 2DG solution was added to each well (apart from background controls, which were given an equal volume of PBS). The plate was shaken and left at room temperature for 10 minutes. 25µl Stop Buffer was added and plate shaken briefly, before 25µl Neutralisation Buffer was added and shaken briefly again. Finally, 100µl 2DG Detection Reagent was added to all wells, the plate was shaken and then dark-adapted for one hour. Luminescence was measured using the ThermoScientific VarioSkan plate reader. Control wells, without 2DG treatment, provided the assay background and were subtracted from all conditions.

2.5. Functional assays

2.5.1. Enzyme-linked Immunosorbent Assay (ELISA)

ELISAs were performed using eBioscience Antibody ELISA kits, targeting mouse TNFα or mouse IL-6 following the manufacturer's instructions. The day prior to assay, 44µl capture antibody was diluted in 11ml Coating Buffer, and 100µl of this loaded into wells

of a 96-well High-Binding ELISA plate. The plate was sealed and incubated overnight at 4°C. On the morning of assay, the plate was first washed using the Bio-tek ELX-50 Plate Washer. Wash Buffer was made of 0.5M NaCl, 2.5mM NaH_2PO_4, 7.5mM Na_2HPO_4 and 0.1% Tween-20 at pH 7.2. 200µl of Assay Diluent (AD) was added to all wells and left to incubate for 1 hour at room temperature, during which Antibody Standards were made, providing either 1000pg/ml TNFα or 500pg/ml IL-6. Up to eight serial dilutions of the standards were performed, to give standard curves of between 15-1000pg/ml for TNFα and 8-500pg/ml for IL-6. The plate was washed again, and 100µl standards and samples added in duplicate. The plate was sealed and incubated at room temperature for at least 2 hours to allow binding. After a further wash, 44µl Detection Antibody was diluted in 11ml AD, and 100µl of this solution loaded into each well, and left at room temperature for one hour. The plate was washed again, and Avidin-HRP Antibody added, in the same dilution and volumes as for the Detection Antibody. This was left to incubate for 30 minutes. After a final plate wash, 100µl TMB Substrate Buffer was added and left for 15 minutes, and 50µl/well of H_2SO_4 Stop Buffer added after this time to halt the reaction. The plate was then read for absorbance at 450nm, using a Thermoscientific MRX Plate Reader with Biolinx S. Cytokine quantification was carried out using standards and GraphPad Prism software.

2.5.2. 4-amino-5-methylamino-2',7'-difluorofluorescein diacetate (DAF-FM) staining

DAF-FM Diacetate is a cell-permeable reagent used to quantify nitric oxide (NO). It is non-fluorescent until it becomes de-acetylated in the intracellular environment to give DAF-FM. This form is highly fluorescent once reacted with NO and can be measured by flow cytometry and other fluorescence readers.

Cell culture media was discarded and cells washed twice with 1ml PBS. 5µM DAF-FM was added to phenol red-free RPMI, supplemented with 2mM L-Glutamine, with 500µl pipetted into each well and incubated at 37°C for 30 minutes. Unstained controls were incubated in phenol-free RPMI for this same duration. Cells were then washed twice in 1ml PBS, and 500µl phenol red-free RPMI supplemented with 2mM L-glutamine only, was added to all wells before incubation for a further 30 minutes. This allowed time for the reaction and fluorescence to develop. Two more 1ml PBS washes were carried out, and finally cells were scraped in 300µl PBS, ready for assessment via flow cytometry.

Cells were separated by forward scatter and side scatter, with debris excluded and DAF-FM measures taken in the FLH-1 channel. Geometric means of all conditions were recorded, and values for unstained controls subtracted from corresponding stained samples.

2.5.3. 2',7'–dichlorofluorescin diacetate (DCF-DA) staining

DCF-DA is a cell-permeable reagent used to quantify Reactive Oxygen Species (ROS). It is non-fluorescent until it becomes be acetylated in the intracellular environment. This form is then highly fluorescent after reacting with ROS and can be measured by flow cytometry and other fluorescence readers.

Cell culture media was discarded and cells washed twice with 1ml PBS. 20µM DCF-DA was added to phenol red-free RPMI supplemented with 2mM L-Glutamine, at 500ul per well. The plate was incubated for 45 minutes at 37°C. Unstained controls were incubated with an equal volume of phenol red-free RPMI with 2mM L-glutamine. Cells were then washed in duplicate with 1ml PBS, and scraped in 300ul PBS, ready for flow cytometry. Cells were separated by forward scatter and side scatter, with debris excluded and DCF-DA measures taken in the FLH-1 channel. Geometric means of all conditions were recorded, and values for unstained controls subtracted from corresponding stained samples.

2.5.4. Latex bead internalisation and calculations

10µl aqueous red-fluorescent latex bead suspension was diluted into 990µl PBS, to provide ~$5.7x10^9$beads/ml. Beads were spun at 13,000rpm for 5 minutes, and the final pellet resuspended in 225µl DMEM with 25µl mIS. This was incubated with shaking at 37°C for 30 minutes. During this time, cells on coverslips were washed twice with 1ml PBS and 500µl assay media was added. Beads were then spun at 3400rpm for 3 minutes and washed twice in 1ml PBS. Opsonised beads were left in 1ml PBS and added to cell culture media in a volume that provided ~10 beads per cell. The cell culture plate was kept on ice for one hour, then transferred to incubator at 37°C. After a total of 4 hours, cells were washed, mounted and counted as stated in section 2.5.6. From each coverslip,

the following variables were counted: Total macrophages, total beads, and number of macrophages with beads. From these measures, the following calculations were made:

Calculation Name	**Calculation Method**
Phagocytic Index	Total beads / Total macrophages
% Phagocytosis	(Number of macrophages with beads / Total macs)*100
Average Bead Uptake	Total beads / Number of macrophages with beads

2.5.6. DAPI staining and microscopy

Cells cultured on coverslips were fixed, stained, and mounted for microscopy. Media was removed and wells washed three times with 1ml PBS. 0.5ml of 2% Paraformaldehyde (BDH Ltd.) was added and left at 4°C overnight. The following morning, Paraformaldehyde was removed, coverslips washed three times in 1ml PBS, then left in 0.5ml PBS ready for mounting, to prevent cells drying out and aid removal of coverslip from the well. The DAPI staining reagent used was VECTASHIELD® Mounting Medium with DAPI (Vector Laboratories Inc.). Two small drops of this were placed on a labeled microscope slide. Coverslips were maneuvered out of wells using a hooked needle and tweezers, gently blotted to remove excess PBS, and inverted into the VECTASHIELD® solution (i.e. cells in contact with the stain). After mounting, slides were blotted to remove excess solution, before being fixed in position using nail varnish around the outer edges. The reagent remains liquid during microscopy; therefore coverslips must be securely fixed in place. Microscopy was carried out immediately, using a Leica DMRB Type 301-371.010 fluorescent microscope, under blue light and 40-100x magnification, with oil immersion. At least three hundred cells were counted from each coverslip.

2.5.7. Protein extraction and quantification

Cells were lysed at room temperature, and protein was extracted using a trichloroacetic acid (TCA) method. Cells were first washed with 1ml PBS three times, then 600µl TBS-EDTA-SDS lysis buffer (2% 1M Tris pH 7.4, 6% 1M NaCl, 1% 0.5M EDTA, 1% 0.5M EGTA, 2% SDS (20%) H_2O) with complete protease inhibitor added, at a ratio of 1:25,

immediately prior to use. DNA was aggregated and protein precipitated using 100% TCA. The protein pellet was obtained by centrifugation at 13,000rpm for 5 minutes. This was washed in 1ml 2.5% TCA before being dissolved in 40µl 3M Tris base, which was diluted to 1.5M Tris base with water after an hour solubilisation at room temperature. Protein samples were stored at -20°C.

Protein was quantified using a colorimetric DC Protein Assay Kit. BSA protein standards were dissolved in lysis buffer to a concentration range of 0.5-10mg/ml, allowing the construction of a standard curve. 5µl of samples and protein standard were added to a 96-well plate, with 25µl Reagent A' (made using 20µl Reagent S in 1ml Reagent A). 200µl Reagent B was then added, the plate was shaken and left to incubate at room temperature for 15 minutes. Absorbance was measured at 750nm and protein concentrations calculated from interpolation of the standard curve, using GraphPad Prism.

2.5.8. Western blotting

Proteins were first separated via sodium dodecyl sulphate polyacrylamide gel electrophoresis. Protein samples were denatured by adding equal amounts of protein and Lammeli buffer (4% SDS, 20% Glycerol, 0.004% Bromophenol Blue, 10% 2-mercaptoethanol, 0.125M Tris Hcl), and boiling at 95°C for 5 minutes. Proteins were then loaded into lanes of a 1.5mm thick 10% polyacrylamide gel (see Table 2.1) in running buffer (0.025M Tris-base, 0.19M glycine, 0.1% SDS). An electrical current of 100V was applied when passing proteins through the stacking gel, which was increased to 140V for passing through the resolving gel. The molecular weight of proteins was determined by the addition of 5µl Color Prestained Protein ladder (Broad range, 11-245kDa). Once the gel had completely run, the resolving gel was cut from the stacking gel, and discarded. The resolving gel was placed on top of a nitrocellulose paper membrane, with filter paper either side, soaked in transfer buffer (0.047M Tris-base, 0.038M glycine, 0.04% SDS, 10% methanol, H_2O). The sandwiched gel was then transferred using the semi-dry Trans-Blot SD transfer cell (Bio-Rad), with an electric current of 15V for 45 minutes.

After transfer, the nitrocellulose membrane was washed in water and transfer of protein was confirmed by Poncheau S staining. The membrane was incubated in Poncheau S for 2 minutes, and could be removed by washing in TBS (0.1M Tris-HCl, 0.16M NaCl, H_2O) with agitation. The membrane was then blocked for 1 hour in blocking buffer (TBS with 5% skimmed milk powder). Membranes were incubated over night at 4°C overnight, in TBS-Tween (TBS with 0.05% Tween-20) containing 5% skimmed milk powder and a 1:1000 dilution of the primary antibody. Primary antibodies used included murine iNOS, COX-2 and α-tubulin. After primary incubation, the membrane was washed three times in TBS-Tween, each for 10 minutes. Horse radish peroxidase-conjugated polyclonal goat anti-mouse antibody was diluted 1:2500 in TBS-Tween with 5% skimmed milk powder, and the membrane was incubated in this for 1 hour at room temp. The membrane was washed a further three times in TBS-Tween and incubated with Bio-Rad Clarity™ ECL substrate for 5 minutes at room temperature. The membrane was then sealed in clear film and analysed using the ChemiDoc™ XRS+ System (BioRad). The membrane could then be stripped with 0.2M NaCl and water, to be re-probed with α –tubulin as the loading control, which was also diluted at 1:1000 in TBS-Tween in 5% skimmed milk powder.

Table 2.1. Ingredients of resolving and stacking gels

	Resolving Gel (µl)	**Stacking Gel (µl)**
H_2O	7200	3000
40% Acrylamide 29-1	3800	620
1.5M Tris, pH 8.8	3800	-
0.5M Tris, pH 0.8	-	1260
20% SDS	75	25
20% Ammonium persulphate	150	50
T-Med	6	5

2.6. Statistics

All statistical analyses were performed using GraphPad Prism v.7, with data represented as mean ± standard deviation, unless otherwise stated. For comparison between multiple groups, a One-Way ANOVA test was used. For multiple comparisons to the

mock/unstimulated group, Dunnett's multiple comparisons were used, and for comparisons between all groups, Tukey's multiple comparisons were used.

Chapter 3 – The optimisation and use of Seahorse XF Analysis to study BMDM glycolytic responses after *S. pneumoniae* challenge

3.1. Introduction

Immunometabolism is an emerging field that aims to reveal the importance of metabolism in immune responses. As described previously, macrophages have been shown to shift towards CAM metabolism following stimulation with LPS, with up-regulated glycolysis and a repressed Krebs cycle both noted as key changes (Tannahill et al. 2013; O'Neill et al. 2016). With increased interest in this field, new techniques and methods of studying metabolism have emerged – one such technique is the Seahorse XF Analyser. The Analyser assesses real-time changes to glycolysis and respiratory metabolism in cell cultures, through measuring hydrogen ion and oxygen availability in the extracellular environment. These measures are herein referred to as ECAR and OCR respectively. This technique provided an ideal candidate for assessing central metabolic changes during macrophage stimulation. Therefore, by using the Seahorse XF Analyser and the Glycolysis Stress Test, *S. pneumoniae*-induced changes to macrophage metabolism could be assayed, with comparisons made to CAM and AAM metabolic changes, as promoted using the singular stimuli, LPS and IL-4, respectively.

This chapter describes optimisation of the Seahorse XF Analyser, specifically for use with murine BMDMs. This includes finding appropriate cell densities, inhibitor concentrations and protocol timings to gain robust results. Optimisation was further required when considering specific use of the Glycolysis Stress Test, as media composition varied between recommended kits and profiling assays. This optimised technique was then used to test the effect of *S. pneumoniae* challenge on BMDM glycolytic metabolism, compared to LPS stimulation. The application of this technique was also demonstrated for human cells.

3.2. Results

3.2.1. Seahorse XF Optimisation: Cell Density and Command Protocol

Firstly, an appropriate cell density and timings for mixing, waiting and measuring were identified. Figure 3.1 and 3.2 show a representative experiment for simultaneous testing of both these factors, with ECAR and OCR responses and changes to oxygen pressure shown respectively. Changes to pH are not shown, as fluctuations were negligible. BMDMs were seeded in the microplate at the indicated densities, 24 hours prior to XF assay. DMEM was substituted for un-supplemented XF assay media (XFAM) one hour prior to assay. XFAM is similar to DMEM, however it is non-buffered, to allow accurate assessment of pH changes, as required for measuring ECAR. It also lacks sodium bicarbonate, glucose, glutamine and sodium pyruvate, allowing users to customise XFAM for individual experiments. It is recommended that serum not be added to XFAM, unless required to maintain cell viability or phenotype, as it alters XFAM buffer capacity (Agilent Technologies 2017a). Upon visual inspection, 300,000 cells/well were most confluent, therefore changes to the protocol timings were designed to restore oxygen pressure after each cycle, to the baseline seen for this density. A confluent cell monolayer was required to measure steady state metabolism, as cell aggregates cause false readings and are likely to detach during assays. It was important that the density chosen also provided a large and detectable output – raw data measurements for basal ECAR were within 2-10mpH/min and were over 100pmol/min for OCR. After measuring, baseline ECAR/OCR were restored by mixing and waiting, to avoid acidic or hypoxic conditions being formed within the microchamber. Changes to protocol timings were made after the injection point, indicated by the black vertical line in Figures 3.1 and 3.2. Equilibration of oxygen pressure was achieved, as shown for the final reading in Figure 3.2B, by an increase in wait time, from 2 to 12 minutes. Table 3.1 lists the changes made to the command protocol timings, during the representative assay shown for Figure 3.1 and 3.2. Amendments were also made to mix timings, however this did not effectively improve equilibration of oxygen pressure. The results also suggest that 500,000 cells/well metabolised too rapidly in this system, and that timings would need to be considerably increased to re-equilibrate the baseline oxygen pressure in the media. Therefore, to prevent long run times and maintain low costs, the cell densities of 200,000 and 300,000 cells/well were deemed more suitable.

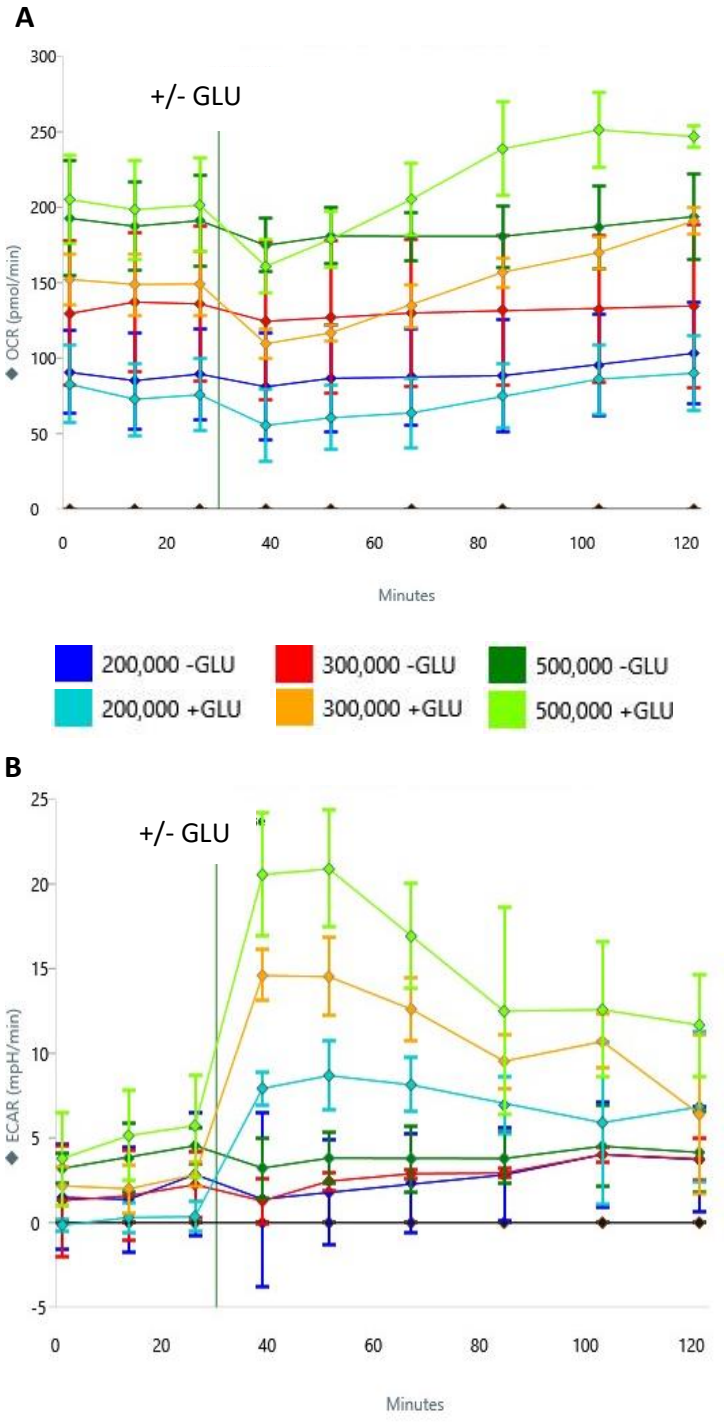

Figure 3.1: Seahorse optimisation - Cell density and command protocol (1)

A representative OCR (A) and ECAR (B) plot during optimisation of cell density and command protocol timings. BMDMs were cultured for 14 days prior to reseeding into the XF microplate at the different cell densities indicated. XFAM was injected during the assay, either with or without glucose (GLU, 10mM). This experiment aimed to identify the optimal cell number for measurements, with the opportunity to find suitable timings for BMDM assays. Data represents mean of 3-4 experimental repeats ±SD. Representative of n=3.

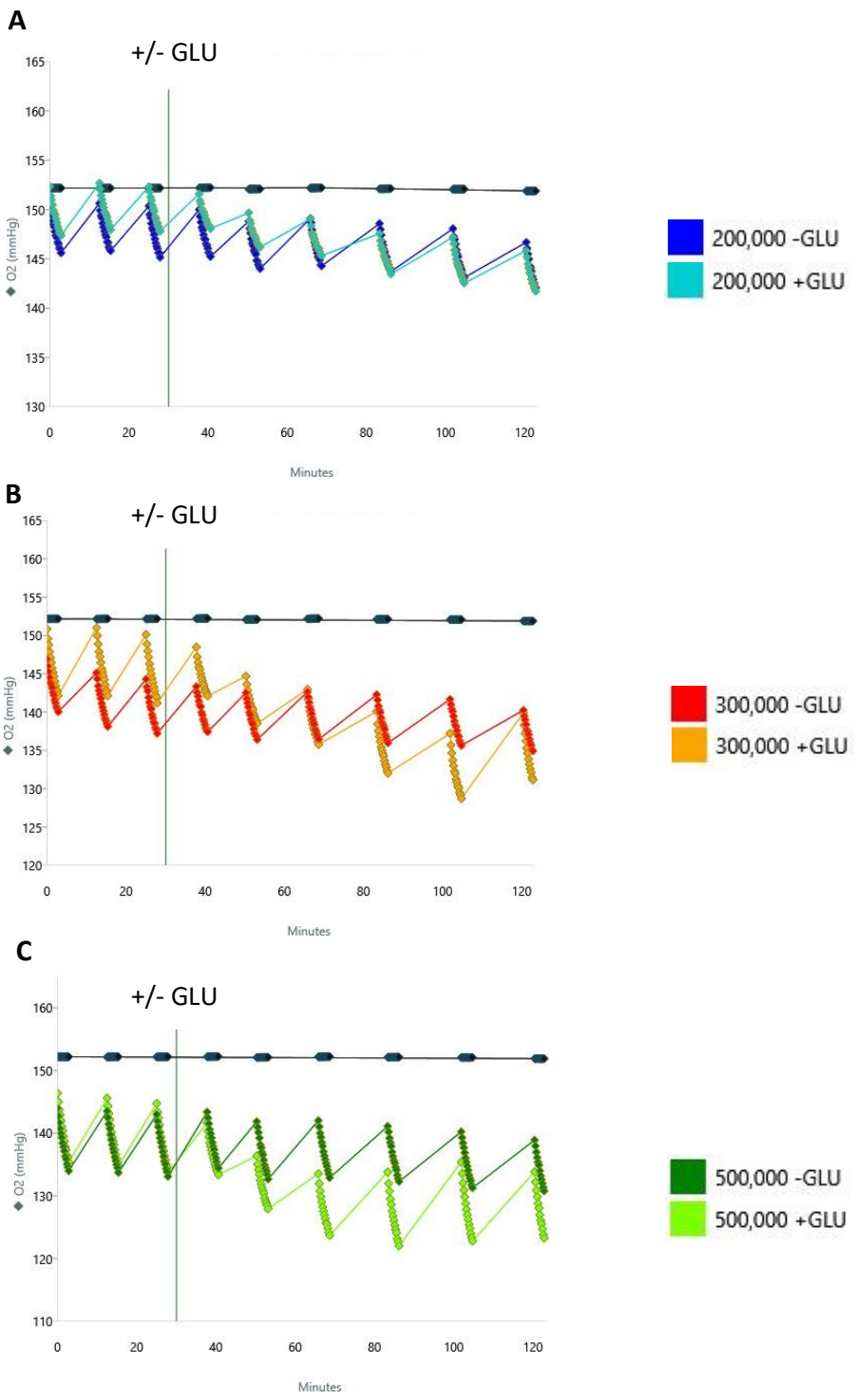

Figure 3.2: Seahorse optimisation - Cell density and command protocol (2)

Representative oxygen pressure changes, during optimisation of cell density and command protocol timings. BMDMs were cultured for 14 days prior to reseeding into the XF microplate at three cell densities: (A) 200,000 cells/well; (B), 300,000 cells/well; (C) 500,000 cells/well. XF media was injected during the assay, with or without glucose (GLU, 10mM). The experiment aimed to identify which cell number would give optimal outputs, and to provide an opportunity to find suitable timings for a BMDM assay. Changes to protocol timings aimed to restore oxygen pressure to the original baseline for 300,000BMDMs/well stimulated with glucose, compared to unstimulated cells. This was achieved by the final cycle, as seen in (B). Coloured circles indicate measuring points and coloured lines indicate the mixing and waiting periods. The bold black line indicates atmospheric oxygen pressure within the XF analyser. Data represent mean summary of 3-4 experimental replicates. Representative of n=3.

Cycle (post-injection)	Mix (min)	Wait (min)	Measure (min)
1	3	6	3
2	3	6	3
3	4	8	3
4	4	10	3
5	3	12	3
6	3	12	3

Table 3.1: Seahorse optimisation – Command protocol timings

An example of the changes made to the command protocol timings during optimisation stages. These timings are taken from the representative data plots shown in Figures 3.1 and 3.2. Protocol timings are shown for the six cycles following the glucose injection. (min = minutes). Representative of n=1.

One final test was conducted, to confirm the suitability of 200,000 cells/well and the timings stated in Table 3.1. This time, however, XFAM contained 25mM D-glucose in solution, as opposed to the 10mM injection. This higher concentration of glucose was used to culture BMDMs from initial harvest through to experimental use, therefore it was considered a more suitable concentration than the Agilent recommendation of 10mM. The result is shown in Figure 3.3. The assay verified that 200,000 cells/well was enough to provide a measurable reading for both ECAR and OCR. The assay also highlighted a slight increase and possible artefact in ECAR, following glucose injection into glucose-containing XFAM. This could be due to a variation in pH or temperature in the injection port, or alternatively a small increase in glycolysis after addition of more glucose. To eliminate potential changes to pH after injection, all compounds were injected into blank wells and used for background correction in subsequent assays.

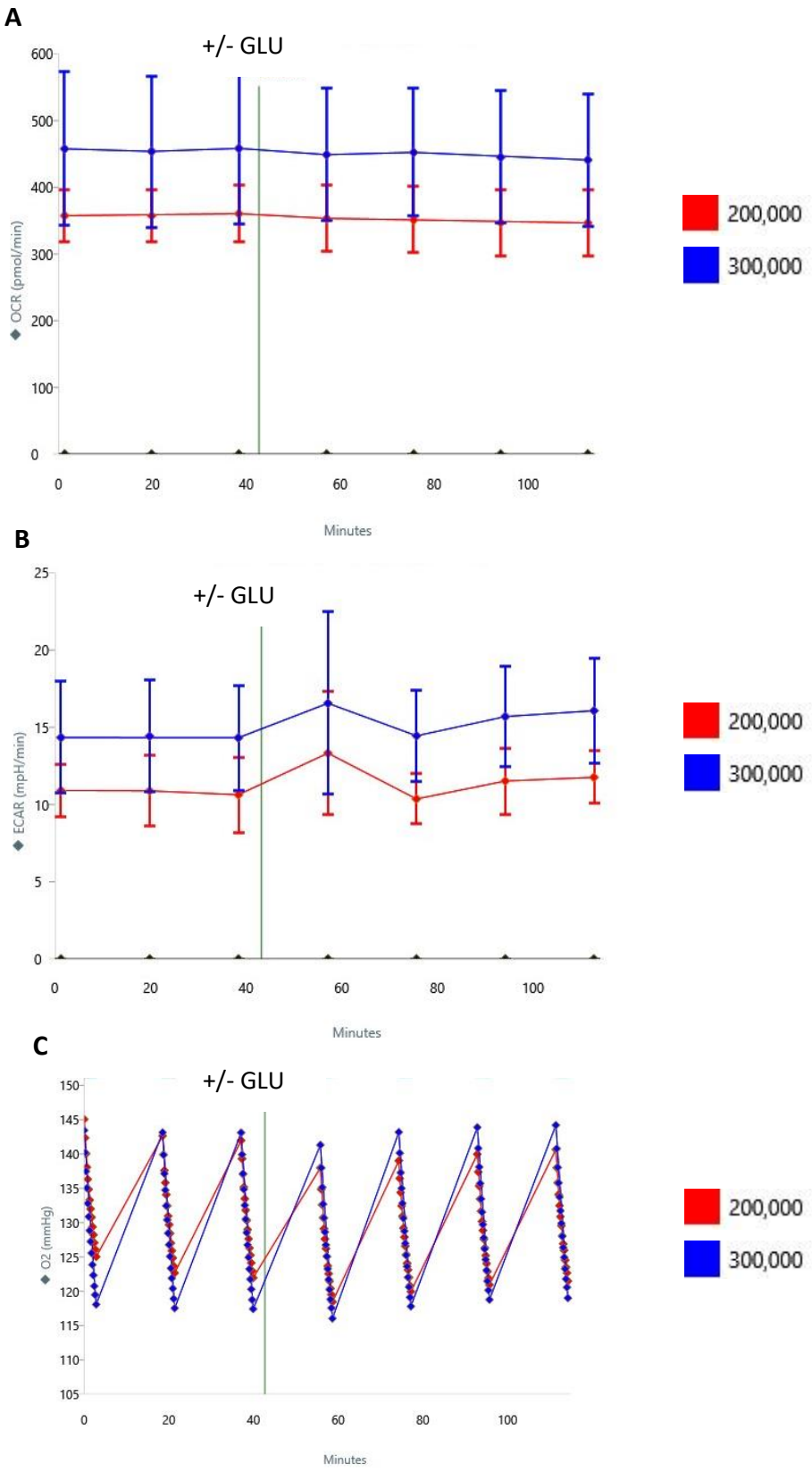

Figure 3.3: Seahorse optimisation - Protocol confirmation

BMDMs were cultured for 14 days and reseeded at either 200,000 or 300,000 cells/well, with metabolic responses to a single glucose stimulus assessed using the XF Analyser. A representative OCR plot (A), ECAR plot (B) and oxygen pressure changes (C) are shown. XF media contained 25mM D-Glucose and the vertical line on all graphs indicates the glucose injection (GLU, 25mM). Data in (A) and (B) represent mean ±SD of up to ten experimental replicates. Data in (C) represent measuring points (coloured circles), linked by mixing and waiting times (coloured lines). Representative of n=1

3.2.2. Seahorse XF Optimisation: Inhibitor Concentrations

Prior to using the XF Analyser with BMDMs, suitable concentrations were identified for inhibitors used in the XF assay kits. Inhibitors were tested at a range of concentrations, to achieve a maximal change in metabolic output, with the explicit ECAR and OCR changes for each inhibitor noted. The Glycolysis Stress Test recommends sequential injection of glucose, followed by Oligomycin A (Oligo) and then 2-Deoxyglucose (2DG). The first injection is a concentration of glucose, which saturates the cells, prompting them to utilise glucose and begin glycolysis at a basal metabolic rate. Oligo is an ATP Synthase inhibitor that prevents mitochondrial ATP production, causing a backlog stress on the electron transport chain, and shifting energy production from respiration to glycolysis. The inhibitor therefore causes a maximal increase in glycolysis, to indicate the glycolytic capacity of the cells. This inhibitor is also used in the Mito Stress Test to cause maximal inhibition of respiration. Lastly, 2DG is an analogue of glucose, which enters cells and competitively inhibits both Hexokinase and Phosphoglucose Isomerase, the first two enzymes of glycolysis. This halts glycolytic activity, allowing indication of non-glycolytic acidifications. By using this combination of inhibitors, the assay measures glycolytic activity under stress, allowing basal glycolysis, glycolytic capacity, the glycolytic reserve, and non-glycolytic acidification of cells to be calculated from ECAR results - as previously shown in Figure 1.5.

To identify a suitable concentration of Oligo, for use with 200,000 cells/well and the corresponding protocol timings, concentrations ranging between 0.5-2.5µM were tested, as shown in Figure 3.4. XFAM was supplemented with 25mM D-Glucose, to reduce the running time of the Analyser whilst mimicking the glucose-containing environment into which Oligo would be injected. Results were not normalised to cell number or protein content during these inhibitor optimisation assays, which could indicate why error bars remain quite large for the 'Oligo NIL' group. Here, the most appropriate inhibitor concentration was selected after repeat assays and by identifying the lowest concentration to induce the greatest increase in ECAR – also associated with a reciprocally large decrease in OCR. A working concentration of 1µM was chosen, which correlated with concentrations previously seen for similar cells in the literature and also recommended by Agilent Technologies (Covarrubias et al. 2016; Seahorse Bioscience & Agilent Technologies 2016)

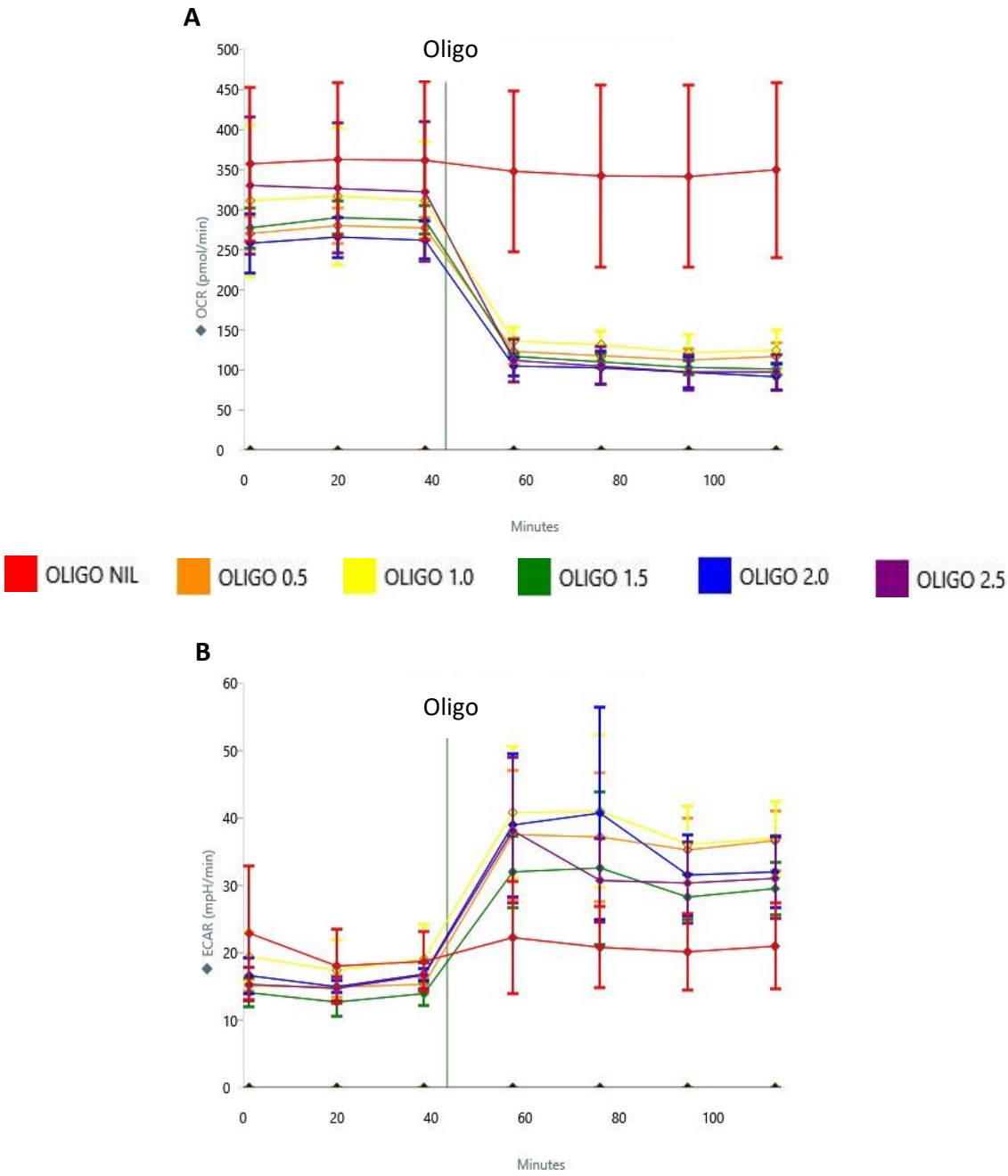

Figure 3.4: Seahorse optimisation – Oligomycin A (Oligo) concentration

A representative OCR plot (A) and representative ECAR plot (B) of BMDMs, following injection with Oligo concentration range of 0.5-2.5µM. BMDMs were grown for 14 days prior to reseeding for XF Analysis, at $2x10^5$cells/well. Assessment of ECAR and OCR responses of BMDMs, at a range of concentrations, helped to identify the optimal Oligo concentration. The ideal concentration should induce the greatest increase in ECAR, associated with a major decrease in OCR. Assay media used was XF DMEM supplemented with 25mM D-Glucose. The optimal, lowest Oligo concentration was 1.0µM. Data represent mean ±SD for 3-4 experimental replicates. Representative of n=3

To identify a suitable concentration of 2DG, concentrations ranging between 50-200mM were tested, as shown in Figure 3.5. XFAM was supplemented with 25mM D-Glucose, and the 2DG injection preceded by an Oligo injection - as would be the case during a Glycolysis Stress Test. Once again, the results here were not normalised to protein content and the optimal concentration was chosen by inspecting the data after repeat experiments, to identify the lowest concentration to produce the largest decrease in ECAR. The chosen working concentration for 2DG was 100mM. Seahorse specialists and colleagues, who had previously used the XF Analyser to study immune cells, also recommended this concentration at the time, and it had been used at this concentration in the literature (Na et al. 2015). However, Agilent have since recommended 50mM working concentration for 2DG rather than 100mM (Seahorse Bioscience Inc. 2012; Seahorse Bioscience & Agilent Technologies 2016).

The optimal conditions for XF Analysis of BMDMs are listed in Table 3.2.

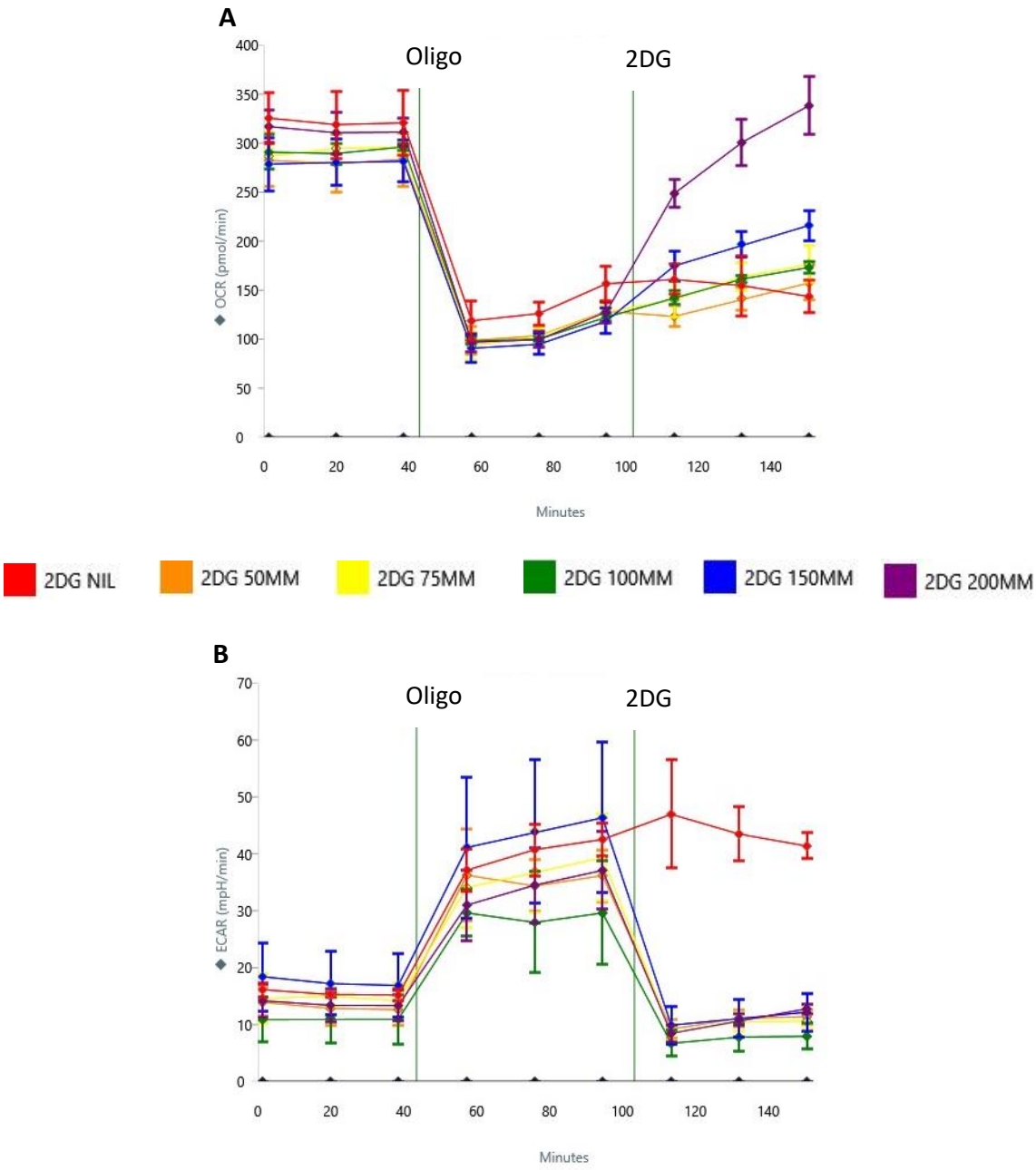

Figure 3.5: Seahorse optimisation – 2-Deoxyglucose (2DG) concentration

A representative OCR plot (A) and representative ECAR plot (B) of BMDMs, following injection with 2DG concentration range of 50-200mM. BMDMs were grown for 14 days prior to reseeding for XF analysis, at $2x10^5$cells/well. The ideal concentration would dramatically reduce ECAR after Oligo stimulation (1µM). Assay media was supplemented with 25mM D-Glucose. The optimal, lowest 2DG concentration was identified as 100mM. Data represent mean ±SD for 3-4 experimental replicates. Representative of n=3

	Glycolysis Stress Test	Mito Stress Test
Inhibitors: *(Working concentrations - must be made up 10-fold higher for injection ports):*	*Glucose (25mM) Oligomycin (1µM) 2DG (100mM)	Oligomycin (1µM) FCCP (2µM) Rotenone (1µM) and Antimycin A (1µM)
XFAM *supplemented with:*	*Glucose (25mM) L-Glutamine (2mM) **Penicillin (50U/ml) **Streptomycin (50µg/ml)	Glucose (25mM) L-Glutamine (2mM) Sodium Pyruvate (1mM) **Penicillin (50U/ml) **Streptomycin (50µg/ml)
Injection port volumes:	A – 70µl B – 77µl C – 85µl D – 94µl	
Timings	Mix – 3 minutes Wait – 12 minutes Measure – 3 minutes	
Cell Density	200,000 cells/well (Detach and re-suspend cells $2x10^6$/ml, then use 100µl/well for optimal coverage without clumping)	

Table 3.2: Summary of optimal Seahorse XF analyser conditions for BMDMs

Table summarises optimal conditions, required for using BMDM cell cultures in the Seahorse XF Analyer. *Glucose injection can be omitted and replaced with glucose supplemented in XFAM (NB. Do not require both); **Antibiotics can be added; to ensure no extracellular bacteria are present after live bacterial challenge. Alternatively antibiotic treatment can occur prior to assay, and remain omitted from XFAM.

3.2.3. Real-time effect of heat-killed *S. pneumoniae* on glycolytic metabolism of BMDMs

After optimising the XF protocol, BMDMs were assessed for their responses to different stimuli, using the Glycolysis Stress Test. This experiment aimed to see whether cells responded to *S. pneumoniae* by increasing their glycolytic rate after a one hour stimulation, compared to responses induced by LPS and IL-4 – stimuli that induce CAM and AAM phenotypes respectively (Van den Bossche et al. 2015).

Heat-killed (HK)-*S. pneumoniae* was used as this would interact with cells, without contributing to metabolic outputs. The experiment was set-up using injection ports in the sensor cartridge plate, with stimulants and inhibitors injected within the machine and changes assessed directly over the experimental time course. The injection ports followed the sequence: Port A: stimulus (see Figure 3.6 legend and graph key for details), Port B: glucose (25mM working concentration), Port C: Oligo (1µM working concentration) and Port D: 2DG (100mM working concentration). Figure 3.6 shows a representative ECAR plot of this set-up, with post-stimulation and glycolytic basal rates calculated from measurements immediately before the glucose, and immediately before the Oligo injections respectively. From this, it appears that LPS increased glycolytic metabolism within just one hour of stimulation, compared to mock-stimulated BMDMs, although this was not found to be statistically significant. HK-*S. pneumoniae* also did not induce any significant changes. Additionally, Oligo is used to provoke increased glycolytic capacity of cells and help metabolic profiling of cells, as demonstrated in Figure 1.5B. However, in these experiments it did not produce the desired effect on ECAR, after glucose injection.

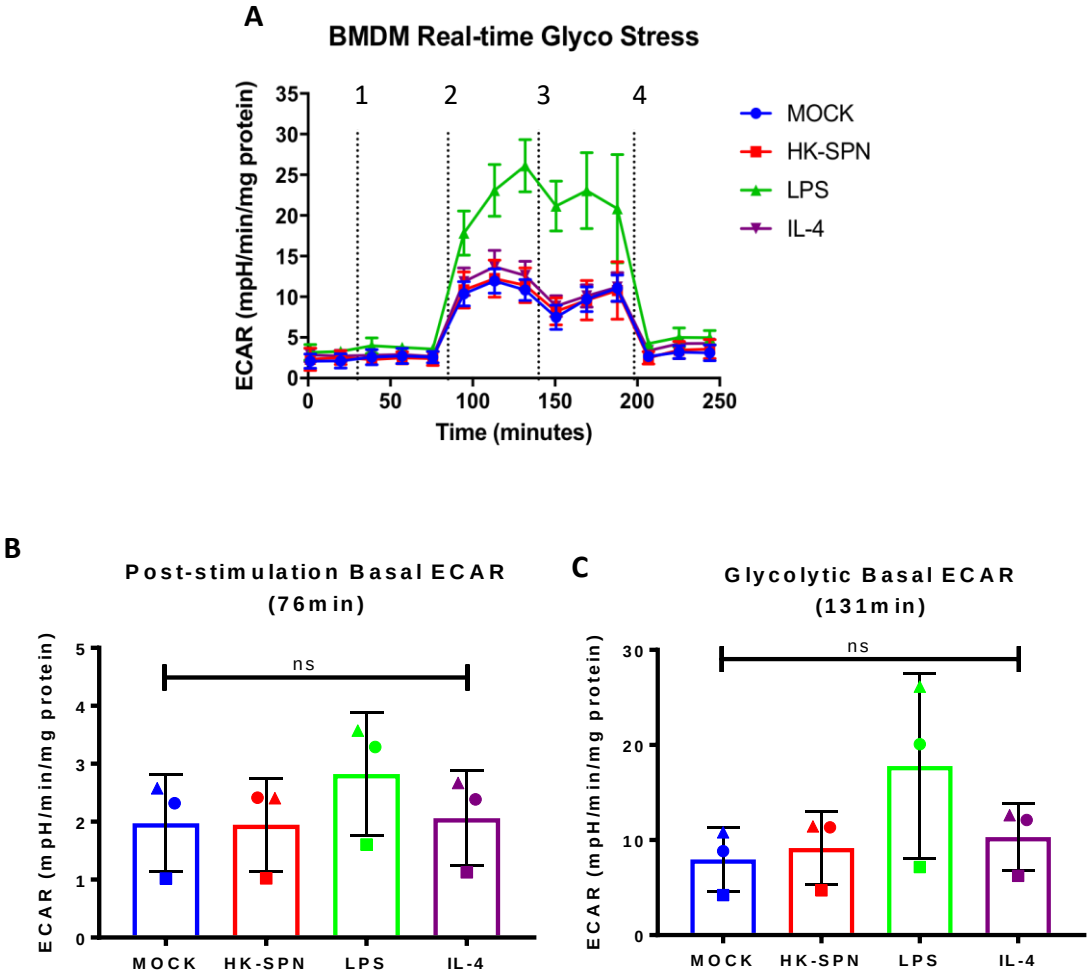

Figure 3.6: Glycolysis Stress Test – Real-time (1hr) BMDM stimulation

BMDMs were cultured for 14 days prior to seeding for XF Analysis at $2x10^5$cells/well. Media was replaced with XFAM, and stimuli injected using the XF Analyser apparatus. A representative and normalised ECAR plot (A) is shown, with a reciprocal key. Injection points are indicated by the dotted lines, and in the following order: 1=Stimulus (as shown in key: HK-SPN, D39 at MOI 10, LPS at 100ng/ml, IL-4 at 10ng/ml), 2=Glucose (25mM), 3=Oligomycin A (1µM), 4=2DG (100mM); Post-stimulation basal ECAR (B) and glycolytic basal ECAR (C) are shown, as taken from the 76th and 131st minutes of the experiment, to correlate with immediately before the glucose and oligomycin injections respectively. A one-way ANOVA with Dunnett's multiple comparisons calculated no significance (ns) compared to the mock condition. Each donor is indicated by a different shape and is the mean value of 4-5 experimental replicates; Representative of biological n=3. (HK-SPN = heat-killed D39 *S. pneumoniae*)

3.2.4. Re-optimisation of Oligo and Glucose for Glycolysis Stress Test

To test for discrepancies after Oligo stimulation, different concentrations of Oligo and glucose were tested, to see if these concentrations and/or stocks were still appropriate. The results of these experiments can be found in Figures 3.7 and 3.8. First, concentrations of Oligo between 1-10µM, after a preliminary 25mM glucose injection, were trialled to see if this would help stimulate an increased shift from respiration to glycolysis. Regardless of the Oligo concentration used, ECAR was not increased further than the original 1µM concentration. Secondly, lower concentrations of glucose, between 5-25mM, were trialled to prevent overwhelming the cells with glucose and to test whether this could reduce their basal glycolytic rates, leaving greater opportunity to increase the subsequent capacity with Oligo. There appeared to be a small concentration-dependent change in the glycolytic rate, with decreased glycolysis seen for lower glucose concentrations; however, this same pattern remained after Oligo injection, with low glucose availability diminishing the total measurable metabolic shift. The original Oligo concentration of 1µM was therefore still deemed suitable.

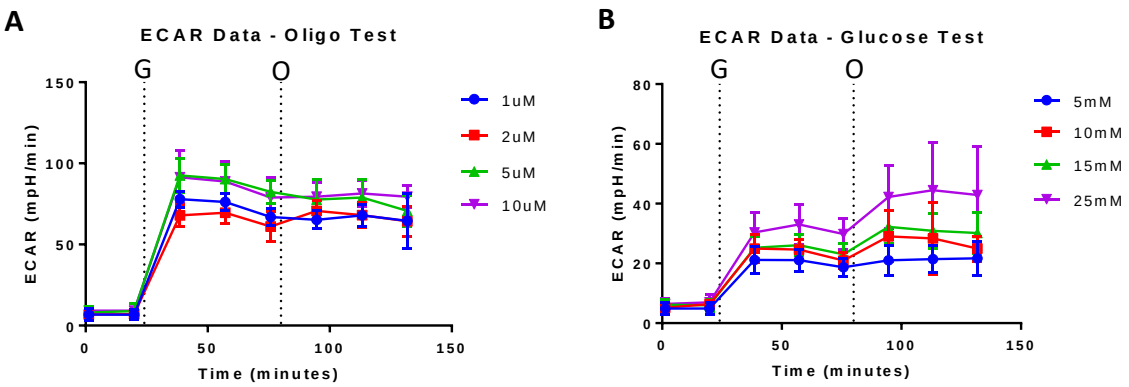

Figure 3.7: Glycolysis Stress Test – Re-optimisation of Oligo usage

(A) BMDMs were cultured for 14 days prior to seeding for XF Analysis at $2x10^5$cells/well. Media was replaced with XFAM supplemented with 2mM L-glutamine. Glucose (G; 25mM) and oligomycin (O; 1-10µM, see key) were added using the injection ports, indicated by the dotted lines respectively. Figures represent raw data, as protein normalisation was not used. n=1

(B) BMDMs were cultured for 14 days prior to seeding for XF Analysis at $2x10^5$cells/well. Media was replaced with XFAM supplemented with 2mM L-glutamine. Glucose (G; 5-25mM, see key) and Oligo (O; 1µM) were added using the injection ports, as indicated by the dotted lines respectively. Figures represent raw data, as protein normalisation was not used. n=1

Following this, an alternative Oligo stock was tested to see: 1) if this new stock would consistently increase glycolytic capacity after glucose injection and 2) whether there were differences in sensor cartridge port loading for Oligo or solubility in XFAM. Figure 3.8A shows the changes seen across the plate, as separated by plate row and Oligo loading order (rows loaded chronologically, 1→4). This secondary Oligo stock did work effectively, although there were slight differences after Oligo stimulation, depending on how this was loaded in the cartridge plate. That said, as there was no normalisation to protein content after this experiment, these variances could primarily be due to differences in cell number rather than the effect of the compound. From this experiment onwards, the secondary Oligo stock was used. The final experiment shown in Figure 3.8B shows a test run of the new stock, used to measure the glycolytic capacities of cells following mock-stimulation, *S. pneumoniae*-challenge, or stimulation with IL-4 or LPS for 4 hours. Despite attempts to re-optimise this protocol, the Oligo did not induce the desired effect. It was hypothesised here that cells had metabolised maximally after the glucose injection and that this could not be pushed further with Oligo treatment; therefore from here on, the glucose was no longer injected as a stimulus, but was instead added to the XFAM, to improve output measures and further reduce time on the analyser.

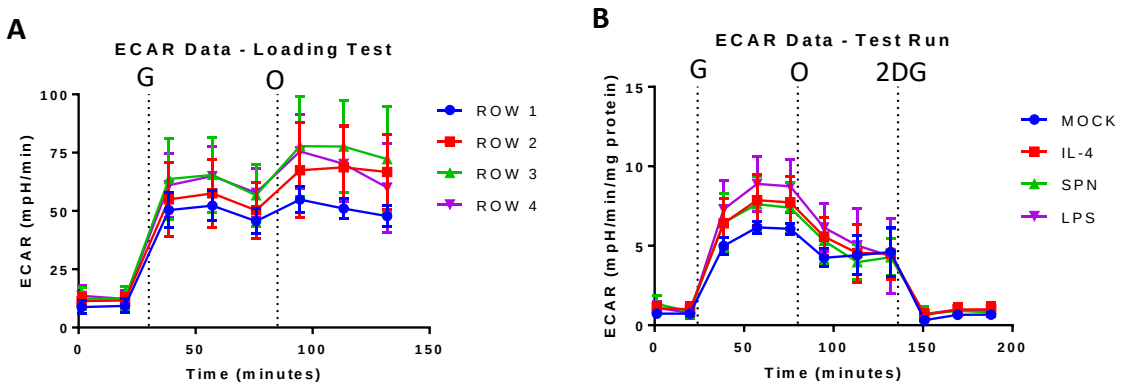

Figure 3.8: Glycolysis Stress Test – Re-optimisation of Oligo usage, with new stock

(A) Experimental set-up was as described for Figures 3.7A-B, with glucose (25mM) and oligomycin (1µM) injected by the dotted lines respectively. However, a different oligo stock was used and groups here indicate the rows of the cell microplate, to reveal any differences caused by loading order. Figures represent raw data, as protein normalisation was not used. n=1
(B) BMDMs were cultured for 14 days prior to seeding for XF Analysis at $2x10^5$cells/well. Cells were infected/stimulated for 4hrs (as per key: IL-4 =interleukin-4 (10ng/ml); SPN = D39 *S. pneumoniae* MOI 10; LPS = 100ng/ml), treated with penicillin and gentamycin to kill extracellular bacteria, washed with PBS, and XFAM supplemented with 2mM L-glutamine was added. Injection ports are indicated by the dotted line, containing glucose (25mM), oligomycin (1µM, new stock) and 2DG (100mM) in this order. Data was normalised to protein content. n=1 (G = glucose; O = oligomycin; 2DG = 2-deoxyglucose)

3.2.5. Glycolysis Stress Test – Glycolytic changes after 4 hour bacterial challenge

Using the amended Glycolysis Stress Test, with glucose in the XFAM as opposed to the first injection port, BMDMs were assessed for differences in basal and maximal glycolytic rates, following 4 hours mock-stimulation, live *S. pneumoniae* challenge, IL-4- or LPS-stimulation. The results of these experiments are displayed in Figure 3.9. Upon initial inspection of the ECAR data plots, it seemed that LPS and *S. pneumoniae* increased glycolysis in BMDMs, compared to mock-stimulation; however, the results in Figure 3.9 suggest there were no statistically significant changes between these groups after 4 hours stimulation. Interestingly, this contradicts findings previously shown in Figure 3.6, which suggest that LPS induces an increase in glycolytic metabolism after one hour. One cause of this discrepancy could be in the experimental design: in previous assays, LPS was injected, without any media changes or disruptions; however, assays involving live bacterial infections were treated with antibiotics prior to performing the XF assay and therefore required prior preparation. Additionally, there were differences in the XFAM, as glucose was supplemented during these experiments with live bacteria. Additionally, macrophage metabolism is very plastic, and any induced changes in glycolytic metabolism by these stimuli could have been reversed – or overwritten – by the subsequent media changes and delay in assaying this model.

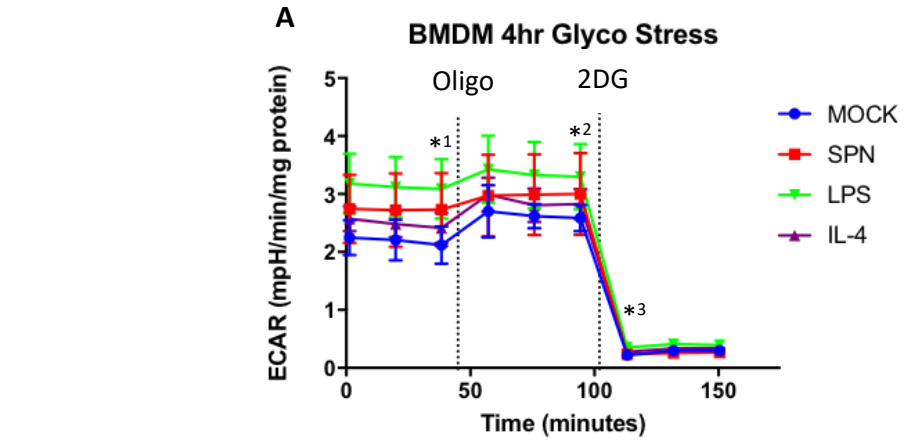
A
BMDM 4hr Glyco Stress
Oligo
2DG
*1
*2
*3
ECAR (mpH/min/mg protein)
Time (minutes)
MOCK
SPN
LPS
IL-4

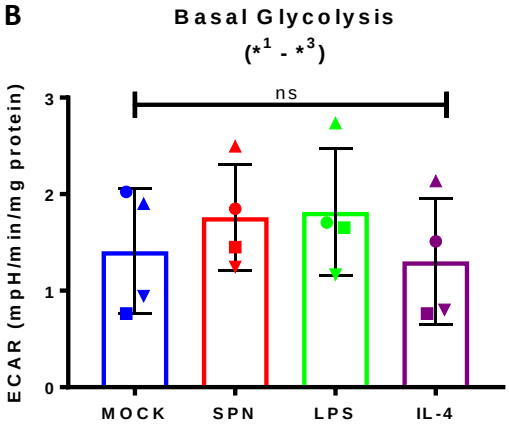
B
Basal Glycolysis
(*1 - *3)
ns
ECAR (mpH/min/mg protein)
MOCK
SPN
LPS
IL-4

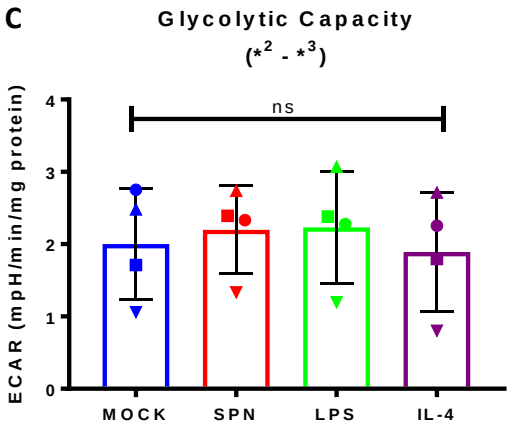
C
Glycolytic Capacity
(*2 - *3)
ns
ECAR (mpH/min/mg protein)
MOCK
SPN
LPS
IL-4

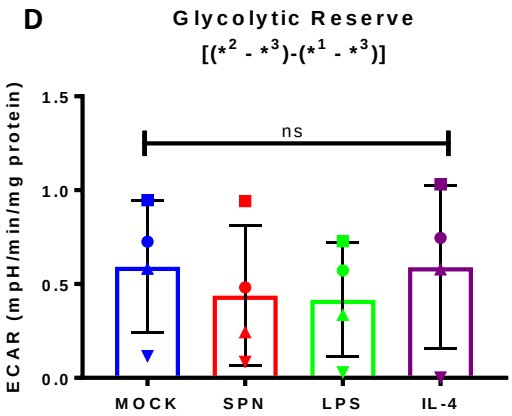
D
Glycolytic Reserve
[(*2 - *3)-(*1 - *3)]
ns
ECAR (mpH/min/mg protein)
MOCK
SPN
LPS
IL-4

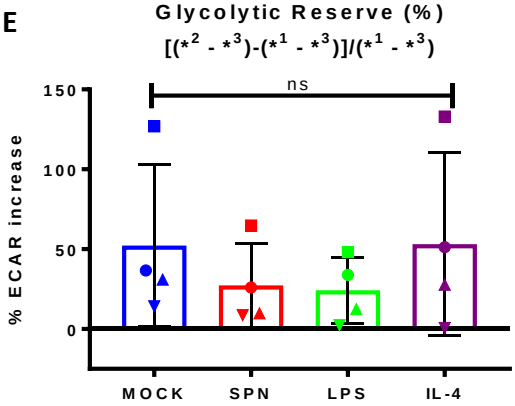
E
Glycolytic Reserve (%)
[(*2 - *3)-(*1 - *3)]/(*1 - *3)
ns
% ECAR increase
MOCK
SPN
LPS
IL-4

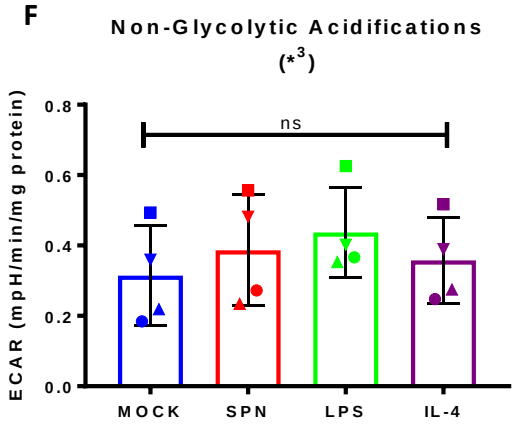
F
Non-Glycolytic Acidifications
(*3)
ns
ECAR (mpH/min/mg protein)
MOCK
SPN
LPS
IL-4

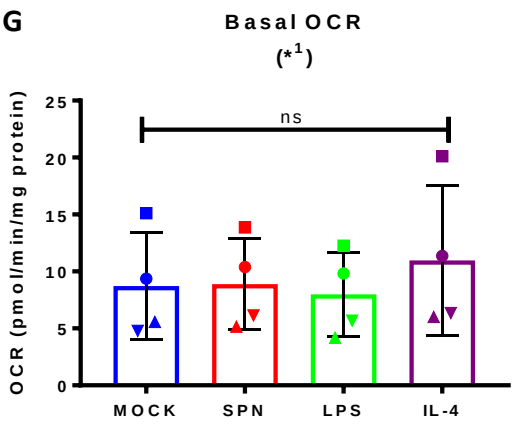
G
Basal OCR
(*1)
ns
OCR (pmol/min/mg protein)
MOCK
SPN
LPS
IL-4

Figure 3.9: Glycolytic Stress Test – 4 hour bacterial challenge of BMDMs

A) A representative ECAR profile of four experiments. BMDMs were cultured for 14 days prior to seeding for XF Analysis at $2x10^5$cells/well. Cells were infected/stimulated for 4hrs (as per key: IL-4 = interleukin-4 (10ng/ml); SPN = D39 *S. pneumoniae* MOI 10; LPS = 100ng/ml), treated with penicillin (40U/ml) and gentamycin (20ug/ml) to kill extracellular bacteria, washed with PBS, and XFAM supplemented with 2mM L-glutamine and 25mM D-glucose was added. Injection ports are indicated by the dotted lines, containing oligomycin (Oligo; 1µM) and 2DG (2DG; 100mM) respectively. Results were normalised to total protein content, which was collected for every well and assayed for after XF analysis. B) - G) Calculated values from four independent biological repeats, as follows (* indicate points represented in 3.8A):
Basal Glycolysis = Basal ECAR ($*^1$) – Non-Glycolytic Acidifications ($*^3$)
Glycolytic Capacity = Maximal ECAR ($*^2$) – Non-Glycolytic Acidifications ($*^3$)
Glycolytic Reserve = Glycolytic Capacity ($*^2$ - $*^3$) – Basal Glycolysis ($*^1$ - $*^3$)
Glycolytic Reserve % = ((Glycolytic Capacity – Basal Glycolysis)/Basal Glycolysis)*100
Non-Glycolytic Acidifications = Immediately after 2DG ($*^3$)
Basal OCR = Immediately before Oligo ($*^1$)
Statistics calculated using One-way ANOVA with Tukey's multiple comparisons. Data represent mean summary of 5 experimental replicates. Representative of biological n=4; different shapes indicate different donors.

3.2.6. Glycolysis Stress Test – Glycolytic changes after 12 hour bacterial challenge

To further study the glycolytic responses exhibited by BMDMs during live *S. pneumoniae* challenge, a later 12 hour time point was assayed. These results are shown in Figure 3.10. The representative ECAR plot in Figure 3.10A shows a distinction between the basal glycolysis of LPS-stimulated and *S. pneumoniae*-challenged cells, compared to the mock-infected group. However, no statistical significance was found for basal glycolysis of *S. pneumoniae*-challenged cells, compared to the mock. Furthermore, the percentage glycolytic reserve - the difference between basal and maximal glycolytic rates - was reduced in both LPS-stimulated and *S. pneumoniae*-challenged cells, suggesting that BMDMs may only have a finite inducible capacity for glycolysis. Another interesting observation is shown in Figure 3.10F, whereby 12 hours LPS-stimulation or bacterial challenge increased non-glycolytic acidifications – that being acidic pH changes not contributed by increased glycolysis, and the production of lactate and H^+. It is difficult to stipulate what might have caused this, but it indicates that an acidic environment and/or intracellular change could influence BMDM metabolism. Finally, basal OCR was assessed and there were no significant differences between groups, suggesting that respiration remains unchanged after this time.

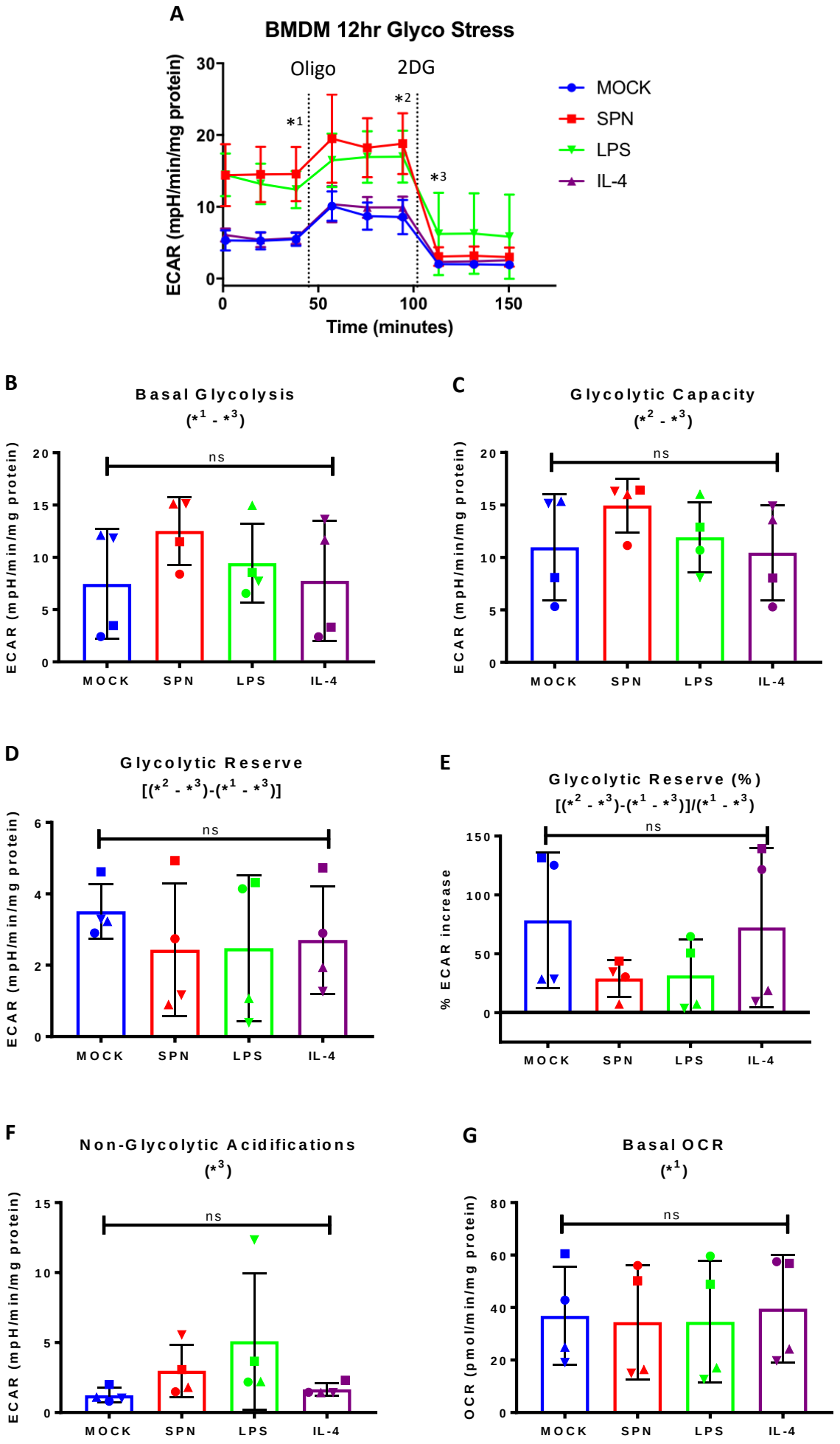
A
BMDM 12hr Glyco Stress
Oligo
2DG
*1
*2
*3
ECAR (mpH/min/mg protein)
Time (minutes)
MOCK
SPN
LPS
IL-4
B
Basal Glycolysis
(*1 - *3)
C
Glycolytic Capacity
(*2 - *3)
D
Glycolytic Reserve
[(*2 - *3)-(*1 - *3)]
E
Glycolytic Reserve (%)
[(*2 - *3)-(*1 - *3)]/(*1 - *3)
% ECAR increase
F
Non-Glycolytic Acidifications
(*3)
G
Basal OCR
(*1)
OCR (pmol/min/mg protein)
ns

Figure 3.10: Glycolysis Stress Test – 12 hour bacterial challenge of BMDMs

A) A representative ECAR profile of four experiments. BMDMs were cultured for 14 days prior to seeding for XF Analysis at $2x10^5$cells/well. Cells were infected/stimulated for 4hrs (as per key: IL-4 =interleukin-4 (10ng/ml); SPN = D39 *S. pneumoniae* MOI 10; LPS = 100ng/ml). Cells were then treated with penicillin (40U/ml) and gentamycin (20ug/ml) to kill extracellular bacteria, washed with PBS and culture media +/- LPS/IL-4 was replaced until 12hr post-stimulation. Cells were washed in PBS and XFAM supplemented with 2mM L-glutamine added and 25mM D-glucose. Injection ports are indicated by the dotted lines, containing oligomycin (Oligo; 1μM) and 2DG (2DG; 100mM) respectively. Results were normalised to total protein content, which was collected and assayed for every well.
B) - G) Calculated values from four independent biological repeats, as follows (* indicate points represented in 3.8A):
Basal Glycolysis = Basal ECAR ($*^1$) – Non-Glycolytic Acidifications ($*^3$)
Glycolytic Capacity = Maximal ECAR ($*^2$) – Non-Glycolytic Acidifications ($*^3$)
Glycolytic Reserve = Glycolytic Capacity ($*^2$ - $*^3$) – Basal Glycolysis ($*^1$ - $*^3$)
Glycolytic Reserve % = ((Glycolytic Capacity – Basal Glycolysis)/Basal Glycolysis)*100
Non-Glycolytic Acidifications = Immediately after 2DG ($*^3$)
Basal OCR = Immediately before Oligo ($*^1$)
Statistics calculated using One-way ANOVA with Tukey's multiple comparisons. Data represent mean summary of 5 experimental replicates. Representative of biological n=4; different shapes indicate different donors.

3.2.7. Mito Stress Test to study human monocyte-derived macrophage metabolic responses to pneumococcal challenge

Following earlier work in this chapter on murine BMDMs, the XF procedure was used to consider a human cell model of infection. For this, collaboration was made with PhD student Joby Cole, who was also part of the Dockrell research group. The research question addressed 'tolerisation' of human monocyte-derived macrophages (MDMs) and how this could affect respiratory metabolism during *S. pneumoniae* challenge. Here, the Mito Stress Test was used, which had been optimised for use with human cells, in collaboration with a third Dockrell PhD student, MD Mohasin.

The aim of this experiment was to address the respiratory modifications in MDMs, following 24 hour pre-treatment, or 'tolerisation', with either LPS or heat-killed *S. pneumoniae*, and to assess how this influenced MDM respiratory metabolism when followed by a live 4 hour *S. pneumoniae* challenge. The results of these experiments are shown in Figure 3.11. Whilst no statistically significant differences are seen for any of the calculated measures shown, there are still some interesting trends in this data. For example, the basal and maximal respiration rates of MDMs are lower after encountering bacteria, regardless of whether their exposure involved heat-killed or live *S. pneumoniae*. This may suggest that MDMs shift their mitochondrial functioning away from respiration, upon contact with bacteria, and potentially towards other functions, for example the production of ROS (Liemburg-Apers et al. 2015). The results of Figure 3.11G are also very interesting: whilst MDM contact with bacteria produced a trend of increased Basal ECAR, a 24 hour tolerisation with LPS did not. This contrasts with the published literature and results shown previously in Figure 3.10. Despite this, it could be proposed that increases in ECAR after bacterial challenge are sustained for longer periods, compared to stimulation with LPS. There was also no difference in ECAR or OCR for tolerised cells with *S. pneumoniae* challenge, suggesting that these different stimuli do not induce a lasting influence on metabolism that could be observed after bacterial infection.

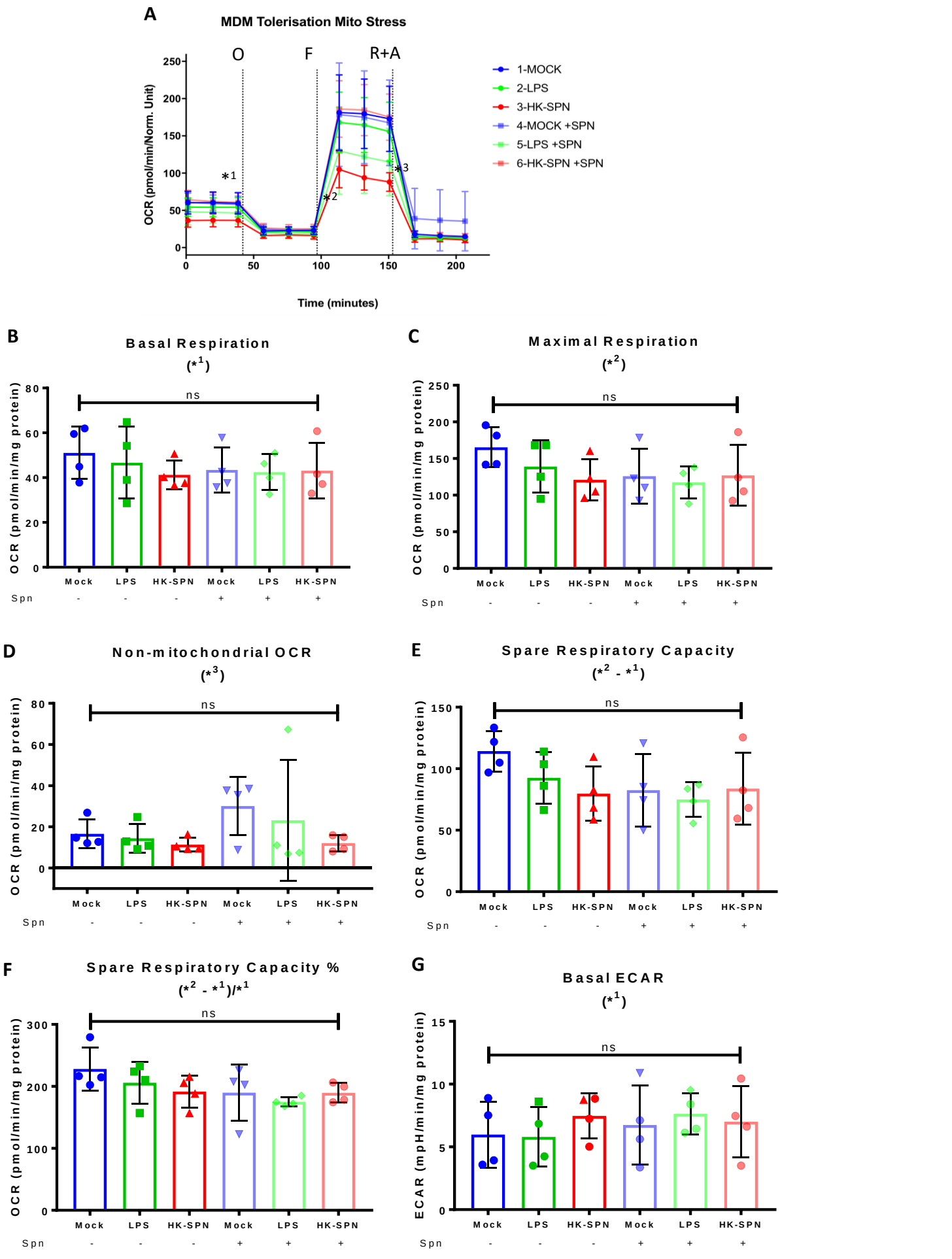
A
MDM Tolerisation Mito Stress
O
F
R+A
OCR (pmol/min/Norm. Unit)
Time (minutes)
1-MOCK
2-LPS
3-HK-SPN
4-MOCK +SPN
5-LPS +SPN
6-HK-SPN +SPN
*1
*2
*3
B
Basal Respiration
(*1)
C
Maximal Respiration
(*2)
D
Non-mitochondrial OCR
(*3)
E
Spare Respiratory Capacity
(*2 - *1)
F
Spare Respiratory Capacity %
(*2 - *1)/*1
G
Basal ECAR
(*1)
OCR (pmol/min/mg protein)
ECAR (mpH/min/mg protein)
ns
Mock
LPS
HK-SPN
Spn

Figure 3.11: Mito Stress Test in tolerised MDMs

A) Representative OCR profile of four MDM Mito Stress experiments. MDMs were cultured for fourteen days, prior to reseeding at 200,000 cells/well for XF analysis. Cells were tolerised as per the key for 24hrs (MOCK = no stimulus; LPS = 100ng/ml; HK-SPN = heat-killed D39 *S. pneumoniae* MOI 10), then either *S. pneumoniae*-challenged (D39, MOI 10) or mock-infected for 4 hours. At this time, cells were washed 2x with XFAM, supplemented here with 25mM D-glucose, 2mM L-glutamine, 1mM Na-pyruvate, 50U/ml penicillin, 50ug/ml streptomycin and pH adjusted to 7.4 at 37°C. A final volume of 630µl XFAM was added to the plate, ready for XF assay. The injection ports, indicated by the dotted lines, contained oligomycin (O = 10µM), FCCP (F = 20µM) and Rotenone + Antimycin (R+A, both 10µM) respectively. Results were normalised to total protein content, which was collected for every well and assayed for after XF analysis.
B) - G) calculated values from four independent repeats as follows:
Basal Respiration = Basal OCR (*[1])
Maximal Respiration = Maximal OCR (*[2])
Non-mitochondrial OCR = Immediately after Rotenone + Antimycin A (*[3])
Spare Respiratory Capacity = Max OCR (*[2]) – Basal OCR (*[1])
Spare Respiratory Capacity % = ((Spare Respiratory Capacity – Basal OCR)/Basal OCR)*100
Basal ECAR = Immediately before Oligo (*[1])
No statistically significant differences were found for any measures, after One-way ANOVA with Tukey's multiple comparisons; Data represent mean summary of 3-4 experimental replicates. Representative of biological n=4;

3.3. Discussion

3.3.1. Chapter Summary

In this chapter, optimisation of the Seahorse XF Analyser has been shown, with the adjusted technique used to study glycolytic metabolism of BMDMs after *S. pneumoniae*-challenge. XF analysis has been used to study a wide range of disease models, including neurodegenerative disorders, cancer, obesity and inflammation, however, few studies have used it to look at the metabolic effects of cell cultures challenged with whole, live bacteria (Agilent Technologies 2017b). The optimisation of this technique aimed to suit the specific cell type, however many users and publications do not detail these stages, as it has been overlooked for the convenience of using standard protocols recommended by the manufacturer. This optimisation can be critical, to avoid false metabolic measurements, particularly concerning oxygen pressure and OCR readings.

The optimal cell density and protocol timings were first identified: 200,000 cells/well were shown to be effective, in combination with mix, wait, measure timings of 3, 12, 3 minutes respectively. Suitable concentrations of inhibitors for the Glucose Stress Test, Oligo and 2DG, were then identified as 1µM and 100mM respectively. Concentrations for inhibitors used in the Mito Stress Test kit, including Carbonyl cyanide-4-(trifluoromethoxy)phenylhydrazone (FCCP), Antimycin A and Rotenone were also identified, using the same experimental set-up as that seen of Oligo and 2DG. Establishing an appropriate concentration for FCCP can be critical, as it can cause loss of inner mitochondrial transmembrane potential, leading to toxicity and cell death (Gottlieb et al. 2003; Held et al. 2010). However, the Mito Stress assay was not relevant to the research aims of this thesis; therefore these have been omitted. Table 3.2 provides a summary of all the optimal conditions required for both the Glycolysis and Mito Stress Tests with BMDMs.

Optimisation of the technique was further continued after Oligo did not induce the desired effect. This could have been because cells were already working maximally after glucose injection, and it was not feasible to increase this further. A second plausible theory could be that macrophages were starved of glucose prior to the injection, during both XFAM equilibration and initial XF analysis; therefore cutting off the glucose supply for prolonged periods and suddenly returning it could affect the outcome of this assay,

as macrophages are highly reliant on glycolysis when differentiating or converting to a CAM phenotype (Suzuki et al. 2016; Kelly & O'Neill 2015). Furthermore, preliminary Oligo optimisations were carried out with glucose present in the XFAM, as opposed to being injected, which may also change the expected outcome. Finally, there could have been technical problems with the Oligo stock itself. Oligo solubility might have influenced the assay, with loading of this compound varying between injection ports. This could be caused by the compound dropping out of solution upon dilution into a different solute, or by inadequate mixing of the central stock prior to aliquoting for storage. Therefore, further optimisations and checks were required to continue using this glycolytic profiling experiment effectively.

Once optimisations were finalised, metabolic responses of BMDM were assessed. After both 4 and 12 hours stimulation, no significant differences were observed between mock-stimulated, LPS-stimulated or *S. pneumoniae*-challenged macrophages. However, there was a notable trend of increased non-glycolytic acidification and decreased glycolytic reserve with both LPS and *S. pneumoniae* stimulation. Lastly, XF analysis was used to dissect the importance of mitochondrial respiration in human macrophages, following stimulation with LPS or *S. pneumoniae*. This also revealed no significant differences between these stimulatory groups regarding oxidative metabolism.

3.3.2. Chapter Discussion

Seahorse XF analysis was used to measure glycolytic metabolism of *S. pneumoniae*-challenged BMDMs, and to compare this with BMDMs stimulated with LPS – a prototypic bacterial and inflammatory stimulus that induces distinct metabolic changes and a CAM phenotype (Haschemi et al. 2012; Freemerman et al. 2014). There were no significant differences seen between different stimulations of BMDMs at a 4 hour time point; that said, notable differences were seen at a later 12 hour time point, as bacterial challenge stimulated an increase in glycolysis. Interestingly, LPS stimulation did not produce a statistically significant change in basal glycolysis, in either murine BMDMs or human MDMs. This contradicts what was expected following LPS stimulation and does not align with the current literature (Van den Bossche et al. 2015; Tannahill et al. 2013). This could be due to the type or concentration of LPS used here, or could potentially have been

influenced by macrophage plasticity, with the cells adapting to the different media changes required both prior to and during the assay. That said, an interesting observation was the significant increase in non-glycolytic acidifications by LPS stimulation of BMDMs, as this has not been widely reported on. This may suggest that media acidifications, usually indicative of glycolysis, were being produced by an alternative mechanism. One plausible suggestion could be CO_2 release during Krebs Cycle metabolism – this pathway has also been reported as broken following LPS stimulation (O'Neill et al. 2016).

Since these assays were carried out, Lachmandas et al published a similar experimental set-up, using Seahorse XF analysis but with bacterial isolates and lysates to demonstrate changes in ECAR and OCR of human monocytes, comparing microbial stimulation to LPS (Lachmandas et al. 2016). Intriguingly, they too indicate distinct differences between different bacterial stimuli, with the Gram-positive bacterium, *Staphylococcus aureus*, inducing the smallest changes in both measures, compared to the mock. This work is particularly provocative as it suggests that changes seen after LPS stimulation are not necessarily mirrored by complex bacterial stimulation. It could be proposed that the complex stimulation seen during microbial infection, by multiple ligands and diverse host receptors, are causing changeable levels of downstream pathway activation, resulting in pathway convergence and/or receptor redundancy. For example, whilst LPS is known to activate TLR4 in isolation, it could be that TLRs and other surface receptors are synergising upon contact with further bacterial stimuli. This is shown to be the case for the recognition of LPS and lipoteichoic acid, which can both co-ordinate activation of TLR4 with CD14 (Kusunoki et al. 1995). It is also seen in the cooperation of TLR2 and TLR6 in detecting bacterial lipoproteins (Takeuchi et al. 2001). Further literature, describing the use of Seahorse XF analysis to uncover the effects of live bacterial infection on host immune cells, is quite limited. However, it has been briefly used to highlight an increased glycolytic metabolism during *M. tuberculosis* infection of alveolar macrophages (Gleeson et al. 2016), a role for *S. aureus* metabolic stress during infection of keratinocytes (Wickersham et al. 2017) and a proposed role for the *P. aeruginosa* toxin Pyocyanin in mediating bioenergetic changes to neutrophils (Managò et al. 2015). To date, no further publications have been shown to use the Seahorse XF Analyser to make comparisons between the metabolism of cells stimulated with extracellular bacteria, versus others stimulated with PAMPS or bacterial components such as LPS.

Instead, research has focused on using this technique to study bacterial metabolism independent of mammalian host cells, which has been demonstrated for *S. aureus, M. tuberculosis* and *E. coli* (Lamprecht et al. 2016; Lobritz et al. 2015). Further work is required in this area, to truly understand the unique detection and responses induced by different bacteria, and what this means for downstream responses – including the typical antimicrobial responses such as cytokine release, but also for immunometabolic responses and their importance in tackling specific bacterial infections.

The Seahorse XF Analyser is beneficial for monitoring live cell culture metabolism in real time, without the need for labelled substrates or complex data analysis. The technique requires relatively few cells, compared to traditional radiolabelling methods, and does not require any further specialist equipment or training to analyse the resulting data. However there are some limitations to this technique. The analyser used here was housed in a neurobiology lab, and as *S. pneumoniae* is a hazard Category II pathogen, any live bacterial work was limited. Care was taken to ensure only heat-killed or intracellular bacteria were present, with extracellular antibiotics used as required, to limit the effects of extracellular bacterial metabolism on XF analyser measurements. This therefore increased the preparation time and media changes prior to assessment, which could have influenced subsequent metabolism, in both murine BMDMs and human MDMs. Additionally, XF Analysis can only be presented as an indirect measure of glycolysis, as media acidification could occur through other means. It provides limited pathway information; therefore, additional techniques should be implemented to confirm these findings.

Assays that complement XF Analysis could involve the quantification of metabolites. Simple assays include direct quantification using commercially available assay kits, for example measuring glucose or lactate in the cell culture media, or ATP inside the cell. Glucose uptake can also be measured with a fluorescent glucose analog, such as 2-[N-(7-nitrobenz-2-oxa-1,3-diazol-4-yl) amino]-2-deoxy-d-glucose, or 2NBDG (Zou et al. 2005). Alternatively, more detailed and complex assay designs can be used. The 'gold standard' in this case would be heavy or radioactive labelling of glucose, which can be traced through glycolysis and subsequent pathways, and separated for high-resolution analysis via NMR Spectroscopy or tandem Mass Spectrometry techniques, such as gas or liquid chromatography. This provides extensive information on metabolic pathway

engagement, but also requires extensive experience in data handling and analysis methods, compared to XF Analysis (Everts et al. 2012; Dupuy et al. 2013).

3.3.2. Future work

The XF Analyser has been used here to consider glycolytic changes at distinct intervals post-infection; however, Agilent have opened this technique up to greater opportunities, as they now supply a wider range of profiling kits, including assays for fatty acid oxidation and the dependency of mitochondria for different fuel sources. Therefore, these assays could be used to further understand other metabolic changes that occur during infection. Alternatively, the injection ports could be used to inject metabolites of interest, to examine their importance in macrophage health or their utilisation during macrophage responses to bacterial challenge. An example here could be using XFAM free from glucose, glutamine and/or galactose, and injecting these into the system, observing their importance during metabolic switches, such as those seen in the literature after LPS stimulation.

For these experiments, the use of live *S. pneumoniae* was not permitted and antibiotics were used to prevent extracellular bacteria from influencing XF readings; however, it would be interesting to follow real-time metabolic changes during bacterial challenge, to observe how rapidly this occurs and if they compare to responses seen with LPS. That said, Lachmandas et al used bacterial lysates, which could be alternative method to take forward (Lachmandas et al. 2016). A modification of this bacterial experiment would be to use extracellular bacterial components, such as the pneumococcal capsule polysaccharide, peptidoglycan or pneumolysin toxin, rather than whole bacteria, and to see how the responses to these stimuli compare to those seen for LPS.

Finally, as noted earlier in this discussion, XF Analysis should be accompanied by other metabolic measures where possible. It would have been favourable to assay metabolic enzymes and transporters, such as Hexokinase and GLUT1 – either at a transcriptional, protein or enzymatic level – to supplement this data further.

Chapter 4 – The optimisation and use of NMR Spectroscopy to study global metabolic changes of BMDMs after *S. pneumoniae* challenge

4.1. Introduction

Metabolomic researchers employ NMR Spectroscopy, to analyse changes to metabolite profiles in a wide range of samples. It has been particularly valuable for researchers considering the metabolome as a potential diagnostic tool for disease, and it has been heavily applied to analysis of clinical samples such as bloods, urines, and tissues. By analysing these biological samples, NMR Spectroscopy may aid identification of metabolomic phenotypes or biomarkers that distinguish healthy patients from those with disease, aiding patient diagnosis or in evaluating the effectiveness of treatments (Emwas et al. 2013). NMR approaches have also been used to consider metabolic changes in cell cultures, as seen with drug testing in cancer cells (Lauri et al. 2016), and in microbiological studies, for example, in studying metabolic changes seen in biofilm formation (Zhang & Powers 2012).

Different sample preparations and NMR approaches for cell culture systems are found across the literature. Two specific papers provided opposing approaches to this: Ramm Sander et al. described the use of whole cell suspensions, to assess live, real-time metabolism with minimal preparation and in the absence of culture media, whereas Lamour et al. compared the extracellular supernatant and intracellular extracts of cells, which required more processing prior to running on the NMR spectrometer (Lamour et al. 2012; Ramm Sander et al. 2013). Both approaches are considered in this chapter, as ^{1}H-NMR can be used to measure metabolite levels, making it an appropriate method to study the metabolic changes correlated with CAM activation.

This chapter demonstrates the optimisation and use of ^{1}H-NMR Spectroscopy to identify metabolomic changes that occur during the host-pathogen interaction, between murine BMDM cell cultures exposed to *S. pneumoniae*. This research aimed to optimise a novel NMR Spectroscopy protocol and to compare the metabolic changes observed during bacterial infection, with spectra acquired from BMDMs stimulated with LPS - a stimulus shown to induce a CAM phenotype with distinct metabolic changes, including changes to glycolysis, arginine and TCA cycle metabolisms.

4.2. Results

4.2.1. Initial NMR Spectroscopy protocols

Firstly, the Ramm Sander and Lamour protocols were tested, to assess which provided the most effective output for BMDM analysis. To identify significant differences in BMDM metabolite profiles, a comparison was made between healthy, unstimulated cells, and cells stimulated with INFy+LPS for 24 hours; this stimulation is shown to convert macrophages into a classically-activated, inflammatory phenotype, which increases their glycolytic metabolism and lactate release (Van den Bossche et al. 2015).

For the Ramm Sander protocol, samples were run in 5mm Shigemi NMR tubes. These tubes are engineered like a standard NMR tube, but with a large, solid base and small inner tube. This allows for smaller volumes and more concentrated samples to be assessed within the optimal sampling region of the magnet, but without compromising data acquisition quality. Figure 4.1 shows an example Shigemi tube and the spectra observed from whole BMDMs, using the protocol adapted from Ramm Sander et al. on a 600MHz magnet. Some compounds have been tentatively assigned in the comparative spectral view in Figure 4.1C, identified using spectral tables and open access databases, such as the Human Metabolome Database (HMDB). The spectra achieved were relatively reproducible between the two conditions, with small increases seen for, what was tentatively assigned as, lactate, succinate and potentially a choline-related product.

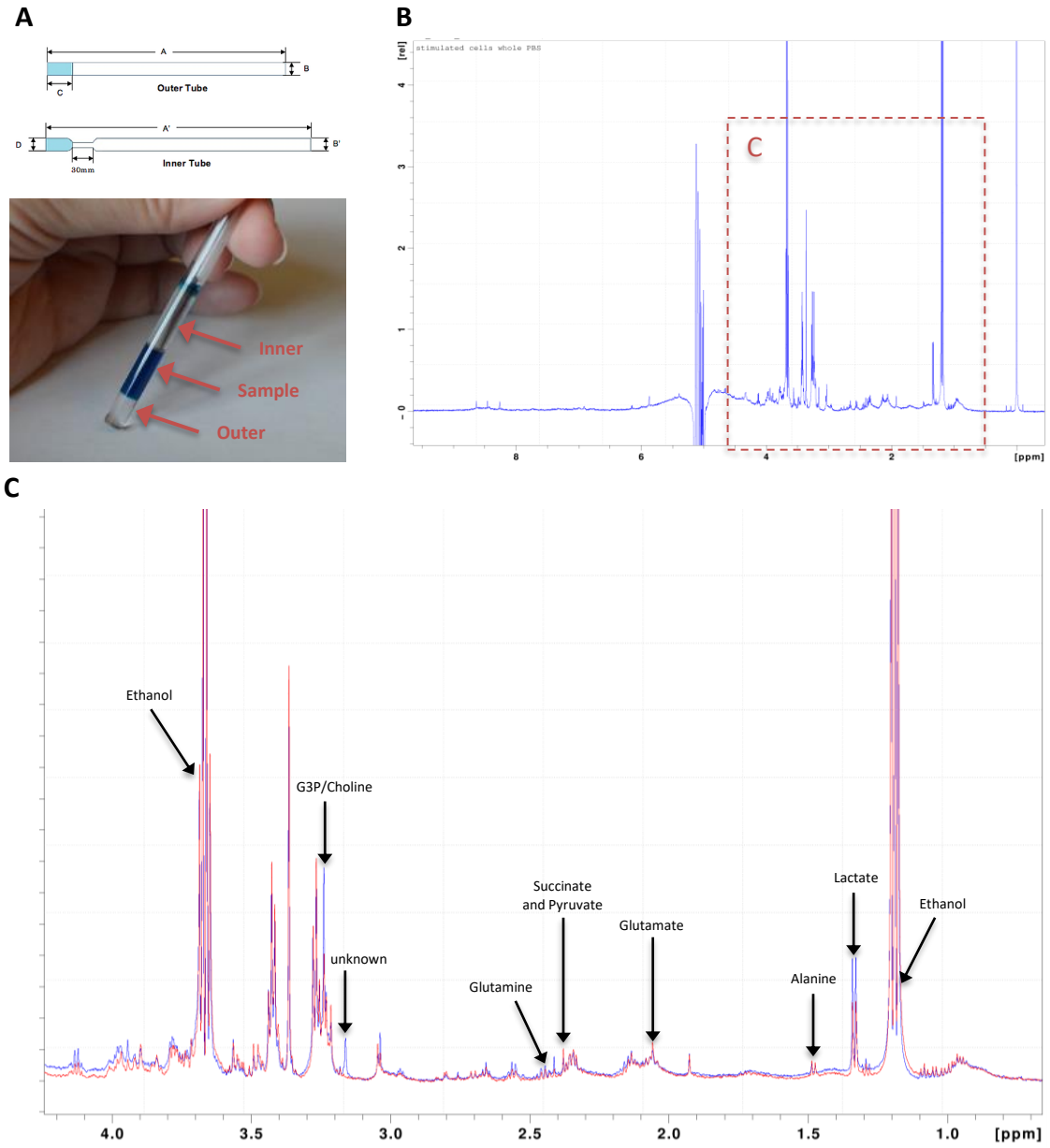

Figure 4.1: NMR Spectroscopy protocol test – Ramm Sander whole cells

Cells were reseeded at a density of 600,000 cells/well, and left overnight to adhere, before being mock-stimulated or stimulated with IFNγ +LPS (both at 10ng/ml). After 24 hours, cells were washed, scraped in 10% D_2O PBS with 1µM of 100mM Trimethylsilylpropanoic acid (TSP), and assessed via NMR spectroscopy on a 600MHz magnet with 5mm Shigemi NMR tubes; n=1.
A) A diagram and representative image of a Shigemi tube. Images taken with permission from http://www.shigeminmr.com/
B) The full spectral acquisition window, from 0-10ppm, is shown from an IFNγ+LPS stimulated cell sample. The TSP reference peak is shown at 0ppm, water peak at 5ppm and the central region of interest indicated by the hashed square.
C) An enlarged and tentatively labelled region of Figure 4.1B, showing a comparative view between mock-stimulated (red) and IFNγ+LPS stimulated (blue) cells. Compounds were assigned using open access spectral tables and databases, such as HMDB.

Following this, the Lamour et al. protocols for intracellular versus extracellular metabolomic components were tested. This required more preparation of samples prior to NMR acquisition. Supernatant samples only were first used to trial the Lamour et al. protocol for extracellular spectral acquisition and were loaded into standard 5mm NMR tubes. Using this protocol, comparable spectra were achieved, to those shown in Lamour et al., with the addition of a few extra peaks, which could result from components of the specific culture media. These spectra are shown in Figure 4.2. The supernatants required minimal preparation and only had a short acquisition time of 8-10 minutes. Therefore, the Lamour protocol was deemed suitable, and optimised for metabolic assessment of *S. pneumoniae*-challenged BMDM cell cultures.

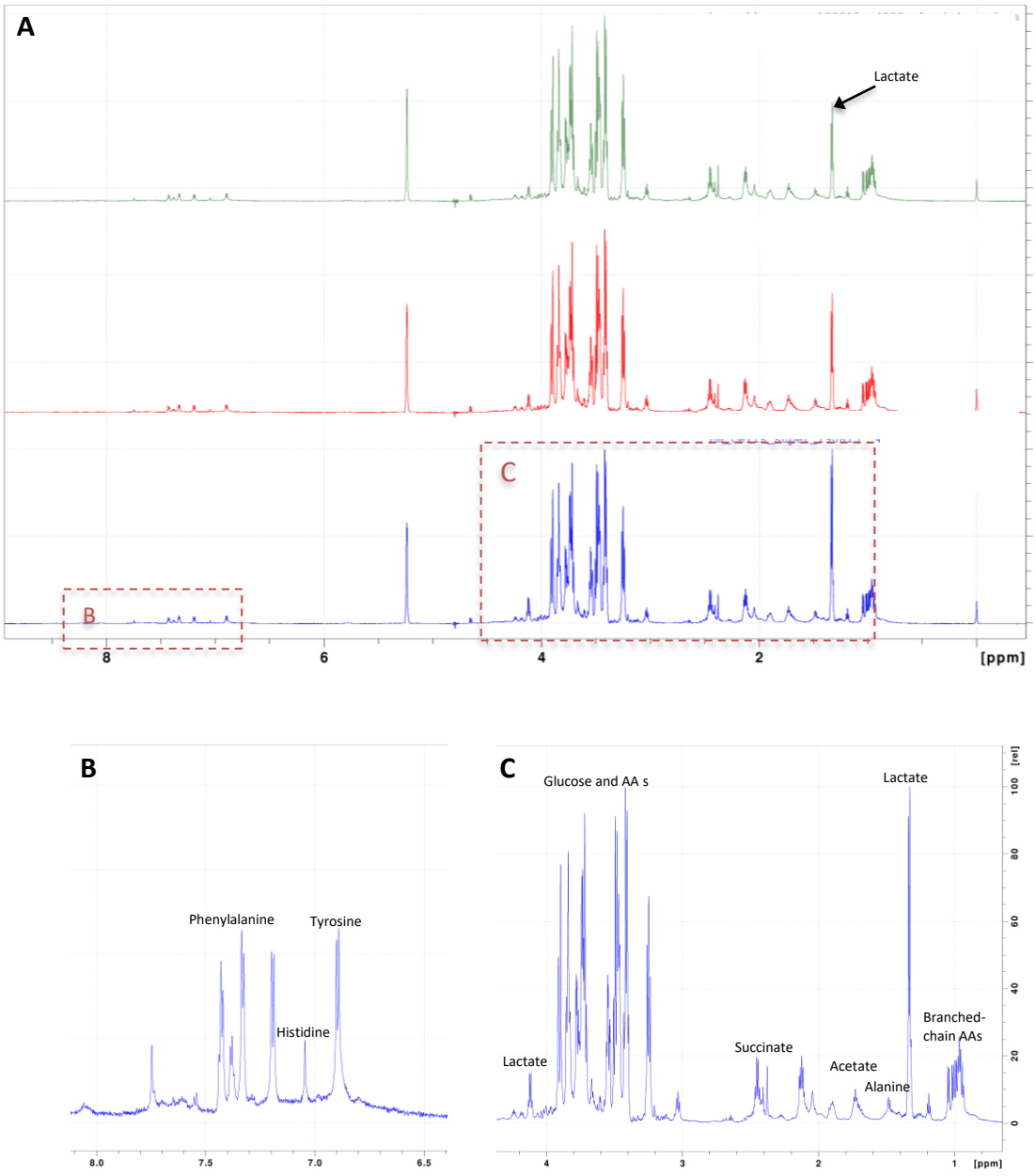

Figure 4.2: NMR Spectroscopy protocol test – Lamour cell supernatants

Cells were reseeded using accutase, to a density of 600,000 cells/well, left overnight, then mock-stimulated or stimulated with IFNγ+LPS (both at 10ng/ml) for 24 hours. At this time, supernatants were frozen at -80°C, whilst whole cells were prepared for analysis seen in Figure 4.1. Supernatants we diluted 300µl:300µl in 70% D2O PBS, with 1µM of 100mM Trimethylsilylpropanoic acid (TSP), and assessed on a 800Hz magnet; n=1.
A) 1H-NMR spectra of culture media are shown, from the absence of cells (BLANK - green), for supernatants from unstimulated BMDMs (UNS - red) and from IFNγ+LPS stimulated BMDMs (IFNγ+LPS - blue) after 24 hours. Lactate has been tentatively labelled, the TSP reference peak is shown at 0ppm and water peak at 5ppm.
B) – C) Enlarged versions of the IFNγ+LPS supernatant 1H-NMR spectra, as indicated in Figure 4.2A, with annotations of suggested metabolic identifications, identified using open-access spectral tables and databases, such as HMDB;(AA=Amino Acid).

Following this, both supernatants and cell extracts were prepared from three biological BMDM donors, using the adapted Lamour et al. protocol. BMDMs were reseeded and left unstimulated for 24 hours. Supernatants were collected directly and intracellular metabolites extracted using an 80% methanol extraction procedure. The results of these experiments are shown in Figure 4.3, with the comparison between supernatants from cell-free conditions (i.e. blank) and supernatants from healthy BMDMs. This provided an insight into the profiles expected in repeat supernatant samples from unchallenged, healthy cells – for example, increases in the lactate peak only happened when cells were present. It also indicated that there could be differences in media prepared on different days, as this was different for each donor preparation. Despite this, spectra here could still be closely compared to those found in Figure 4.2. With regards to the cell extracts, these spectra are far less concentrated than the supernatants, requiring an increased number of scans and longer acquisition time within the spectrometer. This resulted in an increased level of noise and distortion to the baseline. These spectra also suggest there could be carry-through of media components, altering the cell extract spectra; for example, as seen for the peak present at ~1.5ppm. From these trial experiments, the Lamour protocols were deemed suitable to take forward, to assess metabolic changes in the extracellular versus intracellular environments, as the protocol provided clear peaks for analysis and acquisition times that were reasonable for the quality of spectra achieved.

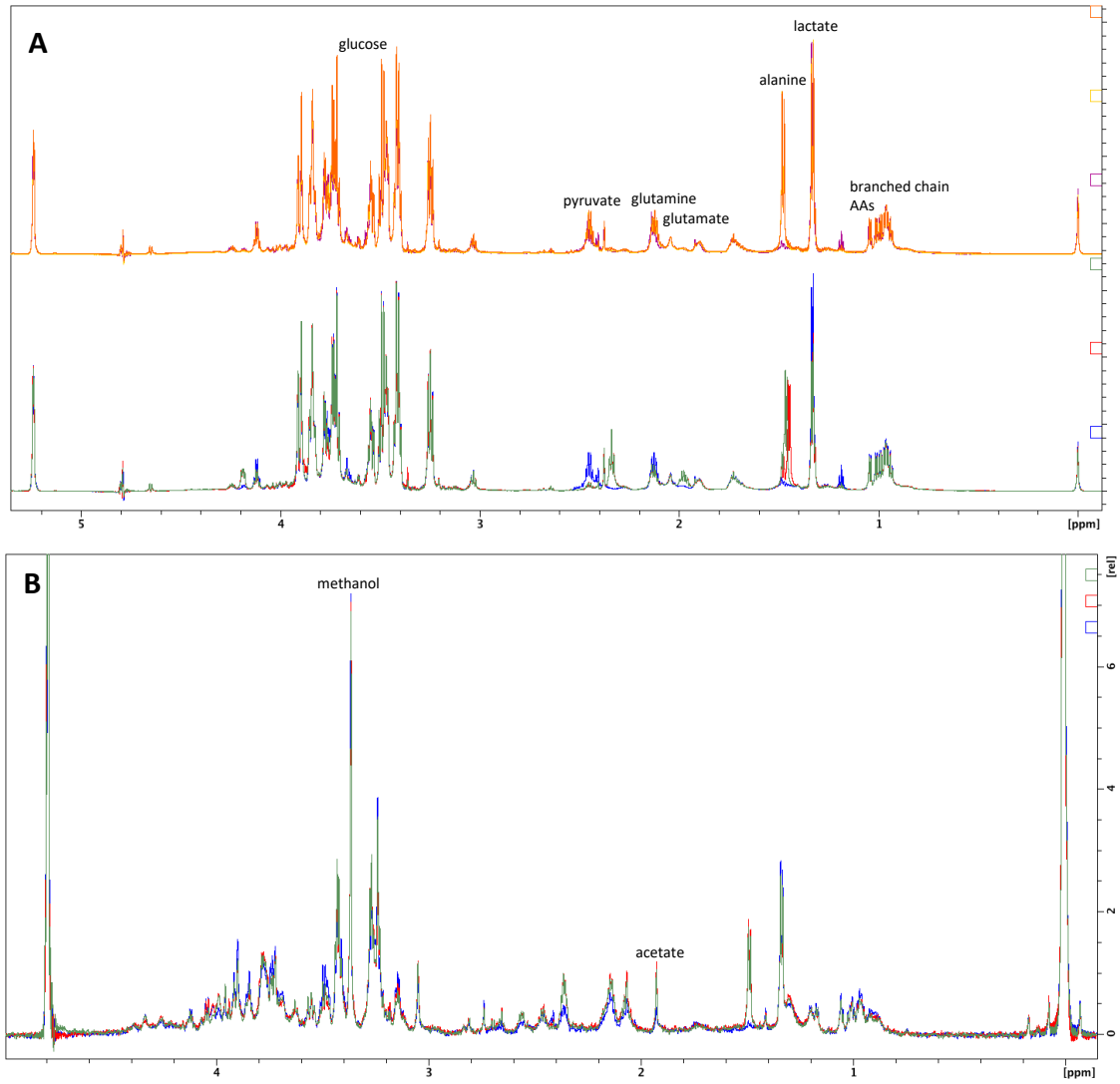

Figure 4.3: NMR Spectroscopy protocol test – Lamour cell supernatants and extracts

Cells were reseeded at $1x10^6$ cells/well via accutase and haemocytometer counting, and left to adhere for 24 hours. Supernatants were stored at -80°C and cell extracts prepared using 80% methanol extraction. 70% D_2O PBS with 167µM TSP was used in both supernatant and cell extract acquisitions, in an 800Hz NMR magnet. The TSP reference peak is shown at 0ppm and water peak at 4.8ppm. Biological n=3, experimental n=1.

A) Triplicate supernatant spectra each from cell-free, blank samples (top) and BMDM-containing samples (bottom). Metabolites are tentatively assigned using references tables and HMDB.

B) Triplicate cell extract preparations from healthy, unstimulated BMDMs only. Metabolites are tentatively assigned using references tables and HMDB.

4.2.2. NMR Spectroscopy preliminary screen

The metabolism of *S. pneumoniae*-challenged BMDMs had not previously been examined; therefore, a preliminary screen, sampling at intervals over a 24 hour time course was first used. The effect of bacterial metabolism was minimised by using external antibiotics for all samples after 4 hours, and with utilisation of a bacteria-only supernatant control (shown in the Appendix). This initial assessment also provided a data set with which to trial some preliminary analysis methods. Both supernatants and cell extracts were prepared, with representative spectra shown in Figures 4.4 and 4.5.

The supernatant spectra of healthy, unstimulated BMDMs are shown in Figure 4.4A. There are no visually distinct or obvious changes upon overlaying the spectra, apart from peaks at 1.3 and 4.1ppm, which correlated with lactate production. In comparison, there were several peaks following infection that appeared to change in pneumococcal-challenge samples, particularly at 16 hours, as indicated in Figure 4.4B. Analysis against known spectral patterns suggested these could potentially correlate with changes in the peaks of acetate and glutamate. The supernatant spectra after 24 hours also had greatly decreased glucose peaks, between 3.2-4.9ppm, which associated with a large increase in lactate peaks at 1.3 and 4.1ppm.

With regards to cell extract profiles, most changes were notable between the 8-16 hour timeframe, as indicated by the small black arrows in Figure 4.5. These were tentatively identified as changes to lactate, acetate, glutamate, choline and glucose. The 8 hour spectrum in Figure 4.5B also demonstrates how difficult spectral analysis can be if the baseline is warped – i.e. if it is not flat.

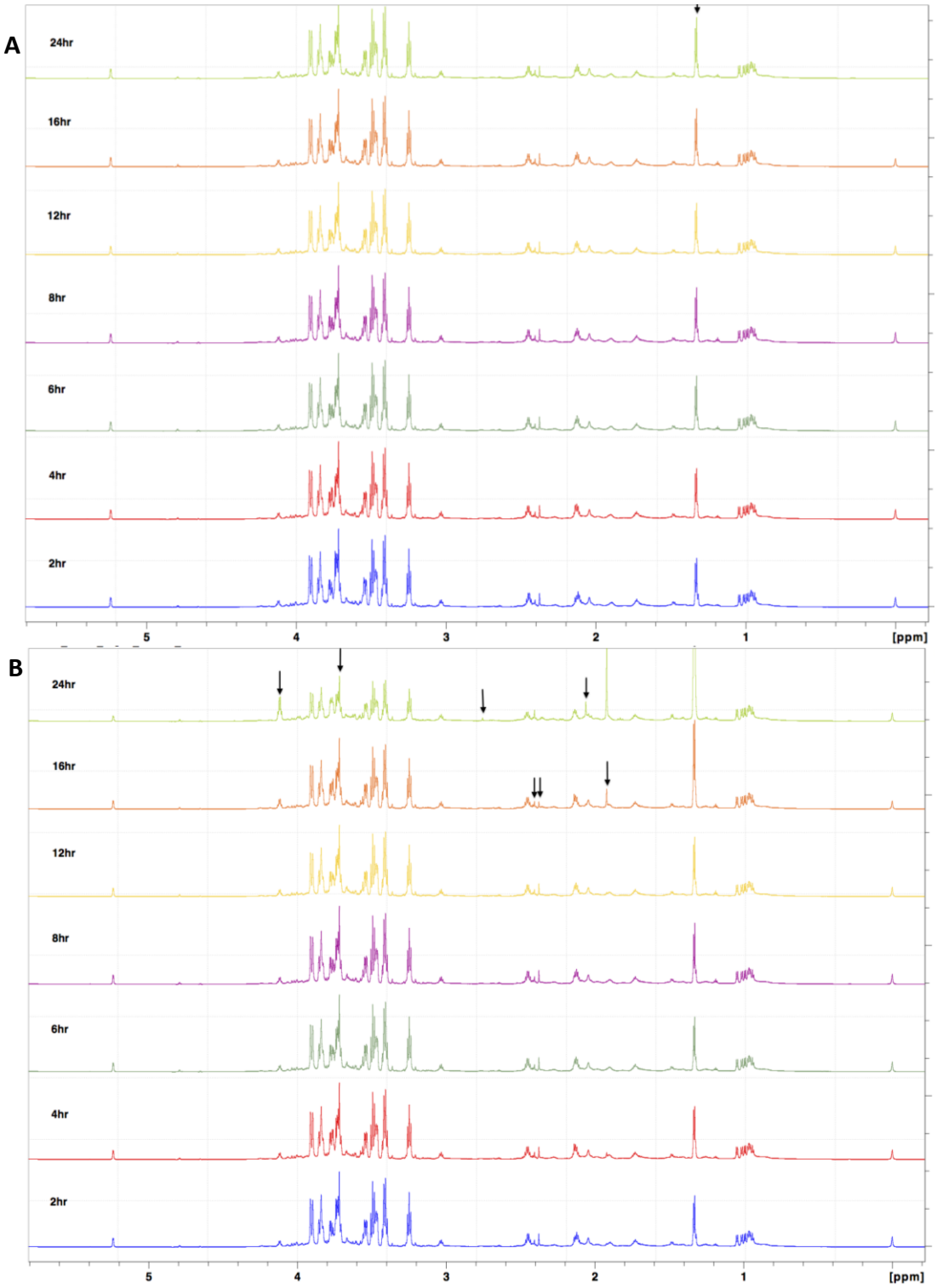

Figure 4.4: Preliminary 1H-NMR screen -BMDM cell supernatants

Supernatants taken from cells seeded at 600,000 cells and either mock-infected or challenged with *S. pneumoniae* (D39, MOI 10), and sampled over a 24 hour period. For NMR spectroscopy, supernatants were diluted 300µl:300µl in 70% D_2O PBS with 167µM TSP. Black arrows indicate noted differences between spectra. Supernatant control samples (no cells with/without *S. pneumoniae*) were used, as shown in the Appendix.

A) Spectra of between 0-6ppm from supernatants of mock-infected cells. The only clear differences were increases to peaks at 1.3 and 4.1ppm, correlating with lactate production.

B) Spectra of supernatants from *S. pneumoniae*-challenged cells. Differences in peak intensity identified by black arrows at 1.9, 2.4, 2.7, 3.7 and 4.1ppm. These correlated with increases to lactate, and tentative increases in acetate, glutamate and glucose.

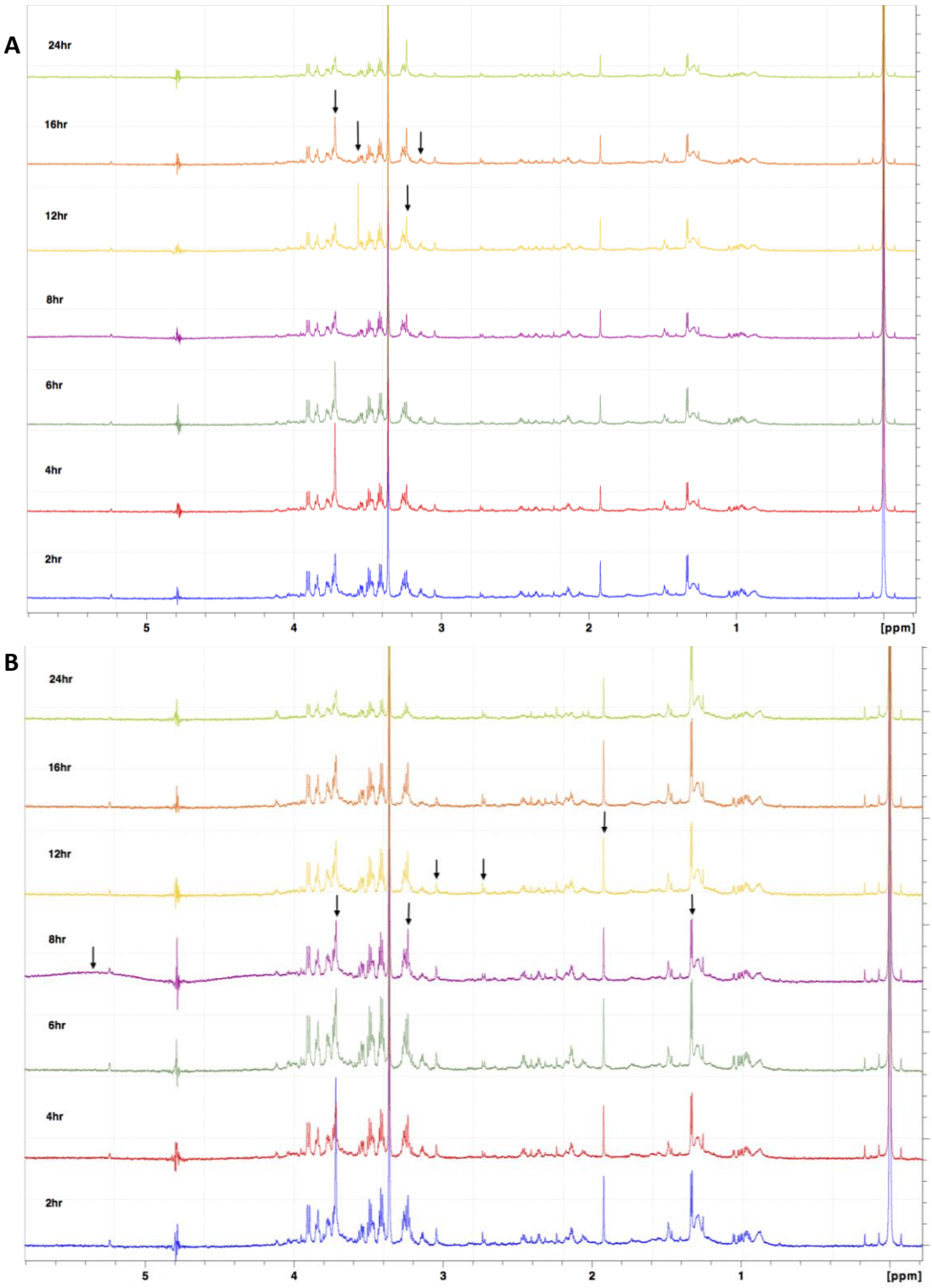

Figure 4.5: Preliminary 1H-NMR screen – BMDM cell extracts

Cell extract samples prepared from cells seeded at 600,000 cells, and either mock-infected or challenged with *S. pneumoniae* (D39, MOI 10), and sampled over 24 hours. Cell extract preparation performed using 80% methanol-water extraction. For NMR spectroscopy, cell extract pellets were re-suspended in 600µl 70% D_2O PBS with 167µM TSP. Black arrows indicate noted differences.

A) Spectra of between 0-6ppm from cell extracts of mock-infected cells. Differences observed at 3.2-3.7ppm, correlating with glucose and other unidentifiable compounds.

B) Spectra of between 0-6ppm from cell extracts of *S. pneumoniae*-challenged cells. Differences observed at 1.3, 1.9, 2.7, 3.1-3.7ppm, correlating with lactate and tentative changes in acetate, glutamate, choline and glucose. The 8hr sample also has a distorted baseline and poor phasing.

4.2.2.1. Preliminary screen data handling – metabolite identification

When viewing supernatant spectra, they were dominated by components found within the cell culture media. Whilst this may have masked smaller metabolite peaks, it also provided a starting point for metabolite identification, as the media components were listed by the manufacturer. Therefore, an initial identification method involved correlating the components of Lonza's DMEM, with spectral references and peak information from the Human Metabolome Database (HMDB). The HMDB has an extensive collection of metabolites and provides information on expected ppm shifts and peak shapes. Therefore, preliminary analyses were carried out by eye, comparing the HMDM expected spectra, to those shown in Figures 4.4 and 4.5.

A second metabolite identification method involved using a trial-version of Chenomx, a software that allows manual fitting of reference compounds to experimental spectra, aiding metabolite identification and with the potential for automated quantification. A screenshot and example of this process is shown in Figure 4.6. In this figure, an example supernatant spectrum is shown, with a glucose reference spectrum used to demonstrate the automated fitting of compounds. Here you can see that only 338 compound spectra are available in this trial version, and that appropriate alignment to these reference spectra can be quite difficult. Using these preliminary methods, a reference table was produced, listing potential compounds of interest and their expected spectral information. Table 4.1 provides this list of metabolites and their expected ppm shifts, which were predominantly identified in DMEM and supernatant samples.

Figure 4.6: Chenomx Profiler

A) Screenshot of Chenomx Profiler Suite, showing an experimental spectrum. Here the cell supernatant of *S. pneumoniae*-challenged cells at 6 hours is shown. The table in the lower half of the image lists the 338 compounds available in the free trial version of this software.
B) Example spectral fitting of 6 named compounds, with a focused view on the glucose peaks. The red line shows summary fit (ie of all 'fitted compounds' listed in table) and blue shading shows expected shape of a chosen compound, here showing the peaks produced by glucose. The numbers in the top left corner indicate mid-point ppm of the expected peaks.

Metabolite	ppm (in H_20, +/-0.03, pH7.0) and peak shape
Amino Acids	
L-Alanine	• 1.460 (doublet) • 3.760 (quadruplet)
L-Arginine	• 1.68 (multiplet ~11) • 1.90 (multiple ~6) • 3.23 (triplet) • 3.76 (triplet)
L-Aspartate	• 2.66 (quadruplet, steep) • 2.80 (quadruplet, split) • 3.89 (quadruplet)
L-Cysteine	• 3.06 (quadruplet) • 3.97 (multiplet ~8, split)
L-Glutamate	• 2.040 (multiplet ~5) • 2.119 (?) • 2.341 (multiplet ~7) • 3.748(quadruplet)
L-Glutamine	• 2.125 (multiplet ~8) • 2.446 (multiplet ~11) • 3.766 (triplet)
L-Glycine	• 3.54 (singlet) •
L-Histidine	• 3.16 (quadruplet) • 3.23 (doublet) • 3.98 (quadruplet) • 7.09 (singlet) • 7.90 (singlet)
L-Isoleucine	• 0.926 (triplet) • 0.997 (doublet) • 1.248 (multiplet ~6) • 1.457 (multiplet ~6) • 1.968 (multiplet ~8) • 3.661 (doublet)
L-Leucine	• 0.948 (triplet) • 1.700 (multiplet ~12) • 3.722 (quadruplet)
L-Lysine	• 1.46 (multiplet ~10) • 1.71 (quadruplet) • 1.89 (multiplet ~12) • 3.02 (triplet) • 3.74 (triplet)
L-Methionine	• 2.157 (multiplet ~10, 1 long) • 2.631 (triplet) • 3.851 (quadruplet)
L-Phenylalanine	• 3.19 (wide/split multiplet) • 3.98 (quadruplet) • 7.32 (doublet) • 7.36 (singlet/doublet) • 7.42 (doublet)
L-Proline	• 1.99 (multiplet ~7) • 2.06 (quadruplet) • 2.34 (multiplet ~5) • 3.33 (quadruplet) • 3.41 (quadruplet) • 4.12 (quadruplet)
L-Serine	• 3.832 (quadruplet) • 3.958 (multiplet ~8)
L-Threonine	• 1.316 (doublet) • 3.575 (doublet) • 4.244 (multiplet ~6)
L-Tryptophan	• 3.292 (quadruplet) • 3.472 (quadruplet) • 4.046 (quadruplet) • 7.194 (quadruplet) • 7.274 (multiplet ~5) • 7.310 (singlet) • 7.531 (doublet) • 7.723 (doublet)
L-Tyrosine	• 3.024 (quadruplet) • 3.170 (triplet) • 3.921 (quadruplet) • 6.877 (quadruplet) • 7.170 (triplet?)
L-Valine	• 0.976 (doublet) • 1.029 (doublet) • 2.261 (multiplet ~9) • 3.601 (doublet)
Carbohydrate metabolism and intermediates	
D-Glucose	• 3.233 (quadruplet) • 3.398 (multiplet ~6) • 3.458 (multiplet ~9) • 3.524 (quadruplet) • 3.728 (multiplet ~10) • 3.824 (multiplet ~7 • 3.889 (quadruplet) • 4.634 (doublet) • 5.223 (doublet)
Glucose-6-phosphate	• 3.27 (quadruplet) • 3.50 (multiplet ~7) • 3.56 (mutliplet ~10) • 3.71 (triplet) • 3.87 (triplet) • 3.92 (mutliplet ~8) • 3.99 (quadruplet) • 4.03 (multiplet ~7)

	• 4.64 (doublet) • 5.22 (doublet)
Ribose-5-phosphate	• 3.85 (multiplet ~5) • 3.93 (quadruplet) • 4.06 (quadruplet) • 4.20 (multiplet ~5) • 4.30 (triplet) • 5.22 (doublet) • 5.39 (multiplet ~9)
6-Phosphogluconate	• 3.84 (singlet) • 3.96 (multiplet ~9) • 4.09 (doublet) • 4.19 (doublet)
Glyceraldehyde-3-phosphate	• *Not in HMDB*
Glycerol-3-phosphate	• 3.61 (multiplet ~6) • 3.67 (multiplet ~6) • 3.82 (multiplet ~20)
Fructose-2,6-bisphosphate	• 1.17 (triplet) • 3.34 (singlet) • 3.64 (quadruplet) • 3.81 (singlet) • 3.84 (singlet) • 3.93 (quadruplet) • 3.98 (quadruplet) • 4.03 (doublet) • 4.05 (doublet) • 4.18 (triplet)
Fructose-6-phosphate	• 3.55 (quadruplet) • 3.65 (multiplet ~7) • 3.92 (multiplet ~18) • 4.11 (triplet) • 4.23 (triplet)
Pyruvic Acid/ Pyruvate	• 2.46 (singlet)
cis-Aconitic Acid/ Aconitate	• 3.43 (doublet) • 6.58 (singlet)
Citric Acid/ Citrate	• 2.65 (doublet) • 2.53 (doublet)
Isocitric acid/ Isocitrate	• 2.46 (mutliplet ~8) • 2.97 (mutliplet ~6) • 3.98 (doublet)
Oxoglutaric acid/ alpha-ketoglutarate	• 2.43 (triplet) • 2.97 (triplet)
Oxaloacetate	• 2.377 (singlet)
Succinic Acid/ Succinate	• 2.393 (singlet)
Fumaric Acid/ Fumarate	• 6.51 (singlet)
L-Malic acid/ Malate	• 2.35 (quadruplet) • 2.66 (doublet) • 4.29 (doublet)
L-Lactic acid	• 1.324 (doublet) • 4.101 (quadruplet)
Itaconic Acid/ Itaconate	• 3.40 (singlet) • 5.85 (singlet) • 6.33 (singlet)
2-Ketobutyrate	• 1.07 (triplet) • 2.76 (quadruplet)
Miscellaneous	
Choline	• 3.189 (singlet) • 3.507 (doublet) • 4.056 (quadruplet)
Citrulline	• 1.56 (multiplet ~12) • 1.87 (multiplet ~11) • 3.14 (multiplet ~6) • 3.74 (quadruplet)
Ornithine	• 1.727 (multplet ~5) • 1.826 (multiplet ~5) • 1.933 (multiplet ~7) • 3.046 (triplet) • 3.774 (triplet)
Acetic Acid/ Acetate	• 1.91 (singlet)
L-Cystine	• 3.18 (quadruplet) • 3.38 (quadruplet) • 4.10 (quadruplet)
Glycerophosphocholine	• 3.20 (singlet) • 3.63 (quadruplet) • 3.90 (multiplet ~13) • 4.30 (multiplet ~9)
Phosphoenolpyruvate	• 5.18 (singlet) • 5.36 (singlet)
Phosphocholine	• 3.21 (singlet) • 3.59 (singlet) • 4.17 (singlet)
3-Hydroxybutyrate	• 1.204 (doublet) • 2.314 (quadruplet) • 2.414 (quadruplet) • 4.160 (multiplet ~6)
Hydroxyacetone	• 2.172 (singlet) • 3.257 (singlet) • 4.260 (singlet)
Creatine Phosphate/ Phosphocreatine	• 3.03 (singlet) • 3.93 (singlet)

Creatine	• 3.02 (singlet) • 3.92 (singlet)
Creatinine	• 3.03 (singlet) • 4.05 (singlet)
Glycolate	• 3.94 (singlet)
Urea	• 5.78 (singlet
Malonate	• 3.11 (singlet)
Formic Acid/ Formate	• 8.44 (singlet)
Fumarate	• 6.51 (singlet)
Pantothenate (Vit B5?)	• 0.88 (singlet) • 0.92 (singlet) • 2.41 (triplet) • 3.39 (singlet) • 3.43 (quadruplet) • 3.51 (doublet) • 3.98 (singlet)
Folate/Folic Acid	• 2.11 (mutliplet ~10) • 2.33 (mutliplet ~6) • 4.20 (quadruplet) • 4.30 (triplet) • 6.42 (doublet) • 7.50 (doublet) • 8.01 (doublet) • 8.49 (singlet)
Niacinamide (Nicotinamide)	• 7.58 (quadruplet) • 8.24 (quadruplet) • 8.70 (quadruplet) • 8.92 (singlet)
Inosinic Acid	• 4.02 (quadruplet) • 4.36 (doublet) • 4.50 (triplet) • 6.13 (doublet) • 8.21 (singlet) • 8.55 (singlet)
Glutathione	• 2.15 (multiplet ~6) • 2.54 (multiplet ~10) • 2.97 (quadruplet) • 3.78 (multiplet ~5) • 4.20 (quadruplet)
Purine/Pyrimidine metabolism	
AMP	• 4.01 (doublet) • 4.36 (doublet) • 4.50 (doublet) • 6.12 (doublet) • 8.23 (singlet) • 8.58 (singlet)
ATP	• 4.211 (multiplet ~5) • 4.284 (quadruplet) • 4.394 (triplet) • 4.507 (singlet) • 4.619 (triplet)
	• 6.127 (doublet) • 8.239 (singlet) • 8.526 (singlet)
Allantoin/ Allantoic Acid	• 5.38 (singlet) OR • 5.34 (triplet)
Cytosine	• 5.96 (doublet) • 7.49 (doublet
Cyclic AMP	• 4.34 (doublet) • 4.53 (doublet) • 6.16 (singlet) • 8.22 (singlet)
NAD(H)	• 4.225 (multiplet ~5) • 4.353 (doublet) • 4.373 (multiplet ~3) • 4.434 (multiplet ~4) • 4.499 (triplet) • 6.027 (doublet) • 6.088 (doublet) • 6.122 (doublet) • 8.142 (singlet) • 8.207 (multiplet ~4) • 8.406 (singlet) • 8.839 (doublet) • 9.152 (doublet) • 9.332 (singlet)
NADP(H)	• 4.23 (multiplet ~5) • 4.29 (multiplet ~5) • 4.37 (triplet) • 4.45 (triplet) • 4.52 (triplet) • 4.56 (multiplet ~5) • 4.65 (triplet) • 5.10 (triplet) • 6.12 (doublet) • 6.21 (doublet) • 8.21 (singlet) • 8.24 (quadruplet) • 8.49 (singlet) • 8.88 (doublet) • 9.19 (doublet) • 9.36 (singlet)

Table 4.1: 1H-NMR identifiable compounds

A list of metabolites and their expected ppm, according to the HMDB, Chenomx and NMR reference tables. Each compound will produce all peaks indicated in the table, if it is truly present in samples. This served as a metabolite ID resource and a personal reference during subsequent work.

4.2.2.2. Preliminary screen data handling – integral analysis

To compare changes between conditions and over time, spectra were 'binned' into specific ppm segments and integrals were calculated from these defined regions. For this preliminary data set, variable size integral regions were chosen, rather than uniform and regular regions that spanned the full ppm scale. This aimed to reduce the data load for analysis and allowed selection of whole peaks within individual integrals. Integral bins were selected as one bin per spectral peak, with ppm regions as listed in Table 4.2. These integrals were then plotted as stimulatory conditions versus time. Representative and tentatively assigned graphs are shown in Figures 4.7 and 4.8 for supernatant and cell extract integrals respectively. From these graphs, it is clear there was considerable variability between spectra, and that further data processing is required prior to analysing in this way. This screening experiment was not repeated as further technical optimisations were identified.

Integral Number	Integral Region (ppm)	
1	8.511	8.432
2	8.291	8.136
3	8.125	7.981
4	7.905	7.842
5	7.823	7.780
6	7.772	7.725
7	7.722	7.676
8	7.668	7.643
9	7.642	7.572
10	7.569	7.532
11	7.456	7.408
12	7.408	7.357
13	7.357	7.309
14	7.309	7.272
15	7.219	7.168
16	7.168	7.095
17	7.095	7.024
18	7.024	6.970
19	6.97	6.835
20	6.835	6.716
21	6.716	6.572
22	6.076	5.952
23	5.952	5.591
24	5.282	5.186
25	4.28	4.211
26	4.206	4.161
27	4.161	4.094
28	4.094	4.055
29	4.048	4.030
30	4.03	4.014
31	4.014	3.993
32	3.993	3.958
33	3.958	3.931
34	3.925	3.876
35	3.872	3.812
36	3.811	3.791
37	3.79	3.770
38	3.77	3.755
39	3.755	3.748
40	3.748	3.697
41	3.687	3.649
42	3.644	3.620
43	3.618	3.598
44	3.598	3.586

Integral Number	Integral Region (ppm)	
45	3.585	3.571
46	3.57	3.553
47	3.553	3.519
48	3.518	3.477
49	3.477	3.445
50	3.444	3.381
51	3.372	3.344
52	3.344	3.308
53	3.307	3.278
54	3.276	3.223
55	3.218	3.195
56	3.195	3.177
57	3.17	3.084
58	3.081	2.998
59	2.794	2.737
60	2.714	2.661
61	2.661	2.621
62	2.583	2.530
63	2.529	2.491
64	2.491	2.471
65	2.471	2.429
66	2.428	2.390
67	2.389	2.368
68	2.366	2.331
69	2.33	2.234
70	2.226	2.171
71	2.147	2.100
72	2.075	2.012
73	2.011	1.950
74	1.953	1.858
75	1.858	1.775
76	1.767	1.711
77	1.711	1.625
78	1.583	1.500
79	1.494	1.467
80	1.359	1.305
81	1.303	1.217
82	1.217	1.164
83	1.064	1.028
84	1.028	1.000
85	1	0.980
86	0.98	0.946
87	0.946	0.909
88	0.06	-0.054

Table 4.2: Integral regions for preliminary 1H-NMR screen data handling

Cells seeded at 600,000 cells and either mock-infected or challenged with *S. pneumoniae* (D39, MOI 10), then sampled over a 24 hour period. Supernatants and cell extract spectra were acquired via the Lamour protocol on a 800Hz magnet. Spectra were binned and integrals calculated from these regions in Bruker TopSpin software, using raw NMR spectra data. Integral regions were selected as one peak per bin. Binned ppm regions and Integral numbers are indicated above with corresponding ppm regions shown for each; n=1.

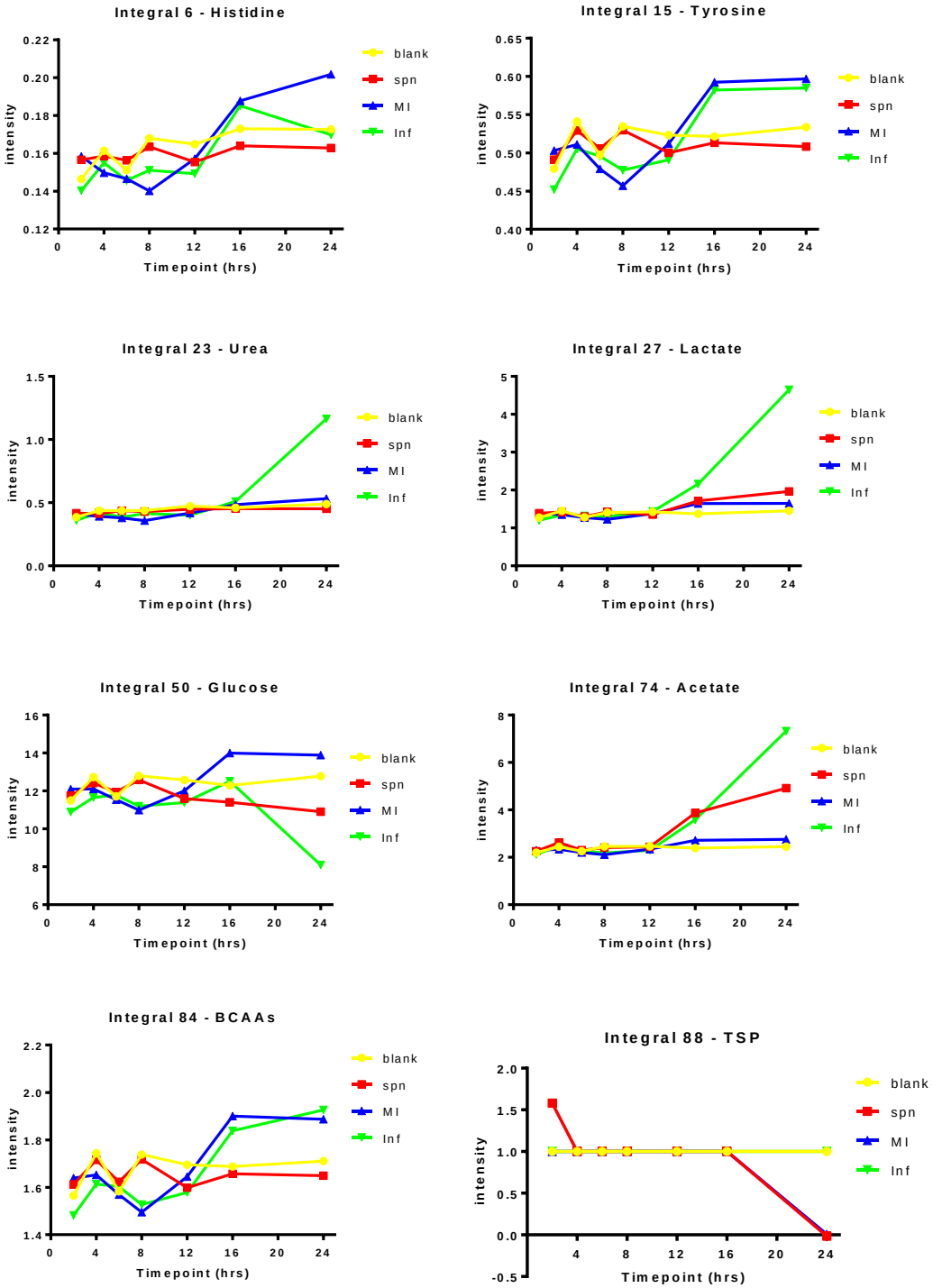

Figure 4.7: NMR spectroscopy preliminary data handling – supernatant integrals

Cells seeded at 600,000 cells and either mock-infected or challenged with *S. pneumoniae* (D39, MOI 10), then sampled over a 24 hour period. Supernatant spectra were acquired via the Lamour protocol on a 800Hz magnet. Spectra were binned and integrals calculated from raw NMR spectral data, using Bruker TopSpin software. Integrals were plotted using GraphPad, to show specific changes within that integral region, both over time and between the four supernatant conditions. Here just eight representative integral regions are shown, with tentative assignments; n=1.
Blank = no cells, no bacteria; spn = no cells with *S. pneumoniae*; MI = mock-infected BMDMs; Inf = *S. pneumoniae*-challenged BMDMs. (BCAAs = Branched-chain amino acids, TSP = Trimethylsilylpropanoic acid,)

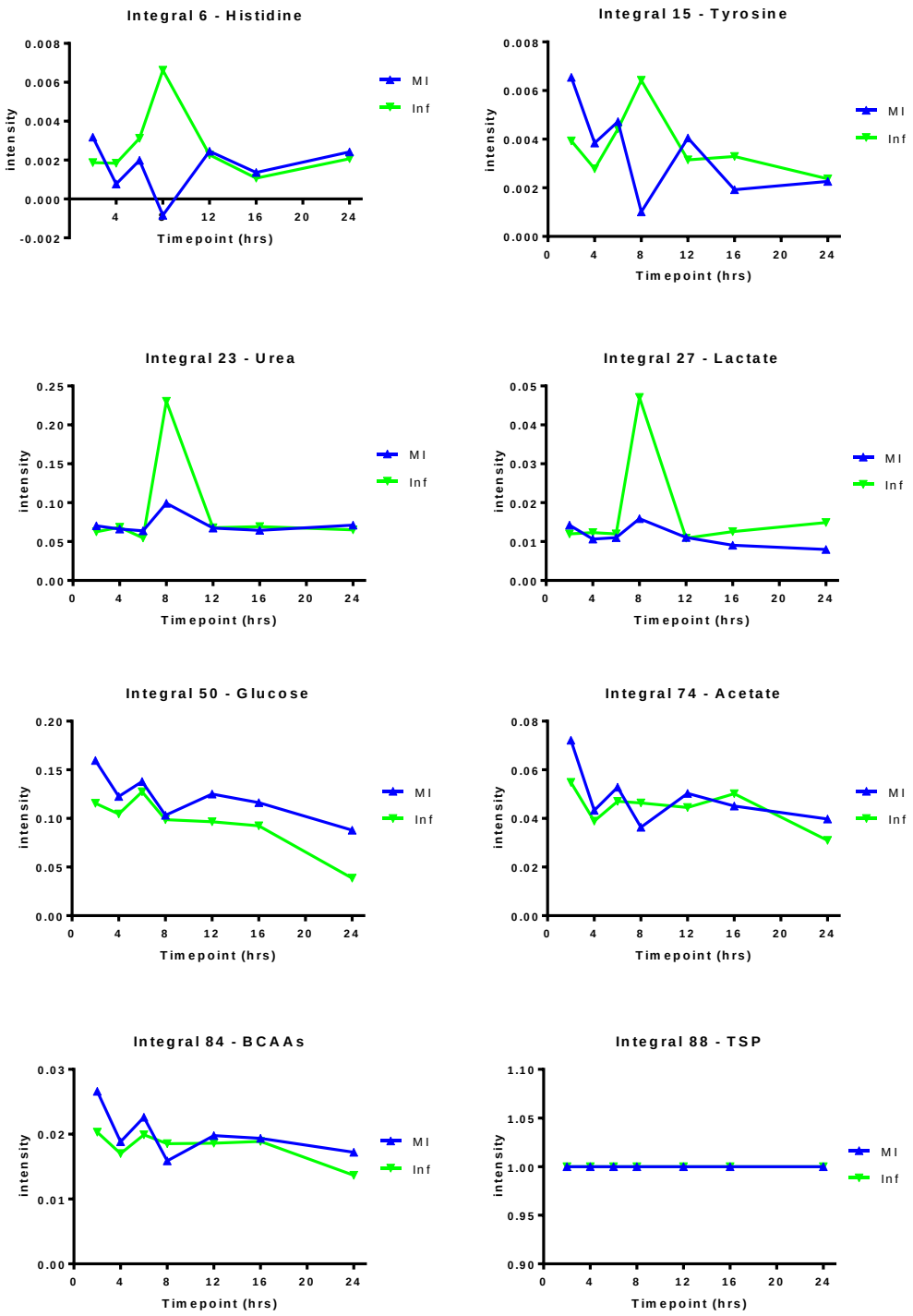

Figure 4.8: NMR spectroscopy preliminary data handling – cell extract integrals

Cells seeded at 600,000 cells and either mock-infected or challenged with *S. pneumoniae* (D39, MOI 10), then sampled over a 24 hour period. Cell extract spectra were acquired via the Lamour protocol on a 800Hz magnet. Spectra were binned and integrals calculated from raw NMR spectral data, using Bruker TopSpin software. Integrals were plotted using GraphPad, to show specific changes within that integral region, both over time and with comparison made between the two cell extract conditions. Here just eight representative integral regions are shown, with tentative assignments; n=1.

MI = mock-infected BMDMs; Inf = *S. pneumoniae*-challenged BMDMs. (BCAAs = Branched-chain amino acids, TSP = Trimethylsilylpropanoic acid,)

4.2.3. NMR Spectroscopy method optimisation

Following the preliminary screen, there were aspects of the technique and experimental design that required further optimisation. This included optimising the number of cells used in preparations, understanding the influence of culture media and the bacterial challenge protocol on the resulting spectra, and characterising the expected spectral profiles after BMDM CAM and AAM stimulation, as potential controls for macrophage activation status.

4.2.3.1. Method optimisation – The influence of cell number

Increasing the cell number in sample preparations aimed to improve both spectral resolution and intensity, for supernatant and cell extract profiles. BMDMs were seeded at either a low ($5x10^5$cells) or high ($2x10^6$cells) density. Samples were taken from both an early 4 hour and late 12 hour time point, following mock-infection or *S. pneumoniae* challenge. The resulting spectra are shown in Figures 4.9 and 4.10. By overlaying the supernatant spectra, there were no identifiable differences between the 4 hour profiles. The most discernible difference after 12 hours was the increased lactate peak at ~1.3ppm. This increase correlated with increased cell number, and with the presence of bacteria. Additionally, the peak corresponding to acetate at ~1.9ppm was very distinct when bacteria were grown independently but was also detectable in *S. pneumoniae*-challenged cells, particularly those at a higher cell density. The minimal differences seen between supernatant samples could be due to the overwhelming metabolite content of DMEM, and the low sensitivity of NMR spectroscopy, thus making analysis of these spectra quite challenging. When examining the cell extract spectra in the same way, an increased cell number produced more prominent and defined peaks, allowing comparative analysis of spectra to be much easier. However, due to the limited cell numbers available from each murine bone marrow preparation, the use of $2x10^6$cells per condition was not feasible for future studies; therefore an intermediate density of $1x10^6$cells was chosen as a suitable compromise for further work.

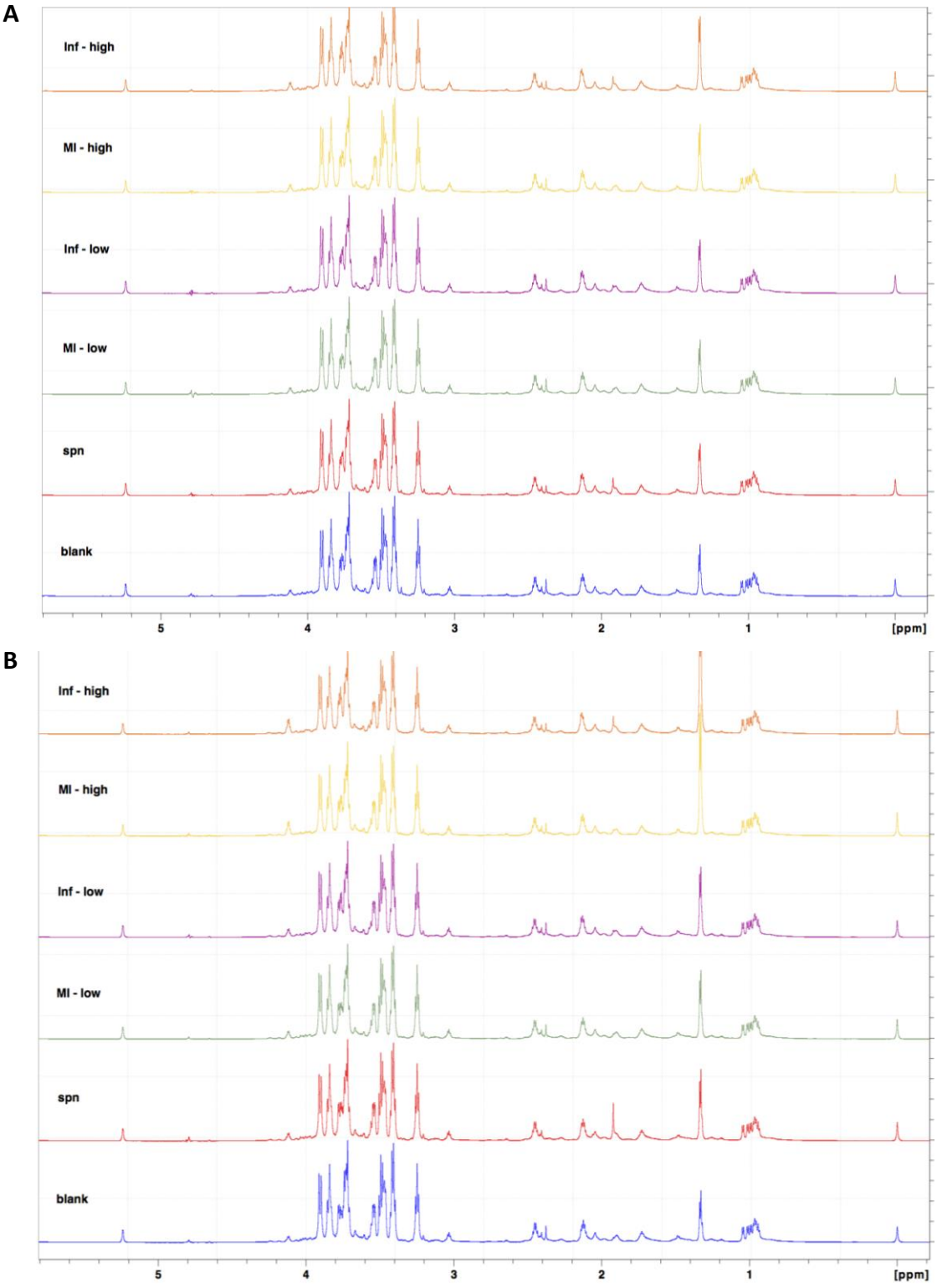

Figure 4.9: NMR spectroscopy optimisation: different cell densities – cell supernatants

Cells were seeded at either a low ($5x10^5$cells) or high ($2x10^6$cells) density, before being mock-infected or challenged with *S. pneumoniae* (D39 MOI 10). Supernatants were collected directly, and NMR spectra acquired on a 800Hz magnet. Figures are annotated to indicate sample condition: blank = no cells, no bacteria; spn = no cells with *S. pneumoniae*; MI = mock-infected BMDMs; INF = *S. pneumoniae*-challenged BMDMs. n=1

A) Supernatant samples collected after 4 hour stimulation. No discernible differences seen.

B) Supernatant samples collected after 12 hour stimulation, following 4 hour PBS wash and media replacement. Increases at 1.3ppm (lactate) and 1.9ppm (acetate) with bacterial challenge.

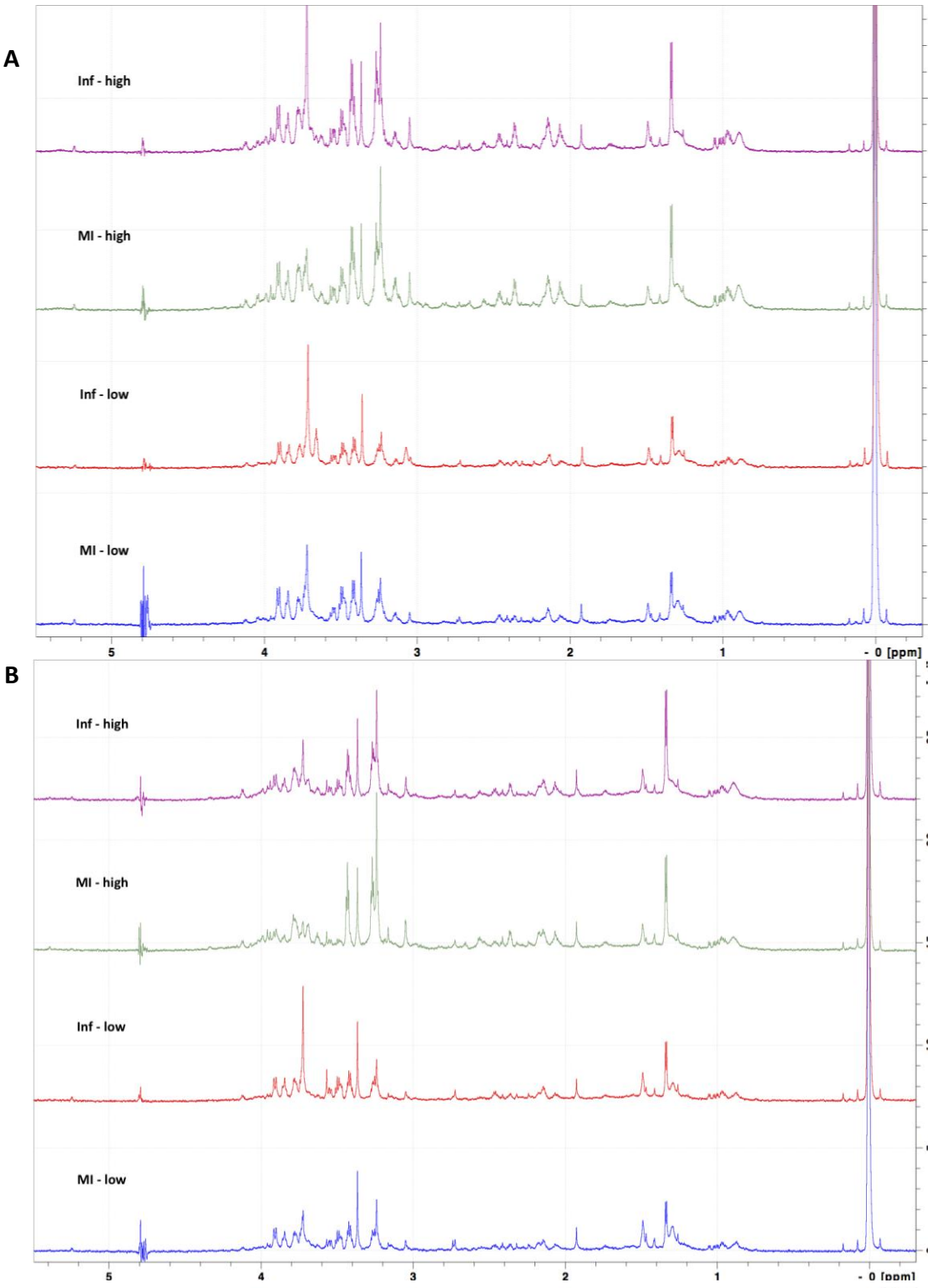

Figure 4.10: NMR spectroscopy optimisation: different cell densities – cell extracts

Cells were seeded at either a low ($5x10^5$cells) or high ($2x10^6$cells) density, before being mock-infected or challenged with *S. pneumoniae* (D39 MOI 10). Cell extracts were prepared via methanol extraction and NMR spectra acquired on a 800Hz magnet. Figures are annotated to indicate sample condition: MI = mock-infected BMDMs; INF = *S. pneumoniae* challenged BMDMs ($5x10^5$cells). n=1

A) Cell extract samples after 4 hour stimulation. Spectra definition improved with increased cell number.

B) Cell extract samples prepared after 12 hour stimulation, following 4 hour PBS wash and media replacement. Spectra definition improved with increased cell number.

4.2.3.2. Method optimisation – The influence of culture media on spectral profiles

To understand how cell culture media contributed to the spectra of supernatants, the influence of HIFCS was specifically assessed. There are no definable lists for what can be found in calf serum, and it can be subject to batch variation from suppliers, hence it incurs unwanted variation between spectra. To investigate this, DMEM and HIFCS were sampled both independently and in combination, as shown in Figure 4.11. This confirmed the technical challenges that HIFCS may present for analysis; it is rich in protein, which distorts the 1H-NMR baseline, making phasing and peak definition very poor. It was also difficult to scale the TSP in the HIFCS-only spectra to align with the two other spectra shown, without getting incredibly high background noise. However, as HIFCS was only used at 10% in DMEM during experiments, these issues are lessened, as shown in the red spectra of Figure 4.11. The two compounds that look like they were dominant in HIFCS are at ~1.33 and ~2.04ppm, which may correlate with metabolite chemical shifts of lactate and/or threonine, and glutamate respectively. HIFCS is used as an essential supplement in the BMDM culture system, therefore it was not omitted, but precaution was taken from this point to use the same batch for all comparable experiments, where physically possible.

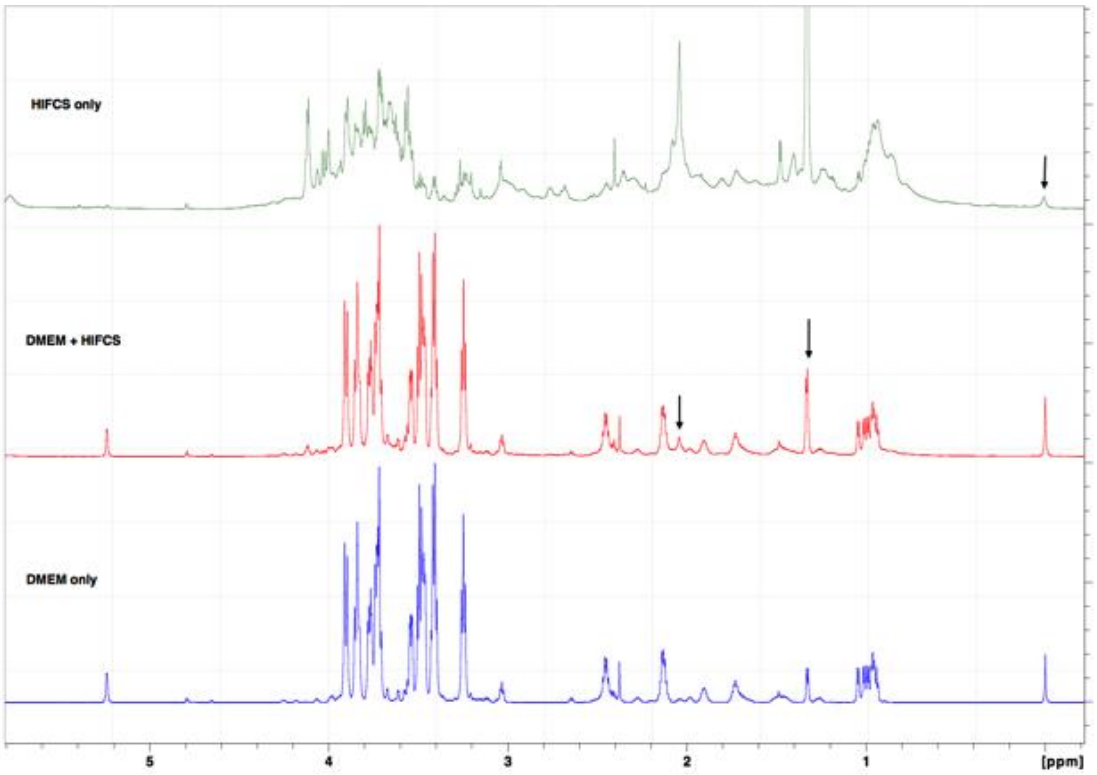

Figure 4.11: NMR spectroscopy optimisation: HIFCS

1H-NMR spectra are shown for HIFCS only (top, green), DMEM+10% HIFCS (middle, red) and DMEM only (bottom, blue). Samples were diluted 300µl:300µl in 70% D_2O PBS with 167µM TSP and measured on a 800Hz magnet. Black arrows indicate regions of interest as follows: 0ppm indicates TSP, 1.3ppm indicates lactate and/or threonine, and 2.04ppm correlates with glutamate. n=1

Metabolite spiking of DMEM was also trialled, as an aid to metabolite identification (ID). Figure 4.12 shows the resulting spectra of DMEM spiked with saturated solutions of glucose, glycine, glutamine and glutamate. Each of the indicated compounds produce a clear and distinct chemical shift. That said, some compounds, for example glutamate, produced a more acidic pH and could therefore cause an undesirable pH shift, making spectra harder to align and ID. Additionally, the concentrated spike of glycine dominated the spectrum intensity, making it difficult to reliably scale and align to TSP. This spiking technique is ideally used for identifying compounds in clustered regions, compounds at low concentrations or for confirming tentative metabolite IDs.

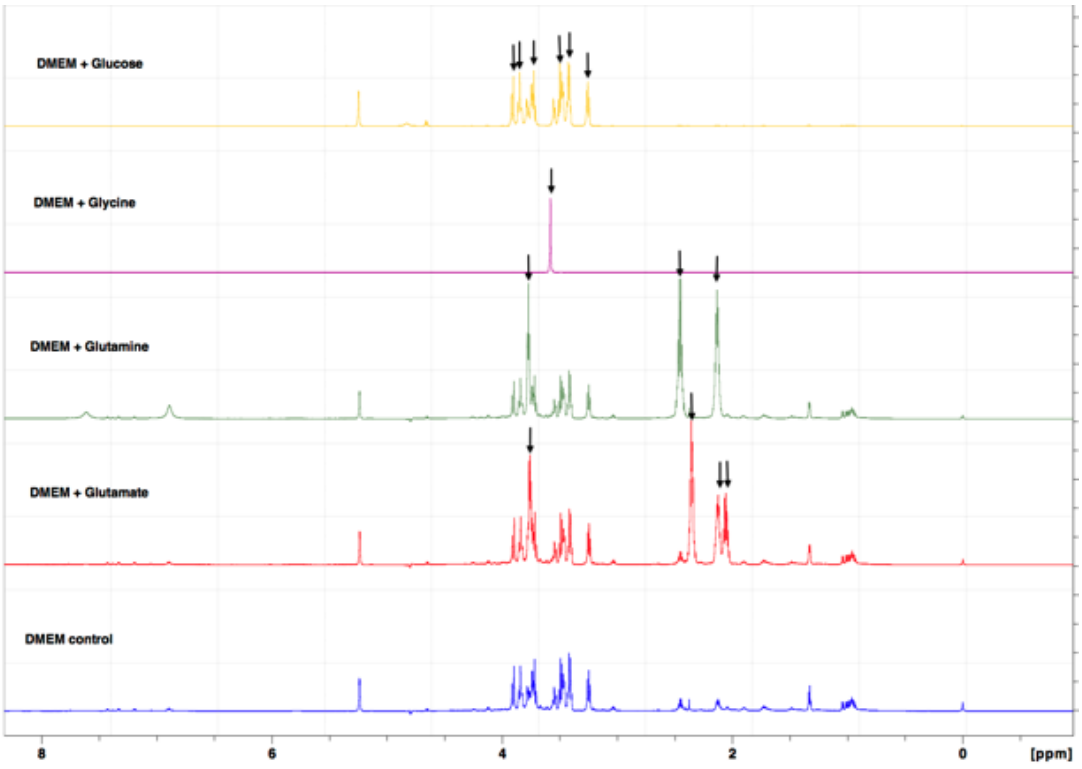

Figure 4.12: NMR spectroscopy optimisation: metabolite spiking

DMEM was spiked with powdered D-glucose, L-glycine, L-glutamine or L-glutamate, then diluted 300µl:300µl in 70% D_2O PBS with 167µM TSP. Spectra were obtained on a 800Hz magnet. Spectra are annotated to indicate compound name and suspected resulting peaks: DMEM only (bottom, blue), DMEM with glutamate (red), DMEM with glutamine (green), DMEM with glycine (purple), DMEM with glucose (top, yellow). Black arrows indicate the proposed peaks for the metabolites used. Spectra have been aligned to a TSP reference but have been scaled to aid the visualisation of spiked compound peaks.

4.2.3.3. Method optimisation – A comparison between CAM and AAM stimuli to *S. pneumoniae* challenge in BMDMs

To study the effects of *S. pneumoniae* challenge on BMDM metabolism, and to compare to responses reported in the literature, LPS and IL-4 were used as stimuli associated with the CAM and AAM phenotypes respectively. After 4 hours, all cells were washed, treated with antibiotics to remove extracellular bacteria, and media replaced until samples were collected at either 8 hours or 20 hours post-stimulation. Spectral comparisons were conducted via manual inspection in TopSpin software, with spectra from supernatants and cell extracts shown in Figures 4.13 and 4.14 respectively.

In Figure 4.13, apart from changes to lactate and acetate peaks at ~1.3 and ~1.9ppm respectively, there were no visually discernible differences between the supernatant spectra of mock-stimulated or *S. pneumoniae*-stimulated cells, at either time point. Both *S. pneumoniae* challenge and LPS stimulation increased lactate in the supernatant. Likewise, in cell extract samples, one of the most distinct changes was the increase to lactate after both LPS and *S. pneumoniae* stimulation. Furthermore, the cell extract spectra were not dominated by high levels of glucose or DMEM components, making it much easier to identify changes and ID metabolites; for example, differences can be seen in Figure 4.14A at 2.42ppm for *S. pneumoniae*-challenged and LPS-stimulated spectra compared to the rest, and in Figure 4.14B, differences can be seen at 1.17ppm for IL-4, at 3.06 and 3.72ppm for mock-infected, and at 3.24ppm for both IL-4- and *S. pneumoniae*-challenged conditions. While these could be genuine differences induced by the conditions, it must be considered that carry through of external metabolites or contaminates could be present – this is likely to be the case for the large singlet peak at 3.72ppm for the mock-infected spectrum of Figure 4.14B. These results advocate the use of cell extract profiles, to provide more detailed changes to metabolite levels, than those seen for supernatant spectra. Fewer regions of these spectra overlap and are not dominated by components of the cell culture media. It also demonstrated that LPS can induce a CAM status, making it a useful pro-inflammatory control stimulus, whilst IL-4 would be less valuable in this study.

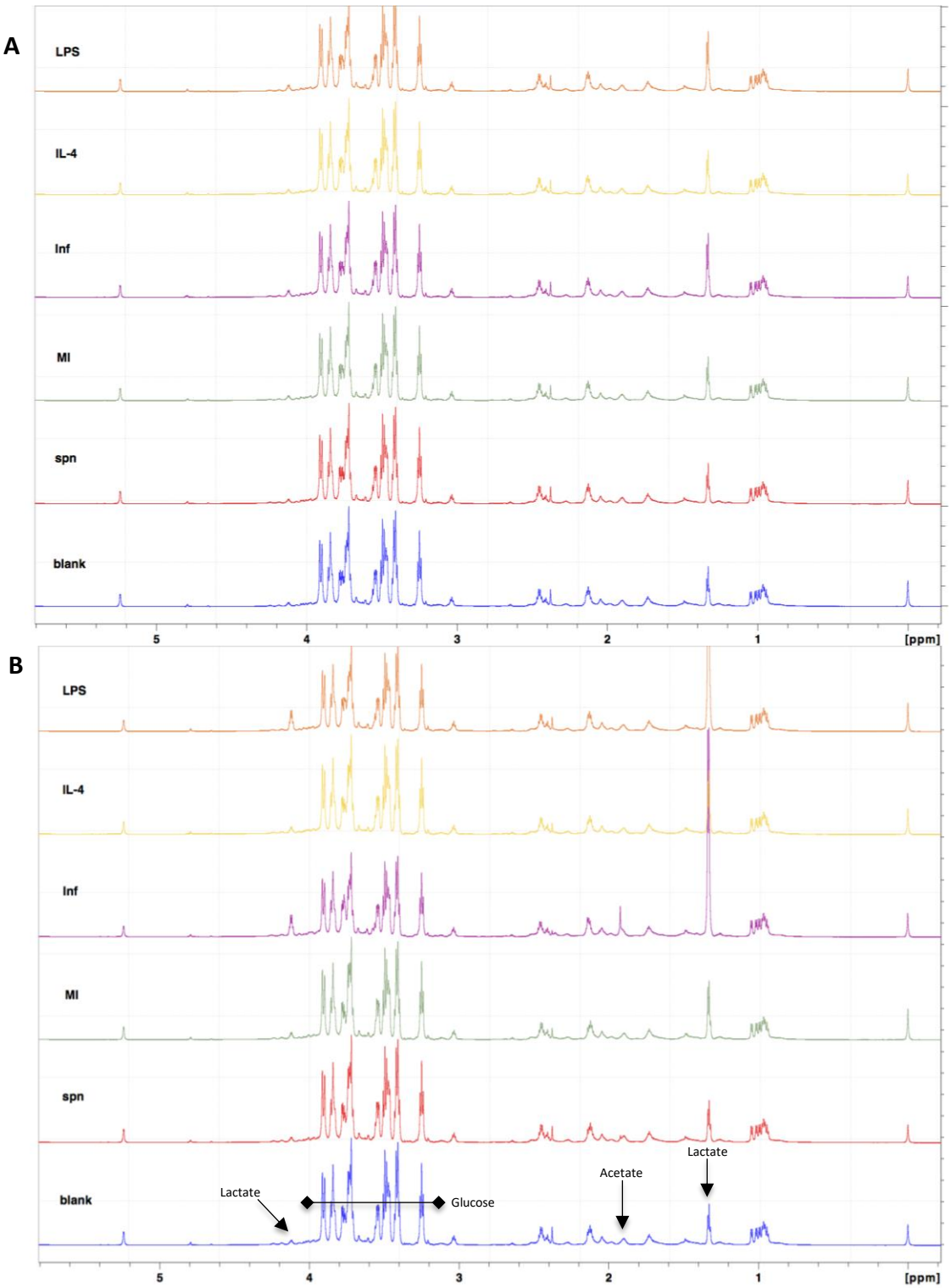

Figure 4.13: NMR spectroscopy optimisation: comparison of BMDM supernatant profiles after *S. pneumoniae* challenge, CAM or AAM stimulation after 8 and 20 hours

Cells were seeded at 1x10^{6}cells, treated as per key, with 1 hour on ice and 3 hours incubation. At 4 hours, all cells were treated with 20ug/ml Gentamycin and 40U/ml Penicillin, before media was replaced and cells returned to incubator. Supernatants were collected directly, and spectra acquired on a 800Hz magnet. Images are annotated as follows: Blank = no cells, no bacteria; spn = no cells with *S. pneumoniae*; MI = mock-infected BMDMs; Inf = *S. pneumoniae*-challenged BMDMs (D39, MOI 10); IL-4 = BMDMs with 10ng/ml IL-4; LPS = BMDMs with 100ng/ml LPS. n=1

A) Supernatant profiles from 8 hours post-stimulation

B) Supernatant profiles from 20 hours post-stimulation. Glucose, lactate and acetate are labelled.

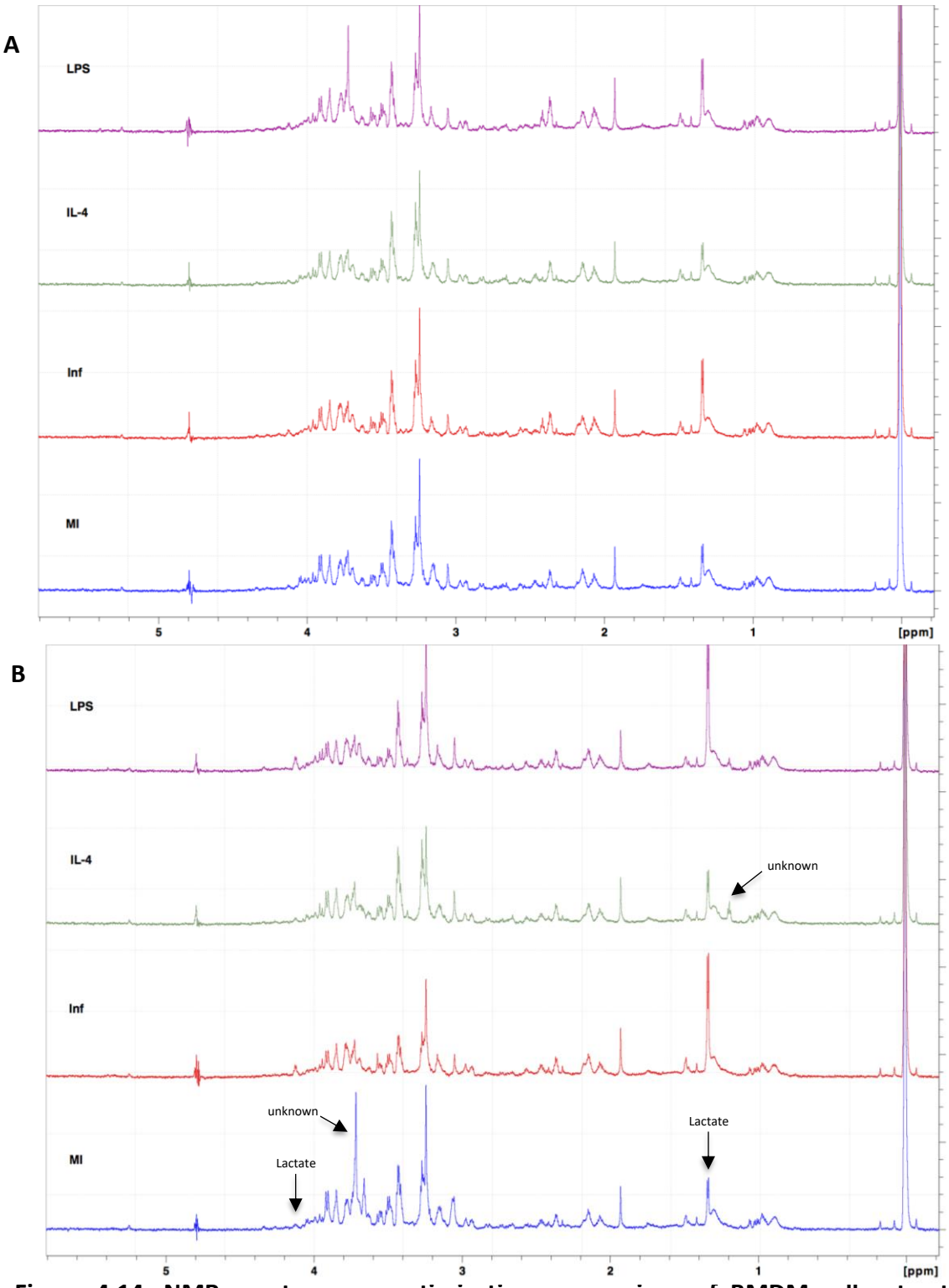

Figure 4.14: NMR spectroscopy optimisation: comparison of BMDM cell extract profiles after *S. pneumoniae* challenge, CAM or AAM stimulation after 8 and 20 hours

Cells were seeded at 1x10^{6}cells, treated as per key, with 1 hour on ice and 3 hours incubation. At 4 hours, all cells were treated with 20ug/ml Gentamycin and 40U/ml Penicillin, before media was replaced and cells returned to incubator. Cell extracts were prepared by methanol extraction, and spectra acquired on a 800Hz magnet. Images are annotated as follows: MI = mock-infected BMDMs; Inf = *S.pneumoniae*-challenged BMDMs (D39, MOI 10); IL-4 = BMDMs with 10ng/ml IL-4; LPS = BMDMs with 100ng/ml LPS. n=1

A) Cell extract profiles from 8 hours post-stimulation

B) Cell extract profiles from 20 hours post-stimulation. Lactate and peaks of unknown origin are labelled. Unknowns were contaminants or metabolites not identified by spectral tables.

4.2.3.4. Method optimisation - The influence of temperature on early metabolite profiles

The use of a 4°C incubation immediately after bacterial stimulation was questioned. It was hypothesised to affect the immediate responses of macrophages to bacteria, and that cellular responses could be different if cells were instead able to immediately respond at 37°C. Therefore, an alternative protocol was tested, whereby cells were stimulated, and the culture plate centrifuged briefly, before immediately transferring to a 37°C incubator. This aimed to increase adherence of bacteria to macrophage surfaces, without needing a reduced temperature. It also assessed whether early metabolite changes could be detected within four hours post-stimulation. Supernatant and cell extract samples were collected at 1, 2, 3, and 4 hours post-stimulation, both with and without the initial hour at 4°C. Once again, visual comparisons of spectra were carried out in TopSpin software.

Gradual differences could be seen over this time, with the most significant comparisons between the 1 hour and 4 hour post-stimulation groups. After one hour, the main noticeable difference in supernatant spectra was the emergent singlet peak at ~1.92ppm, in *S. pneumoniae*-only and BMDM *S. pneumoniae*-challenged groups. This correlated with acetate production by the bacterium, and was not previously observed in supernatant spectra until after 2 hours, when cells were first cooled upon addition of bacteria. Figure 14.15 specifically shows the 4 hour supernatant spectra from the six conditions sampled, with overlaid regions of interest indicated. After 4 hours stimulation, changes in the supernatant spectra were seen at: 1.33ppm (lactate), whereby presence of cells and/or bacteria increased this peak and the largest increase seen for *S. pneumoniae*-challenged BMDMs and LPS-stimulated BMDMs; 1.92ppm (acetate), which only increased in *S. pneumoniae*-only or *S. pneumoniae*-challenged BMDMs; 2.38ppm (oxaloacetate, not confirmed by spiking but displayed similar ppm shift), which only decreased in *S. pneumoniae*-only or *S. pneumoniae*-challenged BMDMs and could be associated with the emergent peak at 1.92ppm, as a product of streptococcal metabolism. The rest of the supernatant spectra could be overlaid without any other discrepancies or misalignments; hence this further supported the idea that supernatant samples were not going to be as valuable in revealing metabolic changes

between these conditions, due to dominance of media components in these samples. The focus of future work from here on was therefore on the analysis of cell extracts.

Upon analysing the cell extracts, no differences between spectra or conditions could be identified after 1 hour stimulation, but small changes became visible after 2 hours, for example, at 3.56ppm (choline/phosphocholine, not confirmed by spiking but displayed expected ppm shift), which increased in IL-4 stimulated cells. The most distinct changes were seen after 4 hours, suggesting that this should be the earliest time point sampled. Figure 14.16 shows an overview of regions 0-5ppm of cell extracts after 4 hours stimulation, with overlaid regions of interest highlighted. After 4 hours *S. pneumoniae*-challenge, the intensity of the spectrum had lowered compared to other conditions, with only a few regions remaining consistent between all groups – such as at 1.40ppm, 2.31ppm and 3.36ppm, each of which cannot accurately be correlated with a specific metabolite. Despite this, it was suggested that LPS and *S. pneumoniae* stimulation could induce different metabolic changes. These results suggest that the preliminary hour at 4°C, as part of the infection protocol, does not make a difference to cell extract spectra, if sampling at or after a 4 hour period.

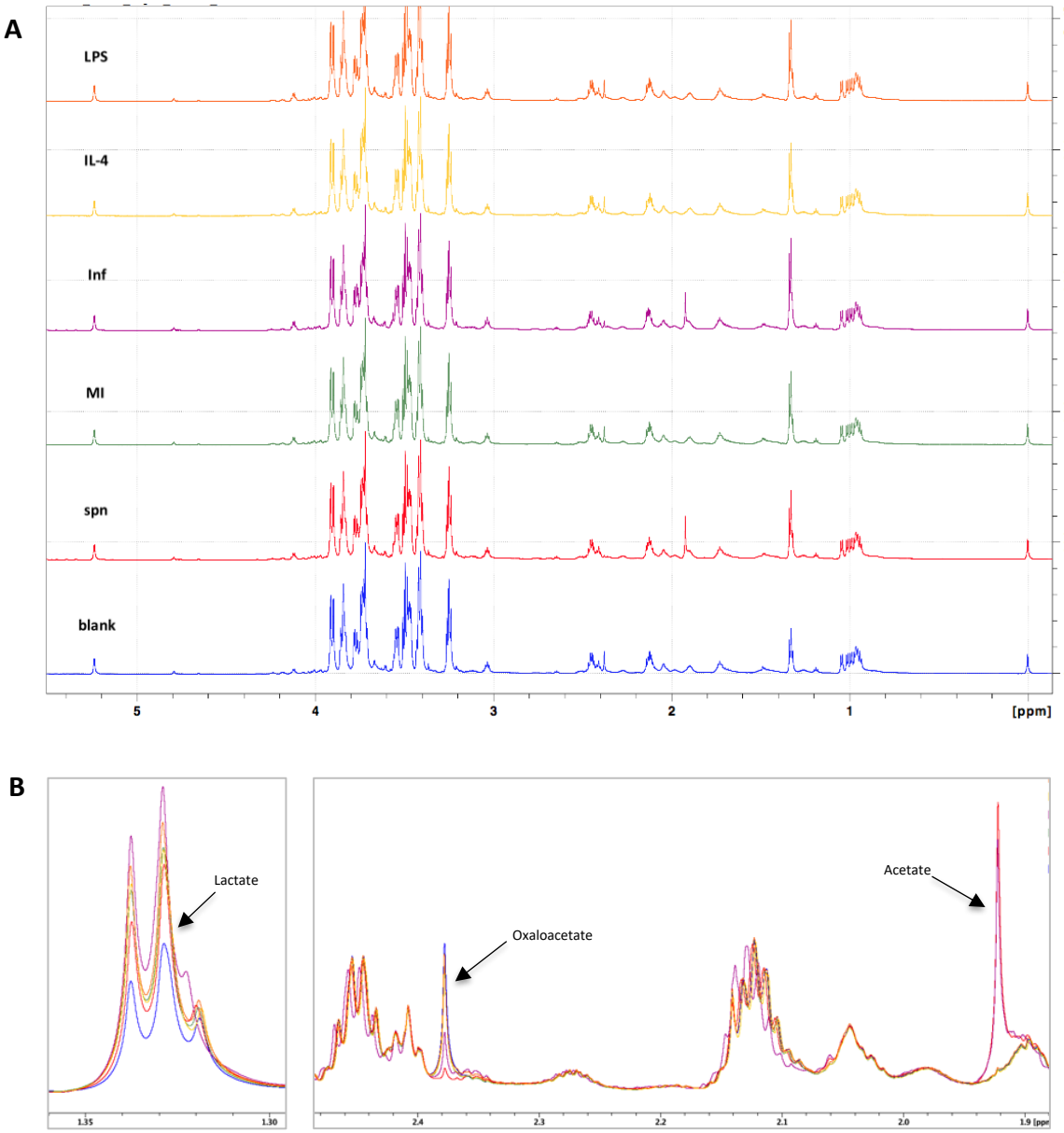

Figure 4.15: NMR spectroscopy optimisation: the effect of immediate incubation on supernatant metabolite profiles

Cells were seeded at 1x10^{6}cells, treated as per key, centrifuged at 9000rpm for 3 minutes and immediately incubated for 4 hours. Supernatants were collected directly and spectra obtained on a 800Hz magnet. Images annotated as follows: Blank = no cells, no bacteria; spn = no cells with *S. pneumoniae*; MI = mock-infected BMDMs; Inf = *S. pneumoniae*-challenged BMDMs (D39, MOI 10); IL-4 = BMDMs with 10ng/ml IL-4; LPS = BMDMs with 100ng/ml LPS.

A) Supernatant spectra from 4 hour post-stimulation samples only.

B) Regions of interest from all 4 hour post-stimulation groups, showing overlaid spectra from Figure 4.15A. Lactate, oxaloacetate (tentative assignment) and acetate and have labelled.

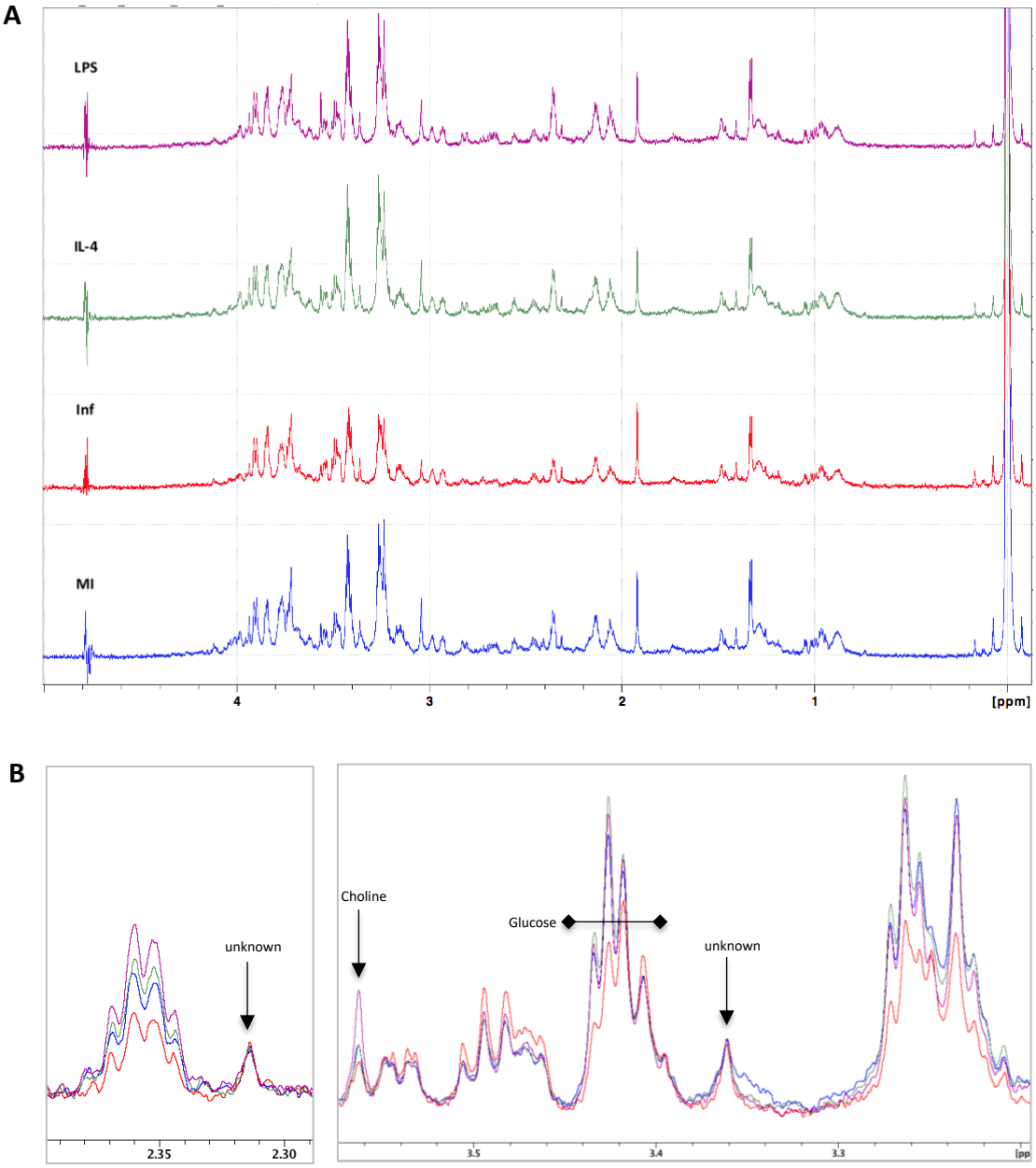

Figure 4.16: NMR spectroscopy optimisation: the effect of immediate incubation on cell extract metabolite profiles

Cells were seeded at 1x10^{6}cells, treated as per key, centrifuged at 9000rpm for 3 minutes and immediately incubated for 4 hours. Cell extracts were obtained by methanol extraction and spectra obtained on a 800Hz magnet. Images annotated as follows: MI = mock-infected BMDMs; Inf = *S.pneumoniae* challenged BMDMs (D39, MOI 10); IL-4 = BMDMs with 10ng/ml IL-4; LPS = BMDMs with 100ng/ml LPS.
A) Cell extract spectra from 4 hours post-stimulation samples only.
B) Regions of interest from all 4 hour post-stimulation groups, showing overlaid 4 hour spectra from Figure 4.16A. Glucose, choline (tentative assignment) and peaks of unknown origin are labelled. Unknowns are contaminants or not metabolites not identified by spectral tables.

To verify any effect of cooling versus centrifugation on BMDM metabolism, three biological preparations were collected from mock-stimulated BMDMs, with one triplicate set from each donor exposed to a temperature shift from ~4°C to 37°C, and a second triplicate set centrifuged and immediately transferred to 37°C. All samples were prepared after a total of 4 hours. In Figure 4.17, representative spectra are shown from just one donor. Interestingly, cells exposed to an hour at 4°C produced more consistent and reproducible cell extract preparations, with fewer variations both between donors and experimental replicates. Therefore this method was continued with, and time points were restricted to no earlier than 4 hours, to allow plenty of time for cells to respond at 37°C, prior to sampling.

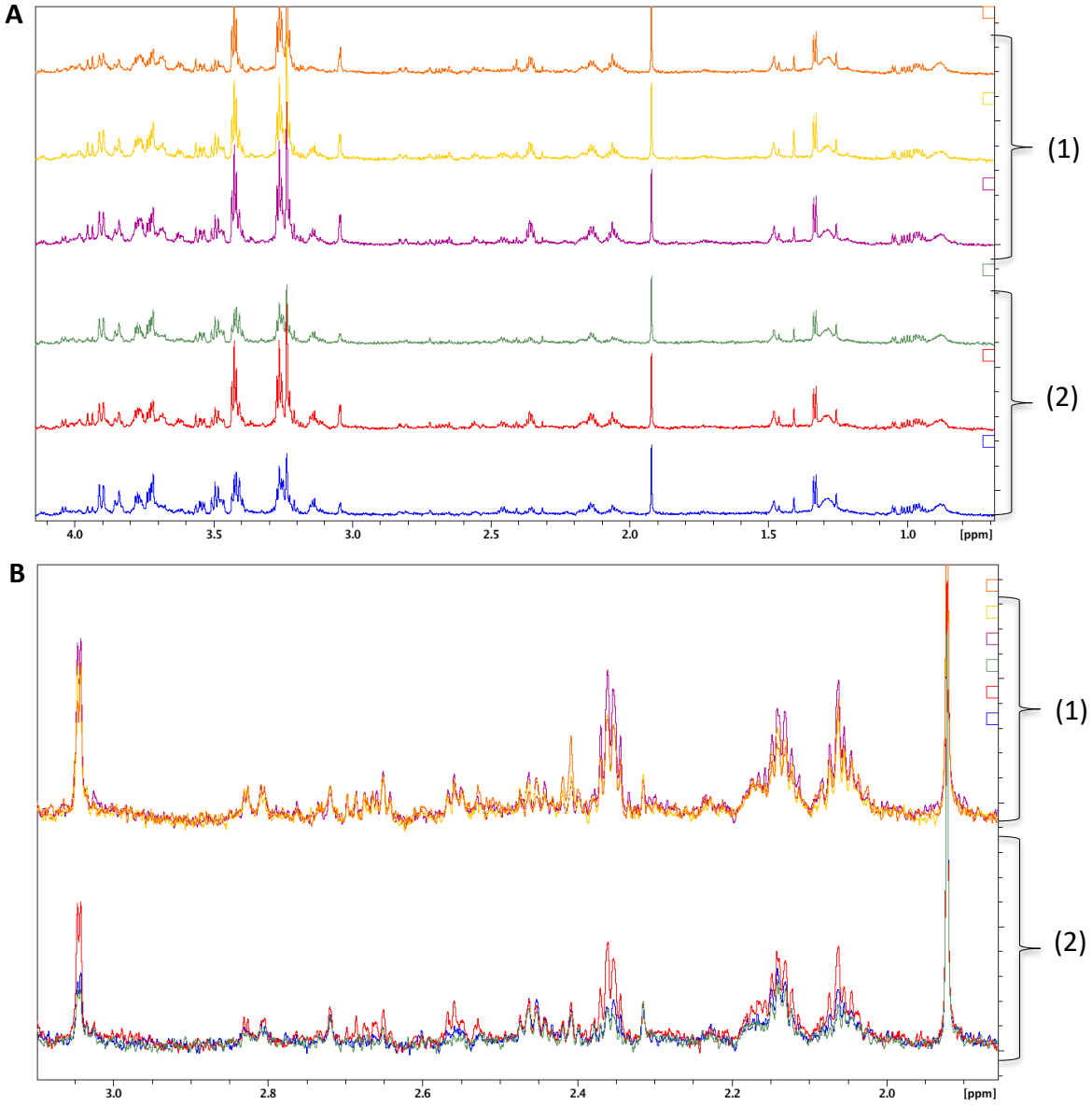

Figure 4.17: NMR spectroscopy optimisation: The effect of varying temperature on unstimulated BMDM cell extracts

Cells were seeded from three biological donors at 1x10^{6}cells. One triplicate set from each donor was sampled after 1 hour at 4°C (on ice) followed by 3 hours incubation at 37°C. A second triplicate set was sampled after centrifugation at 9000rpm for 3 minutes and immediate incubation for 4 hours at 37°C. Cell extracts were obtained via methanol extraction and spectra obtained on a 800Hz magnet. Biological n=3, experimental n=2.
A) Spectra from cells left at 4°C for 1 hour followed by 3 hours incubation (1) or after centrifugation and immediate incubation at 37°C for 4 hours (2). Only the 4.1-0.7ppm region is shown, for clear visualisation of spectra. Representative cell extract spectra shown from one biological donor.
B) Higher resolution image of overlaid spectra from Figure 4.16A, showing between 3.10-1.85ppm, indicating the reproducibility of these preparations. Spectra from cells left on ice for 1 hour followed by 3 hours incubation are shown at the top of the figure (1). Spectra from cells provided centrifugation and immediate incubation for 4 hours are shown at bottom of figure (2). Spectra are more defined and consistent for group (1).

4.2.9. Using 1H-NMR Spectroscopy to assess metabolic changes in BMDMs, following stimulation with LPS or *S. pneumoniae*

One-dimensional 1H-NMR Spectroscopy was used to consider the metabolic changes of murine BMDMs during *S. pneumoniae* challenge or LPS stimulation. To complement work shown previously using the Seahorse Extracellular Flux Analyser in Chapter 3, an early 4 hour and late 12 hour time point were both assessed. Following optimisation of this technique, only cell extract spectra were acquired and analysed, as they offered a more robust strategy for identifying changes to metabolic profiles after BMDM stimulation.

As described previously, the cell extracts of samples were prepared using an 80% methanol:water extraction method and acquired on a 800MHz spectrometer, via the pulse sequence 'ah_robust5.ptg'. A total of four murine donors were used, with duplicate extractions for each condition. To process the raw NMR data, a MATLAB algorithm was used to align, normalise, and calculate integral regions. An external collaborator, Dr. Stephen Reynolds from the University of Sheffield Jessop Fertility Research Centre, developed and ran this MATLAB script. The script processed all spectra, aligning to the average spectral position, replacing the water region (4.5-5.2ppm) with random integral values, binning the whole spectral region in equal 0.04ppm segments (-0.5-11ppm), and normalising to the area under each spectrum, before exporting the integral values of the processed data in plain text files. A copy of the MATLAB script can be found in the Appendix. The data produced from this script was used for the subsequent statistical analysis.

One of the most accessible resources in the field of metabolomics is the free online tool MetaboAnalyst. This is an online R-based server, currently maintained by the Jianguo Xia lab at McGill University in Québec, Canada. It provides different methods of processing and analysing metabolomic data, from both Mass Spectrometry (MS) and NMR Spectroscopy sources (Xia Lab 2017). Using this program, a 'Time series/Two-factor Design' analysis was performed on the integral bins calculated from the MATLAB algorithm, with a Two-factor independent sample study design, and using the data format shown in Figure 4.18. In this model, statistical functions were calculated, including an interactive Principal Component Analysis (iPCA), Heatmap visualisation, Two-way ANOVA and ANOVA Simultaneous Component Analysis (ASCA). Initially, all

samples and all binned integrals were used, to assess for variability and overall trends in the data. However, three samples varied significantly from the rest, and were identified as outliers via interactive PCA and heatmap analysis. These spectra were affected by either carry-through of supernatant metabolites or ineffective spectral alignment, therefore they were eliminated from further analysis. Regions of spectra known to be noise were also unwantedly flagged up as regions of interest. With this in mind, the data used for subsequent analysis was modified, to eliminate the problematic samples (MI4.2.1502, INF4.1.0203 and INF4.1.1403) and the following spectral regions: Bins1-50 (11-9ppm, spectral noise), Bins73-92 (8-7.3ppm, spectral noise), Bins147-164 (5.1-4.4ppm, water region) and Bins262-287 (0.5--0.5ppm, TSP region). This aimed to provide a more directed analysis, on robust samples and using only the regions of spectra containing peaks.

The revised data set was analysed, with the resultant heatmap and iPCA plot shown in Figures 4.19 and 4.20 respectively. From the heatmap, it could be stated that *S. pneumoniae* challenge induces a very different intracellular metabolic profile, compared to mock-stimulated or LPS-stimulated cells, after 12 hours. From this figure, regions of interest were selected, which increased either during *S. pneumoniae* or LPS challenge of BMDMs, compared to the mock condition. This provided specific spectral regions to identify, rather than identifying the whole spectrum. To identify the metabolites found in these spectral regions, Table 4.1, the HMDB, Bruker TopSpin and Chenomx software were used. When considering the interactive PCA plot, 12 hours *S. pneumoniae*-challenge caused the largest inherent sample variation compared to other sample groups, demonstrated by their group separation and high PC1 values. This further demonstrated that cells challenged with *S. pneumoniae* present a very different NMR spectra and metabolic phenotype compared to unstimulated or LPS-stimulated cells.

	A	B	C	D	E	F	G	H	I	J	K	L	M	N	O
1	Sample	Time	Subject	Bin1	Bin2	Bin3	Bin4	Bin5	Bin6	Bin7	Bin8	Bin9	Bin10	Bin11	Bin12
2	MI4.1.1502	4	MI	-0.00197589	-0.0016838	-0.0019698	-0.0017201	-0.0014283	-0.0016817	-0.0013215	-0.0013749	-0.0007098	-0.0007599	-0.0010596	-0.0011662
3	MI4.2.1502	4	MI	-0.00365602	-0.0034816	-0.0032891	-0.0030245	-0.003283	-0.0028656	-0.002321	-0.0024998	-0.002431	-0.0025204	-0.0019613	-0.002173
4	MI4.1.2202	4	MI	-0.00201134	-0.0022602	-0.0018771	-0.0020734	-0.0018595	-0.0019778	-0.0011925	-0.0010216	-0.0010973	-0.0009074	-0.0013598	-0.0007554
5	MI4.2.2202	4	MI	-0.00090799	-0.000795	-0.0007515	-0.0011313	-0.001201	-0.000993	-0.0008093	-0.0009724	-0.0013985	-0.0014832	-0.0009018	-0.0011806
6	MI4.2.0203	4	MI	-0.00155245	-0.0015913	-0.0014311	-0.0014776	-0.0014815	-0.0014524	-0.0012824	-0.0014226	-0.0017042	-0.0009466	-0.0010207	-0.0008662
7	MI4.1.1403	4	MI	-0.0012903	-0.0011095	-0.0009609	-0.0011413	-0.0010432	-0.0007244	-0.0012504	-0.0011375	-0.0010171	-0.0012672	-0.0010804	-0.0009452
8	MI4.2.1403	4	MI	-0.00148072	-0.0012966	-0.0015782	-0.0009369	-0.0014692	-0.0010949	-0.0011116	-0.0011314	-0.0014823	-0.0012049	-0.0013318	-0.0010496
9	MI12.1.1502	12	MI	-0.00166779	-0.0015577	-0.0013863	-0.0016695	-0.0012933	-0.0012692	-0.0012058	-0.0015104	-0.0010541	-0.0016228	-0.0014936	-0.0012963
10	MI12.2.1502	12	MI	-0.0019542	-0.0019002	-0.0017345	-0.0016267	-0.0014069	-0.0014912	-0.0013251	-0.0014908	-0.0015716	-0.0016602	-0.0013339	-0.0008442
11	MI12.1.2202	12	MI	-0.00147106	-0.0015173	-0.0015332	-0.0014597	-0.0015061	-0.0014183	-0.001311	-0.0010449	-0.0012421	-0.0013488	-0.0008485	-0.0009781
12	MI12.2.2202	12	MI	-0.00137511	-0.0012478	-0.0010739	-0.0010544	-0.0011508	-0.0008763	-0.0010248	-0.0013788	-0.0008553	-0.000913	-0.0006829	-0.0010168
13	MI12.1.0203	12	MI	-0.00123469	-0.0009521	-0.0013046	-0.0011595	-0.0008127	-0.0012595	-0.0011291	-0.0005465	-0.0008677	-0.000983	-0.0008142	-0.0008552
14	MI12.2.0203	12	MI	-0.00259888	-0.0025316	-0.0027083	-0.0023994	-0.0023398	-0.0025083	-0.0017557	-0.0011859	-0.00145	-0.0010979	-0.0009774	-0.00091
15	MI12.1.1403	12	MI	-0.00075124	-0.0011471	-0.0007812	-0.0010753	-0.0008097	-0.000873	-0.0010241	-0.000915	-0.0013116	-0.0011204	-0.0010721	-0.0010023
16	MI12.2.1403	12	MI	-0.00164687	-0.0016489	-0.0013497	-0.0021106	-0.0014101	-0.0014863	-0.0015703	-0.0012499	-0.001419	-0.0012781	-0.0013351	-0.0011155
17	INF4.1.1502	4	INF	-0.00311362	-0.002449	-0.0031442	-0.0024711	-0.0023623	-0.0026561	-0.0023354	-0.002089	-0.0009153	-0.0009618	-0.001051	-0.0015644
18	INF4.2.1502	4	INF	-0.00128734	-0.0005815	-0.0006961	-0.0008697	-0.0008794	-0.0007478	-0.0012313	-0.0011379	-0.000998	-0.0013888	-0.0015257	-0.0009369
19	INF4.1.2202	4	INF	-0.00144328	-0.0013196	-0.0012213	-0.0010743	-0.0009817	-0.0010339	-0.0009756	-0.001767	-0.0014382	-0.0011552	-0.0014506	-0.0008907
20	INF4.2.2202	4	INF	-0.00138428	-0.0017464	-0.001935	-0.0015488	-0.0014214	-0.0018945	-0.0009581	-0.0012032	-0.0011658	-0.0012496	-0.0009954	-0.001253
21	INF4.1.0203	4	INF	0.00083076	0.00041366	0.0001395	0.00043257	-1.018E-05	-0.0001018	0.00017761	0.00034353	0.00030014	0.0003177	0.00071621	0.00037604
22	INF4.2.0203	4	INF	-0.00075098	-0.0010806	-0.0009171	-0.0007803	-0.0006913	-0.0007148	-0.0011057	-0.0015109	-0.0013982	-0.0008787	-0.0013329	-0.0011348
23	INF4.1.1403	4	INF	-0.00185513	-0.0017672	-0.0018504	-0.0013363	-0.0018896	0.00152041	-0.0013038	-0.0015531	0.00106382	-0.0018822	-0.0014735	0.00086722
24	INF4.2.1403	4	INF	-0.00128352	-0.0010963	-0.0011813	-0.0013059	-0.0009845	-0.0011753	-0.0011834	-0.0008434	-0.0012904	-0.0015856	-0.001601	-0.0012665
25	INF12.1.1502	12	INF	-0.00167688	-0.0015205	-0.0020642	-0.0020527	-0.0015951	-0.0019136	-0.0015638	-0.0016949	-0.0018845	-0.0013732	-0.0017399	-0.0019236
26	INF12.2.1502	12	INF	-0.00160034	-0.0014863	-0.0014059	-0.0017096	-0.0013849	-0.0011563	-0.0020324	-0.0020881	-0.0013016	-0.001924	-0.0018821	-0.0019914
27	INF12.1.2202	12	INF	-0.00231582	-0.0024521	-0.0026433	-0.0022175	-0.0020594	-0.0021718	-0.0015564	-0.0017774	-0.002276	-0.0022051	-0.0013419	-0.0016614
28	INF12.2.0203	12	INF	-0.00270274	-0.0030933	-0.0024548	-0.0028048	-0.0029395	-0.0021712	-0.0029229	-0.0028455	-0.0022468	-0.0021594	-0.0014246	-0.0017111
29	INF12.1.1403	12	INF	-0.00286065	-0.0023038	-0.0025186	-0.0026298	-0.0024663	-0.0023117	-0.0016082	-0.0020546	-0.0022395	-0.0022422	-0.0020514	-0.0019942
30	INF12.2.1403	12	INF	-0.0038406	-0.0035762	-0.003173	-0.0028633	-0.003157	-0.0026435	-0.0025954	-0.0023501	-0.0025327	-0.0022316	-0.0021823	-0.0015652
31	LPS4.1.1502	4	LPS	-0.00081563	-0.0010423	-0.0007893	-0.0005347	-0.0008573	-0.0006248	-0.0010874	-0.0015979	-0.0010422	-0.0007581	-0.001087	-0.0009557
32	LPS4.2.1502	4	LPS	-0.00208327	-0.0019989	-0.0017762	-0.0018212	-0.0016432	-0.0014838	-0.0019074	-0.0017793	-0.0009232	-0.0009447	-0.0010253	-0.0014135
33	LPS4.1.2202	4	LPS	-0.00161628	-0.001708	-0.0017479	-0.0015363	-0.0016489	-0.0016895	-0.0011024	-0.0012483	-0.0015951	-0.0009119	-0.0011942	-0.0008854
34	LPS4.2.2202	4	LPS	-0.00121472	-0.0009862	-0.000904	-0.0010083	-0.0011465	-0.0006711	-0.0010799	-0.0010765	-0.0015912	-0.0011375	-0.0009098	-0.0008235
35	LPS4.1.0203	4	LPS	-0.00142088	-0.0016508	-0.0019052	-0.0012187	-0.0012116	-0.0016913	-0.0008995	-0.0015801	-0.0012933	-0.0015111	-0.0011414	-0.0011501
36	LPS4.2.0203	4	LPS	-0.00149324	-0.0007034	-0.0012286	-0.0010794	-0.0009207	-0.0009231	-0.0011876	-0.0011456	-0.0009394	-0.0010755	-0.0012768	-0.0013885
37	LPS4.1.1403	4	LPS	-0.00160862	-0.0013639	-0.0012567	-0.0013001	-0.0010155	-0.0013297	-0.0014584	-0.0011609	-0.0011485	-0.0012748	-0.0013596	-0.0010644
38	LPS4.2.1403	4	LPS	-0.00113186	-0.0017337	-0.0013548	-0.0013701	-0.0011402	-0.0014658	-0.0011844	-0.0017663	-0.0010712	-0.0008891	-0.0014896	-0.0013487
39	LPS12.1.1502	12	LPS	-0.00114027	-0.0011843	-0.0012876	-0.0012553	-0.0008426	-0.0015462	-0.0014309	-0.0009511	-0.0012741	-0.001314	-0.0017492	-0.0012943
40	LPS12.2.1502	12	LPS	-0.00173056	-0.0018966	-0.0015207	-0.0013488	-0.0011549	-0.0012565	-0.0012206	-0.0021368	-0.0020713	-0.0014828	-0.0013912	-0.0008081
41	LPS12.1.2202	12	LPS	-0.00164185	-0.0013305	-0.0016523	-0.0011368	-0.0012968	-0.0013596	-0.0012715	-0.0009711	-0.0010668	-0.0011931	-0.001446	-0.0006592
42	LPS12.2.2202	12	LPS	-0.00120267	-0.0014332	-0.0011701	-0.0011494	-0.0014615	-0.0009281	-0.0009815	-0.0009106	-0.0005818	-0.0006145	-0.000893	-0.0007434
43	LPS12.1.0203	12	LPS	-0.00177172	-0.0020498	-0.0017253	-0.0015692	-0.001969	-0.0014515	-0.0013945	-0.0011095	-0.0012817	-0.0013091	-0.0008382	-0.000796
44	LPS12.2.0203	12	LPS	-0.00126476	-0.0011948	-0.0014783	-0.000892	-0.0013529	-0.0011931	-0.001362	-0.0008285	-0.0012618	-0.0011135	-0.0010949	-0.0010988
45	LPS12.1.1403	12	LPS	-0.00126336	-0.0014122	-0.0010152	-0.001123	-0.0011047	-0.0009537	-0.0014567	-0.0008871	-0.001342	-0.0009345	-0.0009139	-0.0006205
46	LPS12.2.1403	12	LPS	-0.00010243	-7.924E-05	-0.0001253	0.00010658	5.8095E-05	-0.0001005	-0.0005354	-0.0013712	-0.000964	-0.0011609	-0.0012511	-0.0012422
47															

Figure 4.18: Format of processed 1H-NMR integrals for MetaboAnalyst analysis

Data inputted to MetaboAnalyst must be formatted appropriately. Here shown is the format required for a 'Time Series or Two-factor Design' module, where data used are 'spectral bins', separated as 'samples in rows'. Cell extract integrals are shown, and normalised against the sum of all 287 integrals, from -0.5-11ppm. The columns are titled: Sample (ID code for each sample spectra), Time (4 or 12), Subject (stimulatory condition) and Bin numbers (1-287).

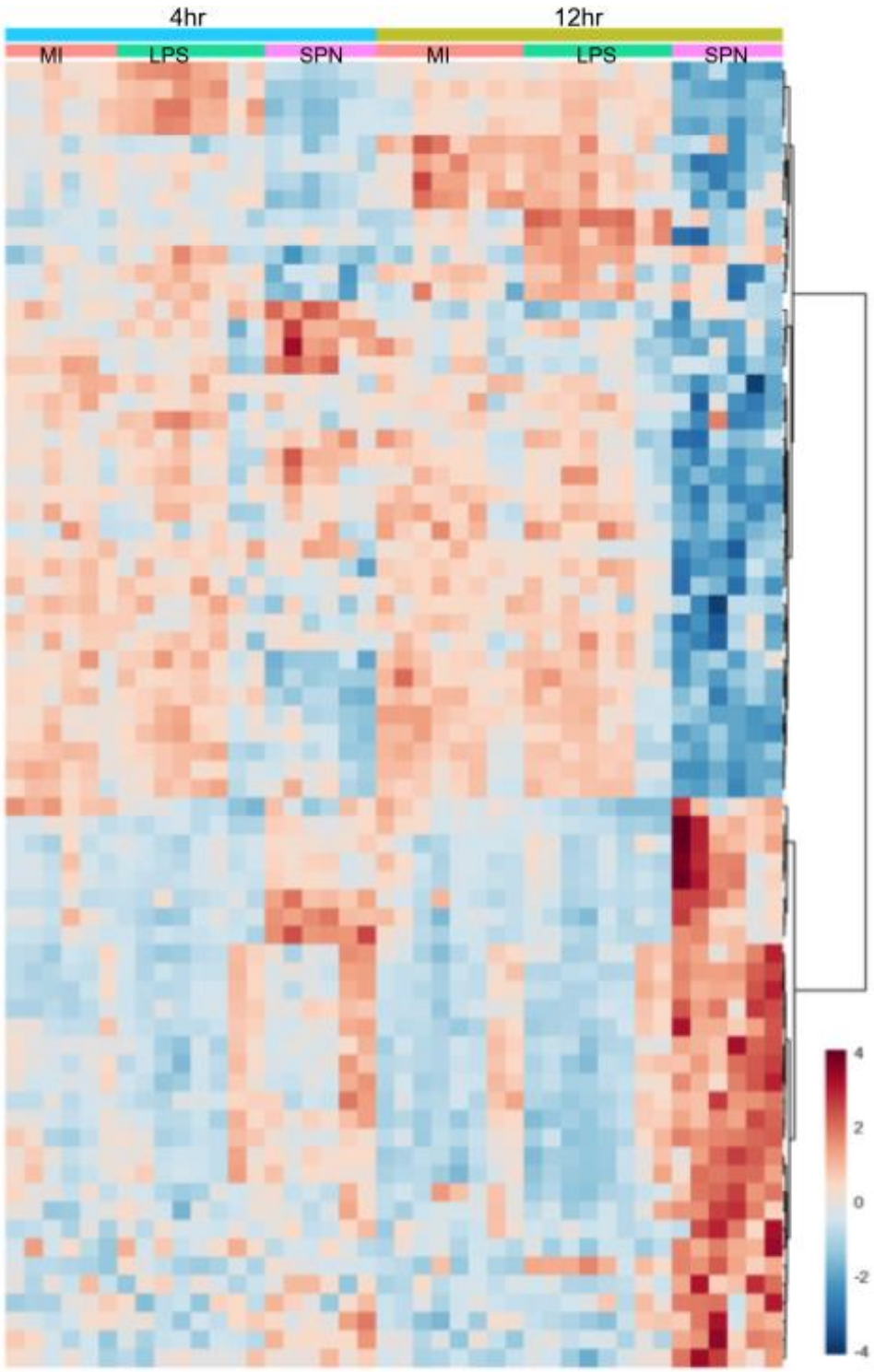

Figure 4.19: 1H-NMR MetaboAnalyst Results - Heatmap

Cells were seeded at 1x10^{6}cells, treated as per key, with one hour on ice and 4 hours incubation. Cell extracts were obtained by methanol extraction, after either 4 hour stimulation, or 12 hour stimulation, following antibiotic treatment and media replacement at 4 hours. Spectra were obtained on a 800Hz magnet. Image annotated as follows: MI = mock-infected; Inf = *S. pneumoniae* challenge (D39, MOI 10); LPS = 100ng/ml LPS. Heatmap generated using MetaboAnalyst, after data was processed via MATLAB. Data was sum normalised and auto-scaled. Three samples were excluded as outliers due to contamination, and ppm regions containing noise were eliminated from analysis. The most significant bins are shown, as calculated via Two-way ANOVA with Bonferroni multiple testing correction ($p<0.05$). Rows represent spectral bins, and columns indicate stimulation groups. Colours specify a relative increase (red) or decrease (blue) in this area of the spectrum, as shown by the key.

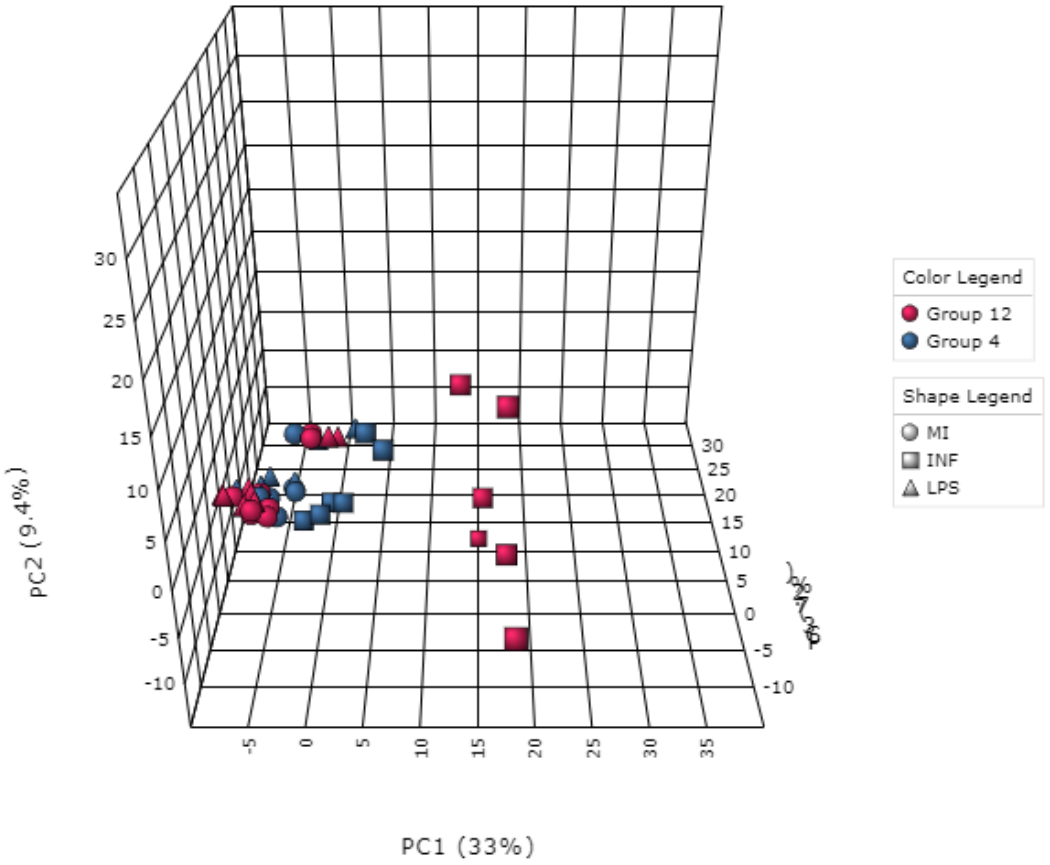

Figure 4.20: 1H-NMR MetaboAnalyst Results – PCA plot

Cells were seeded at 1x10^{6}cells, treated as per key, with one hour on ice and 4 hours incubation. Cell extracts were obtained by methanol extraction, after either 4 hour stimulation, or 12 hour stimulation, following antibiotic treatment and media replacement at 4 hours. Spectra were obtained on a 800Hz magnet. Image annotated as follows: MI = mock-infected; Inf = *S.pneumoniae* challenge (D39, MOI 10); LPS = 100ng/ml LPS. The interactive PCA plot generated using MetaboAnalyst online software. Data was sum normalised and auto-scaled prior to analysis. Three samples have been excluded as outliers, and ppm regions containing noise eliminated from analysis. Here, it is shown that 12 hour *S. pneumoniae*-challenged samples have a higher variation compared to all other samples, as separated by three principal component analyses. (NB. PCA analysis of original data set was used to distinguish outliers for subsequent analyses)

From the MetaboAnalyst results, integral regions of interest were further investigated. Once again, the HMDB, Chenomx Profiler and Table 4.1 were used to ID metabolites that corresponded to these integrals. The proposed metabolite IDs are shown in Table 4.2, and are listed as tentative/partial similarity, or high similarity. The partial similarity group present similar but weak spectral alignments and chemical shifts between this data set and compounds in spectral databases, whilst the high similarity demonstrate stronger correlations and more confident matches. These integral regions, or 'bins', have also been plotted separately in Figure 4.21, to show the changes between conditions. That said, further metabolite ID confirmation was needed, as these integral regions could result from multiple metabolite signals.

Bin no.	Metabolite ID – tentative/partial similarity	Metabolite ID – high similarity
Bin128	-	Itaconic Acid
Bin140	Allantoin, Phosphoenolpyruvate,	-
Bin170	Phophocholine, 6-Phosphogluconate, Fruc-2,6-bis-P,	-
Bin173	Creatinine, Lactate, Rib-5-P, Isocitrate	Choline
Bin174	Fruc-2,6-bis-P, Inosinic Acid, Glu-6-P,	-
Bin177	Betaine, Glycerophosphocholine	Creatine/Creatine-P
Bin178	Aspartate, Methionine, Serine, Glucose	-
Bin179	Glucose, 6-Phosphogluconate, Glycerol-3-P	-
Bin182	Dimethylglycine, Leucine, Glucose, Glu-6-P	-
Bin215	Oxaloacetate, Succinic acid, Pyruvate	Glutamate, Glutamine
Bin216	Proline, Malate	Glutamate
Bin221	Glutathione, Methionine, Acetylcholine	Glutamine, Glutamate
Bin223	Proline	Glutamate
Bin 227	-	Acetate
Bin 241	Threonine	Lactate

Table 4.3: 1H-NMR spectral regions of interest following MetaboAnalyst assessment: metabolite IDs

Binned regions of interest identified from the data displayed in Figures 4.18, 4.19 and 4.20. Metabolite IDs have either been assigned to these regions, as tentative/partial similarity or as high similarity, compared to the expected chemical shifts and peak shapes of metabolites, as seen in spectral data tables and online databases.

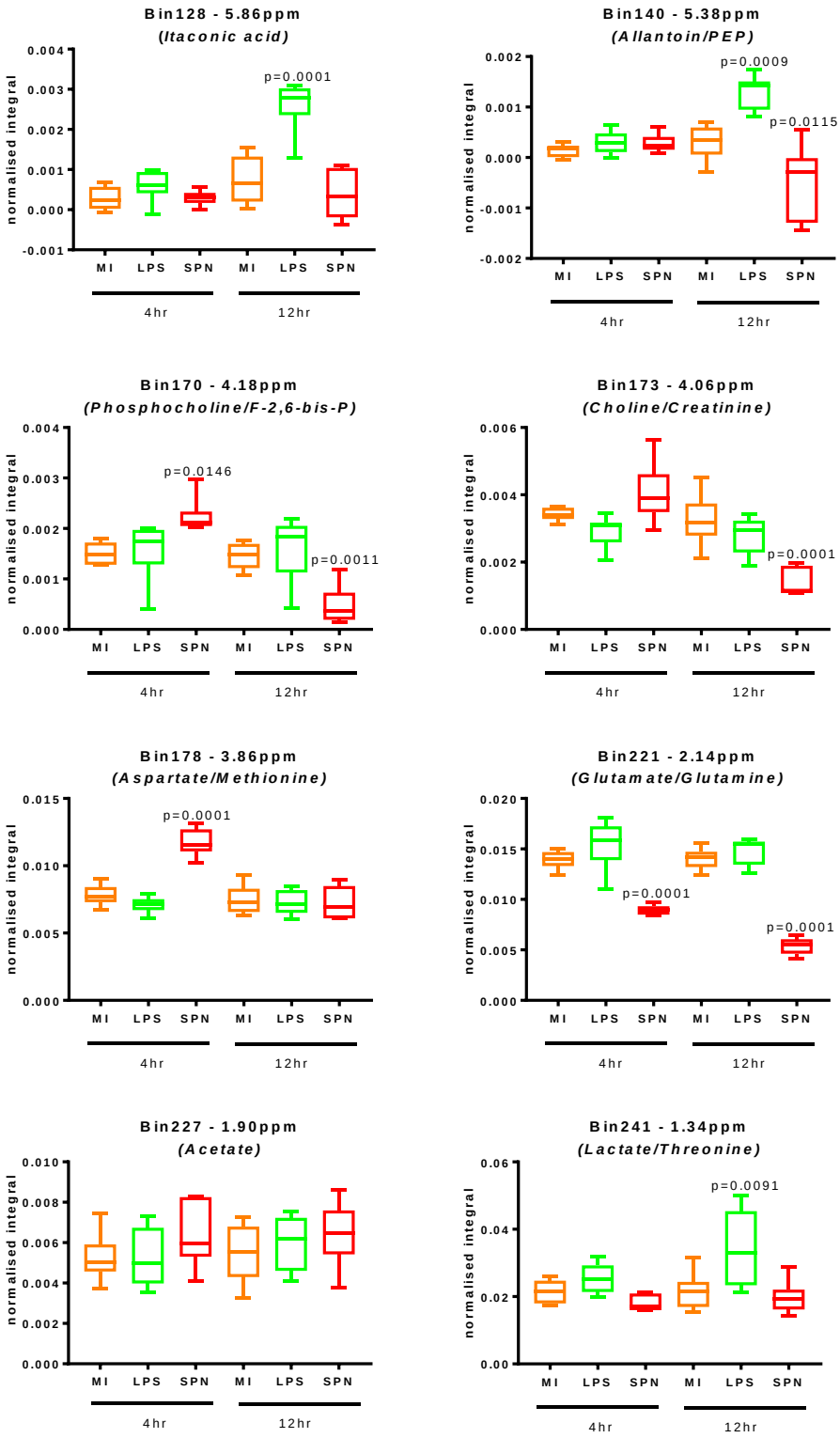

Figure 4.21: 1H-NMR spectral regions of interest – processed integrals

Cells were seeded at 1x10^{6}cells, treated as per key, with one hour on ice and 4 hours incubation. Cell extracts were obtained by methanol extraction, after either 4 hour stimulation, or 12 hour stimulation, following antibiotic treatment and media replacement at 4 hours. Spectra were obtained on a 800Hz magnet. Image annotated as follows: MI = mock-infected; Inf = *S.pneumoniae* challenge (D39, MOI 10); LPS = 100ng/ml LPS. Integral regions are plotted to show proposed changes to metabolite levels, following stimulation with either *S. pneumoniae* or LPS. Integrals were processed via MATLAB and plotted via GraphPad. Metabolites tentatively assigned using Table 4.1, 4.2 and online databases. Statistics were calculated via One-Way ANOVA with Dunnett's multiple comparisons to the MI group from the same time point.

To ascertain whether these metabolite IDs were both correct and present in cell extract samples, individual compounds were used to spike D_2O-PBS. This opportunity was also taken to test the detection of other compounds of interest, including arginine and succinic acid (succinate). Powdered metabolites were added to separate aliquots of buffer and pH adjusted to 7.8, to avoid ppm shift changes caused by strong acid or alkali solutions. This pH adjustment also correlated with standards seen for spectral libraries. An unstimulated cell extract was used for alignment and comparison, with the resultant and appropriate spectral regions shown for these spiked compounds in Figure 4.22. It was clear that arginine was not detectable in the cell extracts; therefore its utilisation in CAM metabolism could not be traced using this NMR Spectroscopy methodology. The same was also true of glutamine: some but not all its peaks are detected, which could be due to the high structural similarity with glutamate - which was detectable in the cell extract samples. Metabolite spiking also confirmed itaconic acid and glycine presence in cell extract samples, and a tentative confirmation of choline and succinic acid, both potentially present at low concentrations. Itaconic acid, a distinguishable marker of the broken TCA cycle during CAM metabolism, was shown to be produced by BMDMs within 12 hours LPS stimulation. Contrastingly, the same response was not seen for *S. pneumoniae*-challenged cells, indicating that the reported metabolic changes seen after LPS-stimulation, may not occur during live infection with this pathogen.

To identify further metabolites in Figure 4.20, crosschecks were made using Table 4.1, the HMDB, Bruker TopSpin and Chenomx software. Other distinguishable compounds were acetate (Bin227) and lactate (Bin240-243), both of which increased during a 12 hour challenge with *S. pneumoniae* and correlated with earlier findings.

.

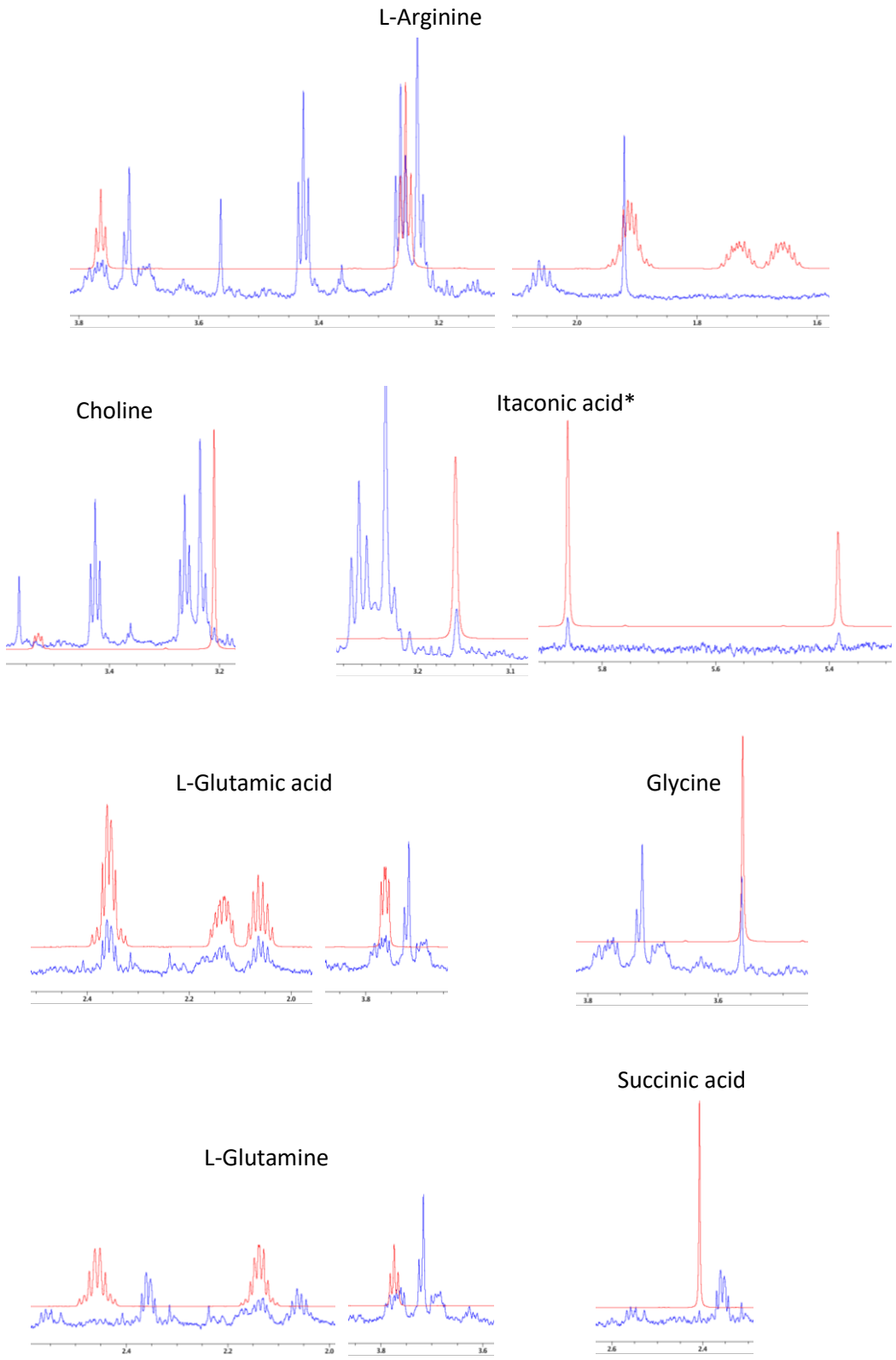

Figure 4.22: 1H-NMR spectral regions of interest – spiked compounds

Powdered metabolites of interest were added to 70% D_2O PBS with 167µM TSP, and pH adjusted to 7.8. Cells were seeded at $1x10^6$cells, and cell extracts were obtained by methanol extraction. Spectra were obtained on a 800Hz magnet. The spectra of an unstimulated cell extract (blue) is shown, overlaid with spectra from spiked metabolites (red) - **cell extract of a previous 12hr LPS-stimulated sample is shown here, as itaconic acid is not produced by unstimulated cells;* n=1.

4.3. Discussion

4.3.1. Chapter Summary

This chapter outlines the attempted optimisation of NMR Spectroscopy to study murine BMDM metabolites, and the processes required for metabolomic analysis of spectra. Attention was made to ensure appropriate cell numbers were used for preparations, and to consider the influence of culture media and temperature changes of this model on the resultant spectra. The technique was then used to consider the metabolome of unstimulated BMDMs, compared to LPS-stimulated and *S. pneumoniae*-challenged cells. The overarching, novel conclusion of this chapter is that *S. pneumoniae* does not induce the same global metabolic changes as seen for LPS.

Optimisation of NMR Spectroscopy, for the analysis of metabolic changes in cell culture samples, was initially discussed. Firstly, appropriate protocols were identified in the literature, with Ramm Sander and Lamour providing the two principal methods tested (Ramm Sander et al. 2013; Lamour et al. 2012). With the Ramm Sander whole cell approach, the preparation and run time for each sample was approximately half an hour, during which the cells settled and adhered to the bottom of the Shigemi tubes. This was problematic as samples were not homogenous during acquisition time, which could affect the resulting spectra. Additionally, the adherence of cells made it difficult to clean the tubes, which hindered upscaling this experiment to a larger sample set. Finally, the cells were still viable, metabolising and reacting to the environment inside the spectrometer, which was below 5°C and absent of nutrients. Therefore, it was considered that this protocol was not suitable to take forward. Contrastingly, the Lamour method was more labour-intensive, but provided a simple way of measuring changes between the intracellular and extracellular environment. Cell preparation required destruction of samples, therefore real-time analysis was not possible, but the Lamour protocols were used in favour of the shorter acquisition times and spectral quality.

A preliminary screen of *S. pneumoniae*-challenged BMDMs was carried out, to assess visible metabolic changes over a 24 hour period. This data set was used to test preliminary analysis techniques, such as Chenomx and integral calculations. No distinct differences were seen for supernatants, apart from an overall decrease in the intensity of glucose peaks with pneumococcal challenge, which amplified over time. This could

have been due to an increased metabolic demand and elevated glycolysis; however, it was also considered that increased cell death typically occurs 16-24 hours after *S. pneumoniae* challenge (Dockrell et al. 2003b), therefore fewer viable cells may have contributed to these spectra. BMDMs could also have been overwhelmed and shifted towards increased apoptosis by excess bacterial growth at these later time points. This idea of reduced cell numbers was supported upon viewing the 16-24 hour spectra from corresponding cell extracts, as the intensity of the spectra also decreased with time. Another noted problem in this data set concerned warping of spectral baselines. These warped spectra could have been a result of poor manual phasing and baseline correction, or the presence of contaminants such as excess protein in the culture media. When plotting integrals with this data set, mis-alignments and potential contamination were identified. Prior to calculating or comparing integrals, spectra should be normalised and aligned appropriately. According to the literature, metabolomic NMR data processing and analysis is typically performed using numerical programming; for example with the use of programs such as R or MATLAB, many of which are written in-house (Lamour et al. 2012; Ellinger et al. 2013). From here, technical optimisation was needed, particularly regarding sample extraction, metabolite ID and data handling methods.

Initial optimisations included assessing the impact of cell number, culture media and the infection protocol on resulting spectra. An intermediate cell number was found to give clear and visible spectral readouts, and the undesirable effect of HIFCS in supernatant spectra was highlighted. The expected spectral profiles from CAM and AAM stimuli were assessed, for both supernatants and cell extracts. This demonstrated that LPS would be a worthwhile control for CAM activation, whilst IL-4 was not of primary interest, as this work focused instead on pro-inflammatory and CAM-type activation patterns rather than AAM-type. Upon reflection of these results, the appropriateness of a cell extract after 20 hour pneumococcal-challenge could be questioned. It has been documented by the Dockrell group that BMDMs undergo apoptosis from 16hr post-infection with *S. pneumoniae* (Marriott et al. 2005). Therefore sampling should occur prior to this to avoid cell loss, to provide more cells for NMR preparation and therefore increase the signal:noise ratio in cell extract spectra.

The influence of temperature changes in the infection protocol were also evaluated. Within the typical infection procedure, cells were first kept at 4°C (on ice) for one hour immediately after stimulation, before being transferred to a 37°C incubator for a further 3 hours. This initial cooling correlates with previous studies carried out by the Dockrell group, and aims to increase bacterial adhesion to the BMDM cell surfaces, promoting synchronous phagocytosis across the whole cell population, once cells are transferred to 37°C (Gordon et al. 2000; Ali et al. 2003). It was considered that this temperature shock could hinder the immediate cellular responses to bacteria or hamper bacterial growth and virulence in this system. However, upon comparison between cooled and non-cooled conditions, no undesirable differences were observed in the spectrum. The original infection procedure was therefore continued with, to remain in-line with current practice by the Dockrell-Marriott group.

Following these optimisation stages, NMR Spectroscopy was used to analyse the cell extract samples of BMDMs, after stimulation with LPS or *S. pneumoniae,* compared to the mock condition. Duplicate samples from four biological donors were used, and data was aligned and normalised via a collaboration with the University of Sheffield Jessop Fertility Research Centre. The subsequent data was analysed and visualised via MetaboAnalyst. Regions of interest were identified by assessing for increased/decreased integral values after pneumococcal or LPS challenge compared to the mock. Compounds such as glucose, glutamate, choline, succinate and itaconic acid were identified as key changes during these experiments. However, parts of the spectral regions of interest were in overlapped metabolite regions, making identification quite restricted. One of the largest issues here regarded glucose, which has seven major peaks between 3.1-3.9ppm. This could therefore mask changes to other low concentration compounds that produce similar chemical shifts. An analogous situation to this was also seen regarding the multiple ppm shifts for glutamate. Due to this, a limited number of metabolite IDs were confirmed. That said, a major finding here was the production of itaconic acid by LPS-stimulated macrophages, which was not seen during mock-stimulation or pneumococcal challenge of BMDMs.

4.3.2. Chapter Discussion

LPS is well documented as being a strong pro-inflammatory stimulus, known to cause distinct metabolic changes including increases to glycolysis, elevated succinate production and a shift in arginine metabolism towards NO production (Tannahill et al. 2013; Rath et al. 2014). Here, 1H-NMR was used to identify metabolites in central carbon metabolism of BMDMs, including lactate, itaconic acid and glutamic acid, to propose that *S. pneumoniae* does not induce a strong change to CAM metabolism, like LPS does. A key finding here is the identification and confirmation of itaconic acid, specifically at 5.68ppm, following LPS stimulation. This is interesting and noteworthy because this did not occur during *S. pneumoniae* challenge of BMDMs. The production of itaconic acid during LPS stimulation is thought to occur during arrest of the Krebs cycle, and is considered to play a part in antimicrobial activity of macrophages (O'Neill et al. 2016). This is a hallmark of pro-inflammatory macrophage activation, further supporting the idea that *S. pneumoniae* does not induce the same, strong CAM phenotype or metabolic changes. In addition to this, *S. pneumoniae* induced increases in lactate and acetate, which are likely due to increases in glycolysis and from pneumococcal metabolism respectively. Furthermore, it was considered that glutamate levels decreased during bacterial challenge, which could be due to an increased need to feed glutamate into the Krebs cycle, through conversion to α-ketoglutarate. Finally, with noted changes to arginine metabolism during pro-inflammatory stimulation, it was discouraging not to be able to identify this compound in our samples, particularly following LPS stimulation. This could be due to the low sensitivity of this technique, particularly in comparison to MS strategies.

An explanation for the difference between LPS- and *S. pneumoniae*-stimulation could involve the strength of the initial host-pathogen interaction and subsequent activation of receptor pathways. LPS has been characterised as a TLR4 agonist, with well-defined intracellular pathway activation, via factors such as MyD88, which ultimately lead to NF-kB activation (Koppe et al. 2012; Opitz et al. 2010); however *S. pneumoniae* presents an assorted range of surface proteins and PAMPs, as opposed to just one, with many antigens also hidden beneath the thick polysaccharide capsule of the bacteria. This could mean they remain undetected, perhaps until the capsule is degraded in the phagolysosome. This would therefore make it hard for the macrophage to bind,

recognise and respond to the pathogen in a swift manner. Wolf et al. previously discussed a related theory. They showed that intracellular degradation of lysozyme-sensitive *S. aureus* – a pathogen normally capable of resisting lysosomal degradation – produced an elevated IFNβ cytokine response following activation of intracellular PRRs, compared to the wild-type strain. They describe how inflammation appeared in two waves: an initial activation after surface receptor engagement, followed by a second wave that correlated with bacterial phagosomal breakdown (Wolf et al. 2011). Further to this, macrophage responses to bacteria have been shown to be case-dependent, with cellular polarisation often variable in each instance. For example, Goldmann et al. described an unusual phenomenon following *S. pyogenes* infection of murine macrophages, whereby typical pro-inflammatory responses, such as cytokine release, were induced but were observed in association with up-regulation of Arginase, an AAM phenotypical marker, instead of the CAM-associated marker iNOS (Goldmann et al. 2007). This could suggest that macrophage responses are unique to each pathogen, and/or that bacteria are able to subvert and/or manipulate some CAM-associated host responses, to sustain their own survival. The latter is thought to be the case for *M. tuberculosis*, which avoids lysosomal killing and persists in the intracellular environment through promoting macrophages into a more AAM phenotype (Lugo-villarino & Neyrolles 2014).

4.3.3. Future work

NMR Spectroscopy for metabolomic assessment of cell cultures had not previously been assessed at the University of Sheffield. This work provided a novel methodology both in the field and at this University. However, the lack of initial expertise resulted in a slow-going experimental process, compared to well-established centres such as those found in London, Liverpool and Birmingham. Therefore in order to progress this work and verify findings at an increased pace, collaboration with external NMR metabolomic facilities would be desirable. This would allow access to informed workflows that have continuously evolved with the field – from initial NMR acquisition through to statistical and pathway analyses. This would also provide potential for high sample throughput, with the use of automated samplers and in-house spectral processing methods, all of which contribute to high quality and reproducible spectra that provide more informative

outcomes (Aranı´bar et al. 2006). Many publications in this field increasingly use tandem techniques, to achieve superior metabolite coverage, separation and sensitivity - for example by using chromatography with MS and NMR (Zhang et al. 2012); therefore working with metabolic centres would allow these set-ups to be accessed. A further benefit to this collaboration would also be the experience in data analysis, particularly concerning multivariate statistical analysis with reciprocal metabolite and pathway identification.

One of the biggest challenges of this chapter concerned confirmation of metabolite ID, therefore this would be a major theme to continue with. A method that was not trialled here was 2D-NMR. This allows metabolites to be identified simultaneously via both 1H and 13C NMR, providing a way of cross-referencing the two spectra to aid metabolite ID. However, analysing this 2D-spectra requires specialist understanding and interpretation of J-coupling patterns, therefore it was not utilised here. Additionally, metabolite spiking was used to aid metabolite ID, however this can be a limitless activity – hence it was only performed with a select batch of compounds. That said, this targeted identification method could be continued, and accompanied using databases and software with wider metabolite ranges, to identify more compounds across the spectral region. Finally, a further method that could be used to aid metabolite ID is Statistical Total Correlation Spectroscopy (STOCSY), which looks for correlations in changes to peak intensities, which are statistically likely to be contributed by the same molecule. This only works on compounds with multiple peaks, but has been previously shown to aid metabolite ID of complex mixtures (Cloarec et al. 2005).

NMR Spectroscopy could alternatively be used to trace isotope-labelled metabolic precursors through predetermined metabolic pathways using ^{13}C-labelled compounds - glucose and glutamine are two of the most commonly used (Walther et al. 2012; Metallo et al. 2009). This allows the user to trace metabolism, through chasing an isotope label in metabolic compounds. However, this technique has a few drawbacks: *a priori* knowledge is required for the metabolic pathway of choice, making it difficult to use during extensive pathway discovery or screening; labelled compounds must be taken up by cells, so often central carbon metabolism is the focus of experimentation as this is typically rate-limiting for growth and survival in mammalian cells; the technique is very costly, as expensive labelled compounds, long acquisition times and a high demand for

computational or mathematical modelling are required (Cascante & Marin 2008; Malloy et al. 2013). Therefore this may not be suitable in the immediate future but would be ideal for longer term future studies.

The field of NMR metabolomics is still progressing, and the use of NMR to study metabolomics has been largely overshadowed by MS techniques. However, it is developing to assess a wide range of samples, from bacteria and cell cultures, through to samples obtained directly from patients, such as blood, urine and tissue. This therefore brings with it a complex and varied methodology, with different preparations, extraction and acquisition steps required in each case. Here, only cell cultures were used. This allowed an experimental design that considered metabolites in both the extracellular and intracellular environments, using simple 1H-NMR. The Lamour et al. protocol was chosen, as it provided a convenient method for BMDM model analysis, using unprocessed supernatants and a methanol-water extraction of cell extracts. That said, extraction methods are extremely variable across the field, with different combinations of solvents used including water, chloroform, acetonitrile and/or perchloric acid, and also different variations in quenching, including ice-cold PBS, liquid nitrogen and sonication (Lin et al. 2007; Kostidis et al. 2017). Therefore, it could be worth assessing the benefits of these processes to aid sample extraction and analysis. For example, a two-phase extraction using methanol, water and chloroform, could be used to produce two separate fractions, consisting of aqueous water-soluble metabolites and organic non-polar molecules respectively. This could also allow greater precipitation of proteins and other large macromolecules prior to NMR acquisition, which would further improve baseline correction and phasing of spectra (Lauri et al. 2016; Teng et al. 2009).

Looking to the future, it would be interesting to apply metabolomic NMR Spectroscopy to samples obtained from patients or animal models infected with *S. pneumoniae* and/or other respiratory pathogens. This has already been touched upon by Slupsky et al. with their analysis of urine from patients of pneumococcal pneumonia (Slupsky et al. 2009) and also by McClay et al. who looked for metabolic biomarkers of lung disease, in the blood and urine of chronic obstructive pulmonary disease patients (McClay et al. 2010). Whilst *ex vivo* and patient sample analysis has focused on blood and urine, it would be interesting to observe metabolic signatures in sputum, to consider metabolite biomarkers that may arise during different types of respiratory infection. These

applications, however, focus mainly on potential diagnostic applications while my work has been focused more upstream on understanding key steps in the host-pathogen interaction, whose application could be therapeutic, prognostic or diagnostic.

Chapter 5 – The importance of glucose metabolism during BMDM challenge with *S. pneumoniae*

5.1. Introduction

It is shown that LPS increases glycolytic metabolism in macrophages and that this is important in priming the cell to fight infection (Tannahill et al. 2013). To test whether this was also true for BMDM responses to *S. pneumoniae*, three inhibitors were used to interrupt glycolysis and the PPP, mirroring work that had previously been done with LPS and macrophages (Haschemi et al. 2012; Tannahill et al. 2013). The glucose analogue 2-deoxyglucose (2DG) competitively inhibits Hexokinase and leads to intracellular accumulation of 2DG-phosphate, which cannot be used by Phosphoglucose Isomerase. It has been used in the literature as a method of halting glycolysis and depleting cellular ATP (Pelicano et al. 2006). Dehydroepiandrosterone (DHEA) is an androgen precursor, which inhibits Glucose-6-phosphate Dehydrogenase, the rate-limiting enzyme of the pentose phosphate pathway (PPP), and Iodoacetate (Iodo) inhibits Glyceraldehyde-3-phosphate Dehydrogenase, an enzyme at the branch-point of glycolysis, by irreversibly binding cysteine residues in the enzyme active site and preventing substrate interaction (Haschemi et al. 2012). The chosen compounds were tested simultaneously to dissect the role of glucose in these responses, as they acted at different stages of the glucose pathway: 2DG restricted glucose entry and glycolysis entirely, Iodo allowed glucose entry and the PPP, but blocked glycolysis halfway through the pathway, whilst DHEA allowed glycolysis but inhibited PPP metabolism. Figure 5.1 highlights the action of the inhibitors in these pathways. The inhibitors were used in the context of macrophage effector functions assays, to establish the importance of glucose metabolism in these processes during *S. pneumoniae* challenge.

Further to this, supporting functional and metabolic experiments were performed, to compare BMDM responses induced by LPS with those seen after *S. pneumoniae* challenge. These experiments aimed to understand the role of glucose metabolism in macrophage activation and innate immune functions, comparing bacterial challenge to LPS-induced responses, as a stimulus of the CAM phenotype. These experiments also complemented the work shown in Chapters 3 and 4.

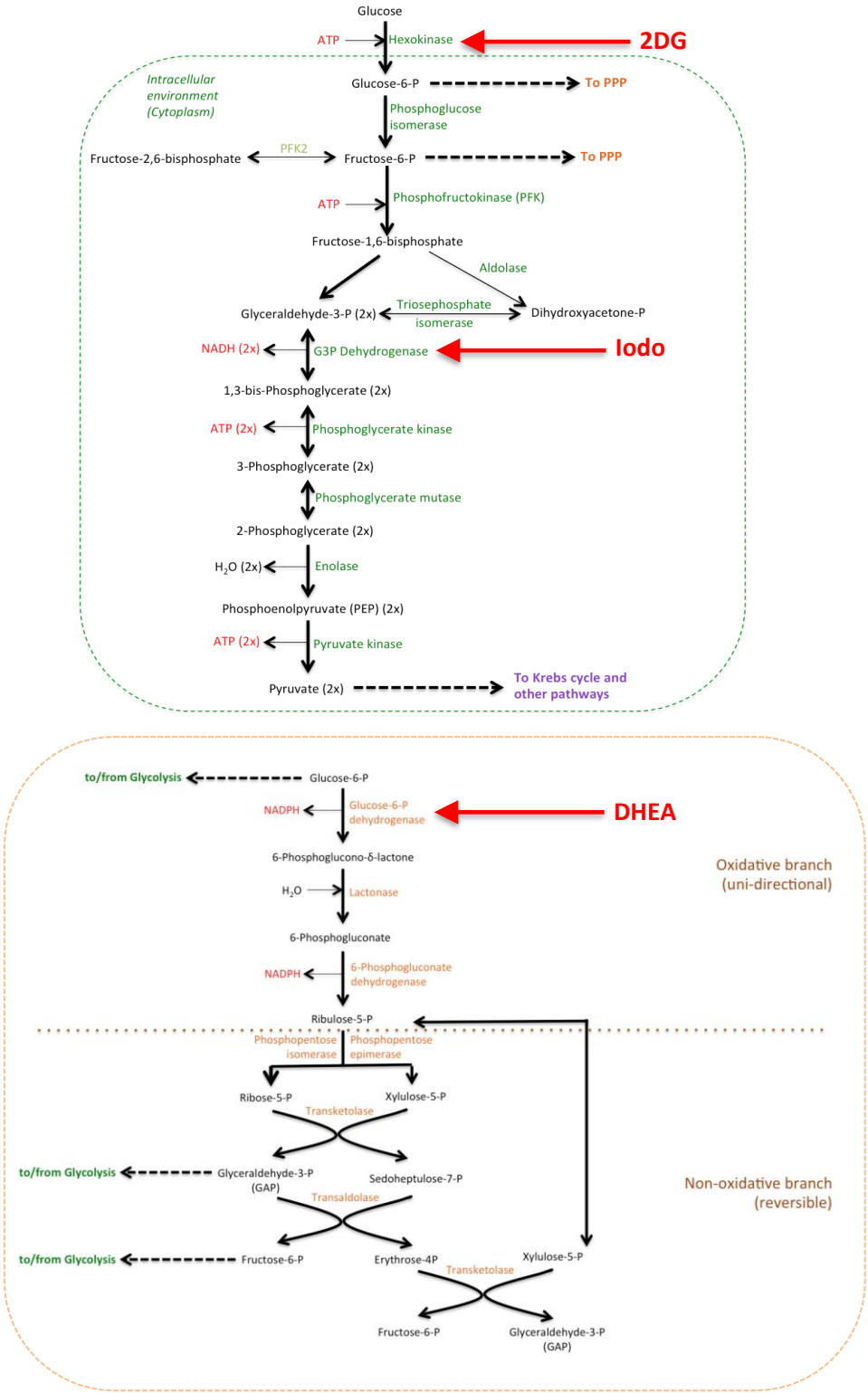

Figure 5.1: Glycolysis and PPP metabolism indicating glycolytic inhibitor activities

Details of the pathways for glycolysis (green) and the PPP (orange) are shown, highlighting enzymes, intermediates, and key interlinking regions in both. The inhibitory action of the compounds used in this chapter are shown in **bold red**.
(ATP = adenosine triphosphate, PFK = phosphofructokinase, PFK2 = phosphofructokinase-2, G3P = glyceraldeyde-3-phosphate, NADH = nicotinamide adenine dinucleotide, NADPH = nicotinamide adenine dinucleotide phosphate, PEP = phosphoenolpyruvate)

5.2. Results

5.2.1. The role of glycolysis in BMDM bacterial internalisation and TNFα release during *S. pneumoniae* challenge

The inhibitors - 2DG, Iodoacetate and DHEA - were used to consider the impact of glucose metabolism on TNFα cytokine release, following *S. pneumoniae* challenge of BMDMs. BMDMs were inhibited for one hour, followed by addition of *S. pneumoniae* for 4 hours. This is referred to here as the inhibit-then-infect strategy, with results shown in Figure 5.2. In the absence of bacteria, 2DG induced a trend of increased TNFα release; however this change was not statistically significant. All other conditions induced cytokine changes narrowly within the detection limit of this ELISA kit (~5pg/ml). During pneumococcal challenge, unstimulated cells (UNS - cells with no metabolic inhibition) demonstrated the anticipated increased release of TNFα. A similar level was also seen during Iodo treatment. However, both 2DG and DHEA significantly reduced TNFα release during bacterial challenge. The effect of DHEA could be suggested to be partly caused by it's solvent, as the DHEA vehicle control also caused a drop in TNFα after pneumococcal challenge, although this was not found to be statistically significant. That said, the large reduction in cytokine release, following 2DG treatment and *S. pneumoniae* challenge, could suggest here that glucose uptake and/or glycolysis play a role in early macrophage cytokine responses to pneumococci.

In Figure 5.2, bacterial growth curves of *S. pneumoniae* in the presence of the glycolytic inhibitors are shown. These inhibitors were not specific to murine macrophage metabolism, so were tested for their effects against bacterial growth and metabolism. It was hypothesised that if the inhibitors affected bacterial growth, this could impact on the virulence of the bacteria and therefore the host-pathogen interaction (Peterson 1996). Here, 2DG slowed bacterial replication, as measured by OD, whilst DHEA seemed to halt it completely. This inhibition of viable bacterial growth could have been the cause of the low cytokine release in Figure 5.2B. From these findings, an alternative experimental method was proposed, whereby simultaneous use of the inhibitors and bacteria were avoided, to avoid undesirable inhibition of bacterial metabolism or growth in the extracellular environment.

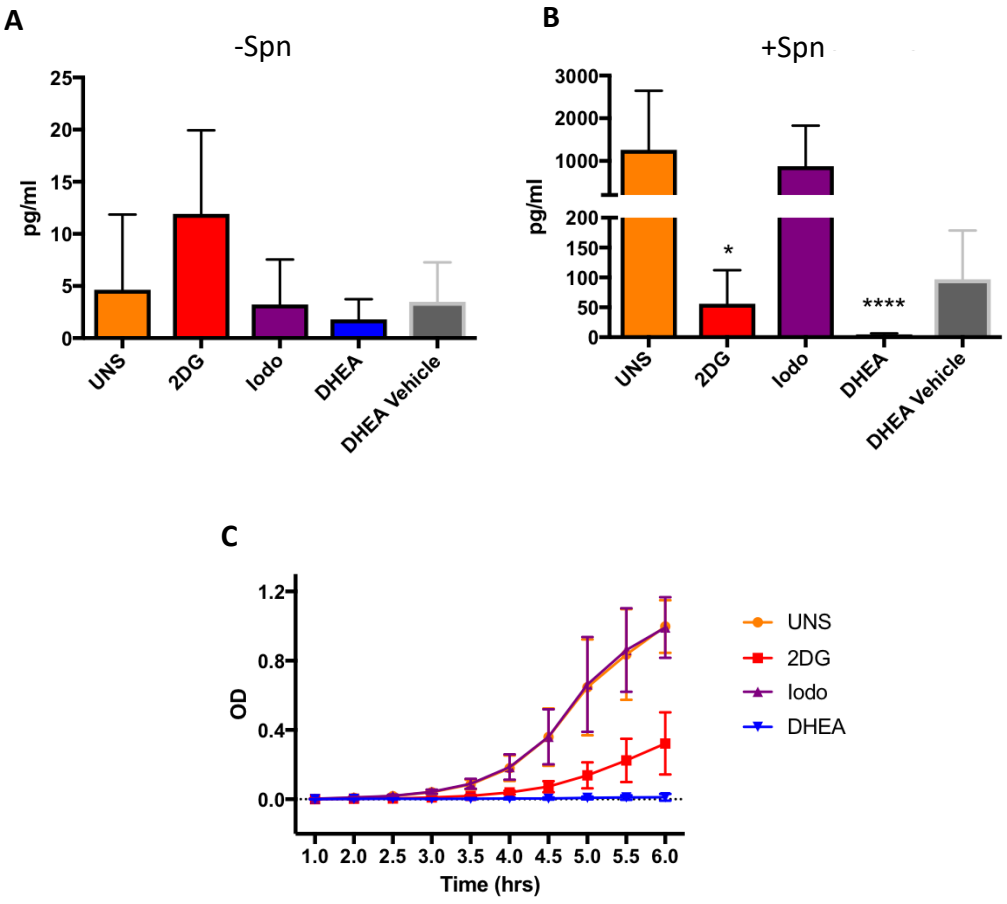

Figure 5.2: TNFα release of BMDMs following inhibit-then-infect model, and pneumococcal growth in the presence of glycolytic inhibitors

A) BMDMs were seeded at 2x10^{5}cells/ml, and treated as per x-axis for one hour, followed by 4 hours mock-infection (-Spn). Supernatants were collected and assayed for TNFα release. (2DG = 100mM, Iodo = 100µM, DHEA = 200µM, DHEA Vehicle = methanol). Biological n=4, in duplicate. Analysed using Kruskal-Wallis test, with Dunn's multiple comparisons, using the unstimulated group (UNS) as the control in each data set. Data shows mean ±SD.
B) BMDMs were seeded at 2x10^{5}cells/ml, and treated as per x-axis for one hour, followed by 4 hours *S. pneumoniae* challenge (+Spn; D39, MOI 10). Supernatants were collected and assayed for TNFα release. (2DG = 100mM, Iodo = 100µM, DHEA = 200µM, DHEA Vehicle = methanol). Biological n=4, in duplicate. Analysed using Kruskal-Wallis test, with Dunn's multiple comparisons, using the unstimulated group (UNS) as the control in each data set; *p=0.011, ****p<0.0001. Data shows mean ±SD.
C) Growth curves of *S. pneumoniae* (Spn) with glycolytic inhibitors, assayed in 5ml Brain-Heart-Infusion (BHI) broth with 20% HIFCS, and 100µl D39 bacterial stock. n=4. (UNS=unstimulated/no inhibitors, 2DG = 100mM, Iodo = 100µM, DHEA = 200µM, DHEA Vehicle = methanol). Data shows mean ±SD.

5.2.3. The role of glycolysis on BMDM internalisation of latex beads

With the glycolytic inhibitors shown to manipulate bacterial growth, the importance of glucose metabolism during BMDM phagocytosis was instead evaluated using fluorescent latex beads. The beads were opsonised using murine immune serum and internalisation quantified via fluorescence microscopy after 4 hours. BMDMs were pre-treated with the inhibitors for one hour prior to adding the beads, allowing metabolic changes to occur before this interaction. LPS was also used here as an additional condition, to compare responses to a CAM-inducing stimulant. The results of these counts are shown in Figure 5.3. Three different calculations were used, to ascertain the phagocytic index, the percentage of macrophages demonstrating active phagocytosis and average bead uptake per macrophage, for each condition. The results suggest that LPS significantly increased phagocytosis, whilst DHEA significantly reduced it. No further trends were found to be significant after 2DG or Iodo treatment compared to the unstimulated condition, suggesting that glucose metabolism is not essential for phagocytosis of opsonised beads by murine BMDMs.

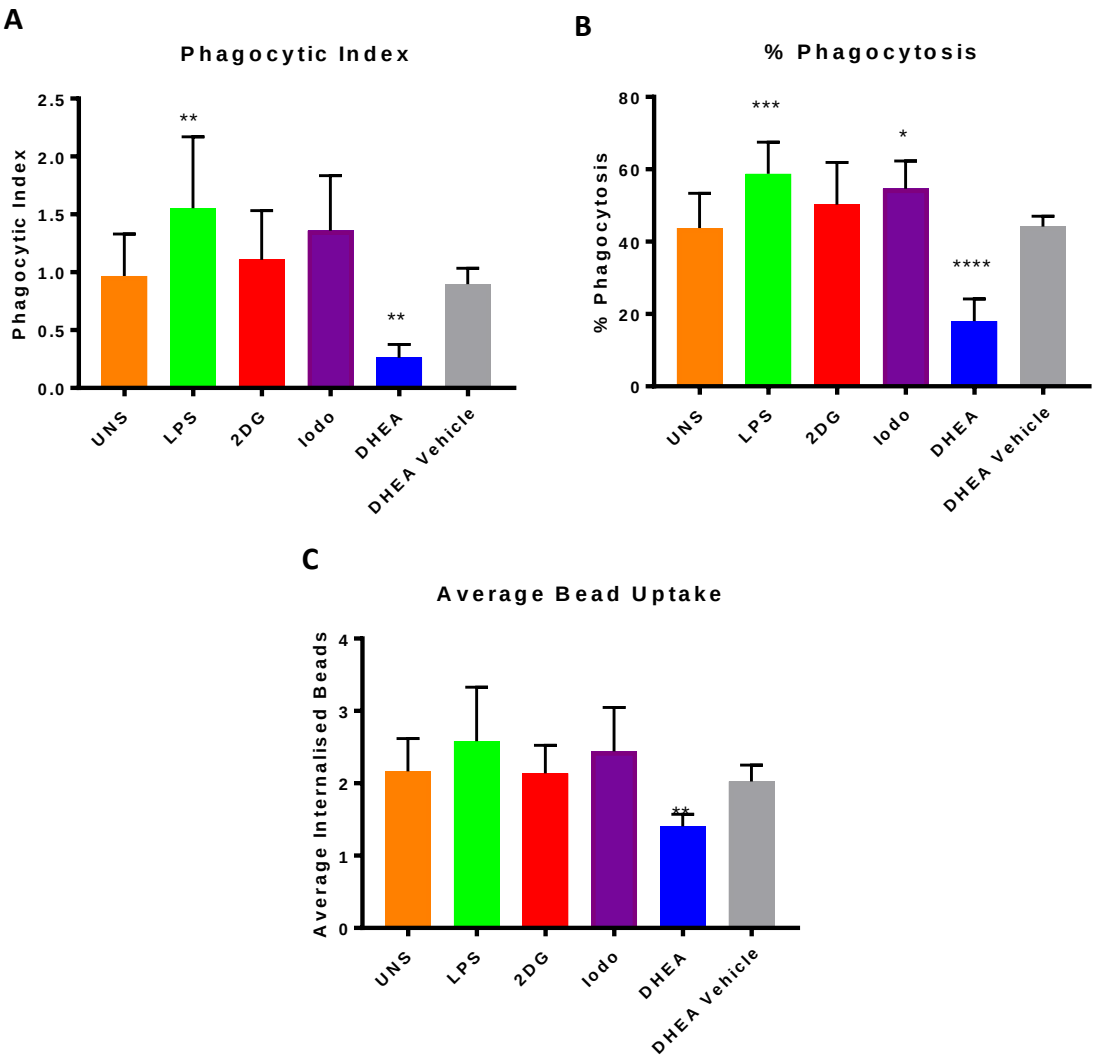

Figure 5.3: The effect of glycolytic inhibition on BMDM phagocytosis of latex beads

BMDMs were seeded at $2x10^5$cells/ml, and challenged with red-fluorescent latex beads opsonised with mouse immune serum. After 4 hours, cells were washed and fixed in paraformaldehyde before DAPI staining and counting via fluorescent microscopy. 300 cells were counted per condition.
A) Phagocytic Index = (Total beads/Total macrophages)
B) % Phagocytosis = (Macrophages with internalised beads/Total macrophages)
C) Average Bead Uptake = (Total beads/Macrophages with internalised beads)
Statistics were calculated via One-way ANOVA with Dunnett's multiple comparisons to the unstimulated (UNS) group (*= $p<0.05$; **= $p<0.01$; ***= $p<0.001$; ****= $p<0.0001$); n=5, in duplicate. Data shows mean ±SD.

5.2.4. The role of glycolysis in BMDM killing of intracellular *S. pneumoniae* by reactive nitrogen species.

A different experimental approach was taken to establish the role of glycolysis in early macrophage responses – specifically the production of nitric oxide (NO). Here, BMDMs were first mock infected or *S. pneumoniae* challenged for 4 hours, washed to remove extracellular bacteria, and then given glycolytic inhibitors or left unstimulated for a further 4 hours. This will be referred to as the infect-then-inhibit model. This allowed bacterial internalisation to occur uniformly for all conditions, prior to adding the inhibitors. Once again, LPS was added as an extra condition, to allow comparison of *S. pneumoniae*-induced responses to a CAM phenotype that should also induce NO release. To measure NO production, DAF-FM diacetate was used. This is a non-fluorescent, cell-permeable dye that emits high levels of fluorescence upon reaction with NO in the intracellular space. The dye was measured via flow cytometry, with unstained controls subtracted from all conditions. These results are shown in Figure 5.4.

For NO production in the absence of infection, DHEA increased release compared to unstimulated cells, although this was not statistically significant. 2DG also induced a trend of increased NO, however this was also not found to be statistically significant, whilst LPS did not induce detectable increases in NO. After *S. pneumoniae* challenge NO production was very similar and not significantly different between all groups. This could suggest that pneumococcal stimulation induces NO production, that this is not dependent on glycolytic metabolism.

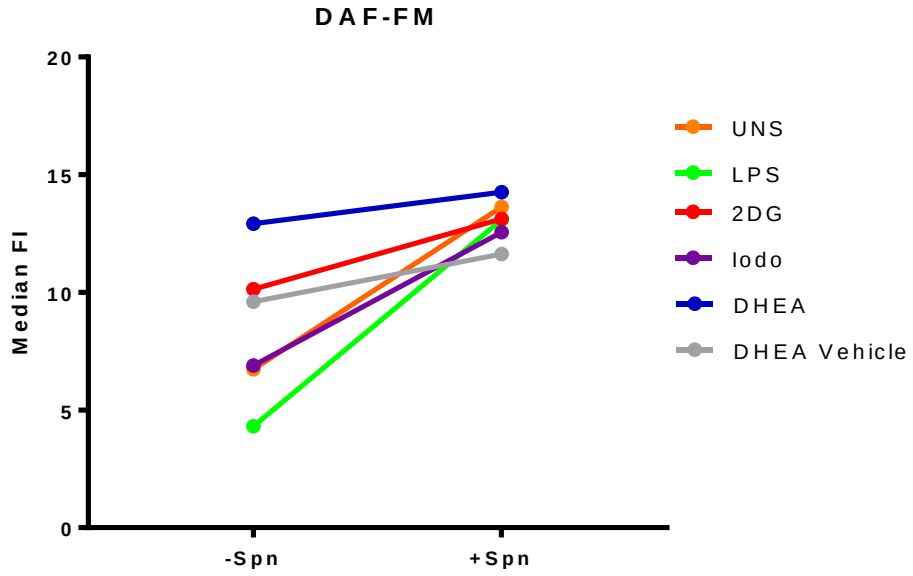

Figure 5.4: The effect of glycolytic inhibition on BMDM NO production

BMDMs were seeded at 2x10^{5}cells/ml, and mock-infected (-Spn) or *S. pneumoniae* challenged (+Spn) for 4 hours. Cells were then washed with PBS and treated with compounds for 4 hours, as per key. After a total of 8 hours, cells were stained with DAF-FM and Median Fluorescence Intensity (FI) measured via flow cytometry in the FLH-1 channel, and analysed with FlowJo software. Median FI values from unstained controls were subtracted from DAF-FM stained values for each condition. Experimental duplicates used, and data represents mean of biological n=5.
Statistics calculated via Two-Way ANOVA indicate a statistical difference between the mock-infected and *S. pneumoniae*-challenged group (p=0.001); however there were no statistical differences found within each of these two groups, after Sidak's multiple comparisons.

5.2.5. The role of glycolysis in BMDM cytokine release during *S. pneumoniae* infection

In parallel with measuring NO, TNFα and IL-6 inflammatory cytokine release was assessed, using the same infect-then-inhibit format. Supernatants were collected from both mock-infected and *S. pneumoniae* challenged cells, with glycolytic inhibitors used as presented in Figure 5.5.

In the absence of bacteria, cytokine release was barely within the limit of detection for the ELISA kits used. *S. pneumoniae* exposure alone stimulated a significant 5-fold and 15-fold increase in IL-6 and TNFα release respectively, compared to unchallenged cells. However, *S. pneumoniae*-induced release was much lower than LPS stimulation - almost 10-fold less than LPS for both IL-6 and TNFα. No significant differences were found between unstimulated and inhibitor groups in the absence of bacteria. The release detected for pneumococcal-challenged cells was not significantly altered in the presence of 2DG and Iodoacetate. 2DG produced a trend of lower cytokine release after pneumococcal challenge, but DHEA and its vehicle control significantly reduced IL-6 release during bacterial exposure.

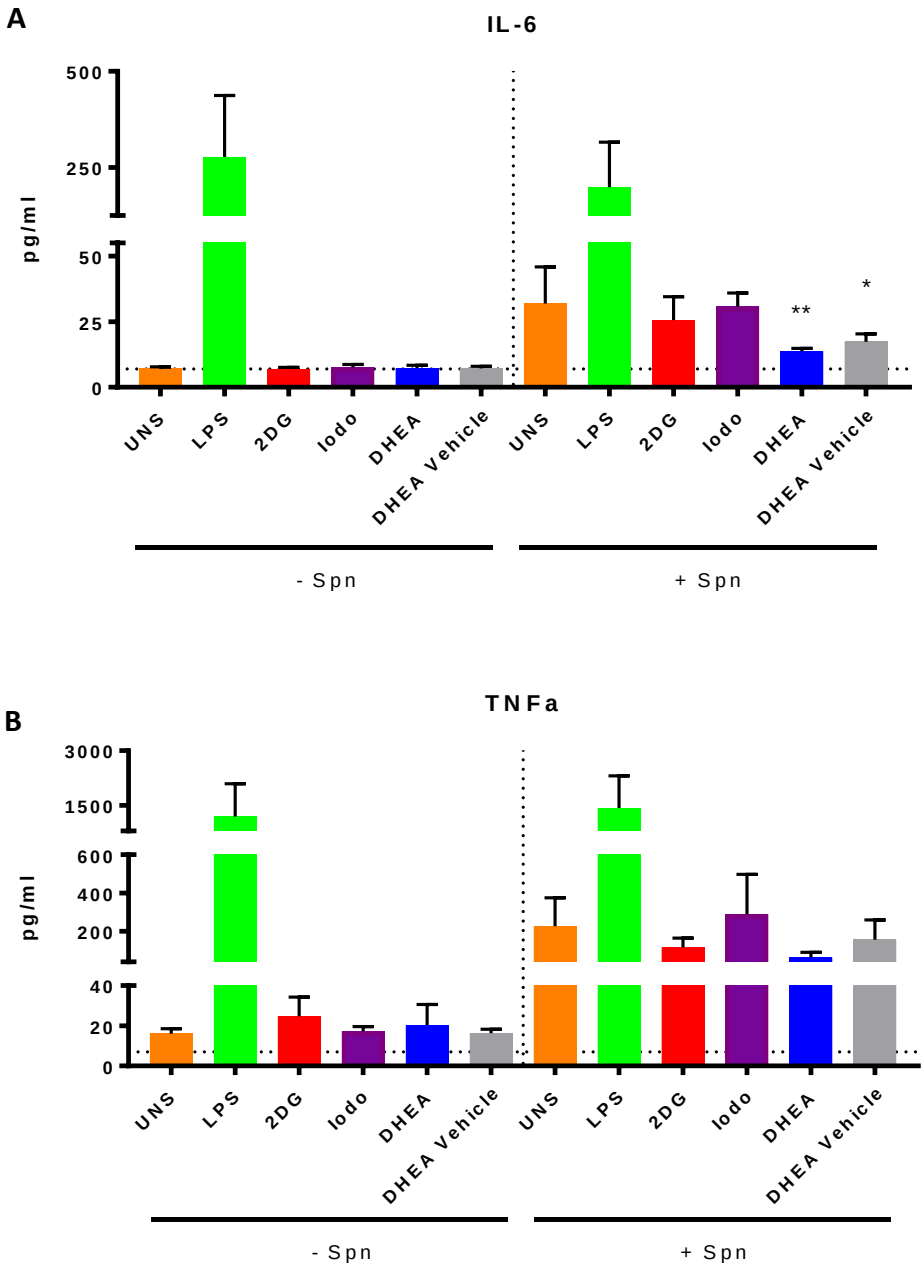

Figure 5.5: The effect of glycolytic inhibition on BMDM cytokine production

BMDMs were seeded at 2x10^{5}cells/ml, and mock-infected (-Spn) or *S. pneumoniae* challenged (+Spn) for 4 hours. Cells were then washed with PBS and treated with compounds for 4 hours, as per key. Supernatants were collected and ELISAs performed to measure IL-6 release (A) and TNFα release (B). Statistical differences calculated via One-Way ANOVA with Dunnett's multiple comparisons, excluding the LPS group and comparing all conditions to the unstimulated group in each data set (i.e. either with or without bacterial exposure) ($p<0.005$; *=0.02, **=0.009); Biological n=3, with duplicates. Data shows mean ±SD. Dotted line indicates lower assay detection limit.

5.2.6. Verifying the effects of glycolytic inhibition on key macrophage effector functions

A combination of methods were used to study the effects of glycolytic inhibition on key macrophage effector functions; however it was difficult to draw conclusions from some of these results. Therefore, repeats of key assays were conducted to assess the influence specifically of 2DG and Iodoacetate on macrophage effector functions. DHEA was excluded here due to its proposed negative influence on bacterial growth and cell viability. A comparison was also made between the D39 encapsulated pneumococcal strain, obtained from Professor Tim Mitchell at the University of Birmingham, and an R6 unencapsulated pneumococcal strain, obtained from Dr Andrew Fenton at the University of Sheffield.

In Figures 5.6 and 5.7, TNFα cytokine release, reactive oxygen species (ROS) detection and bacterial phagocytosis are shown, after stimulation with either the D39 or R6 strain respectively. TNFα was detected after D39 stimulation but was not detectable within the limits of the ELISA kit following mock-stimulation. Interestingly, 2DG appeared to increase cytokine release during D39 challenge, which contrasted to previous results. In comparison, cytokine levels were much higher during challenge with the R6 unencapsulated strain. That said, no significant differences were identified for cytokine release, following R6 stimulation with glycolytic inhibition. This supports the conclusion from prior experiments, whereby no effect of glycolytic inhibition was observed, that was not explicable by confounding effects on bacterial replication or macrophage viability.

There was no evidence of ROS generation after bacterial challenge, with no further effect induced by the inhibitors, when measured via DCF-DA staining. IFNγ was used as a positive control during D39 stimulation, whilst IFNγ and Antimycin A were used during R6 stimulation. The efficacy of these controls could be challenged and is discussed later in this chapter.

Lastly, internalisation of the two strains was assessed. Colony forming units (CFU) were measured from both the extracellular supernatant, and the intracellular cell lysate after antimicrobial treatment. 2DG inhibited detectable growth of D39 in the extracellular media during this assay, as shown in the pre-treatment CFU counts. This confirmed the confounding effect of altered bacterial replication on results with this inhibitor.

Internalisation of D39 was very low for all conditions. Contrastingly, higher levels of internalisation were achieved for the R6 strain. There appeared to be no difference in internalisation following Iodoacetate treatment but there was a significant reduction in intracellular CFU counts with 2DG treatment. Consistent with this, there were significantly fewer bacteria in the extracellular environment following 2DG treatment; this therefore supports the idea that 2DG impacts extracellular bacterial replication, with knock-on consequences for intracellular bacterial burden and stimulation of innate immune effector responses, which would otherwise hamper interpretation of results.

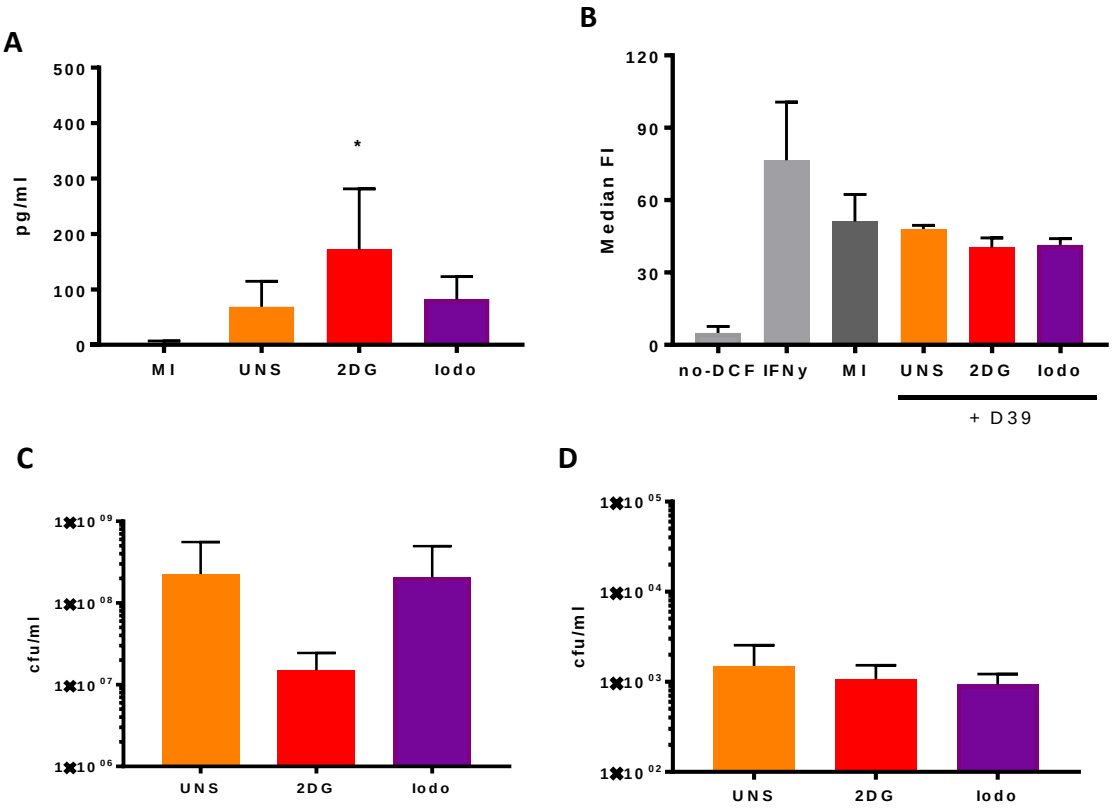

Figure 5.6: The effects of glycolytic inhibition on BMDM cytokine release, ROS production and bacterial phagocytosis, using D39 *S. pneumoniae*

A) BMDMs were seeded at 2x10^{5}cells/ml and challenged with *S. pneumoniae* (D39, MOI 10) for 4 hours, followed by a PBS wash and 4 hours treatment with compounds 2DG or Iodoacetate (Iodo), or left unstimulated (UNS), as indicated on x-axis; Supernatants were collected and used to measure TNFα release via ELISA. Biological n=3, with duplicates.
B) BMDMs were seeded at 2x10^{5}cells/ml, treated with the indicated inhibitors or left unstimulated (UNS) for 1 hour, prior to being mock-challenged (MI) or *S. pneumoniae*-challenged (+D39, MOI 10) for 4 hours. Cells were stained with DCF-DA, scraped in PBS and assessed by flow cytometry. Figure indicates negative control and positive controls used (no DCF and 24 hour stimulation with 20µg/ml IFNγ, respectively). Biological n=2, with duplicates.
C) BMDMs were seeded at 2x10^{5}cells/ml, treated with the indicated inhibitors or left unstimulated (UNS) for 1 hour, prior to being challenged with *S. pneumoniae* (D39, MOI 10) for 4 hours. CFU counts were calculated from extracellular supernatants. Biological n=3, with duplicates.
D) BMDMs were seeded at 2x10^{5}cells/ml, treated with the indicated inhibitors or left unstimulated (UNS) for 1 hour, prior to being challenged with or *S. pneumoniae* (D39, MOI 10) for 4 hours. CFU counts were calculated from lysed cells, with extracellular bacteria removed via antimicrobial treatment. Biological n=3, with duplicates.

Statistical differences identified via One-Way ANOVA with Dunnett's multiple comparisons to the unstimulated (UNS) group; ($p<0.05$, * = <0.03.) Data shows mean ±SD.

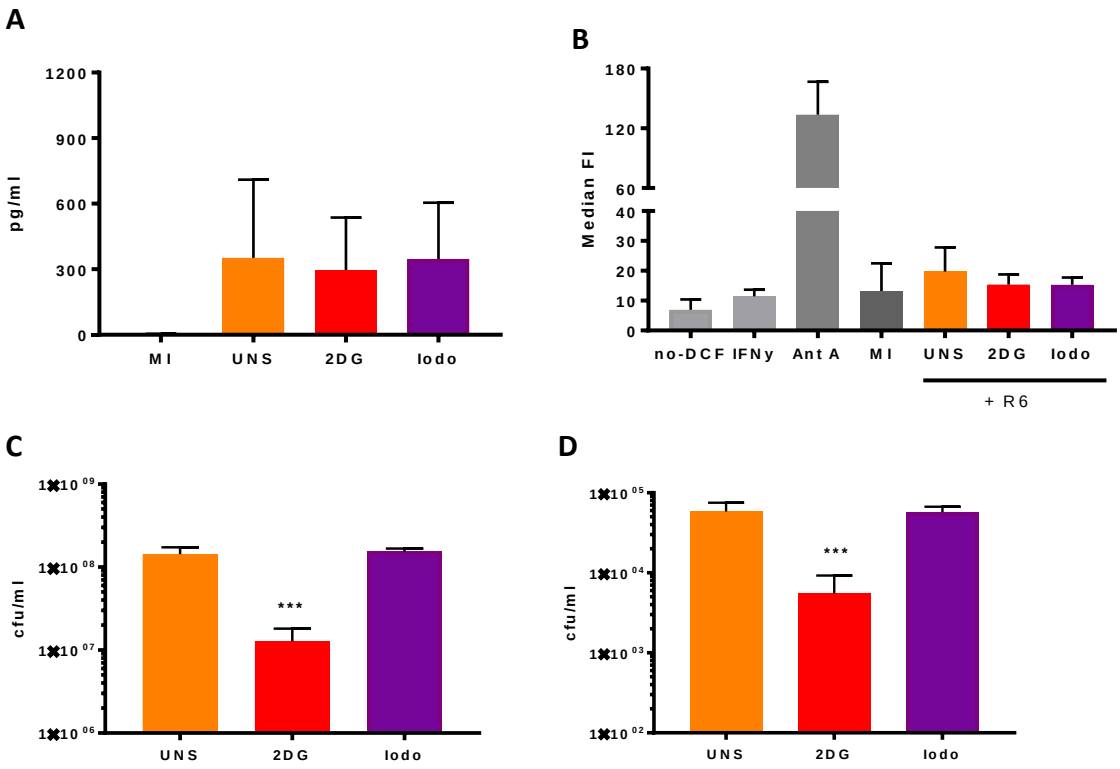

Figure 5.7: The effects of glycolytic inhibition on BMDM cytokine release, ROS production and bacterial phagocytosis, using R6 *S. pneumoniae*

A) BMDMs were seeded at 2x10^{5}cells/ml and challenged with *S. pneumoniae* (R6, MOI 10) for 4 hours, followed by a PBS wash and 4 hours treatment with compounds 2DG or Iodoacetate (Iodo), or left unstimulated (UNS), as indicated on x-axis; Supernatants were collected and used to measure TNFα release via ELISA. Biological n=3, with duplicates.
B) BMDMs were seeded at 2x10^{5}cells/ml, treated with the indicated inhibitors or left unstimulated (UNS) for 1 hour, prior to being mock-challenged (MI) or *S. pneumoniae*-challenged (+R6, MOI 10) for 4 hours. Cells were stained with DCF-DA, scraped in PBS and assessed by flow cytometry. Figure indicates negative control and positive controls used (no DCF and 24 hour stimulation with 20µg/ml IFNγ or 4 hour 10µM Antimycin A (Ant A) treatment, respectively). Biological n=2, with duplicates.
C) BMDMs were seeded at 2x10^{5}cells/ml, treated with the indicated inhibitors or left unstimulated (UNS) for 1 hour, prior to being challenged with *S. pneumoniae* (R6, MOI 10) for 4 hours. CFU counts were calculated from extracellular supernatants. Biological n=3, with duplicates.
D) BMDMs were seeded at 2x10^{5}cells/ml, treated with the indicated inhibitors or left unstimulated (UNS) for 1 hour, prior to being challenged with or *S. pneumoniae* (R6, MOI 10) for 4 hours. CFU counts were calculated from lysed cells, with extracellular bacteria removed via antimicrobial treatment. Biological n=3, with duplicates.

Statistical differences found via One-Way ANOVA, with Dunnett's multiple comparisons to the unstimulated (UNS) condition ($p<0.05$; *** = 0.001). Data shows mean ±SD.

5.2.7. A comparison of polarisation status between LPS-stimulated and *S. pneumoniae* challenged BMDMs

The use of glycolytic inhibitors during *S. pneumoniae* challenge was shown to be problematic, after experiments showed reduced numbers of BMDMs and increased numbers of trypan blue positive cells after exposure to DHEA (data not shown). DHEA also reduced bacterial viability, and therefore altered the nature of the host-pathogen interaction. 2DG was still used with relative confidence as it was shown to be effective in Chapter 3 of this thesis; however, this inhibitor also affected bacterial growth (Figure 5.2C) and could have impacted bacterial interaction with host cells. In parallel with these observations, it became apparent that the responses of BMDMs after LPS stimulation versus *S. pneumoniae* were different, as shown for the metabolic profiles shown in Figures 4.19 and 4.21. Therefore subsequent experiments examined the differences between LPS-stimulated and *S. pneumoniae*-challenged cells, rather than utilising the metabolic inhibitors further. These remaining experiments were performed using D39 pneumococci only.

To appropriately respond to bacterial infection, macrophages develop a CAM phenotype, with LPS stimulation often used to induce this (Mosser & Edwards 2008). However, whether activation of BMDMs occurs on a similar scale or timeframe after *S. pneumoniae* challenge is yet to be shown. To consider this, two markers of theCAM phenotype were examined: inducible nitric oxide synthase (iNOS), as a marker of CAM metabolism, and cyclooxygenase-2 (COX2), as a marker of CAM pro-inflammatory activation (Rodriguez-Prados et al. 2010). These proteins were assayed via western blot, after BMDMs were stimulated for 12 hours. The representative gel images are shown in Figure 5.8. The amount of loading control protein, α-tubulin, was low after bacterial challenge, which is a common finding in cells at later time points, as proteases become activated (Schmeck & Gross 2004). The upregulation of iNOS following LPS stimulation was evident, especially when compared to the mock condition. Contrastingly, iNOS was not present after bacterial challenge with *S. pneumoniae*. Prior findings have shown iNOS induction in macrophages after *S. pneumoniae* challenge (Marriott et al. 2004), but the absence of comparable upregulation here suggested that any induction levels were lower than with LPS. On the other hand, COX2 expression was upregulated after *S. pneumoniae*-challenge, but was not detectable after mock- or LPS-stimulation.

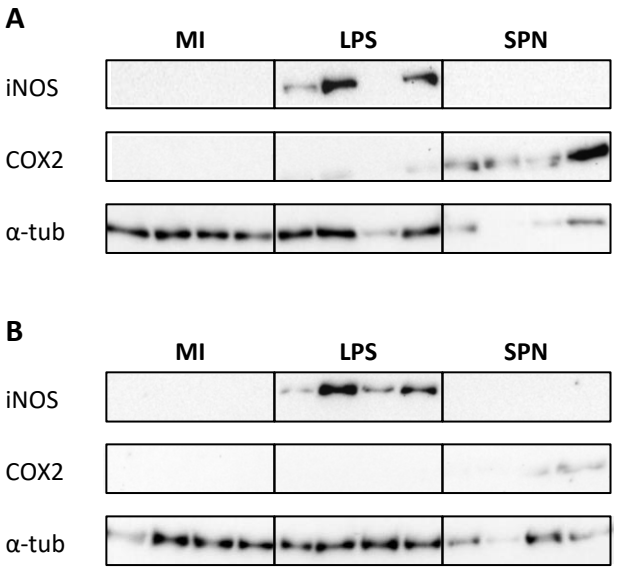

Figure 5.8: Expression of CAM protein markers, following 12 hour stimulation with LPS versus 12 hour *S. pneumoniae* bacterial challenge

BMDMs were seeded at $2x10^5$cells/ml, and mock-infected (MI), treated with LPS (100ng/ml) or *S. pneumoniae* challenged (SPN, D39 MOI 10) for 4 hours. Cells were washed with PBS and media replaced until 12 hours post-infection. Cells were washed and protein extracted via trichloroacetic acid, before separation on a 1.5mm 10% polyacrylamide gel. Protein samples were either loaded with equal volumes (A) or equal estimated protein, after total protein calculation using a Bradford assay (B). Lysates from 4 biological donors were used. (iNOS = inducible nitric oxide synthase; COX2 = cyclooxygenase-2; α-tub = α-tubulin.)

5.2.8. A comparison of glucose uptake and ATP production between LPS-stimulated and *S. pneumoniae* challenged BMDMs

To complement Chapters 3 and 4 of this thesis, ATP production and glucose uptake were compared between mock-infected, LPS-stimulated and *S. pneumoniae*-challenged BMDMs after 12 hours. To do this, the Perkin Elmer ATPlite and Promega Glucose Uptake-Glo™ assay kits were used, with the results shown in Figure 5.9. ATP levels were significantly decreased following *S. pneumoniae* challenge, whilst both mock-infected and LPS-stimulated cells were not significantly different. On the other hand, there was a trend of increased glucose uptake following LPS stimulation, although no statistical differences were found. This trend correlates with the literature, regarding increased glycolysis with LPS stimulation, which could be significant with increased experimental repeats. That said, there was no concurrent increase in glucose uptake after pneumococcal challenge.

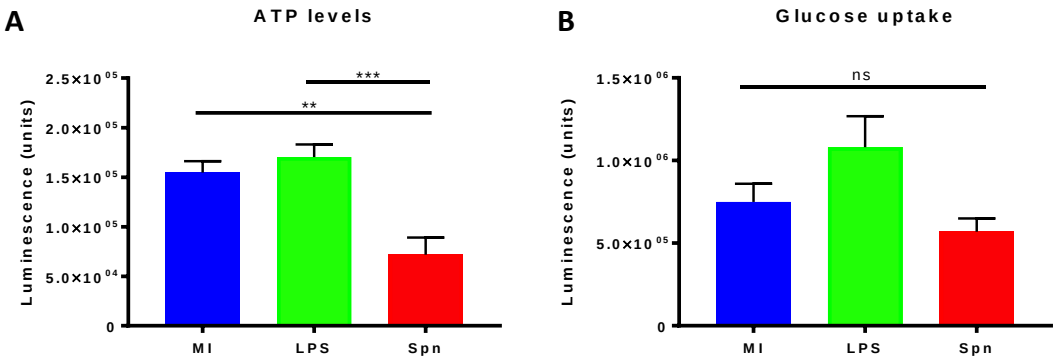

Figure 5.9: A comparison of ATP levels and glucose uptake after 12 hours mock-infection, LPS stimulation or *S. pneumoniae* challenge

A) BMDMs were seeded at 2x10^{5}cells/ml, and mock-infected (MI), treated with LPS (100ng/ml) or *S. pneumoniae*-challenged (SPN, D39 MOI 10) for 4 hours. Cells were washed with PBS and media replaced until 12 hours post-infection. ATP uptake was measured using a Perkin Elmer ATPlite assay kit. Statistical analysis via One-Way ANOVA with Tukey's multiple comparisons, comparing all conditions with each other ($p<0.005$); Biological n=4, with duplicates. Data shows mean ±SD.
B) BMDMs were seeded at 2x10^{5}cells/ml, and mock-infected (MI), treated with LPS (100ng/ml) or *S. pneumoniae*-challenged (SPN, D39 MOI 10) for 4 hours. Cells were washed with PBS and media replaced until 12 hours post-infection. Glucose uptake measured using Promega Glucose Uptake-Glo™ assay kit. No statistical differences were found after One-Way ANOVA with Tukey's multiple comparisons; Biological n=3, with duplicates. Data shows mean ±SD.

5.3. Discussion

5.3.1. Chapter Summary

In this chapter, methods to study macrophage effector functions, following bacterial challenge and metabolic inhibition, have been shown. Glycolytic inhibitors were chosen, as they offered a simple method for testing the influence of glycolysis and the PPP, on BMDM responses to *S. pneumoniae* challenge. Glucose metabolism has previously been shown to be important in the conversion to a CAM phenotype (Rodriguez-Prados et al. 2010), therefore it was hypothesised to play an important role during live bacterial challenge of macrophages, prompting activation of functional responses against bacteria. The difficulties in using glycolytic inhibitors with live bacteria are described, with experiments shown utilising metabolic inhibitors after bacterial internalisation, to limit adverse effects of the inhibitors on the initial bacterial replication, prior to internalisation. Additionally, an interesting contrast was once again shown between macrophage responses to *S. pneumoniae* compared to LPS stimulation, specifically regarding changes to protein expression, ATP levels and glucose uptake. This could suggest that the metabolic and immunological phenotype of BMDMs following *S. pneumoniae* challenge, differs from that seen after stimulation with LPS.

5.3.2. Chapter Discussion

To use the inhibitors in conjunction with live bacteria, their effects on bacterial replication were first assayed. DHEA and 2DG both hindered bacterial growth, as measured via CFU counts. It was hypothesised that inhibition of metabolism or metabolite availability could impact on the virulence of *S. pneumoniae* (Paixao et al. 2015; Somerville & Proctor 2009). Therefore assays were designed to only use the inhibitors after bacteria were internalised, and to focus on the effects of metabolic inhibition on later, downstream responses.

To study the effect of metabolic inhibition on BMDM internalisation, phagocytosis of fluorescent latex beads was measured. The results suggest that LPS stimulation increased phagocytic index and the percentage of cells ingesting; however, the average number of internalised beads in those BMDMs ingesting remained consistent, compared to unstimulated cells. This implied that LPS stimulated more cells within the population

to actively phagocytose beads, inducing BMDMs towards a pro-inflammatory CAM phenotype. This is in line with previous reports demonstrating increased phagocytosis during LPS stimulation of both murine and human macrophages (Patel et al. 2012; Scheraga et al. 2016). 2DG and Iodoacetate did not affect bead phagocytosis. On the other hand, DHEA caused a highly significant decrease in all phagocytic measures. This could suggest a role for the PPP in controlling phagocytosis. That said, cell densities of DHEA-stimulated cells appeared lower and were not fully comparable with unstimulated cells, when inspected via microscopy; this implied that DHEA caused adverse effects regarding cell adhesion or viability. DHEA has previously been shown as a compound that can induce apoptosis in murine cells (Tian et al. 1999), further supporting this idea.

Metabolic inhibitors were used to test the role of glucose metabolism in generation of NO. Elevated NO was detected in the absence of bacteria, after both DHEA and 2DG treatments. Increased NO after DHEA treatment could have lead to cell cytotoxicity, since NO production causes mitochondrial dysfunction (Beltrán et al. 2002). The small increase in NO detected after 2DG stimulation could also suggest that inhibition of glucose metabolism induces oxidative stress, consequent upon upregulation of oxidative phosphorylation. This could further alter viability and function in this model. Additionally, the MFI measured after *S. pneumoniae* exposure was lower than expected, which could reflect the early time point studied. It has been shown that NO production in response to *S. pneumoniae* is a delayed response, that is more marked at later times (Marriott et al. 2004). However, studying later time points would have been problematic due to prolonged exposure of cells to the inhibitors, with potential for adverse effects on both bacterial survival and macrophage viability.

The effect of metabolic inhibition on cytokine release by BMDMs was assayed, specifically for TNFα and IL-6. No significant differences were observed in the absence of infection. An increase in both cytokines was detected after bacterial stimulation, but only DHEA and the DHEA vehicle control altered cytokine release. While this might suggest that PPP metabolism influences cytokine production and/or release, the results cannot be interpreted with confidence, in view of the effects of DHEA on bacterial replication, the potential impact on macrophage viability and a reciprocal response by the DHEA vehicle control. Further to this, LPS induced elevated release of both

cytokines. This difference between LPS stimulation and bacterial challenge suggested that *S. pneumoniae* stimulated a reduced and/or slower response by BMDMs.

Further functional experiments were continued, comparing responses seen after either D39 *S. pneumoniae* or R6 *S. pneumoniae* stimulation of BMDMs. It was hypothesised that an R6 strain would elicit stronger responses from BMDMs compared to the D39, due to its lack of capsule and subsequently easier internalisation by BMDMs (Hyams et al. 2010). TNFα release was indeed higher after R6 challenge, suggesting that BMDMs were able to phagocytose and respond to this strain much quicker – as was expected from a strain that lacks capsule and is more easily phagocytosed (Ali et al. 2003). Additionally, 2DG seemed to increase cytokine release after D39 challenge. This contrasts with earlier findings but could largely be due to one hyper-responsive donor skewing the data set – the influence of which could be reduced with increased replicates. The effect of metabolic inhibition on ROS generation was also tested after both D39 and R6 challenge. Two controls, IFNγ and Antimycin A, were included to confirm that the DCF-DA dye effectively measured ROS, as has been previously shown (Jubrail et al. 2016). IFNγ stimulation causes upregulation of gp91phox in macrophages, a component of the nicotinamide adenine dinucleotide phosphate (NADPH) oxidase, which generates ROS immediately after bacterial internalisation (Cassatella et al. 1990). During D39 experiments, IFNγ resulted in a very modest increase in DCF signal. When challenging with the R6 bacterial strain, Antimycin A was also used. This is an inhibitor of Complex III of the electron transport chain in mitochondrial respiration, and causes mitochondrial ROS generation (Liu et al. 2002). During R6 experiments, Antimycin A demonstrated a significant shift in DCF-DA fluorescence, but there was no shift in DCF-DA signal for IFNγ. It is not clear why macrophages in these experiments were unable to generate a DCF-DA signal with either IFNγ or bacteria, as there is extensive evidence in the literature of NADPH oxidase-dependent production of ROS in BMDMs, activated by bacteria and other CAM-inducing stimuli (Zhao et al. 2013). This absence of ROS induction with bacterial stimulation was also unexpected - despite the known anti-oxidant defence systems of pneumococci, which partially neutralise ROS (Aberdein et al. 2013). It is possible that induction occurred earlier or later than assessed, although the time point used here has previously been shown to be sufficient to detect NADPH oxidase activation in macrophages (Jubrail et al. 2016). The absence of ROS induction meant the effect of these inhibitors could not appropriately be examined here. Lastly,

internalisation of the two strains was compared. Similar CFU counts were observed in the extracellular supernatants, however internalisation of R6 was far greater than for D39. The low level internalisation for D39 demonstrates the challenge for BMDMs internalising this pathogen, due to its complex capsular coating and other bacterial factors that inhibit internalisation (Kadioglu et al. 2008).

On the whole, DHEA was seen to hinder BMDM responses, including cytokine release and phagocytosis; however it is debatable whether this was due to inhibition of the PPP in mediating these responses, or adverse effects of the inhibitors. DHEA has previously been shown to increase mitochondrial permeability and obstruct cellular redox (Tian et al. 1999), which may have induced early apoptosis and undesired cell loss in this model. Contrastingly 2DG and Iodoacetate did not induce significant differences during pneumococcal challenge, compared to unstimulated cells. In summary, it could be suggested that glucose metabolism is not critical for macrophage effector responses to *S. pneumoniae;* however, confounding effects on bacterial replication and macrophage viability impede interpretation of the impact of these glycolytic inhibitors on macrophage function.

Protein markers of the CAM phenotype, COX2 and iNOS, were assayed, as a comparison of activated cell status after *S. pneumoniae*- or LPS-stimulation of BMDMs. COX2 transcription and activity has been shown to be upregulated in BMDMs following just 2 hours incubation with LPS (Eliopoulos et al. 2002). However, this was not shown to be the case as COX2 was undetected after LPS stimulation. The difference here could be contributed by LPS concentration, cell culture conditions or different timings of analysis between these studies. The data here demonstrate increased COX2 but lesser induction of iNOS after pneumococcal challenge, compared to LPS stimulation. LPS is a specific TLR4 agonist, whilst *S. pneumoniae* activates a variety of pattern recognition receptors (PRRs) and might induce lower levels of TLR4 activation than other PRRs, with subsequently less induction of iNOS. These findings may suggest a role for COX2, during the specific interaction between BMDMs and *S. pneumoniae.* COX2 is a key enzyme that converts arachidonic acid into prostaglandins, autocrine mediators of inflammation and cytokine release, which could suggest a role in both acute inflammation and inflammation resolution, during bacterial challenge with *S. pneumoniae* (Ricciotti &

Fitzgerald 2011). That said, further verification and testing would be required to understand this more.

Finally, ATP levels and glucose uptake were measured after either stimulation with LPS or D39 *S. pneumoniae*. ATP levels were significantly decreased with bacterial challenge but were unchanged after LPS stimulation. This could indicate that cells struggle to maintain ATP production during bacterial challenge and following bioenergetically demanding processes such as phagocytosis. Rates of phagocytosis of bacteria have previously been linked to reductions of ATP in monocytes (Webster et al. 2010). The reduction in ATP also could be because cells switch mitochondrial function away from producing ATP and towards ROS generation (Mills & O'Neill 2016; West et al. 2011), which facilitates bacterial killing (Garaude et al. 2016). ATP levels could then drop, as the rate at which glycolysis produces ATP does not match that given by uninterrupted mitochondrial respiration (O'Neill et al. 2016). Contrastingly, glucose uptake measurements contradicted the findings of earlier chapters, as it was not significantly increased after LPS stimulation or pneumococcal challenge. It could be proposed that this anomaly was an artefact of the assay kit used; here, glucose uptake was measured through using a labelled glucose analogue that inhibits glycolysis. Therefore, this could cause false positive read outs from metabolically plastic cells, as inhibition of this pathway would cause a back-log stress and prevent typical uptake in this system. Therefore, further verification would be required to confirm this finding.

5.3.3. Future work

The lower than expected readouts – particularly for RNS and ROS production during *S. pneumoniae* challenge – could have been because the time points studied were too early, or because the emergence of oxidative and nitrogenous species is very transient. It is possible that internalisation, degradation, signalling and killing of the pneumococcus occurs slower than anticipated, and that different cell types, host species or bacterial serotypes also influence these interactions. Therefore, it could be valuable to study different combinations of host species, cells and/or *S. pneumoniae* serotypes over a full 24 hour time course, to identify peak readouts in effector function measures. Jonczyk et al have previously shown there are distinctions in the responses of mice to different pneumococcal serotypes, with disparities in readouts such as cytokine release (Jonczyk

et al. 2016). These differences are thought to be influenced both by host genetics and bacterial serotypes. Within the Dockrell research group, both murine and human cell cultures are used, from primary and cell line systems, and with different serotypes and bacterial species used between studies. Therefore not all experimental protocols or results are fully comparable, and a better understanding of each unique case could provide an interesting perspective on these experimental variations. This would also enable verified and optimal time points to be used in subsequent research, when measuring fundamental macrophage effector functions.

In this work, glycolytic inhibitors were used to manipulate host metabolism, however due to the non-specific nature of their chemistry, they proved more challenging to use than predicted. If this work were to be carried on, alternative methods for inhibiting such enzymes could include the use of gene knockdown. This could be achieved by using techniques such as RNA interference (eg. siRNA) or CRISPR (clustered regularly interspaced short palindromic repeats). Tan et al. recently demonstrated this concept, using siRNAs to knockdown pyruvate dehydrogenase kinase to expose its role in macrophage polarisation (Tan, Xie, Cui, et al. 2015). That said, this could be a timely process, as confirmation of a successful enzyme knockdown and of its activity would require evidence, before application in host-pathogen interaction experiments. Therefore a quicker, albeit more expensive, option could be to use the bone marrow or cells of established knockout mice instead. Contrastingly, the metabolic gene transcription, protein expression and enzymatic activity of BMDM cell cultures could be measured during *S. pneumoniae* challenge, with comparisons made to LPS, and potentially also other pathogens or stimuli of interest.

Throughout this work, comparisons have been made between pneumococcal challenge and stimulation with LPS – a Gram-negative component. This theme should be continued, but with the addition of other, more suitable Gram-positive components, such as lipopeptides, peptidoglycan and its components, or pneumolysin. Alternatively, it would be interesting to emulate the work of Lachmandas et al. who used different TLR agonists but also a mix of bacterial types – the Gram-negative *E.coli*, Gram-positive *S. aureus* and *M. tuberculosis*, a species that is neither Gram-positive nor -negative (Lachmandas et al. 2016).

Chapter 6 – Discussion

6.1. Summary of thesis

The first aim of this work was to optimise and use the Seahorse XF Analyser to analyse changes in glycolytic metabolism during *S. pneumoniae* challenge of BMDMs. This was achieved first through manipulation of the cell density and protocol timings, as required for the basic assay set-up. The appropriate concentrations of inhibitors for profiling assay kits were also tested, including for 2DG, oligomycin and FCCP. Following initial tests, the assay design was further modified, to better mimic typical cell culture conditions and reduce cell stress through prolonged absence of glucose. This assay design was used to establish glycolysis rates of BMDMs after 4 hours and 12 hours post-stimulation, with *S. pneumoniae* compared to the CAM and AAM stimuli, LPS and IL-4 respectively. There were no significant differences observed at 4 hours, with an elevated basal glycolysis and glycolytic capacity identified after 12 hours bacterial stimulation, compared to the mock condition. A novel phenomenon was also identified, whereby LPS stimulation did not elevate these parameters, but instead caused a considerable increase in non-glycolytic acidification. This has not previously been reported. The technique was also used to test mitochondrial oxidative stress in human MDMs, as a proof of concept in other cell types. While aspects of this work may not directly correlate with the literature, specifically regarding short-term metabolic responses to LPS, it has identified that LPS and *S. pneumoniae* induce different metabolic responses, specifically in terms of changes to BMDM glycolysis.

The second aim of my work was to optimise and use NMR Spectroscopy to detect global changes to metabolism, during *S. pneumoniae* challenge of BMDMs. This technique had not previously been used and required extensive training and optimisation, by both the doctoral researcher and by the lead technician at the NMR Spectroscopy facility. The biggest challenges involved the reproducibility of preparations and spectral analysis; therefore optimisation aimed to identify appropriate cell numbers, time points, metabolite identification and data handling techniques. A collaborator was also sought for manipulation of the raw spectral data, to allow statistical metabolomic analysis to be done. The main, novel finding was the identification of itaconic acid in LPS-stimulated samples, which was absent from *S. pneumoniae*-stimulated cells. This hallmark of polarisation and altered metabolism demonstrates that *S. pneumoniae* induces a unique

variation on macrophage activation and metabolism compared to LPS with a combination of CAM- and some AAM-associated changes possible. This phenomenon has previously been described for macrophages challenged with other pathogens such as *S. pyogenes* (Goldmann et al. 2007). This thesis also demonstrates that metabolite profiles of macrophages challenged with *S. pneumoniae* are very different to those seen following LPS-stimulation or mock-infection, as few similarities were observed. Some CAM metabolic features were present in LPS-treated macrophages, but not those challenged with *S. pneumoniae*, for examples itaconic acid production, in contrast others such as low glutamine or glutamate were more marked after *S. pneumoniae* challenge. Thus, although both produced M1 features, these features varied. This further emphasised that LPS stimulation cannot be used as a universal model of the CAM phenotype seen during bacterial challenge, and that future experiments and literature should analyse specific pathogen interactions, including responses to Gram-positive bacterial components such as peptidoglycan, in addition to Gram-negative components such as LPS. This theme has been highlighted in transcriptional studies previously, which showed the variations in macrophage polarisation induced by different bacteria despite the predominance of CAM phenotypes (M. Benoit et al. 2008). These studies showed that some pathogens could induce predominantly AAM phenotypes.

The final aim was to manipulate host glycolytic metabolism and assess the impact of this on macrophage effector functions, specifically during stimulation with *S. pneumoniae.* The use of chemical inhibitors of glycolysis proved challenging for studying initial host-pathogen interactions, due to their disruption of bacterial growth. Therefore they were chiefly used to assess later, downstream responses, after initial bacterial internalisation by macrophages. The PPP inhibitor, DHEA, induced dampened macrophage effector functions; however, whether these differences demonstrate a role for the PPP in macrophage responses or toxicity of the inhibitor, remains unconfirmed. On the other hand, the glycolytic inhibitors 2DG and Iodoacetate did not induce any significant changes in macrophage effector functions. These two inhibitors were further tested for their effects during macrophage challenge with two different pneumococcal strains – encapsulated D39 and un-encapsulated R6. No significant differences were seen following use of these inhibitors, but there were noticeable differences between the effects induced by the different pneumococcal strains. Also, whilst 2DG caused differences in internalisation of the R6 strain, lower bacterial numbers in the

extracellular environment may also have led to this finding. These experiments highlighted that different bacterial strains can induce different outcomes, as demonstrated by the lower levels of TNFα cytokine release following D39 versus R6 challenge, in keeping with known differences in rates of internalisation of the encapsulated strain (Ali et al. 2003), which have been replicated here.

Overall, the main conclusion is that *S. pneumoniae* does not induce the same responses in BMDMs as seen for stimulation with LPS. This was true for both metabolic changes and macrophage effector functions. The effects of LPS stimulation on macrophage metabolism is increasingly well documented (Tannahill et al. 2013; Kelly & O'Neill 2015); however this model of macrophage activation does not necessarily predict the activation status induced by live bacterial infection of cell cultures, particularly when using Gram-positive pathogens. These differences could be due to a number of factors: firstly, LPS is predominantly a Gram-negative bacterial component, that is not typically found in Gram-positive cell wall structures (Brown et al. 2015). Therefore this stimulus is not applicable to work with Gram-positive bacteria and that Gram-positive constituents such as peptidoglycan or lipopeptides should be investigated in future studies. Secondly, the initial interaction with *S. pneumoniae* includes an array of signals and receptors - some of which may detect bacterial components at the surface, others which recognise degraded components in the intracellular environment, and further receptors that bind to opsonic factors, such as antibodies coating the bacterial surface (Koppe et al. 2012; Ali et al. 2003). The bacterium is also capable of releasing components, such as pneumolysin, which will further stimulate and cause responses in host cells (McNeela et al. 2010). Additionally, it has been shown that bacterial infection can cause biphasic macrophage activation, correlating with initial surface interaction and later phagosomal degradation (Wolf et al. 2011). On the other hand, LPS is well documented to activate macrophages through binding and activating TLR4-mediated pathways (Takeda & Akira 2001). Live *S. pneumoniae* and free LPS interact with different numbers and groups of receptors, and different patterns of activation can occur during bacterial challenge. Following from this point, if different bacterial species can activate unique receptor subsets during infection of macrophages, they could also induce tailored patterns of macrophage activation. An example of this can be seen for macrophage infection with *S. pyogenes*, which has been shown to induce a combination of both CAM- and AAM-associated markers (Goldmann et al. 2007). It could be proposed

that a similar outcome is likely to exist following *S. pneumoniae* infection of murine macrophages, with a variety of activation markers being differentially expressed to varying extents.

6.2. Model limitations

BMDM cell culture was used as bone marrow preparations yield high cell numbers and this model was readily available within the Dockrell-Marriott research group. These primary cells also presented benefits over cell line cultures as they do not have Warburg metabolism, whereby glycolysis is already elevated in resting cells (Van den Bossche et al. 2015). However, their relevance as a model for AMs could be questioned. The isolation of AMs requires greater labour and yields fewer cells; therefore primary, proof of concept experimentation was carried out in BMDMs, with the availability to use AMs later in the study, when testing key findings. This is in line with the principles of the 3Rs, to reduce animal use in experimentation (Franco & Olsson 2014). Mouse models were also available for testing major findings *in vivo* – which was not done here but could be implemented upon continuation of this work. Lastly, murine BMDMs were primarily used for experiments, as the paradigm of CAM and AAM polarisation is much more established in mice than in humans, allowing for the identification of more widely accepted phenotypic changes (Murray & Wynn 2011).

A second potential limitation here is the type of bacteria used. This work primarily addresses serotype 2 D39 *S. pneumoniae*. This strain was isolated from a patient in the early 1900s and is still shown to induce pathogenicity in murine models. However pneumococcal serotypes and strains have different genetic sequences and could therefore induce different responses in host cells (Lanie et al. 2007). Therefore different pneumococcal strains and/or other Gram-positive bacteria should be tested, to provide a wider scope and understanding of pneumococcal-macrophage interactions and broader host-pathogen implications.

6.3. Future prospects

In 2016, Czaplewski et al proposed 10 methods that should be developed as a priority for the replacement of antibiotic treatment (Czaplewski et al. 2016); one of these

approaches concerned immune stimulation. By understanding the specific interaction between bacteria and host immune cells, valuable new methods for tackling bacterial infections could be revealed. This knowledge could make it possible to manipulate immune cell responses, to improve infection outcomes and provide an alternative treatment to antibiotics. For example, TLR agonists could be used as preventative therapy for patients at risk of pneumonia, aiming to enhance local immune cell responses without excessive cytokine production (Walker et al. 2014). Whilst this shows how manipulation of immune function could be used for infection prevention, it is interesting to consider the therapeutic effects of immunomodulation as a treatment for bacterial infections. Can this occur without causing toxicity or inappropriate immune activation that causes inflammation-associated tissue injury? Could the natural microbiota be manipulated to our immune advantage, to help downregulate harmful inflammatory responses? Interestingly, some modulatory compounds, that chiefly act through TLR-based activity, are already being explored in clinics to treat bacterial infections – for example, Luivac, a combination bacterial lysate drug produced by Daiichi Sankyo, which acts as an agonist for immune cell responses to limit respiratory infection in children (Hancock et al. 2012). By further understanding host—pathogen interactions and the role of metabolic responses, this could be a new potential target in the field of immune therapy. Manipulating metabolic responses in immune cells, such as macrophages, could be one approach to tailoring activation, although this would need to be calibrated to the specific pathogen in question.

Following from this, a related area of interest is the concept of trained immunity. This is the idea that innate immune cells are capable of immunological memory – much like that seen for adaptive immune cells. This phenomenon is thought to be antigen-independent and regulated through mechanisms such as epigenetic modification (Netea et al. 2016). Epigenetic regulation has also been shown to have a strong connection with cellular metabolism, as substrates such as lactate and succinate have been shown to influence this process (Latham et al. 2012; Yang & Pollard 2013). Thus manipulation of metabolism could modulate epigenetic modifications to mediate innate immune responses. Despite these concepts, the idea of immunomodulation is still very much in its infancy, and further basic research and clinical testing is required before a broader range of therapies can be applied in humans. However, understanding the metabolic

changes that occur during host-pathogen interactions could help with infectious diagnostics and treatments in the future.

Metabolomic studies have grown in number and appeared across a broad range of fields, and with new techniques paving the way for high-content profiling of cells, information in this field is only likely to increase. One such example can be seen in single-cell studies, whereby in-depth details of metabolism and bioenergetics can be obtained, following strict biomass separations and even label-free systems (Vasdekis & Stephanopoulos 2015). This increase in hardware sensitivity has also been followed by the expansion of bioinformatic tools and data handling techniques (Fessenden 2016). This will aid development of the metabolomic field, allowing the metabolic statuses of both individual cells and cell populations to be uncovered with incredible detail, and with greater potential for disease biomarker identification. This could also help future development of diagnostics and new treatment approaches, both in infectious and non-communicable diseases. The unique metabolic signatures of specific immune cells to pathogens, could be used both as a diagnostic approach and to help calibrate suitable treatments.

6.4. Concluding remarks

This research highlights the processes taken to understand the importance of macrophage metabolism during immune responses to pathogens, with a focus on using extracellular fluxomics, NMR metabolomics and metabolic inhibition methods. The steps taken to optimise these techniques have been shown, with the challenges of applying these techniques to infectious studies involving live metabolically active micro-organisms. The overarching conclusion is that *S. pneumoniae* does not induce the same metabolic changes in macrophages as seen for LPS stimulation, and that BMDM responses to *S. pneumoniae* are not likely depend on glucose metabolism. The data also demonstrates that further verification of these metabolic changes is required, particularly considering Gram-positive bacteria and their microbial components, to utilise the potential of metabolic studies in infection diagnostics and therapeutics.

References

Aberdein, J.D. et al., 2013. Alveolar macrophages in pulmonary host defence-the unrecognized role of apoptosis as a mechanism of intracellular bacterial killing. *Clinical and Experimental Immunology*, 174(2), pp.193–202.

Adam, D., 2002. Global antibiotic resistance in *Streptococcus pneumoniae*. *Journal of Antimicrobial Chemotherapy*, 50(T1), pp.1–5.

Agilent Technologies, 2017a. Agilent Seahorse XF Base Medium Data Sheet. , p.1. Available at: http://www.agilent.com/cs/library/datasheets/public/XF-base-medium-data-sheet.pdf [Accessed May 1, 2017].

Agilent Technologies, 2017b. Agilent Seahorse XF Technology News and Information. Available at: http://www.agilent.com/en-us/promotions/seahorse-xf-technology [Accessed May 1, 2017].

Agilent Technologies, 2017c. Publications with Seahorse XF Data. Available at: http://www.agilent.com/publications-database/ [Accessed July 20, 2005].

Albertí, S. et al., 1993. C1q binding and activation of the complement classical pathway by *Klebsiella pneumoniae* outer membrane proteins. *Infection and Immunity*, 61(3), pp.852–60.

Albiger, B. et al., 2005. Myeloid differentiation factor 88-dependent signalling controls bacterial growth during colonization and systemic pneumococcal disease in mice. *Cellular Microbiology*, 7(11), pp.1603–1615.

Albiger, B. et al., 2007. Toll-like receptor 9 acts at an early stage in host defence against pneumococcal infection. *Cellular Microbiology*, 9(3), pp.633–44.

Ali, F. et al., 2003. *Streptococcus pneumoniae*-associated human macrophage apoptosis after bacterial internalization via complement and Fcgamma receptors correlates with intracellular bacterial load. *The Journal of Infectious Diseases*, 188(8), pp.1119–31.

Ali, Y.M. et al., 2012. The lectin pathway of complement activation is a critical component of the innate immune response to pneumococcal infection. *PLoS*

Pathogens, 8(7), p.46.

Aliberti, S. et al., 2014. The role of vaccination in preventing pneumococcal disease in adults. *Clinical Microbiology and Infection*, 20(S5), pp.52–58.

Andre, G.O. et al., 2017. Role of *Streptococcus pneumoniae* proteins in evasion of complement-mediated immunity. *Frontiers in Microbiology*, 8(FEB), pp.1–20.

Appelbaum, P.C., 1992. Antimicrobial Resistance in *Streptococcus pneumoniae*: An Overview. *Clinical Infectious Diseases*, 15(1), pp.77–83.

Aranı´bar, N. et al., 2006. Metabolomic analysis using optimized NMR and statistical methods. *Analytical Biochemistry*, 355(1), pp.62–70.

Balachandran, P. et al., 2001. The autolytic enzyme LytA of *Streptococcus pneumoniae* is not responsible for releasing pneumolysin. *Journal of Bacteriology*, 183(10), pp.3108–3116.

Barnes, P.J., Shapiro, S.D. & Pauwels, R.A., 2003. Chronic obstructive pulmonary disease: Molecular and cellular mechanisms. *European Respiratory Journal*, 22(4), pp.672–688.

Barocchi, M.A. et al., 2006. A pneumococcal pilus influences virulence and host inflammatory responses. *Proceedings of the National Academy of Sciences of the United States of America*, 103(8), pp.2857–2862.

Beltrán, B. et al., 2002. Inhibition of mitochondrial respiration by endogenous nitric oxide: a critical step in Fas signaling. *Proceedings of the National Academy of Sciences of the United States of America*, 99(13), pp.8892–8897.

Benoit, M. et al., 2008. Coxiella burnetii, the agent of Q fever, stimulates an atypical M2 activation program in human macrophages. *European Journal of Immunology*, 38(4), pp.1065–1070.

Benoit, M., Desnues, B. & Mege, J.-L., 2008. Macrophage Polarization in Bacterial Infections. *The Journal of Immunology*, 181(6), pp.3733–3739.

Bentley, S.D. et al., 2006. Genetic analysis of the capsular biosynthetic locus from all 90 pneumococcal serotypes. *PLoS Genetics*, 2(3), pp.0262–0269.

Bewley, M. a. et al., 2011. A cardinal role for cathepsin D in co-ordinating the host-mediated apoptosis of macrophages and killing of pneumococci. *PLoS Pathogens*, 7(1).

Blomberg, C. et al., 2009. Pattern of Accessory Regions and Invasive Disease Potential in *Streptococcus pneumoniae*. *The Journal of Infectious Diseases*, 199(7), pp.1032–1042.

Van den Bossche, J., Baardman, J. & de Winther, M.P.J., 2015. Metabolic Characterization of Polarized M1 and M2 Bone Marrow-derived Macrophages Using Real-time Extracellular Flux Analysis. *Journal of Visualized Experiments: JoVE*, (105), pp.1–7.

Bothwell, J.H.F. & Griffin, J.L., 2011. An introduction to biological nuclear magnetic resonance spectroscopy. *Biological Reviews*, 86(2), pp.493–510.

Bowden, S.D. et al., 2009. Glucose and glycolysis are required for the successful infection of macrophages and mice by *Salmonella enterica serovar Typhimurium*. *Infection and Immunity*, 77(7), pp.3117–3126.

Bradley, J.S. et al., 2011. The management of community-acquired pneumonia in infants and children older than 3 months of age: Clinical practice guidelines by the pediatric infectious diseases society and the infectious diseases society of America. *Clinical Infectious Diseases*, 53(7), pp.25–76.

Brittan, J.L. et al., 2012. Pneumococcal neuraminidase A: An essential upper airway colonization factor for *Streptococcus pneumoniae*. *Molecular Oral Microbiology*, 27(4), pp.270–283.

Brown, J.S. et al., 2002. The classical pathway is the dominant complement pathway required for innate immunity to *Streptococcus pneumoniae* infection in mice. *Proceedings of the National Academy of Sciences of the United States of America*, 99(26), pp.16969–74.

Brown, L. et al., 2015. Through the wall: extracellular vesicles in Gram-positive bacteria, mycobacteria and fungi. *Nature Reviews Microbiology*, 13(10), pp.620–630.

Bruyn, G., 1992. Mechanisms of host defense against infection with *Streptococcus pneumoniae*. *Clinical infectious …*, 14(1), pp.251–262.

Cascante, M. & Marin, S., 2008. Metabolomics and fluxomics approaches. *Essays in Biochemistry*, 45, pp.67–82.

Cassatella, M.A. et al., 1990. Molecular basis of interferon-g and lipopolysaccharide enhancement of phagocyte respiratory burst capability. *Journal of Biological Chemistry*, 265(33), pp.20241–20246.

Cellier, M.F., Courville, P. & Campion, C., 2007. Nramp1 phagocyte intracellular metal withdrawal defense. *Microbes and Infection*, 9(14–15), pp.1662–1670.

Centers for Disease Control and Prevention, 2016. Vaccines and Preventable Diseases - Pneumococcal Vaccines. Available at: https://www.cdc.gov/vaccines/vpd/pneumo/index.html [Accessed July 1, 2017].

Cetin, E.T., 1962. Staphlococci Resistant to Methicillin ("Celbenin"). *British Medical Journal*, pp.51–52.

Chaguza, C., Cornick, J.E. & Everett, D.B., 2015. Mechanisms and impact of genetic recombination in the evolution of *Streptococcus pneumoniae*. *Computational and Structural Biotechnology Journal*, 13, pp.241–247.

Chandra, R.K., 1981. Immune Response in Overnutrition. *Cancer Research*, 41, pp.3795–3796.

Clatworthy, A., Pierson, E. & Hung, D., 2007. Targeting virulence: a new paradigm for antimicrobial therapy. *Nature Chemical Biology*, 3, pp.541–548.

Cloarec, O. et al., 2005. Statistical total correlation spectroscopy: An exploratory approach for latent biomarker identification from metabolic 1H NMR data sets. *Analytical Chemistry*, 77(5), pp.1282–1289.

Cohen, P. et al., 2000. Monitoring cellular responses to *Listeria monocytogenes* with oligonucleotides arrays. *The Journal of Biological Chemistry*, 275(15), pp.11181–11190.

Cole, S.T., 2014. Who will develop new antibacterial agents? *Philosophical Transactions*

of the Royal Society of London. Series B, 369(1645), p.20130430.

Conus, S. & Simon, H., 2010. Cathepsins and their involvement in immune responses. *Swiss Medical Weekly*, 140(13042).

Covarrubias, A.J. et al., 2016. Akt-mTORC1 signaling regulates Acly to integrate metabolic input to control of macrophage activation. *eLife*, 5(11612), pp.1–19.

Cox, D., 1999. A Requirement for Phosphatidylinositol 3-Kinase in Pseudopod Extension. *Journal of Biological Chemistry*, 274(3), pp.1240–1247.

Czaplewski, L. et al., 2016. Alternatives to antibiotics-a pipeline portfolio review. *The Lancet Infectious Diseases*, 16(2), pp.239–251.

D'Costa, S.S., Romer, T.G. & Boyle, M.D., 2000. Analysis of expression of a cytosolic enzyme on the surface of *Streptococcus pyogenes*. *Biochemical and Biophysical Research Communications*, 278(3), pp.826–32.

Dagan, R., 2009. Impact of pneumococcal conjugate vaccine on infections caused by antibiotic-resistant *Streptococcus pneumoniae*. *Clinical Microbiology and Infection*, 15(SUPPL. 3), pp.16–20.

Daniely, D. et al., 2006. Pneumococcal 6-phosphogluconate-dehydrogenase, a putative adhesin, induces protective immune response in mice. *Clinical and Experimental Immunology*, 144(2), pp.254–263.

Davis, K., Nakamura, S. & Weiser, J., 2011. Nod2 sensing of lysozyme-digested peptidoglycan promotes macrophage recruitment and clearance of *S. pneumoniae* colonization in mice. *The Journal of Clinical Investigation*, 121(9).

Didierlaurent, A. et al., 2008. Sustained desensitization to bacterial Toll-like receptor ligands after resolutionof respiratory influenza infection. *The Journal of Experimental Medicine*, 205(2), pp.323–329.

Dockrell, D.H. et al., 2003a. Alveolar macrophage apoptosis contributes to pneumococcal clearance in a resolving model of pulmonary infection. *Journal of Immunology (Baltimore, Md. : 1950)*, 171(10), pp.5380–8.

Dockrell, D.H. et al., 2003b. Alveolar macrophage apoptosis contributes to

pneumococcal clearance in a resolving model of pulmonary infection. *Journal of immunology (Baltimore, Md. : 1950)*, 171(10), pp.5380–5388.

Dockrell, D.H. et al., 2001. Immune-mediated phagocytosis and killing of *Streptococcus pneumoniae* are associated with direct and bystander macrophage apoptosis. *The Journal of Infectious Diseases*, 184(6), pp.713–22.

Donnelly, R.P. & Finlay, D.K., 2015. Glucose, glycolysis and lymphocyte responses. *Molecular Immunology*, 68(2), pp.513–519.

Du, J. et al., 2012. Sirt5 Is an NAD-Dependent Protein Lysine Demalonylase and Desuccinylase. *Science*, 334(6057), pp.806–809.

Duits, L.A. et al., 2002. Expression of beta-defensin 1 and 2 mRNA by human monocytes, macrophages and dendritic cells. *Immunology*, 106(4), pp.517–25.

Dunn, W.B. & Ellis, D.I., 2005. Metabolomics: Current analytical platforms and methodologies. *TrAC - Trends in Analytical Chemistry*, 24(4), pp.285–294.

Dupuy, F. et al., 2013. LKB1 is a central regulator of tumor initiation and pro-growth metabolism in ErbB2-mediated breast cancer. *Cancer & Metabolism*, 1(1), p.18.

Eisenreich, W. et al., 2013. Metabolic host responses to infection by intracellular bacterial pathogens. *Frontiers in Cellular and Infection Microbiology*, 3(July), p.24.

Eliopoulos, A.G. et al., 2002. Induction of COX-2 by LPS in macrophages is regulated by Tpl2-dependent CREB activation signals. *EMBO Journal*, 21(18), pp.4831–4840.

Ellinger, J.J. et al., 2013. Databases and Software for NMR-Based Metabolomics. *Current Metabolomics*, 1(1), pp.1–22.

Epelman, S., Lavine, K.J. & Randolph, G.J., 2014. Origin and Functions of Tissue Macrophages. *Immunity*, 41(1), pp.21–35.

Everts, B. et al., 2012. Commitment to glycolysis sustains survival of NO-producing inflammatory dendritic cells. *Blood*, 120(7), pp.1422–1431.

Everts, B. et al., 2014. TLR-driven early glycolytic reprogramming via the kinases TBK1-IKKε supports the anabolic demands of dendritic cell activation. *Nature Immunology*, 15(4), pp.323–32.

Fessenden, M., 2016. Metabolomics: Small molecules, single cells. *Nature*, 540(7631), pp.153–155.

Flamand, L., Tremblay, M.J. & Borgeat, P., 2007. Leukotriene B4 triggers the in vitro and in vivo release of potent antimicrobial agents. *Journal of Immunology*, 178(12), pp.8036–8045.

Flannagan, R.S., Heit, B. & Heinrichs, D.E., 2015. Antimicrobial mechanisms of macrophages and the immune evasion strategies of *Staphylococcus aureus*. *Pathogens*, 4(4), pp.826–868.

Fleming, A., 1929. On the antibacterial action of cultures of a penicillium, with special reference to their use in the isolation of *B. influenzae*. *The British Journal of Experimental Pathology*, 10(3), pp.226–236.

Fleming, A., 1964. *Penicillin. Nobel Lecture, December 11, 1945*, Amsterdam: Elsevier Publishing Company.

Förstermann, U. & Sessa, W.C., 2012. Nitric oxide synthases: Regulation and function. *European Heart Journal*, 33(7), pp.829–837.

Franco, N.H. & Olsson, I.A.S., 2014. Scientists and the 3Rs: attitudes to animal use in biomedical research and the effect. *Laboratory Animals*, 48(1), pp.50–60.

Freemerman, A.J. et al., 2014. Metabolic reprogramming of macrophages: Glucose transporter 1 (GLUT1)-mediated glucose metabolism drives a proinflammatory phenotype. *Journal of Biological Chemistry*, 289(11), pp.7884–7896.

Fromm, H.J. & Hargrove, M.S., 2012. Introduction to Metabolism. In H. J. Fromm & M. Hargrove, eds. *Essentials of Biochemistry*. Berlin, Heidelberg: Springer Berlin Heidelberg, pp. 149–161.

Fukuzumi, M. et al., 1996. Endotoxin-induced enhancement of glucose influx into murine peritoneal macrophages via GLUT 1. *Infection and Immunity*, 64(1), pp.108–112.

G7 Gesundheitsministertreffen, 2015. *Declaration of the G7 Health Ministers 8 - 9 October 2015 in Berlin*,

Gallo, R.L. et al., 1997. Identification of CRAMP, a Cathelin-related Antimicrobial Peptide Expressed in the Embryonic and Adult Mouse. *Journal of Biological Chemistry*, 272(20), pp.13088–13093.

Garau, J. & Calbo, E., 2008. Community-acquired pneumonia. *Lancet*, 371, pp.455–458.

Garaude, J. et al., 2016. Mitochondrial respiratory-chain adaptations in macrophages contribute to antibacterial host defense. *Nature Immunology*, 17(9), pp.1037–1045.

Garcia-Vidal, C. et al., 2009. Aetiology of, and risk factors for, recurrent community-acquired pneumonia. *Clinical microbiology and infection : the official publication of the European Society of Clinical Microbiology and Infectious Diseases*, 15(11), pp.1033–8.

Geno, K.A. et al., 2015. Pneumococcal capsules and their types: Past, present, and future. *Clinical Microbiology Reviews*, 28(3), pp.871–899.

Di Gialleonardo, V. et al., 2016. High-Throughput Indirect Quantitation of ^{13} C Enriched Metabolites Using ^{1} H NMR. *Analytical Chemistry*, 88(22), pp.11147–11153.

Gilbert, R.J.C. et al., 1999. Two structural transitions in membrane pore formation by pneumolysin, the pore-forming toxin of *Streptococcus pneumoniae*. *Cell*, 97(5), pp.647–655.

Gill, M., Brenwald, N. & Wise, R., 1999. Identification of an Efflux Pump Gene, pmrA, Associated with Fluoroquinolone Resistance in *Streptococcus pneumoniae*. *Antimicrobial Agents and Chemotherapy*, 43(1).

Ginsburg, A.S. et al., 2012. Issues and challenges in the development of pneumococcal protein vaccines. *Expert Review of Vaccines*, 11(3), pp.279–285.

Gleeson, L.E. et al., 2016. Cutting Edge: *Mycobacterium tuberculosis* Induces Aerobic Glycolysis in Human Alveolar Macrophages That Is Required for Control of Intracellular Bacillary Replication. *The Journal of Immunology*, 196(6), pp.2444–2449.

Goldmann, O. et al., 2007. Transcriptome analysis of murine macrophages in response

to infection with *Streptococcus pyogenes* reveals an unusual activation program. *Infection and Immunity*, 75(8), pp.4148–4157.

Gordon, S., 2008. Elie Metchnikoff: father of natural immunity. *European Journal of Immunology*, 38(12), pp.3257–64.

Gordon, S., Irving, G. & Lawson, R., 2000. Intracellular Trafficking and Killing of *Streptococcus pneumoniae* by Human Alveolar Macrophages Are Influenced by Opsonins. *Infection and Immunity*, 68(4), pp.2286–2293.

Gordon, S. & Taylor, P.R., 2005. Monocyte and macrophage heterogeneity. *Nature Reviews Immunology*, 5(12), pp.953–64.

Gottlieb, E. et al., 2003. Mitochondrial membrane potential regulates matrix configuration and cytochrome c release during apoptosis. *Cell Death and Differentiation*, 10(6), pp.709–717.

Gray, B., 1980. Epidemiologic studies of *Streptococcus pneumoniae* in infants: acquisition, carriage, and infection during the first 24 months of life. *Journal of Infectious Diseases*, 142(6), pp.923–933.

Hancock, R.E.W. & Diamond, G., 2000. The role of cationic antimicrobial peptides in innate host defences. *Trends in Microbiology*, 8(9), pp.402–410.

Hancock, R.E.W., Nijnik, A. & Philpott, D.J., 2012. Modulating immunity as a therapy for bacterial infections. *Nature Reviews Microbiology*, 10(4), pp.243–254.

Harding, C. & Geuze, H., 1992. Class II MHC molecules are present in macrophage lysosomes and phagolysosomes that function in the phagocytic processing of Listeria monocytogenes for. *The Journal of Cell Biology*, 119(3), pp.531–542.

Harvey, R.M. et al., 2011. Pneumolysin with low hemolytic activity confers an early growth advantage to *Streptococcus pneumoniae* in the blood. *Infection and Immunity*, 79(10), pp.4122–4130.

Haschemi, A. et al., 2012. The sedoheptulose kinase CARKL directs macrophage polarization through control of glucose metabolism. *Cell Metabolism*, 15(6), pp.813–826.

Hashimoto, D. et al., 2013. Tissue-resident macrophages self-maintain locally throughout adult life with minimal contribution from circulating monocytes. *Immunity*, 38(4), pp.792–804.

Heiden, M.G. Vander, Cantley, L.C. & Thompson, C.B., 2009. Understanding the Warburg Effect: The Metabolic Requirements of Cell Proliferation. *Science*, 324(May), pp.1029–1033.

Held, P. et al., 2010. *Fluorescent Detection of Drug-Induced Mitochondrial Toxicity*, BioTek Instruments, University of Vermont, Enzo Life Sciences.

Henderson, B. & Martin, A., 2011. Bacterial virulence in the moonlight: Multitasking bacterial moonlighting proteins are virulence determinants in infectious disease. *Infection and Immunity*, 79(9), pp.3476–3491.

Hirst, R. a et al., 2004. The role of pneumolysin in pneumococcal pneumonia and meningitis. *Clinical and Experimental Immunology*, 138(2), pp.195–201.

Hole, C.R. et al., 2012. Mechanisms of dendritic cell lysosomal killing of *Cryptococcus*. *Scientific Reports*, 2(October 2012), p.739.

Hoskins, J. et al., 2001. Genome of the Bacterium *Streptococcus pneumoniae* Strain R6. *Journal of Bacteriology*, 183(19), pp.5709–5717.

Houghton, A.M. et al., 2009. Macrophage elastase kills bacteria within murine macrophages. *Nature*, 460(July), pp.637–642.

Hyams, C. et al., 2010. The *Streptococcus pneumoniae* capsule inhibits complement activity and neutrophil phagocytosis by multiple mechanisms. *Infection and Immunity*, 78(2), pp.704–15.

Iles, K. & Forman, H., 2002. Macrophage signaling and respiratory burst. *Immunologic Research*, 26(1–3), pp.95–105.

Ip, W.K.E. et al., 2010. Phagocytosis and phagosome acidification are required for pathogen processing and MyD88-dependent responses to *Staphylococcus aureus*. *Journal of Immunology (Baltimore, Md. : 1950)*, 184(12), pp.7071–7081.

Ishikawa, H. & Barber, G.N., 2008. STING is an endoplasmic reticulum adaptor that

facilitates innate immune signalling. *Nature*, 455(7213), pp.674–678.

Ivanov, I.I. & Littman, D.R., 2011. Modulation of immune homeostasis by commensal bacteria. *Current Opinion in Microbiology*, 14(1), pp.106–114.

Iyer, R., Baliga, N.S. & Camilli, A., 2005. Catabolite Control Protein A (CcpA) Contributes to Virulence and Regulation of Sugar Metabolism in *Streptococcus pneumoniae*. *Journal of Bacteriology*, 187(24), pp.8340–8349.

Jagannathan-Bogdan, M. & Zon, L.I., 2013. Hematopoiesis. *Development*, 140(12), pp.2463–2467.

Jevons, M.P., 1961. "Celbenin"- Resistant Staphylococci. *British Medical Journal*, 1, pp.124–125.

Jha, A.K. et al., 2015. Network integration of parallel metabolic and transcriptional data reveals metabolic modules that regulate macrophage polarization. *Immunity*, 42(3), pp.419–430.

Johnson, H.L. et al., 2010. Systematic evaluation of serotypes causing invasive pneumococcal disease among children under five: The pneumococcal global serotype project. *PLoS Medicine*, 7(10).

Jonczyk, M.S. et al., 2016. Variation in inflammatory response during pneumococcal infection is influenced by host-pathogen interactions but associated with animal survival. *Infection and Immunity*, 84(4), pp.894–905.

Jubrail, J. et al., 2016. Inability to sustain intraphagolysosomal killing of *Staphylococcus aureus* predisposes to bacterial persistence in macrophages. *Cellular Microbiology*, 18(1), pp.80–96.

Kadioglu, A. et al., 2008. The role of *Streptococcus pneumoniae* virulence factors in host respiratory colonization and disease. *Nature Reviews. Microbiology*, 6(4), pp.288–301.

Kafri, R., Springer, M. & Pilpel, Y., 2009. Genetic Redundancy: New Tricks for Old Genes. *Cell*, 136(3), pp.389–392.

Kalin, M., 1998. Pneumococcal serotypes and their clinical relevance. *Thorax*, 53,

pp.159–162.

Kang, Y.S. et al., 2006. A Dominant Complement Fixation Pathway for Pneumococcal Polysaccharides Initiated by SIGN-R1 Interacting with C1q. *Cell*, 125(1), pp.47–58.

Kaplan, M.H. & Volanakis, J.E., 1974. Interaction of C-reactive protein complexes with the complement system. I. Consumption of human complement associated with the reaction of C-reactive protein with pneumococcal C-polysaccharide and with the choline phosphatides, lecithin and sphingomyelin. *Journal of Immunology*, 112(6), pp.2135–47.

Kardos, N. & Demain, A.L., 2011. Penicillin: The medicine with the greatest impact on therapeutic outcomes. *Applied Microbiology and Biotechnology*, 92(4), pp.677–687.

Keller, L.E., Robinson, D.A. & McDaniel, L.S., 2016. Nonencapsulated *Streptococcus pneumoniae*: Emergence and pathogenesis. *mBio*, 7(2), pp.1–12.

Kelly, B. & O'Neill, L.A., 2015. Metabolic reprogramming in macrophages and dendritic cells in innate immunity. *Cell Research*, 25(7), pp.771–84.

Kinchen, J. & Ravichandran, K., 2008. Phagosome maturation: going through the acid test. *Nature Reviews Molecular Cell Biology*, 9(10), pp.781–795.

Kirkham, L.A.S. et al., 2006. Identification of invasive serotype 1 pneumococcal isolates that express nonhemolytic pneumolysin. *Journal of Clinical Microbiology*, 44(1), pp.151–159.

Koppe, U., Suttorp, N. & Opitz, B., 2012. Recognition of *Streptococcus pneumoniae* by the innate immune system. *Cellular Microbiology*, 14(4), pp.460–6.

Kostidis, S. et al., 2017. Quantitative NMR analysis of intra- and extracellular metabolism of mammalian cells: A tutorial. *Analytica Chimica Acta*, 980, pp.1–24.

Krawczyk, C.M. et al., 2010. Toll-like receptor–induced changes in glycolytic metabolism regulate dendritic cell activation. *Blood*, 115(23), pp.4742–4749.

Ku, C.-L. et al., 2007. Selective predisposition to bacterial infections in IRAK-4-deficient children: IRAK-4-dependent TLRs are otherwise redundant in protective

immunity. *The Journal of Experimental Medicine*, 204(10), pp.2407–2422.

Kusunoki, T. et al., 1995. Molecules from *Staphylococcus aureus* that bind CD14 and stimulate innate immune responses. *The Journal of Experimental Medicine*, 182(6), pp.1673–82.

Lachmandas, E. et al., 2016. Microbial stimulation of different Toll-like receptor signalling pathways induces diverse metabolic programmes in human monocytes. *Nature Microbiology*, 2, p.16246.

Lambrecht, B.N., 2006. Alveolar Macrophage in the Driver's Seat. *Immunity*, 24(4), pp.366–368.

Lamour, S.D. et al., 2012. Metabolic characterization of *Leishmania major* infection in activated and nonactivated macrophages. *Journal of Proteome Research*, 11(8), pp.4211–4222.

Lamprecht, D.A. et al., 2016. Turning the respiratory flexibility of *Mycobacterium tuberculosis* against itself. *Nature Communications*, 7, p.12393.

Lampropoulou, V. et al., 2016. Itaconate Links Inhibition of Succinate Dehydrogenase with Macrophage Metabolic Remodeling and Regulation of Inflammation. *Cell Metabolism*, 24(1), pp.158–166.

Lanie, J.A. et al., 2007. Genome sequence of Avery's virulent serotype 2 strain D39 of *Streptococcus pneumoniae* and comparison with that of unencapsulated laboratory strain R6. *Journal of Bacteriology*, 189(1), pp.38–51.

Latham, T. et al., 2012. Lactate, a product of glycolytic metabolism, inhibits histone deacetylase activity and promotes changes in gene expression. *Nucleic Acids Research*, 40(11), pp.4794–4803.

Lauri, I. et al., 2016. Development of an optimized protocol for NMR metabolomics studies of human colon cancer cell lines and first insight from testing of the protocol using DNA G-quadruplex ligands as novel anti-cancer drugs. *Metabolites*, 6(1), pp.1–14.

Lee, J. et al., 2006. Macrophage apoptosis in response to high intracellular burden of

Mycobacterium tuberculosis is mediated by a novel caspase-independent pathway. *Journal of immunology (Baltimore, Md. : 1950)*, 176(7), pp.4267–4274.

Lee, J., Hartman, M. & Kornfeld, H., 2009. Macrophage apoptosis in tuberculosis. *Yonsei Medical Journal*, 50(1), pp.1–11.

Lewis, K., 2013. Platforms for antibiotic discovery. *Nature Reviews. Drug Discovery*, 12(5), pp.371–87.

Liemburg-Apers, D.C. et al., 2015. Interactions between mitochondrial reactive oxygen species and cellular glucose metabolism. *Archives of Toxicology*, 89(8), pp.1209–1226.

Lin, C.Y. et al., 2007. Evaluation of metabolite extraction strategies from tissue samples using NMR metabolomics. *Metabolomics*, 3(1), pp.55–67.

Lin, S.-H. et al., 2016. Increased risk of community-acquired pneumonia in COPD patients with comorbid cardiovascular disease. *International Journal of COPD*, 11, pp.3051–3058.

Ling, E. et al., 2004. Glycolytic enzymes associated with the cell surface of *Streptococcus pneumoniae* are antigenic in humans and elicit protective immune responses in the mouse. *Clinical and Experimental Immunology*, 138(2), pp.290–298.

Ling, L.L. et al., 2015. A new antibiotic kills pathogens without detectable resistance. *Nature*, 517(7535), pp.455–459.

Liu, Y., Fiskum, G. & Schubert, D., 2002. Generation of reactive oxygen species by the mitochondrial electron transport chain. *Journal of Neurochemistry*, 80(5), pp.780–787.

Ljungman, P., 2012. Vaccination of immunocompromised patients. *Clinical Microbiology and Infection*, 18(SUPPL. 5), pp.93–99.

Lobritz, M.A. et al., 2015. Antibiotic efficacy is linked to bacterial cellular respiration. *Proceedings of the National Academy of Sciences*, 112(27), pp.8173–8180.

Lugo-villarino, G. & Neyrolles, O., 2014. Manipulation of the Mononuclear Phagocyte

System by *Mycobacterium tuberculosis*. *Cold Spring Harbor Perspectives in Medicine*, 4(11), pp.1–14.

Makarewicz, O. et al., 2017. Whole genome sequencing of 39 invasive *Streptococcus pneumoniae* sequence type 199 isolates revealed switches from serotype 19A to 15B. *PLoS ONE*, 12(1), pp.1–18.

Malley, R. et al., 2003. Recognition of pneumolysin by Toll-like receptor 4 confers resistance to pneumococcal infection. *Proceedings of the National Academy of Sciences*, 100(4), pp.1966–1971.

Malloy, C.R. et al., 2013. Section 4. Metabolomic Nuclear Magnetic Resonance Spectroscopy Techniques for Body Tissue Analysis. In N. . Lutz, J. . Sweedler, & R. . Wevers, eds. *Methodologies for Metabolomics: Experimental Strategies and Techniques*. New York: Cambridge University Press, pp. 415–445.

Managò, A. et al., 2015. *Pseudomonas aeruginosa* Pyocyanin Induces Neutrophil Death *via* Mitochondrial Reactive Oxygen Species and Mitochondrial Acid Sphingomyelinase. *Antioxidants & Redox Signaling*, 22(13), pp.1097–1110.

Mandell, L.A. et al., 2007. Infectious Diseases Society of America/American Thoracic Society Consensus Guidelines on the Management of Community-Acquired Pneumonia in Adults. *Clinical Infectious Diseases*, 44(Supplement 2), pp.S27–S72.

Marie-Anaïs, F. et al., 2016. Dynamin-Actin Cross Talk Contributes to Phagosome Formation and Closure. *Traffic*, 17(5), pp.487–499.

Marion, D., 2013. An Introduction to Biological NMR Spectroscopy. *Molecular & Cellular Proteomics*, 12(11), pp.3006–3025.

Markley, J.L. et al., 2017. The future of NMR-based metabolomics. *Current Opinion in Biotechnology*, 43, pp.34–40.

Marr, K. a et al., 2003. Differential Role of MyD88 in Macrophage-Mediated Responses to Opportunistic Fungal Pathogens. *Infection and Immunity*, 71(9), pp.5280–5286.

Marriott, H. et al., 2005. Dynamic changes in Mcl-1 expression regulate macrophage viability or commitment to apoptosis during bacterial clearance. *Journal of Clinical*

Investigation, 115(2).

Marriott, H.M. et al., 2006. Decreased Alveolar Macrophage Apoptosis Is Associated with Increased Pulmonary Inflammation in a Murine Model of Pneumococcal Pneumonia. *The Journal of Immunology*, 177(9), pp.6480–6488.

Marriott, H.M. et al., 2005. Dynamic changes in Mcl-1 expression regulate macrophage viability or commitment to apoptosis during bacterial clearance. *Journal of Clinical Investigation*, 115(2), pp.359–368.

Marriott, H.M. et al., 2004. Nitric oxide levels regulate macrophage commitment to apoptosis or necrosis during pneumococcal infection. *The FASEB Journal*, 18(5), pp.1126–1128.

Mathis, D. & Shoelson, S., 2011. Immunometabolism: an emerging frontier. *Nature Reviews Immunology*, 11(2), pp.81–83.

McAllister, L.J. et al., 2004. Molecular analysis of the psa permease complex of *Streptococcus pneumoniae*. *Molecular Microbiology*, 53(3), pp.889–901.

McClay, J.L. et al., 2010. (1)H nuclear magnetic resonance metabolomics analysis identifies novel urinary biomarkers for lung function. *Journal of Proteome Research*, 9(6), pp.3083–3090.

McDevitt, C.A. et al., 2011. A molecular mechanism for bacterial susceptibility to Zinc. *PLoS Pathogens*, 7(11).

McNeela, E. a et al., 2010. Pneumolysin activates the NLRP3 inflammasome and promotes proinflammatory cytokines independently of TLR4. *PLoS Pathogens*, 6(11), p.e1001191.

Metallo, C.M., Walther, J.L. & Stephanopoulos, G., 2009. Evaluation of13C isotopic tracers for metabolic flux analysis in mammalian cells. *Journal of Biotechnology*, 144(3), pp.167–174.

Metchnikoff, E. & Binnie, F., 1906. IMMUNITY IN INFECTIVE DISEASES. *American Journal of the Medical Sciences*, 132(6), p.924.

Michelucci, A. et al., 2013. Immune-responsive gene 1 protein links metabolism to

immunity by catalyzing itaconic acid production. *Proceedings of the National Academy of Sciences of the United States of America*, 110(19), pp.7820–5.

Millet, P. et al., 2016. GAPDH Binding to TNF-α mRNA Contributes to Posttranscriptional Repression in Monocytes: A Novel Mechanism of Communication between Inflammation and Metabolism. *The Journal of Immunology*, 196(6), pp.2541–2551.

Mills, C.D., 2012. M1 and M2 Macrophages: Oracles of Health and Disease. *Critical Reviews in Immunology*, 32(6), pp.463–88.

Mills, E.L. et al., 2016. Succinate Dehydrogenase Supports Metabolic Repurposing of Mitochondria to Drive Inflammatory Macrophages. *Cell*, 167(2), p.457–470.e13.

Mills, E.L. & O'Neill, L.A., 2016. Reprogramming mitochondrial metabolism in macrophages as an anti-inflammatory signal. *European Journal of Immunology*, 46(1), pp.13–21.

Mitchell, A.M. & Mitchell, T.J., 2010. *Streptococcus pneumoniae*: virulence factors and variation. *Clinical microbiology and infection : the official publication of the European Society of Clinical Microbiology and Infectious Diseases*, 16(5), pp.411–8.

Mold, C., Rodic-Polic, B. & Du Clos, T.W., 2002. Protection from *Streptococcus pneumoniae* Infection by C-Reactive Protein and Natural Antibody Requires Complement But Not Fc Receptors. *The Journal of Immunology*, 168(12), pp.6375–6381.

Moore, K.J. et al., 2000. Divergent response to LPS and bacteria in CD14-deficient murine macrophages. *The Journal of Immunology*, 165(8), pp.4272–4280.

Mosser, D. & Edwards, J., 2008. Exploring the full spectrum of macrophage activation. *Nature Reviews Immunology*, 8(12), pp.958–969.

Murphy, K. et al., 2012. *Janeway's Immunobiology* 8th ed., New York: Garland Science, Taylor and Francis Group.

Murray, P.J. et al., 2014. Macrophage Activation and Polarization: Nomenclature and

Experimental Guidelines. *Immunity*, 41(1), pp.14–20.

Murray, P.J. & Wynn, T.A., 2011. Obstacles and opportunities for understanding macrophage polarization. *Journal of Leukocyte Biology*, 89(4), pp.557–563.

Musher, D., 1992. Infections caused by *Streptococcus pneumoniae*: clinical spectrum, pathogenesis, immunity, and treatment. *Clinical Infectious Diseases*, 14, pp.801–809.

Na, Y.R. et al., 2015. Proteomic Analysis Reveals Distinct Metabolic Differences Between Granulocyte-Macrophage Colony Stimulating Factor (GM-CSF) and Macrophage Colony Stimulating Factor (M-CSF) Grown Macrophages Derived from Murine Bone Marrow Cells. *Molecular & Cellular Proteomics*, 14(10), pp.2722–32.

Nau, G.J. et al., 2002. Human macrophage activation programs induced by bacterial pathogens. *Proceedings of the National Academy of Sciences of the United States of America*, 99(3), pp.1503–8.

Nelson, A.L. et al., 2007. Capsule enhances pneumococcal colonization by limiting mucus-mediated clearance. *Infection and Immunity*, 75(1), pp.83–90.

Netea, M.G. et al., 2015. Innate immune memory: a paradigm shift in understanding host defense. *Nature Immunology*, 16(7), pp.675–679.

Netea, M.G. et al., 2016. Trained immunity: A program of innate immune memory in health and disease. *Science*, 352(6284), pp.428–435.

Neushul, P., 1993. and the Mass Production of Penicillin. *The Journal of the History of Medicine and Allied Sciences*, 48, pp.371–395.

Newsholme, P. et al., 1986. Metabolism of glucose, glutamine, long-chain fatty acids and ketone bodies by murine macrophages. *The Biochemical Journal*, 239(1), pp.121–125.

Newton, K. & Dixit, V.M., 2012. Signaling in Innate Immunity and Inflammation. *Cold Spring Harbor Perspectives in Biology*, 4(3), pp.a006049–a006049.

NHS Choices, 2016. Vaccinations - Pneumococcal vaccine. Available at:

http://www.nhs.uk/conditions/vaccinations/pages/pneumococcal-vaccination.aspx [Accessed July 1, 2017].

Nielsen, J., 2003. It Is All about Metabolic Fluxes - GUEST COMMENTARY. *Journal of Bacteriology*, 185(24), pp.7031–7035.

Noris, M. & Remuzzi, G., 2013. Overview of complement activation and regulation. *Seminars in Nephrology*, 33(6), pp.479–492.

Norrby, S.R., Nord, C.E. & Finch, R., 2005. Lack of development of new antimicrobial drugs: a potential serious threat to public health. *The Lancet. Infectious Diseases*, 5(2), pp.115–9.

O'Neill, J., 2015. *Securing New Drugs for Future Generations : the Pipeline of Antibiotics. THE REVIEW ON ANTIMICROBIAL RESISTANCE*,

O'Neill, J., 2016. *Tackling Drug-Resistant Infections Globally: Final Report and Recommendations. THE REVIEW ON ANTIMICROBIAL RESISTANCE*,

O'Neill, L.A.J., Kishton, R.J. & Rathmell, J., 2016. A guide to immunometabolism for immunologists. *Nature Reviews. Immunology*, 16(9), pp.553–65.

Obert, C. et al., 2006. Identification of a candidate *Streptococcus pneumoniae* core genome and regions of diversity correlated with invasive pneumococcal disease. *Infection and Immunity*, 74(8), pp.4766–4777.

Ogunniyi, A.D., Giammarinaro, P. & Paton, J.C., 2002. The genes encoding virulence-associated proteins and the capsule of *Streptococcus pneumoniae* are upregulated and differentially expressed in vivo. *Microbiology*, 148(7), pp.2045–2053.

Opitz, B. et al., 2010. Innate immune recognition in infectious and noninfectious diseases of the lung. *American Journal of Respiratory and Critical Care Medicine*, 181(12), pp.1294–309.

Paiva, C.N. & Bozza, M.T., 2014. Are reactive oxygen species always detrimental to pathogens? *Antioxidants & Redox Signaling*, 20(6), pp.1000–37.

Paixao, L. et al., 2015. Transcriptional and metabolic effects of glucose on

Streptococcus pneumoniae sugar metabolism. *Frontiers in Microbiology*, 6, pp.1–19.

Palsson-Mcdermott, E.M. et al., 2015. Pyruvate kinase M2 regulates hif-1a activity and il-1b induction and is a critical determinant of the warburg effect in LPS-activated macrophages. *Cell Metabolism*, 21(1), pp.65–80.

Park, S. & Nahm, M.H., 2011. Older adults have a low capacity to opsonize pneumococci due to low igm antibody response to pneumococcal vaccinations. *Infection and Immunity*, 79(1), pp.314–320.

Patel, N.R. et al., 2012. Cell Elasticity Determines Macrophage Function. *PLoS ONE*, 7(9).

Paustian, T., 2013. 15-14 After attaching to a microbe, phagocytes ingest them. In *Through the Microscope: a look at all things small*. University of Winsconsin-Madison, pp. 1–18.

Van Pee, K. et al., 2016. Unraveling the Pore-Forming Steps of Pneumolysin from *Streptococcus pneumoniae*. *Nano Letters*, 16(12), pp.7915–7924.

Pelicano, H. et al., 2006. Glycolysis inhibition for anticancer treatment. *Oncogene*, 25(34), pp.4633–46.

Pericone, C. & Park, S., 2003. Factors contributing to hydrogen peroxide resistance in *Streptococcus pneumoniae* include pyruvate oxidase (SpxB) and avoidance of the toxic effects of the Fenton. *Journal of Bacteriology*, 185(23), pp.6815–6825.

Pericone, C.D. et al., 2003. Factors Contributing to Hydrogen Peroxide Resistance in *Streptococcus pneumoniae* Include Pyruvate Oxidase (SpxB) and Avoidance of the Toxic Effects of the Fenton Reaction. *Journal of Bacteriology*, 185(23), pp.6815–6825.

Peterson, J.W., 1996. Bacterial Pathogenesis. In S. Baron, ed. *Medical Microbiology,*. Galveston (TX).

Peterson, L.W. et al., 2017. RIPK1-dependent apoptosis bypasses pathogen blockade of innate signaling to promote immune defense. *The Journal of Experimental*

Medicine, pp.1–12.

Philips, B.J. et al., 2003. Factors determining the appearance of glucose in upper and lower respiratory tract secretions. *Intensive Care Medicine*, 29(12), pp.2204–2210.

van der Poll, T. & Opal, S.M., 2009. Pathogenesis, treatment, and prevention of pneumococcal pneumonia. *The Lancet*, 374(9700), pp.1543–56.

Portnoy, D.A., Chen, C. & Mitchell, G., 2016. Strategies Used by Bacteria to Grow in Macrophages. *Microbiology Spectrum*, 4(3), pp.1–22.

Prolo, C., Álvarez, M.N. & Radi, R., 2014. Peroxynitrite, a potent macrophage-derived oxidizing cytotoxin to combat invading pathogens. *BioFactors*, 40(2), pp.215–225.

Promega UK, 2017. Metabolite Detection Assays. Available at: https://www.promega.co.uk/products/energy-metabolism/metabolite-detection-assays/ [Accessed August 1, 2017].

Quintin, J. et al., 2014. Innate immune memory: towards a better understanding of host defense mechanisms. *Current Opinion in Immunology*, 29, pp.1–7.

Ramm Sander, P. et al., 2013. NMR Spectroscopy of Macrophages Loaded with Native, Oxidized or Enzymatically Degraded Lipoproteins. *PLoS ONE*, 8(2).

Rath, M. et al., 2014. Metabolism via arginase or nitric oxide synthase: Two competing arginine pathways in macrophages. *Frontiers in Immunology*, 5, pp.1–10.

Ratner, A.J. et al., 2007. Nod1 mediates cytoplasmic sensing of combinations of extracellular bacteria. *Cellular Microbiology*, 9(5), pp.1343–1351.

Review on Antimicrobial Resistance, 2016. *Declaration by the Pharmaceutical, Biotechnology and Diagnostics Industries on Combating Antimicrobial Resistance*,

Ricciotti, E. & Fitzgerald, G.A., 2011. Prostaglandins and inflammation. *Arteriosclerosis, Thrombosis, and Vascular Biology*, 31(5), pp.986–1000.

Riedel, S. et al., 2007. Antimicrobial use in Europe and antimicrobial resistance in *Streptococcus pneumoniae*. *European Journal of Clinical Microbiology & Infectious Diseases*, 26(7), pp.485–90.

Rodriguez-Prados, J.-C. et al., 2010. Substrate Fate in Activated Macrophages: A Comparison between Innate, Classic, and Alternative Activation. *The Journal of Immunology*, 185(1), pp.605–614.

Roiniotis, J. et al., 2009. Hypoxia Prolongs Monocyte/Macrophage Survival and Enhanced Glycolysis Is Associated with Their Maturation under Aerobic Conditions. *The Journal of Immunology*, 182(12), pp.7974–7981.

Romero, N. et al., 2017. *Improving Quantification of Cellular Glycolytic Rate Using Agilent Seahorse XF Technology. WHITE PAPER*, Agilent Technologies.

Rosenberger, C.M. et al., 2000. *Salmonella typhimurium* Infection and Lipopolysaccharide Stimulation Induce Similar Changes in Macrophage Gene Expression. *The Journal of Immunology*, 164(11), pp.5894–5904.

Rubins, J.B. et al., 1995. Dual function of pneumolysin in the early pathogenesis of murine pneumococcal pneumonia. *Journal of Clinical Investigation*, 95(1), pp.142–150.

Ruiz-García, A. et al., 2011. Cooperation of adenosine with macrophage toll-4 receptor agonists leads to increased glycolytic flux through the enhanced expression of PFKFB3 gene. *Journal of Biological Chemistry*, 286(22), pp.19247–19258.

Savill, J. et al., 1993. Phagocyte recognition of cells undergoing apoptosis. *Immunology Today*, 14(3), pp.131–136.

Scharf, S. et al., 2012. *Streptococcus pneumoniae* induces human β-defensin-2 and -3 in human lung epithelium. *Experimental Lung Research*, 38(2), pp.100–110.

Scheraga, R.G. et al., 2016. TRPV4 Mechanosensitive Ion Channel Regulates Lipopolysaccharide-Stimulated Macrophage Phagocytosis. *The Journal of Immunology*, 196(1), pp.428–436.

Schertzer, J.D. & Steinberg, G.R., 2014. Immunometabolism: the interface of immune and metabolic responses in disease. *Immunology and Cell Biology*, 92(4), p.303.

Schmeck, B. & Gross, R., 2004. *Streptococcus pneumoniae*-induced caspase 6-dependent apoptosis in lung epithelium. *Infection and Immunity*, 72, pp.4940–

4947.

Schwarz, T. & Pauksens, K., 2013. Safety of a 13-Valent Pneumococcal Conjugate Vaccine in Elderly Adults Previously Immunized with a 23-Valent Pneumococcal Polysaccharide Vaccine: An Open-. *World Journal of Vaccines*, 3, pp.123–129.

Seahorse Bioscience & Agilent Technologies, 2016. Seahorse XF Glycolysis Stress Test Kit. , pp.1–9.

Seahorse Bioscience Inc., 2015a. Basic Procedure: Seeding Cells in XF24 Cell Culture Microplates.

Seahorse Bioscience Inc., 2015b. Basic Procedure: Washing Cells in XF24 Cell Culture Microplates.

Seahorse Bioscience Inc., 2015c. Basic Procedures to Run an XFe24 Assay. Available at: http://www.seahorsebio.com/resources/documentation/basicprocedures/XFe24.php?xfe24 [Accessed June 1, 2015].

Seahorse Bioscience Inc., 2012. User Manual: XF Glycolysis Stress Test kit. , pp.1–21.

Shak, J.R. et al., 2013. Novel role for the *Streptococcus pneumoniae* toxin pneumolysin in the assembly of biofilms. *mBio*, 4(5), pp.1–10.

Shelburne, S.A. et al., 2008. The role of complex carbohydrate catabolism in the pathogenesis of invasive streptococci. *Trends in Microbiology*, 16(7), pp.318–325.

Shi, L. et al., 2015. Infection with *Mycobacterium tuberculosis* induces the Warburg effect in mouse lungs. *Scientific Reports*, 5, p.18176.

Shulga, N. & Pastorino, J.G., 2016. Hexokinase II binding to mitochondria is necessary for Kupffer cell activation and is potentiated by ethanol exposure. *Journal of Biological Chemistry*, 291(24), p.12574.

Sigma-Aldrich Co. LLC., 2017. Metabolism Assay Kits A-Z. Available at: http://www.sigmaaldrich.com/life-science/cell-biology/cell-biology-products.html?TablePage=111781140 [Accessed August 1, 2017].

Slauch, J.M., 2011. How does the oxidative burst of macrophages kill bacteria? Still an open question. *Molecular Microbiology*, 80(3), pp.580–583.

Slupsky, C.M. et al., 2009. Pneumococcal Pneumonia : Potential for Diagnosis through a Urinary Metabolic Profile research articles. *Journal of Proteome Research*, 8(12), pp.5550–5558.

Sly, L.M. et al., 2003. Survival of *Mycobacterium tuberculosis* in host macrophages involves resistance to apoptosis dependent upon induction of antiapoptotic Bcl-2 family member Mcl-1. *Journal of Immunology (Baltimore, Md. : 1950)*, 170(1), pp.430–7.

De Smet, K. & Contreras, R., 2005. Human antimicrobial peptides: Defensins, cathelicidins and histatins. *Biotechnology Letters*, 27(18), pp.1337–1347.

Somerville, G.A. & Proctor, R.A., 2009. At the Crossroads of Bacterial Metabolism and Virulence Factor Synthesis in Staphylococci. *Microbiology and Molecular Biology Reviews*, 73(2), pp.233–248.

Sonawane, A. et al., 2011. Cathelicidin is involved in the intracellular killing of mycobacteria in macrophages. *Cellular Microbiology*, 13(10), pp.1601–1617.

Soruri, A. et al., 2007. β-Defensins chemoattact macrophages and mast cells but not lymphocytes and dendritic cells: CCR6 is not involved. *European Journal of Immunology*, 37(9), pp.2474–2486.

Stafford, S.L. et al., 2013. Metal ions in macrophage antimicrobial pathways: emerging roles for zinc and copper. *Bioscience Reports*, 33(4), p.e00049.

Steenbergen, J.N. et al., 2005. Daptomycin: A lipopeptide antibiotic for the treatment of serious Gram-positive infections. *Journal of Antimicrobial Chemotherapy*, 55(3), pp.283–288.

Steinwede, K. et al., 2012. Cathepsin G and neutrophil elastase contribute to lung-protective immunity against mycobacterial infections in mice. *Journal of Immunology*, 188(9), pp.4476–4487.

Stuckey, D.J. et al., 2005. Detection of the inhibitory neurotransmitter GABA in macrophages by magnetic resonance spectroscopy. *Journal of Leukocyte Biology*, 78(2), pp.393–400.

Suzuki, H. et al., 2016. Glycolytic pathway affects differentiation of human monocytes to regulatory macrophages. *Immunology Letters*, 176, pp.18–27.

Takeda, K. & Akira, S., 2001. Roles of Toll-like receptors in innate immune responses. *Genes to Cells*, 6(9), pp.733–742.

Takeuchi, O. et al., 2001. Discrimination of bacterial lipoproteins by Toll-like receptor 6. *International Immunology*, 13(7), pp.933–940.

Tan, Z., Xie, N., Cui, H., et al., 2015. Pyruvate dehydrogenase kinase 1 participates in macrophage polarization via regulating glucose metabolism. *Journal of immunology (Baltimore, Md. : 1950)*, 194(12), pp.6082–9.

Tan, Z., Xie, N., Banerjee, S., et al., 2015. The monocarboxylate transporter 4 is required for glycolytic reprogramming and inflammatory response in macrophages. *Journal of Biological Chemistry*, 290(1), pp.46–55.

Tannahill, G.M. et al., 2013. Succinate is an inflammatory signal that induces IL-1β through HIF-1α. *Nature*, 496(7444), pp.238–42.

Tannahill, G.M. & O'Neill, L. a J., 2011. The emerging role of metabolic regulation in the functioning of Toll-like receptors and the NOD-like receptor Nlrp3. *FEBS Letters*, 585(11), pp.1568–1572.

Taylor, J. et al., 2014. *Estimating the economic costs of antimicrobial resistance: Model and Results*, Santa Monica (Calif.) and Cambridge (UK).

Taylor, P.R. et al., 2005. Macrophage receptors and immune recognition. *Annual Review of Immunology*, 23, pp.901–44.

Teng, Q. et al., 2009. A direct cell quenching method for cell-culture based metabolomics. *Metabolomics*, 5(2), pp.199–208.

Tettelin, H. et al., 2001. Complete Genome Sequence of a Virulent Isolate of *Streptococcus pneumoniae*. *Science*, 293(5529), pp.498–506.

The University of Sheffield, 2015. The Florey Institute for Host-Pathogen Interactions. Available at: http://www.floreyinstitute.com/ [Accessed September 1, 2016].

The White House Administration, 2015. *National Action Plan For Combating Antibiotic-*

Resistant Bacteria,

Thomas, J.L., 1998. Fundamentals of NMR. In *Fundamentals of NMR*. San Francisco: Department of Pharmaceutical Chemistry, University of California, pp. 1–31.

Thompson, S.N., 1990. NMR spectroscopy: Its basis, biological application and use in studies of insect metabolism. *Insect Biochemistry*, 20(3), pp.223–237.

Tian, W.N. et al., 1999. Importance of glucose-6-phosphate dehydrogenase activity in cell death. *The American Journal of Physiology*, 276(5 Pt 1), pp.C1121–C1131.

Tomlinson, G. et al., 2014. TLR-Mediated Inflammatory Responses to *Streptococcus pneumoniae* Are Highly Dependent on Surface Expression of Bacterial Lipoproteins. *The Journal of Immunology*, 193(7), pp.3736–3745.

Trimble, W.S. & Coppolino, M.G., 2005. Phagosome Maturation. In C. Rosales, ed. *Molecular Mechanisms of Phagocytosis*. pp. 1–18.

Tseng, H. et al., 2002. Virulence of *Streptococcus pneumoniae* : PsaA Mutants Are Hypersensitive to Oxidative Stress. *Infection and Immunity*, 70(3), pp.1635–1639.

U.S. Department of Health and Human Services, 2013. *Pneumococcal conjugate vaccines*,

Urenjak, J. et al., 1993. Proton nuclear magnetic resonance spectroscopy unambiguously identifies different neural cell types. *The Journal of Neuroscience*, 13(3), pp.981–989.

Vasdekis, A.E. & Stephanopoulos, G., 2015. Review of methods to probe single cell metabolism and bioenergetics. *Metabolic Engineering*, 27, pp.115–135.

Vazquez, A. et al., 2010. Catabolic efficiency of aerobic glycolysis: the Warburg effect revisited. *BMC Systems Biology*, 4, p.58.

Wahl, D.R. et al., 2012. Distinct metabolic programs in activated T cells: Opportunities for selective immunomodulation. *Immunological Reviews*, 249(1), pp.104–115.

Walker, A.K. et al., 2014. Activation of lung toll-like receptors does not exacerbate sickness responses to lipopolysaccharide in mice. *Brain, Behavior, and Immunity*, 38, pp.211–219.

Walsh, C.T. & Wencewicz, T.A., 2014. Prospects for new antibiotics: a molecule-centered perspective. *The Journal of Antibiotics*, 67(1), pp.7–22.

Walther, J.L. et al., 2012. Optimization of 13C isotopic tracers for metabolic flux analysis in mammalian cells. *Metabolic Engineering*, 14(2), pp.162–171.

Wan, M. et al., 2014. Antimicrobial peptide LL-37 promotes bacterial phagocytosis by human macrophages. *Journal of Leukocyte Biology*, 95(June), pp.1–11.

Warburg, O., Wind, F. & Negelein, E., 1927. THE METABOLISM OF TUMORS IN THE BODY. *Journal of General Physiology*, pp.519–530.

Webster, S.J. et al., 2010. Distinct Cell Death Programs in Monocytes Regulate Innate Responses Following Challenge with Common Causes of Invasive Bacterial Disease. *The Journal of Immunology*, 185(5), pp.2968–2979.

Weiser, J.N. et al., 1994. Phase variation in pneumococcal opacity: Relationship between colonial morphology and nasopharyngeal colonization. *Infection and Immunity*, 62(6), pp.2582–2589.

Weiser, J.N., 2010. The pneumococcus: Why a commensal misbehaves. *Journal of Molecular Medicine*, 88(2), pp.97–102.

Weiss, G. & Schaible, U.E., 2015. Macrophage defense mechanisms against intracellular bacteria. *Immunological Reviews*, 264(1), pp.182–203.

West, A.. et al., 2011. TLR signalling augments macrophage bactericidal activity through mitochondrial ROS. *Nature*, 472, pp.476–480.

White, C. et al., 2009. A role for the ATP7A copper-transporting ATPase in macrophage bactericidal activity. *Journal of Biological Chemistry*, 284(49), pp.33949–33956.

Wickersham, M. et al., 2017. Metabolic Stress Drives Keratinocyte Defenses against *Staphylococcus aureus* Infection. *Cell Reports*, 18(11), pp.2742–2751.

Williams, N.P. et al., 2017. Seasonality, risk factors and burden of community-acquired pneumonia in COPD patients: A population database study using linked health care records. *International Journal of COPD*, 12, pp.313–322.

Wilson, R. et al., 2017. Naturally Acquired Human Immunity to Pneumococcus Is

Dependent on Antibody to Protein Antigens. *PLoS Pathogens*, 13(1), pp.1–26.

Winter, G. & Krömer, J.O., 2013. Fluxomics - connecting 'omics analysis and phenotypes. *Environmental Microbiology*, 15(7), pp.1901–1916.

Wolf, A.J. et al., 2011. Phagosomal Degradation Increases TLR Access to Bacterial Ligands and Enhances Macrophage Sensitivity to Bacteria. *The Journal of Immunology*, 187(11), pp.6002–6010.

Woodruff, P.G. et al., 2005. A distinctive alveolar macrophage activation state induced by cigarette smoking. *American Journal of Respiratory and Critical Care Medicine*, 172(11), pp.1383–1392.

World Health Organization, 2015. *Global action plan on antimicrobial resistance.*,

World Health Organization, 2011. Pneumococcal disease. Available at: http://www.who.int/immunization/topics/pneumococcal_disease/en/ [Accessed September 9, 2016].

World Health Organization, 2017. The top 10 causes of death. *WHO Fact Sheet,*. Available at: http://www.who.int/mediacentre/factsheets/fs310/en/ [Accessed July 20, 2010].

Wynn, T. a., Chawla, A. & Pollard, J.W., 2013. Origins and Hallmarks of Macrophages: Development, Homeostasis, and Disease. *Nature*, 496(7446), pp.445–455.

Xia Lab, 2017. MetaboAnalyst 3.0. Available at: http://www.metaboanalyst.ca/faces/home.xhtml [Accessed August 28, 2017].

Xu, Y. et al., 2001. Complement activation in factor D-deficient mice. *Proceedings of the National Academy of Sciences of the United States of America*, 98(25), pp.14577–82.

Yang, H.C. et al., 2011. The microbicidal and cytoregulatory roles of NADPH oxidases. *Microbes and Infection*, 13(2), pp.109–120.

Yang, M. & Pollard, P.J., 2013. Succinate: A new epigenetic hacker. *Cancer Cell*, 23(6), pp.709–711.

Yang, Z. et al., 2014. Female resistance to pneumonia identifies lung macrophage nitric

oxide synthase-3 as a therapeutic target. *eLife*, 3, pp.1–17.

Yesilkaya, H. et al., 2000. Superoxide Dismutase in Oxidative Stress and Virulence of *Streptococcus pneumoniae*. *Infection and Immunity*, 68(5), pp.2819–2826.

Yu, J. et al., 2001. Characterization of the *Streptococcus pneumoniae* {NADH} oxidase that is required for infection. *Microbiology*, 147(2001), pp.431–438.

Yuste, J. et al., 2005. Additive inhibition of complement deposition by pneumolysin and PspA facilitates *Streptococcus pneumoniae* septicemia. *The Journal of Immunology*, 175(3), pp.1813–1819.

Zhang, A. et al., 2012. Modern analytical techniques in metabolomics analysis. *The Analyst*, 137(2), pp.293–300.

Zhao, G. et al., 2013. Pivotal role of reactive oxygen species in differential regulation of lipopolysaccharide-induced prostaglandins production in macrophages. *Molecular pharmacology*, 83(1), pp.167–78.

Zhao, Y. et al., 2008. Mechanisms and Methods in Glucose Metabolism and Cell Death. In *Methods in Enzymology*. Elsevier Inc., pp. 439–457.

Zou, C., Wang, Y. & Shen, Z., 2005. 2-NBDG as a fluorescent indicator for direct glucose uptake measurement. *Journal of Biochemical and Biophysical Methods*, 64(3), pp.207–215.

Zysk, G. et al., 2000. Detection of 23 immunogenic pneumococcal proteins using convalescent- phase serum. *Infection and Immunity*, 68(6), pp.3740–3743.

Appendices

- **Appendix 1: Flow Cytometry of BMDMs to establish appropriate differentiation (Taken from EFisk MBiolSci project report)**
- **Appendix 2: Supernatant spectra of blank wells and *S. pneumoniae*-containing media only.**
- **Appendix 3: 1H-NMR MATLAB script**

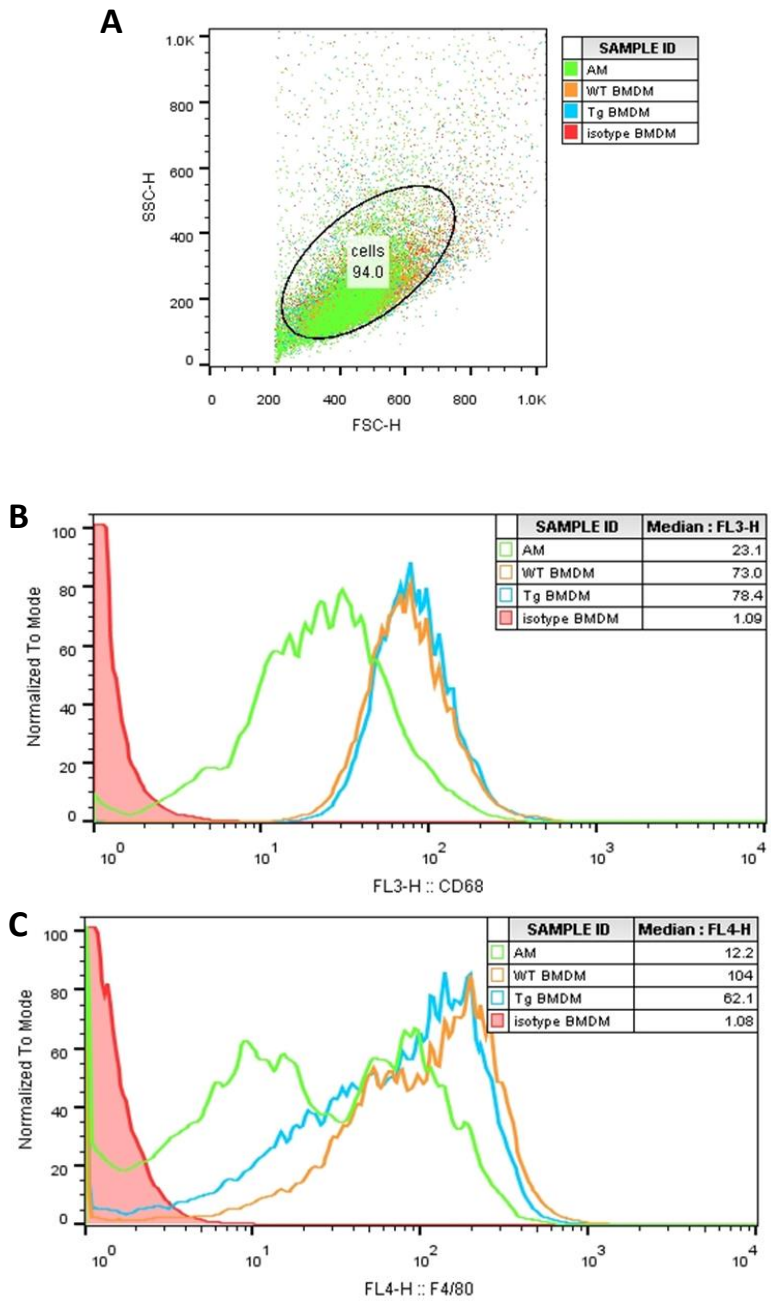

Appendix 1: Flow Cytometry of BMDMs to establish appropriate differentiation (Taken from EFisk MBiolSci project report)

(A) This population of four cell groups, as separated by FSC-H and SSC-H. The black oval indicates gating used, to determine cells used for subsequent analysis. Here this encompasses 94% of the total population, excluding contaminants, debris and cells with unexpected morphologies.
(B) Normalised levels of CD68 expression are shown for alveolar macrophages (AMs), wild type (WT) BMDMs, Mcl-1 transgenic (Tg) BMDMs, and isotype-stained mixed BMDM control. This indicates high level of CD68 expression in both BMDM cell lines, compared to AMs, suggesting appropriate macrophage differentiation occurred in BMDM cultures. Additionally, the isotype control shows non-specific CD68 antibody binding did not occur.
(C) Data presented in the same manner as (B), however here the expression of F4/80 on AMs and BMDMs is shown. Both BMDM cell lines show high expression, and the isotype control confirmed this was not due to non-specific antibody binding. The AM population exhibits two distinct populations; a low expression subset and a high expression subset. This could be due to the functional role of F4/80 in activated alveolar macrophages. This data suggests that BMDMs are appropriately differentiated after fourteen days of culturing.

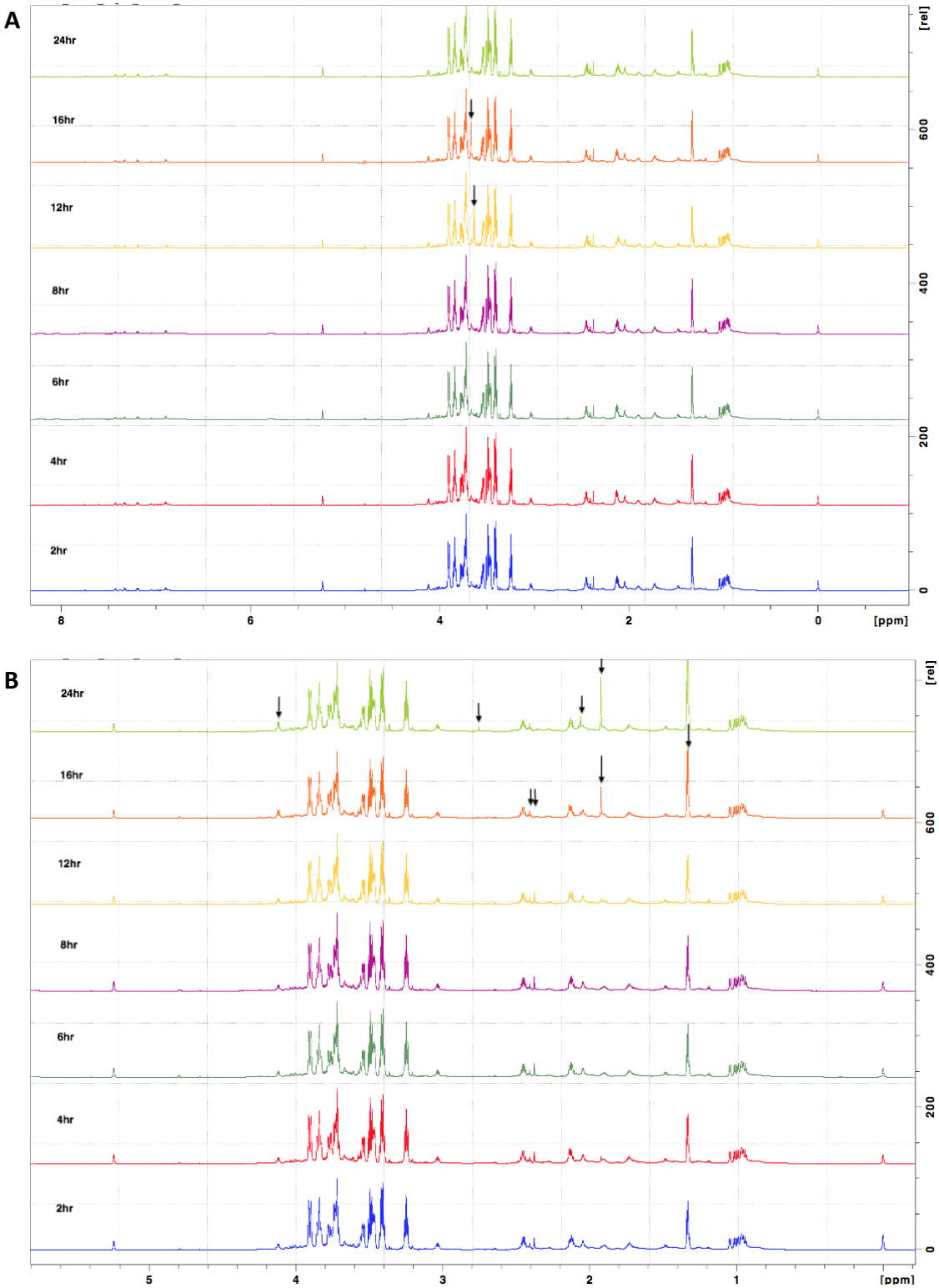

Appendix 2: Supernatant spectra of blank wells and *S. pneumoniae*-containing media only.

Supernatant samples taken from preparations absent of BMDM cell cultures, to act as baseline controls and references. After 4 hours, all wells were treated with antibiotics, to prevent bacterial replication and to correlate with the treatment of the cells. For NMR spectroscopy, supernatants were diluted 50:50 in 70% D_2O PBS with 167µM TSP.

A) Spectral profiles for blank wells (no cells, no bacteria)

B) Spectral profiles for wells containing *S. pneumoniae* (MOI 10, as per infected cells).

```
ccc

workspace;  % Make sure the workspace panel is showing.

pnTop = 'F:\matlab\ProcessData\Emily\NMR\';%Set main directory
fileNm = '\efisk*';%Set filenames to process '*' as a wildcard

%********Option**********
pltFig = 0;%option to plot out spectra
ppm.limits = [11 -0.5];%display limits
ppm.binLimits = [9 0.5];%bin spectra between these values
ppm.noise = [11 9];%define boise region - NOT USED
ppm.water = [5.2 4.5];%replace water region with random numbers
ppm.ref  = 1.30;%reference peak for binning
ppm.binWidth = 0.04;%binning width

%************Spectrum alignment options in icoshift***********************
alignMode.align = 'average';
alignMode.quality = 'b';
alignMode.options = [0 2 0];

%Start of code
pnData = '\pdata\1\';
fn = '1r';
d = dir(strcat(pnTop,fileNm));
tmp = [d.isdir];
d = d(tmp);
dataNms = {d.name}';
numDataSets = length(dataNms);
dataArray = cell(numDataSets,2);

% [~,~,dnData] = xlsread(strcat(pnTop,'ProtonData.xlsx'),'Sheet1','A2:F42');
%     tmp = d(1).name(1:end-1);
%     tmp = strsplit(tmp,'\');
samples = struct;
tmpStrct = struct;
%************get spectra***************
for ii=1:numDataSets
    subDir = dir(strcat(pnTop,dataNms{ii}));
    subDir = subDir(3:end);%take off '.' and '..' directory listing
    tmp = [subDir.isdir];
    subDir = subDir(tmp);
    subDir = {subDir.name};
    numFiles = length(subDir);

    for i2=1:numFiles
        smplPth = [dataNms{ii},'\',subDir{i2},'\pdata\1\'];


        tmpStrct = Open_Bruker_Raw_Data_Spect800([pnTop,smplPth],'1r');
        smplNm = strsplit(smplPth,'\');
        smplNm = smplNm{1};

        ns = tmpStrct.ns;
        tmpStrct.ppm = linspace(tmpStrct.Offset,...
            tmpStrct.Offset-tmpStrct.sweepwidth/tmpStrct.CF,...
            tmpStrct.SI)';
        if i2==1
           holdArray = zeros(numFiles,length(tmpStrct.raw));
        end
        %correct water baseline
        %             tmp = tmpStrct.raw;
        %             SI = numel(tmp);
        %             matFile = sprintf('%s\\%s\\%s_%s.mat',pnTop,smplPth,smplNm,subDir{i3});
        %             if exist(matFile,'file') == 2
        %                 display(sprintf('Previous base line points (%s) exists loading',matFile));
        %                 load(matFile,'bsPts');
        %                 %                     tmpPts = [1,tmp(1);bsPts;SI,tmp(SI)];
        %                 %                     bsCorrRl = splineBsTool(tmpPts,SI,'pchip',[3 81],0);
        %                 fh = figure;
        %                 ha(1) = subplot(2,1,1);
        %                 plot(tmp,'b');
        %                 hold on
        %                 %                 plot(bsPts,'rx')
        %                 plot(bsPts,'r:');
        %                 title('Original')
        %                 ha(2) = subplot(2,1,2);
        %                 plot(tmp-bsPts,'b');
        %                 hold on
        %                 plot(zeros(numel(tmp),1),'k--')
        %                 title('Baseline corrected')
        %                 tmpStrct.corr = tmp-bsPts;
        % %                 linkaxes(ha,'xy')
        %                 pause(2)
        %                 close(fh)
        %             else
        %                 bsPts = [];
        %                 [tmpStrct.corr,bsPts] = bsToolV2(tmp,'interp',3,numel(tmpStrct.raw),'pchip',[3
81],bsPts,1);
        %                 save(matFile,'bsPts')
        %             end
        holdArray(i2,:) = tmpStrct.raw;%place spectra in temporary array for alignment
        samples.(smplNm).(sprintf('Expno_%s',subDir{i2})) =  tmpStrct;
    end

    %***********Align spectra******************
    alignMode.binNo = (knnsearch(tmpStrct.ppm,ppm.limits(1))):(knnsearch(tmpStrct.ppm,ppm.limits(2)));
    trgtSpec = holdArray(1,:);%align to first spectrum
    [alignedSpectra, ~, ~] = icoshiftV2(alignMode.align, trgtSpec,holdArray,...
                                        alignMode.binNo, alignMode.quality,...
                                        alignMode.options,tmpStrct.ppm);
```

```
    if pltFig==1%plot spectra if option on
        figure
        hold on
        for i2=1:numFiles
            plot(tmpStrct.ppm,holdArray(i2,:))
        end
        set(gca,'XDir','reverse')
        legend(subDir,'Location','NorthWest')
        title(strrep(d(ii,1).name,'_',' '))
        xlim(sort(ppm.limits))
    end
end

%**********************Bin Spectra*********************
if exist(sprintf('%s\\%s_BinWdth%s.mat',pnTop,'samples',strrep(num2str(ppm.binWidth),'.','p')),'file') == 2
    reBin = 0;

    reBin = questdlg(sprintf('Previous bindata loaded\nRebin?'), ...
        'Bin data', ...
        'Yes','No','Quit','No');
    if strcmp(reBin,'Quit')==1 || isempty(reBin)==1
        display('Exiting')
        return
    end
    if strcmp(reBin,'No')==1
        load(sprintf('%s\\%s_BinWdth%s.mat',pnTop,'samples',strrep(num2str(ppm.binWidth),'.','p')),'samples')
    end
    if strcmp(reBin,'Yes')==1
        reBin = 1;
    end
else
    reBin = 1;
end

fldNmsL1 = fieldnames(samples);
lvl1 = numel(fldNmsL1);
if reBin==1
    for ii = 1:lvl1
        smplNm = fldNmsL1{ii};%Sample name

        %Determine how many spectra to bin
        fldNmsL2 = fieldnames(samples.(fldNmsL1{ii}));
        tmp = strncmp(fldNmsL2,'Expno',5);
        fldNmsL2 = fldNmsL2(tmp);
        holdArray = samples.(fldNmsL1{ii}).alignedSpectra;
        trgtPnts = 1:size(holdArray,2);

        for i2=1:size(holdArray,1)

            ppm.use = tmpStrct.ppm;

            %replace water peak with random numbers
            tmp = knnsearch(ppm.use,ppm.water(1)):knnsearch(ppm.use,ppm.water(2));
            holdArray(i2,tmp) = rand(numel(tmp),1)-0.5;

            %bin data
            tmp =
binTool(holdArray(i2,:),trgtPnts,ppm.binWidth,ppm,'y',sprintf('%s, %s',smplNm,fldNmsL2{i2}));%bin target spectrum

            if i2==1%only do this for the first loop
                holdCell = cell(size(holdArray,1),4+numel(tmp.binIntegrals));
            end

            %add sample parameters to temporary array for saving
            holdCell(i2,1) = {smplNm};%sample name
            holdCell(i2,2) = fldNmsL2(i2);%expno
            holdCell(i2,3) = {0};% empty for cell concentration
            holdCell(i2,4) = {sum(tmp.binIntegrals)};%total bin integral
            holdCell(i2,5:end) = num2cell(tmp.binIntegrals);%place bin integrals into array

            samples.(fldNmsL1{ii}).(fldNmsL2{i2}) = catstruct(samples.(fldNmsL1{ii}).(fldNmsL2{i2}),tmp);%store
data in main structure
        end

        %************Create text file*************************
%         tmp = ['Sample','Expno','Cell_Conc','Sum_of_Bins',arrayfun(@num2str, 1:size(holdCell,2)-4, 'unif', 0)];
        tmp = ['Sample','Expno','Cell_Conc','Sum_of_Bins',strsplit(sprintf('Bin%d,',1:size(holdCell,2)-4),',')];
        tmp=tmp(1:end-1);
        holdCell = [tmp;holdCell];

writetable(cell2table(holdCell(2:end,:),'VariableNames',tmp),sprintf('%sData_%s.txt',pnTop,fldNmsL1{ii}),'Delimit
er','\t')

        samples.(fldNmsL1{ii}).binIntegrals = holdCell;%store all bin integrals in main structure
    end


save(strcat(pnTop,sprintf('%s_BinWdth%s.mat','samples',strrep(num2str(ppm.binWidth),'.','p'))),'samples')%save
all bin data
```

Appendix 3: 1H-NMR MATLAB script

MATLAB script used to normalise, align and calculate integral regions of raw NMR data, courtesy of Dr. Stephen Reynolds. Green text with '%' at start of line is used here to give information on the proceeding sections of code.